

7. SITE 709¹

Shipboard Scientific Party²

HOLE 709A

Date occupied: 0945 L, 5 June 1987
Date departed: 0200 L, 6 June 1987
Time on hole: 16 hr, 15 min
Position: 03°54.9'S, 60°33.1'E
Water depth (sea level; corrected m, echo-sounding): 3040.8
Water depth (rig floor; corrected m, echo-sounding): 3051.3
Bottom felt (m, drill pipe): 3046.9
Penetration (m): 203.1
Number of cores: 21
Total length of cored section (m): 203.1
Total core recovered (m): 184.74
Core recovery (%): 91
Oldest sediment cored:
Depth (mbsf): 203.1
Nature: nannofossil ooze
Age: late Oligocene
Measured velocity (km/s): 1.518

HOLE 709B

Date occupied: 0720 L, 6 June 1987
Date departed: 0215 L, 7 June 1987
Time on hole: 18 hr, 35 min
Position: 03°54.9'S, 60°33.1'E
Water depth (sea level; corrected m, echo-sounding): 3040.8
Water depth (rig floor; corrected m, echo-sounding): 3051.3
Bottom felt (m, drill pipe): 3048.7
Penetration (m): 254.8
Number of cores: 27
Total length of cored section (m): 254.8
Total core recovered (m): 234.6
Core recovery (%): 92
Oldest sediment cored:
Depth (mbsf): 254.8
Nature: nannofossil ooze
Age: early Oligocene
Measured velocity (km/s): 1.517

HOLE 709C

Date occupied: 0505 L, 7 June 1987

Date departed: 1115 L, 8 June 1987
Time on hole: 30 hr, 10 min
Position: 03°54.9'S, 60°33.1'E
Water depth (sea level; corrected m, echo-sounding): 3040.8
Water depth (rig floor; corrected m, echo-sounding): 3051.3
Bottom felt (m, drill pipe): 3048.7
Penetration (m): 353.7
Number of cores: 37
Total length of cored section (m): 353.7
Total core recovered (m): 330.0
Core recovery (%): 93
Oldest sediment cored:
Depth (mbsf): 353.7
Nature: nannofossil chalk
Age: middle Eocene
Measured velocity (km/s): 1.647

Principal results: Site 709 is located in the western equatorial Indian Ocean at 3°54.9'S and 60°33.1'E, in water depths of 3038.2 m (Fig. 1). The site lies in a small basin perched near the summit of the Madingley Rise, a regional topographic high between the Carlsberg Ridge and the northern Mascarene Plateau. The irregular basement topography is draped with sediment, varying in thickness from less than 50 m to over 400 m. Site 709 was placed in one of the thicker sediment sequences because our primary objective was to study the Neogene history of carbonate preservation at this intermediate-depth site.

Three holes were continuously cored at Site 709. Hole 709A terminated in nannofossil ooze of late Oligocene age at 203.1 mbsf. All 21 cores were taken with the advanced hydraulic piston corer (APC), and the recovery rate was 91%. Hole 709B yielded 27 cores and ended at 254.8 mbsf in lower Oligocene oozes, for a recovery rate of 92%. The 7 deepest cores were taken with the extended core barrel (XCB), and all shallower cores with the APC. Hole 709C was cored to 353.7 mbsf, yielding 20 APC and 17 XCB cores, for a total recovery of 93%. This last hole ended in nannofossil chalks of middle Eocene age (~47 Ma).

The recently modified XCB, with its newly developed cutting shoe with seal, was tested for the first time during Leg 115; it performed extraordinarily well. The XCB recovery rates in Holes 709B and 709C were 91% and 87%, respectively, implying that complete and virtually undisturbed sediment sections can be retrieved from sub-bottom depths beneath the APC-penetration capability.

Cored sediments at Site 709 are fairly homogeneous in composition, comprising a single major lithostratigraphic unit consisting of alternate clay-bearing nannofossil ooze and nannofossil ooze layers. This major unit is tentatively subdivided into three subunits on the basis of distinctive correlatable changes in color. The uppermost 30 m of buff-colored nannofossil oozes, which are of late Pliocene-Pleistocene age, form Subunit IA. An interval between 30 and 115 mbsf containing numerous thin greenish gray horizons forms Subunit IB. This second subunit spans approximately 7 m.y., from 3 Ma to 10 Ma. An interval from 115 to 353.7 mbsf of light gray to white nannofossil oozes and chalks forms the third subunit. This last subunit represents the time interval from 10 (late Miocene) to 47 Ma (middle Eocene).

The first occurrence of more indurated chalk was observed at about 130 mbsf. The amount of chalk increases with depth thereaf-

¹ Backman, J., Duncan, R. A., et al., 1988. *Proc. ODP, Init. Repts.*, 115: College Station, TX (Ocean Drilling Program).

² Shipboard Scientific Party is as given in the list of Participants preceding the contents, with the addition of Isabella Premoli Silva and Silvia Spezzaferria, Dipartimento di Scienze della Terra, Università di Milano, Via Mangiagalli 34, I-20129 Milano, Italy.

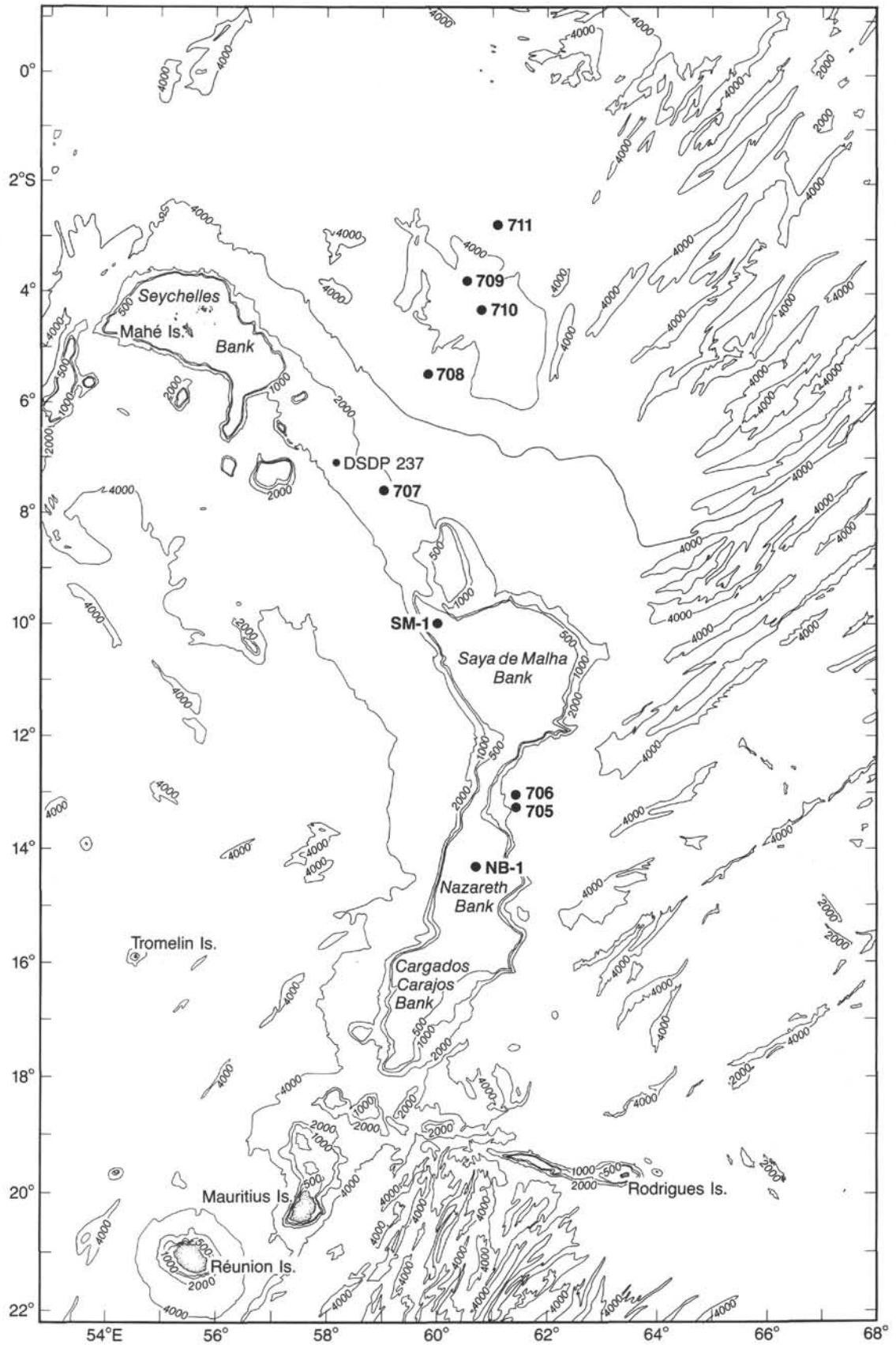


Figure 1. Bathymetric features around the Mascarene Plateau, western Indian Ocean, and the location of Site 709 (after Fisher et al., 1971). Depth in meters.

ter, until chalk occurs consistently toward the bottom of Hole 709C. The cored stratigraphic sequence is summarized in Figure 2.

We observed many ash layers; two particularly prominent ones, observed at the same sub-bottom depth in all three holes, bracket the Miocene/Pliocene boundary. Sedimentation rates are on the order of 13 m/m.y. during late Miocene-Pleistocene times and are followed by a drastic downhole decrease close to the middle/late Miocene boundary. Large portions of both the middle and lower Miocene are stratigraphically disordered. Sediments from the lower part of the lower Miocene are intercalated into sediments of late early

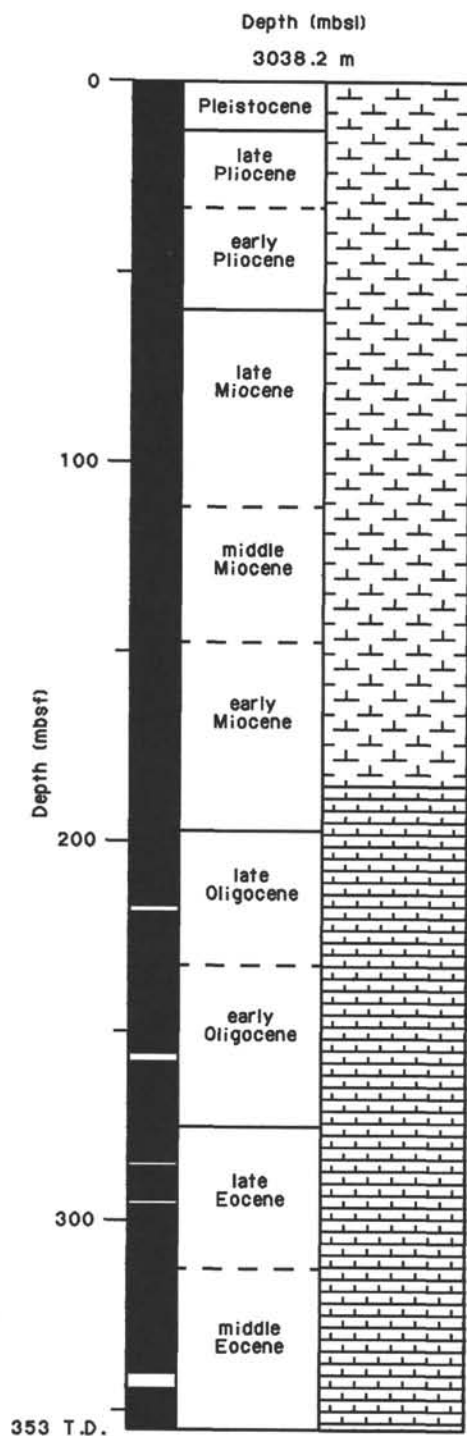


Figure 2. Stratigraphic summary of Site 709. Black column represents recovered section.

and early middle Miocene age. Thus, stratigraphic data are unreliable between approximately 14 and 17 Ma.

All three holes cross the Oligocene/Miocene boundary, although Hole 709A cored just a few meters of Oligocene sediments before being terminated. Oligocene sedimentation rates are on the average around 7 m/m.y., and these comparatively low rates continue well into the middle Eocene.

Measurements of magnetic susceptibility at 5-cm intervals provide the basis for numerous interhole correlations. The resulting high-frequency oscillations reveal inconsistencies in the recovery of the sediment section in all three holes (see "Paleomagnetism" section, this chapter). It is difficult to pinpoint the exact causes for such inconsistencies in the hole-to-hole correlation, as discussed by Ruddiman et al. (1987). We assume, however, that offsets which occur in the middle of the core are associated with minor but true lithostratigraphic differences in the sedimentary column, and that offsets which occur in the vicinity of core boundaries are related to coring problems.

Carbonate contents show a component of "high-frequency" variability, based on one analysis per 0.75 m. When smoothed, the late Neogene carbonate curve displays a "cyclic" character. Only further and more detailed studies, however, will reveal the true nature of these carbonate signals and which periodicities, if any, are involved. With the present sample resolution, only the longer "periodicities" can be observed. Nevertheless, the influence of a parameter which affects the carbonate record on a 0.4–0.5-m.y. periodicity seems, at first sight, to be present in this sediment sequence. The amplitude in these smoothed "cycles" ranges between approximately 88% and 93% carbonate content, except for some early late Miocene extreme values showing lows of about 84%–85%. Low-amplitude changes in carbonate content are also present in the Paleogene record.

By assuming a steady input of both carbonate and noncarbonate fractions to the sediment surface, the Neogene amplitude difference of 5% implies that about 45% of the initial carbonate has been dissolved, according to the formula of Heath and Culbertson (1970):

$$L = 100 [1 - (N_f/N_i)] / (1 - N_i),$$

where L is the loss in percent, N_i is the initial assumed fraction of noncarbonate (7% used in this case), and N_f the final observed fraction (12%). As Piasias and Prell (1985) pointed out, however, changes in carbonate concentration are better described as changing rates of dissolution rather than changing proportions of dissolution, because the mass of carbonate preserved provides more information than carbonate percentages.

Figure 3 shows our preliminary attempt, based on shipboard biostratigraphic data only, to describe the sedimentation history of Site 709 in terms of calculated mass accumulation rates for the carbonate and noncarbonate sediment components. Site 709 shows the greatest variability in bulk mass accumulation rates during late Neogene times, where the values range from 0.4 to 1.8 g/cm²/1000 yr (or 0.7 to 1.8, if we omit the mean values from the 9–11-Ma interval, around the middle/late Miocene boundary). By assuming a constant input of the noncarbonate fraction in the time interval between 0 and 9 Ma (which, of course, is a questionable assumption for such a long period), and using a mean bulk accumulation rate of 1.16 g/cm²/1000 yr, a change in the carbonate mass accumulation of 0.06 g/cm²/1000 yr would explain a 5% amplitude change (88%–93%) in carbonate content.

Bulk accumulation rates vary only from 0.5 to 0.7 g/cm²/1000 yr from 20 through 46 Ma. It appears likely, however, that slightly greater amplitudes will emerge as the time control improves with more detailed shore-based studies. The fourfold increase in the sedimentation rate at 46 Ma is, of course, also apparent in the bulk accumulation rates (Fig. 3). From the point of view of mass accumulation rates, however, the increase of the noncarbonate dilutant is sixfold (from 0.06 to 0.36 g/cm²/1000 yr), using mean carbonate contents of 90.7% (20–46 Ma) and 83.6% (46–47.2 Ma), and mean bulk accumulation rates of 0.59 (20–46 Ma) and 2.22 (46–47.2 Ma) g/cm²/1000 yr. This sixfold increase is probably due to a larger input of siliceous material (radiolarians, diatoms, and sponge spicules) and possibly volcanic ash, implying that the decrease in carbonate content at 46 Ma is due to dilution rather than to dissolution.

The mass accumulation rates indicate major differences in depositional modes between the early Miocene-Oligocene (20–36 Ma)

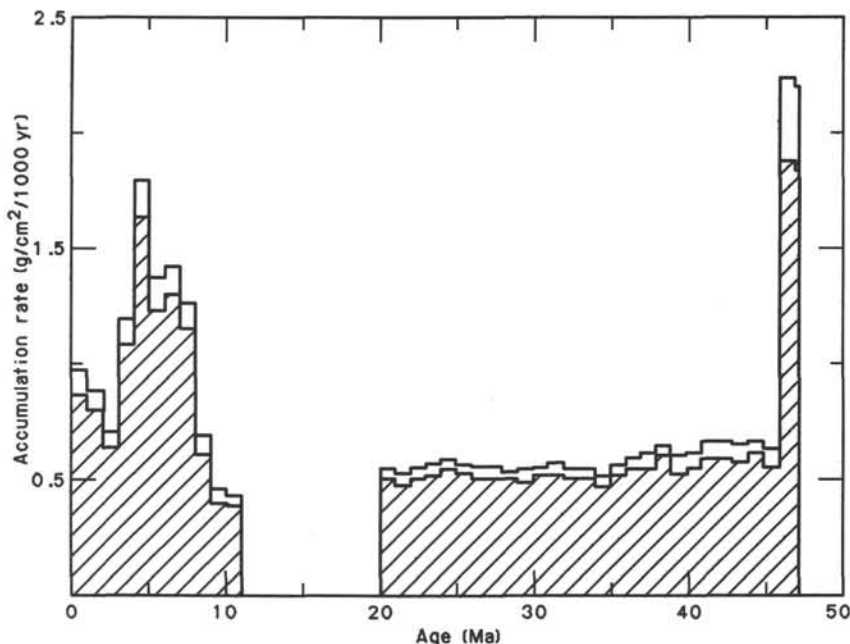


Figure 3. Mass accumulation rates of bulk sediment (unfilled area) and biogenic calcium carbonate (diagonal lines) plotted vs. age at Site 709. The gap in the center of the graph is caused partly by a hiatus (11–15 Ma) and partly by the presence of slump deposits (15–20 Ma), which are excluded. The data represent mean values within 1-m.y. time increments. The graph shows a composite data set as derived from all three holes drilled at Site 709: Hole 709B (0–3.6 Ma), Hole 709A (3.6–11.0 Ma), and Hole 709C (20.0–47.2 Ma).

and the Eocene (36–46 Ma), omitting the oldest peak values, despite the fact that an average sedimentation rate of 5.5 m/m.y. is used as a working hypothesis. The mean carbonate contents are 91.3% (20–36 Ma) and 89.8% (36–46 Ma), respectively, whereas the corresponding bulk accumulation rates are 0.56 and 0.64 g/cm²/1000 yr. Thus, the mean noncarbonate fraction accumulated at a rate of 0.05 g/cm²/1000 yr during the early Miocene–Oligocene interval, and at a rate of 0.07 g/cm²/1000 yr during the later half of the Eocene. This implies a 25%–30% higher mass accumulation rate of the noncarbonate dilutant during the Eocene interval, as compared with the early Miocene–Oligocene interval. The accumulation of carbonate is just over 10% greater during the Eocene (0.57 g/cm²/1000 yr) than during the early Miocene–Oligocene interval (0.51 g/cm²/1000 yr).

BACKGROUND AND OBJECTIVES

Site 709 is one of five sites in a transect drilled at different water depths from the Mascarene Plateau, the Madingley Rise, and the surrounding abyssal plains (Fig. 4). The broader strategy for drilling this bathymetric transect is presented in the chapter on Site 707 (see “Background and Objectives” section, “Site 707” chapter, this volume). The depth difference between the shallowest carbonate-dissolution profile site (Site 707; 1541.4 m) and Site 709, the next deeper one, is close to 1500 m. Site 709 fulfills our requirement for an intermediate-depth site in the carbonate-depth transect. Although it would have been desirable to drill the intermediate site at a somewhat shallower water depth than that at Site 709 (3038.2 m), no suitable target was found that would provide a relatively unbroken, pelagic sediment sequence.

The content of carbonate in the sediment may give a misleading impression of the actual carbonate loss due to dissolution (Berger, 1971; Broecker and Peng, 1982). By assuming a steady input ratio of biogenic carbonate to detrital residue which is 9:1, we can demonstrate that a relatively small decrease in carbonate content is associated with considerable dissolution. Heath and Culberson (1970) used the following formula for estimating the carbonate dissolution:

$$L = 100[1 - (N_f/N_i)] / (1 - N_i)$$

where L is the loss in percent, N_i is the initial content of noncarbonate, and N_f the final noncarbonate content. Thus, a decrease in carbonate content from 90% to 80% indicates a carbonate-dissolution rate of 55%. In view of this relationship, we may expect to find considerable changes in the history of carbonate preservation at Site 709, despite the fact that fluctuations in carbonate content may appear modest.

Our major objective was to retrieve a continuous Neogene sediment sequence from which we can assess the variability in carbonate preservation through time. We particularly hoped to establish how changes in carbonate preservation connect to major perturbations in climatic evolution and in deep-sea circulation. By correcting the water depth at Site 709 for the subsidence of the depositional surface through time, we can model positions and excursions of the lysocline (foraminiferal and nanofossil). Periods of extreme shoaling of the carbonate-compensation depth (CCD) horizon, such as occurred during the middle Miocene (van Andel, 1975), can also be monitored at Site 709.

These objectives require that carbonate-preservation patterns be determined relative to the record of changing paleoenvironments, and that the phasing of different events be accurately assessed. This requires a highly resolved time control in the cored sediments which, in turn, requires direct correlations between biostratigraphy and magnetostratigraphy. Another major goal of our work is, therefore, to improve existing correlations between the major siliceous and calcareous microfossil groups. Leg 115 will recover the only APC material from the equatorial Indian Ocean in the present phase of the Ocean Drilling Program (ODP). We hope that detailed biostratigraphic work in this region will yield valuable insight into the ubiquitous problem of diachroneity vs. synchronicity, important low-latitude datum events, as compared with equatorial regions in the Atlantic and Pacific Oceans.

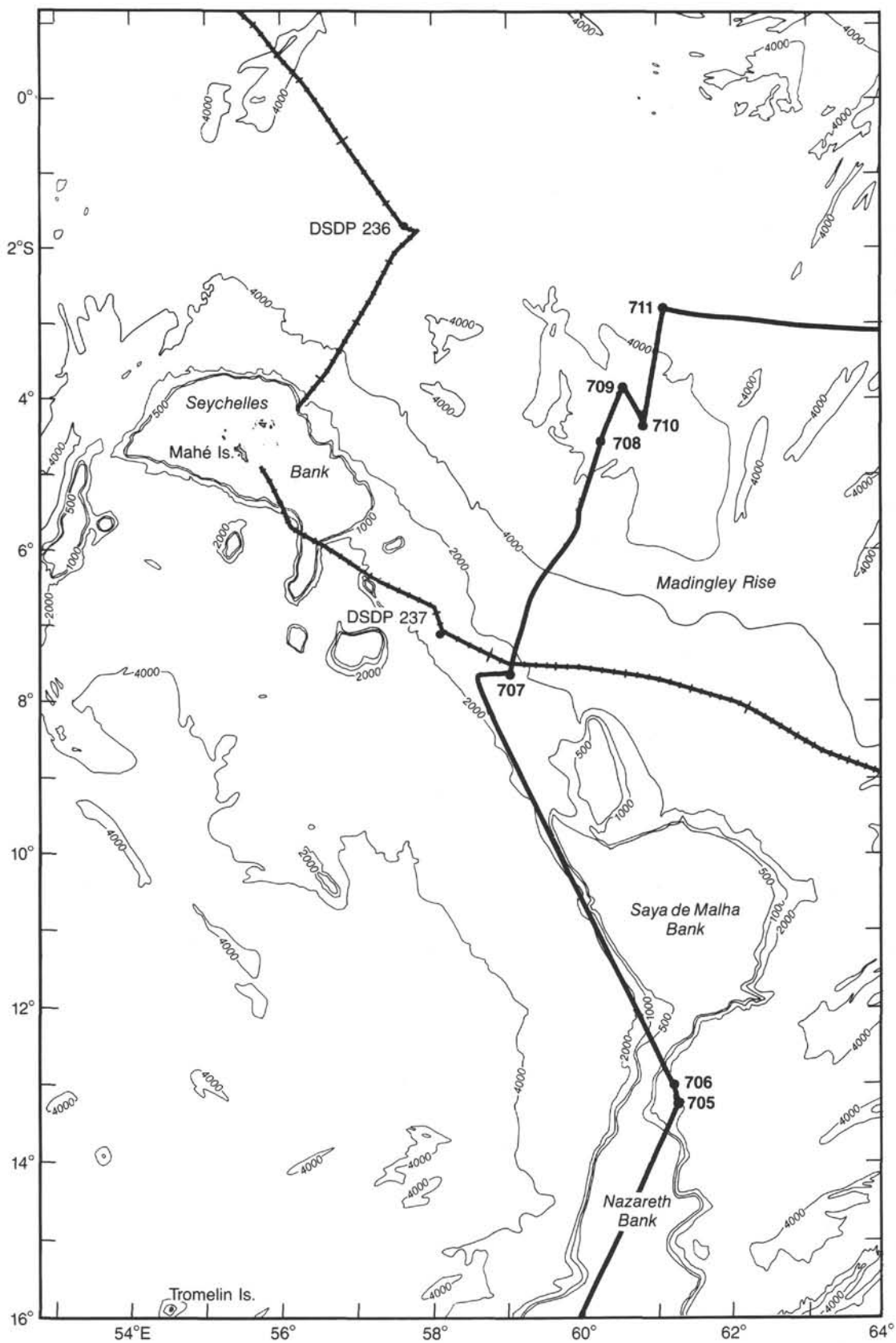


Figure 4. Expanded view of bathymetric features around the northern Mascarene Plateau, with the location of Site 709 and other carbonate depth transect sites (after Fisher, Bunce, et al., 1974). The Leg 115 track line of the *JOIDES Resolution* and the earlier track of the *Glomar Challenger* on Leg 24 are shown for reference. Depth in meters.

OPERATIONS

The pre-site survey for Site 709 did not look promising to the Co-Chiefs. After further surveying and approval from ODP, they selected an alternate site approximately 6 mi north of CARB 2A. The recallable beacon was dropped at 0130 hr, 5 June 1987, and Site 709 was established.

Hole 709A

The standard six-drill collar APC/XCB modified for the XCB cutting shoe with seal and the Monel drill collar were made up and run to the seafloor. We began APC coring with the objective of coring to 250 mbsf. The mud line was established in water depths of 3036.4 m. Orientation instrumentation was deployed beginning with Core 115-709A-4H. Cores 115-709A-18H through -20H had pull-out forces of 20,000 lb. After advancing the hole to 3239.5 m (203.1 mbsf), Core 115-709A-21H had a pull-out force of 30,000 lb. We could not retrieve the next core barrel (it parted in the attempt). Total penetration was 203.1 mbsf to 3239.5 m, with 184.7 m of core recovered for a total recovery rate of 91% (Table 1).

Coring was halted because of the parted core barrel. The hole was filled with heavy mud, the drill string pulled clear of the seafloor, and the ship offset 10 m south to initiate Hole 709B.

Hole 709B

The APC/XCB was lowered back to the seafloor, and the mud line was established at 3038.2 m. We advanced the hole to 3225.4 m with APC coring (187.2 mbsf), recovering 172.9 m of core for a 92% recovery rate. At this point, in anticipation of the formation change which had caused the APC barrel to become stuck in Hole 709A, we deployed the XCB system.

The experimental XCB cutting shoe with seal was used to advance the hole to 3293 m (254.8 mbsf). Core quality was excellent, with 61.6 m of core recovered for a recovery rate of 91%. Total penetration was 254.8 mbsf to 3293 m, with 234.6 m of core recovered for a total recovery rate of 92% (Table 1).

When our 250-mbsf objective was met, we filled the hole with heavy mud, pulled the drill string clear of the mud line, and offset the ship 10 m south to initiate Hole 709C.

Hole 709C

Once again the BHA was lowered to the sea floor and the mud line established at 3038.2 m. We recovered 100% with APC coring in 20 cores to a depth of 3227.3 m (189.1 mbsf). The water sample temperature pressure (WSTP) device was successfully deployed by free falling after Cores 115-709C-11H (3140.4 m, 102.2 mbsf), -15H (3179 m, 140.8 mbsf), and -20H (3227.3 m, 189.1 mbsf) with good water samples and temperature data gathered. Again, in anticipation of a formation change, the XCB system was deployed at this point.

The XCB core barrel was deployed 17 times and recovered 138.7 m of core while advancing the hole 155 m to 3391.9 m (353.7 mbsf), for a recovery rate of 89.4%. Total penetration was 353.7 mbsf to 3391.9 m, with 327.9 m of core recovered for a total recovery rate of 93%. The experimental XCB cutting shoe with seal was also used in this hole. High-quality cores were recovered in both the soupy chalk ooze and the firmer chalk sediment below.

Site 709 to Site 710 (CARB-3)

The hole was filled with heavy mud, the beacon recalled and retrieved at 1500 hr, and the drill string tripped out. A course was laid for Site CARB-3, and at 1700 hr, 8 June 1987, the ship was under way.

Table 1. Coring summary, Site 709.

Core no.	Date (June 1987)	Time (local)	Depth (mbsf)	Cored (m)	Recovered (m)	Recovery (%)
115-709A-						
1H	5	1000	0-10.1	10.1	10.10	100.0
2H	5	1030	10.1-19.7	9.6	8.77	91.3
3H	5	1130	19.7-29.4	9.7	9.73	100.0
4H	5	1200	29.4-39.1	9.7	6.70	69.1
5H	5	1300	39.1-48.7	9.6	0	0
6H	5	1400	48.7-58.3	9.6	9.80	102.0
7H	5	1445	58.3-68.0	9.7	10.09	104.0
8H	5	1545	68.0-77.6	9.6	9.73	101.0
9H	5	1630	77.6-87.3	9.7	9.29	95.8
10H	5	1730	87.3-96.9	9.6	10.06	104.8
11H	5	1830	96.9-106.6	9.7	9.63	99.3
12H	5	1915	106.6-116.2	9.6	9.12	95.0
13H	5	2000	116.2-125.8	9.6	9.86	103.0
14H	5	2045	125.8-135.5	9.7	9.80	101.0
15H	5	2130	135.5-145.2	9.7	9.78	101.0
16H	5	2215	145.2-154.9	9.7	9.76	100.0
17H	5	2300	154.9-164.6	9.7	9.73	100.0
18H	5	1145	164.6-174.3	9.7	9.51	98.0
19H	6	0030	174.3-183.9	9.6	5.63	58.6
20H	6	0115	183.9-193.5	9.6	8.85	92.2
21H	6	0200	193.5-203.1	9.6	8.80	91.6
115-709B-						
1H	6	0730	0-3.8	3.8	3.83	101.0
2H	6	0815	3.8-13.4	9.6	9.77	102.0
3H	6	0900	13.4-23.1	9.7	9.76	100.0
4H	6	0930	23.1-32.8	9.7	9.89	102.0
5H	6	1015	32.8-42.4	9.6	9.65	100.0
6H	6	1100	42.4-52.0	9.6	9.91	103.0
7H	6	1145	52.0-61.7	9.7	9.64	99.4
8H	6	1245	61.7-71.3	9.6	9.99	104.0
9H	6	1330	71.3-81.0	9.7	9.73	100.0
10H	6	1400	81.0-90.6	9.6	9.71	101.0
11H	6	1445	90.6-100.3	9.7	9.26	95.4
12H	6	1515	100.3-109.9	9.6	9.96	104.0
13H	6	1600	109.9-119.5	9.6	9.55	99.5
14H	6	1645	119.5-129.2	9.7	9.83	101.0
15H	6	1730	129.2-138.9	9.7	9.77	101.0
16H	6	1800	138.9-148.6	9.7	3.54	36.5
17H	6	1900	148.6-158.3	9.7	9.53	98.2
18H	6	1945	158.3-168.0	9.7	9.94	102.0
19H	6	2030	168.0-177.6	9.6	9.67	101.0
20H	6	2115	177.6-187.2	9.6	0	0
21X	6	2200	187.2-196.8	9.6	9.49	98.8
22X	6	2245	196.8-206.5	9.7	9.43	97.2
23X	6	2330	206.5-216.1	9.6	8.30	86.4
24X	7	0000	216.1-225.8	9.7	9.18	94.6
25X	7	0045	225.8-235.5	9.7	9.72	100.0
26X	7	0130	235.5-245.1	9.6	6.92	72.1
27X	7	0215	245.1-254.8	9.7	8.58	88.4
115-709C-						
1H	7	0515	0-5.8	5.8	6.17	106.0
2H	7	0600	5.8-15.4	9.6	9.62	100.0
3H	7	0645	15.4-25.1	9.7	9.74	100.0
4H	7	0730	25.1-34.7	9.6	10.02	104.4
5H	7	0800	34.7-44.3	9.6	9.67	101.0
6H	7	0830	44.3-53.9	9.6	9.87	103.0
7H	7	0900	53.9-63.6	9.7	9.74	100.0
8H	7	0945	63.6-73.2	9.6	9.93	103.0
9H	7	1015	73.2-82.9	9.7	9.54	98.3
10H	7	1045	82.9-92.5	9.6	9.63	100.0
11H	7	1130	92.5-102.2	9.7	7.30	75.2
12H	7	1345	102.2-111.8	9.6	9.75	101.0
13H	7	1430	111.8-121.4	9.6	9.83	102.0
14H	7	1500	121.4-131.1	9.7	9.79	101.0
15H	7	1545	131.1-140.8	9.7	9.79	101.0
16H	7	1800	140.8-150.5	9.7	9.92	102.0
17H	7	1845	150.5-160.2	9.7	9.75	100.0
18H	7	1930	160.2-169.9	9.7	9.92	102.0
19H	7	2000	169.9-179.5	9.6	9.89	103.0
20H	7	2030	179.5-189.1	9.6	10.01	104.3

Table 1 (continued).

Core no.	Date (June 1987)	Time (local)	Depth (mbsf)	Cored (m)	Recovered (m)	Recovery (%)
115-709C-						
21X	7	2315	189.1-198.7	9.6	9.24	96.3
22X	8	0000	198.7-208.4	9.7	7.82	80.6
23X	8	0045	208.4-218.0	9.6	7.69	80.1
24X	8	0130	218.0-227.7	9.7	8.04	82.9
25X	8	0215	227.7-237.4	9.7	7.84	80.8
26X	8	0245	237.4-247.0	9.6	9.27	96.5
27X	8	0330	247.0-256.7	9.7	6.61	68.1
28X	8	0415	256.7-266.4	9.7	4.74	48.8
29X	8	0500	266.4-276.1	9.7	9.51	98.0
30X	8	0545	276.1-285.8	9.7	8.68	89.5
31X	8	0630	285.8-295.4	9.6	8.52	88.8
32X	8	0715	295.4-305.1	9.7	9.66	99.6
33X	8	0800	305.1-314.8	9.7	8.41	86.7
34X	8	0845	314.8-324.4	9.6	9.15	95.3
35X	8	0930	324.4-334.1	9.7	9.63	99.3
36X	8	1015	334.1-343.9	9.8	5.68	57.9
37X	8	1115	343.9-353.7	9.8	9.66	98.6

LITHOSTRATIGRAPHY

At Site 709 we drilled three holes in water depths of 3038.2 m in an approximately 400-m-thick sediment section which partially fills a small basin on top of the Madingley Rise. Homogeneous sediment sequences dominated by very pale brown, white, light gray, and light greenish gray clay-bearing nannofossil ooze to nannofossil ooze and nannofossil chalk were recovered in all three holes. In all but a few intervals, nannofossils are the dominant sediment component. Visual core descriptions and smear slide analyses revealed little downcore variation in the above lithology. Consequently, we identified only a single lithologic unit at Site 709, which ranges in age from middle Eocene to Pleistocene.

In general, the carbonate content in Site 709 sediments exhibits small, but systematic, high-frequency fluctuations about an average of approximately 90%, only occasionally falling below 85% or rising above 95% (see Fig. 20, "Geochemistry" section, this chapter). The sediment becomes generally more indurated with depth. Below 130 mbsf, oozes become somewhat stiffer, and the first chalk intervals appear and generally increase in frequency and thickness with depth. The foraminifer content of the oozes and chalks decreases downcore, falling below 10% by 60 mbsf in all three holes, but foraminifers tend to increase above 10% in lower parts of the sediment sequence (below 230 mbsf) in Hole 709B and Hole 709C.

Unit I has been divided into three subunits on the basis of subtle, but consistent, color changes and the appearance of abundant laminae of light greenish gray sediment within middle depth intervals of all three holes. The distribution of the subunits is summarized in Figure 5 and described in detail in the following sections.

Subunit IA: Sections 115-709A-1H-1 to 115-709A-4H-1, 75 cm (0-30.15 mbsf), Sections 115-709B-1H-1 to 115-709B-4H-5, 25 cm (0-29.35 mbsf), and Sections 115-709C-1H-1 to 115-709C-4H-4, 13 cm (0-29.73 mbsf); Age: Pleistocene to late Pliocene.

Subunit IA in all three holes consists of alternating foraminifer-bearing nannofossil to foraminifer-nannofossil ooze, and clay-bearing, foraminifer-bearing nannofossil ooze to clay-bearing nannofossil ooze. Colors generally grade downcore from white to very pale brown (10YR 8/1, 8/2), then to white and very light gray (N9, N8), suggesting a transition to less oxidizing condi-

tions toward the bottom of Subunit IA. The carbonate content is high, ranging from 85.5% to 92.3% and averaging approximately 89% (analyses from Hole 709A), with higher values occurring in the lowest part of the subunit.

Foraminifer content at Site 709 is highest near the top of this subunit, suggesting winnowing or preferential preservation. Estimated abundances of foraminifers vary from 8% to around 35% and are highest in Cores 115-709A-1H and -2H. The non-carbonate component is primarily clay. Siliceous biogenic components are found in minor to trace amounts in isolated sections of Subunit IA.

Subunit IB: Sections 115-709A-4H-1, 75 cm, to 115-709A-13H-1, 95 cm (30.15-117.20 mbsf), Sections 115-709B-4H-5, 25 cm, to 115-709B-13H-5, 90 cm (29.35-116.80 mbsf), and Sections 115-709C-4H-4, 13 cm, to 115-709C-13H-5, 10 cm (29.73-117.90 mbsf); Age: late Pliocene to late Miocene.

The top of Subunit IB is marked by the first appearance of thin, light greenish gray horizons that frequently occur within this interval, particularly in the upper two-thirds of the subunit. Subunit IB colors are distinctly more gray to greenish gray (reducing?) than Subunit IA colors, varying from predominantly very light greenish gray (5G 8/1, 5GY 8/1) to very light gray (N8) and white (N9).

The upper part of Subunit IB is a foraminifer-bearing nannofossil ooze. The sediments grade into nannofossil ooze that alternates with clay-bearing nannofossil ooze, indicating a slight decrease in foraminifer content with depth. As in Subunit IA, Subunit IB contains only minor to trace amounts of biogenic silica. The carbonate content continues to be high, averaging 91%, with only 6% of the analyses (from Hole 709A only) falling below 88%. At the bottom of Subunit IB, the carbonate content is consistently below 90% (Core 115-709A-12H, clay-bearing nannofossil ooze).

The most characteristic feature of Subunit IB is the frequent occurrence of light greenish gray (5G 7/1) and light gray (N7) thin horizons. These are observed as faint to very distinct darker laminae, commonly <1-3 cm in thickness; they often occur in groups, visible on the lighter background of the very light greenish gray to light gray nannofossil ooze. Over 120 of these laminae were observed in Holes 709B and 709C, respectively, while over 75 were observed in Hole 709A (the lower number in Hole 709A is likely due to low recovery in Core 115-709A-4H and to no recovery in Core 115-709A-5H). In some horizons the light greenish gray laminae occur coupled to an underlying thin light gray (N7) horizon (iron-sulfide rich?).

The darker laminae occur most frequently within four intervals in each of the holes at similar sub-bottom depths (Fig. 5). Volcanic-ash layers seem to be associated with these intervals (Fig. 5 and Table 2). Similar pale green laminae were described in sediments cored on the Lord Howe Rise during Leg 90 in the southwest Pacific (Kennett et al., 1986). Detailed post-cruise analysis of these laminae led Gardner et al. (1986) to conclude that they correspond to diagenetically altered volcanic-ash layers. The light greenish gray laminae in Site 709 sediments may have a similar origin and may be associated with pulses of volcanic activity in the Mascarene Plateau region of the Indian Ocean.

The only major sedimentological evidence of naturally disturbed sediment at Site 709 occurs within Subunit IB. An interval of sediment, the structure of which suggests slumping, was observed in all three holes at similar sub-bottom depths (Cores 115-709A-10H to 115-709A-11H?, Sections 115-709B-11H-6 to 115-709B-12H-2, and Sections 115-709C-11H-3 to 115-709C-11H-5; Fig. 5).

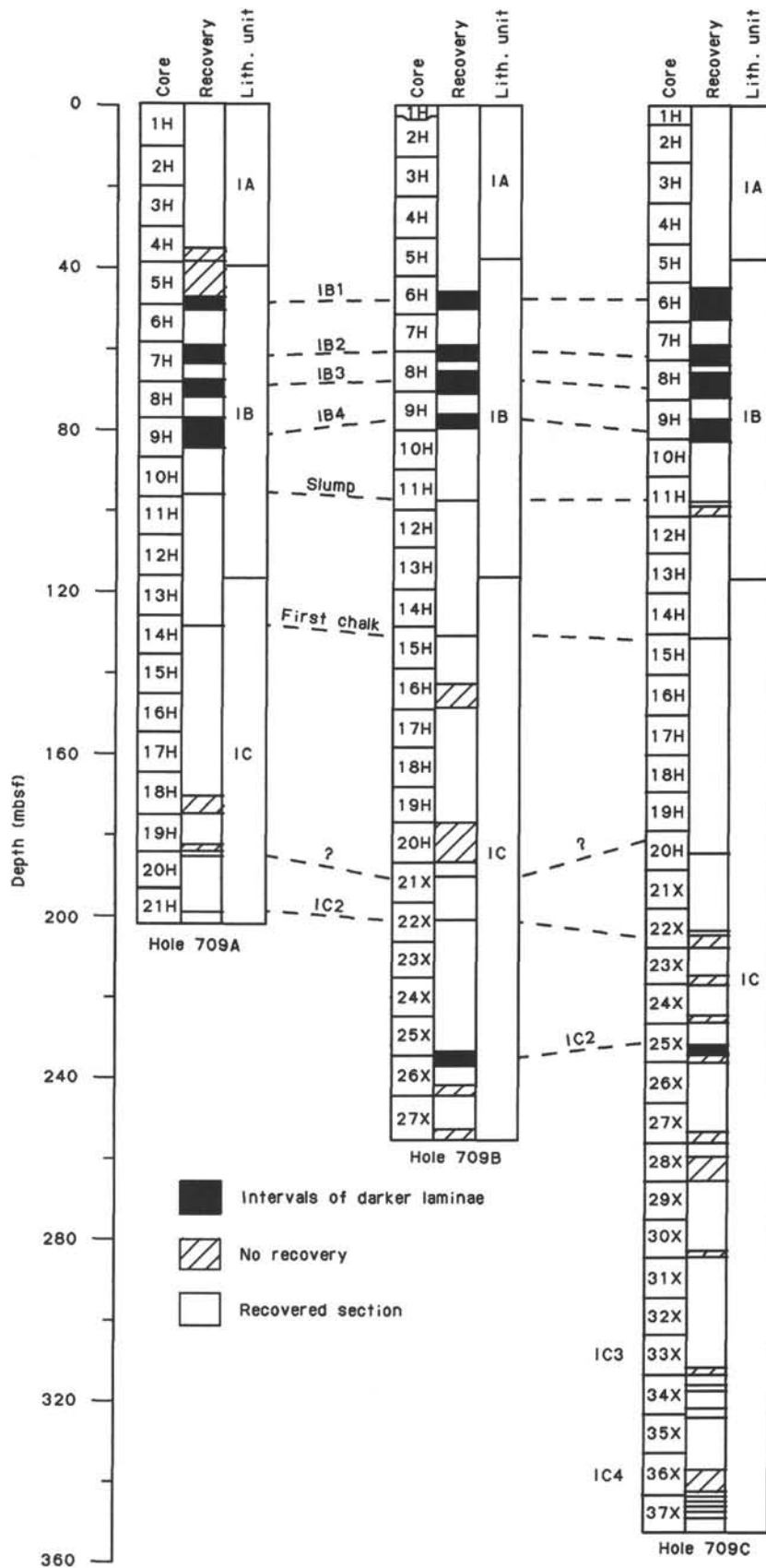


Figure 5. Summary of the stratigraphic distribution of subunits in Holes 709A, 709B, and 709C showing interhole correlations using identified lithostratigraphic markers. See Table 2 for identifications of marked horizons.

Table 2. Summary of the distribution of intervals of abundant greenish gray laminae and volcanic-ash layers in Holes 709A, 709B, and 709C.

	Depth (mbsf)		
	Hole 709A	Hole 709B	Hole 709C
Intervals of concentrated greenish gray laminae:			
IB1	48.7–51.7 (18)	46.9–51.4 (17)	45.8–53.3 (15)
IB2	59.8–64.3 (7)	59.5–63.2 (9)	59.9–64.4 (5)
IB3	68.0–72.5 (9)	66.2–70.7 (15)	66.6–72.6 (9)
IB4	77.6–85.1 (14)	77.3–80.3 (11)	77.7–82.2 (13)
Volcanic-ash layers:			
Subunit IB (in above intervals)			
IB1	a. 50.91 b. 52.04	a. 50.55	
IB2	a. 61.75 *a. 73.65	a. 62.72	a. 60.98
IB4	a. 81.44	a. 85.40	a. 83.60
Subunit IC			
IC1	a. 186.58 b. 187.62 c. 199.20	a. 192.50	a. 185.68
IC2		c. 202.10 a. 235.50? b. 236.06 c. 237.41 d. 237.68	c. 205.63 ? 234.86 ? 235.00
IC3			a. 318.26? b. 318.54? c. 323.74? d. 326.40
IC4			a. 343.92 b. 344.64 c. 344.85 d. 348.73 e. 349.33

Note: Numbers in parentheses indicate the number of greenish gray laminae which occur in each of the identified intervals. Sub-bottom depths for volcanic-ash layers are given for the levels of their bases. Question marks after ash depths indicate tentatively identified altered ashes. Question marks preceding ash depths (in place of lowercase letters) indicate that ashes could not be unambiguously correlated with ashes in other holes.

*Ash layer not within identified intervals of abundant greenish gray laminae.

Subunit IC: Section 115-709A-13H-1, 95 cm, through Core 115-709A-21H (117.20–203.10 mbsf), Section 115-709B-13H-5, 90 cm, through Core 115-709B-27X (116.80–254.80 mbsf), and Section 115-709C-13H-5, 10 cm, through Core 115-709C-37X (117.90–353.70 mbsf); Age: middle Miocene through middle Eocene.

The transition to Subunit IC is marked by a change in color from light gray and greenish gray to white and very pale brown hues (10YR 8/1, 8/2), suggesting a transition back toward more oxidizing conditions in the sediment. Subunit IC is composed predominantly of nannofossil ooze and chalk alternating with clay-bearing nannofossil ooze and chalk. Irregularly spaced chalk nodules first appear in the upper part of Subunit IC (Fig. 5) and increase in abundance with depth.

Regularly spaced chalk biscuits within ooze (drilling paste?) are common in cores split with a band saw as opposed to those cut with piano wire. No noticeable difference was observed in the appearance of the chalk nodules and layers occurring in APC vs. XCB cores, which suggests that alternating oozes and chinks are real diagenetic features and are not produced by rotary drilling (see "Physical Properties" section, this chapter).

The carbonate content in Subunit IC averages around 90% (analyses from Cores 115-709A-14H to -21H and Cores 115-709C-21X to -37X). Average carbonate content for individual cores varies from a low of 81.2% carbonate (Core 115-709C-37X) to a high of 93.7% (Core 115-709C-26X), with the highest

carbonate content occurring between Cores 115-709C-20H and -29X (of course, higher-frequency fluctuations are superimposed upon these general trends). Clay-bearing oozes and chinks are more common in the upper and lower portions of Subunit IC.

Siliceous biogenic components occur in only minor to trace amounts throughout Subunit IC, except in the very lowest intervals (Cores 115-709C-35X and -37X), where a slight increase is observed. Calcspheres occur in minor and trace amounts in Cores 115-709C-30X to -35X.

A number of fresh to altered volcanic-ash layers occur in Subunit IC and appear to be concentrated within four intervals (Fig. 5 and Table 2). The two shallowest ash layers are found in all three holes and seem to bracket the Miocene/Oligocene boundary (Fig. 5). These ash layers are fairly fresh, particularly in Holes 709A and 709B. The topmost ash layers in these two holes occur as distinct horizontal layers in Cores 115-709A-20H and 115-709C-20H. The topmost ash in Hole 709B (Core 115-709B-21X) appears as a distinct, dipping, slightly contorted layer; this core was drilled using the XCB.

Volcanic-ash layers occur further downcore in Sections 115-709B-26X-1 and 115-709B-26X-2 (a total of four, one very altered) and in Section 115-709C-25X-5 (a total of two, both distinct and relatively unaltered). Ashes are observed in two additional intervals in Hole 709C: in Sections 115-709C-34X-4, 115-709C-34X-6, and 115-709C-35X-2 (a total of four), and in Sections 115-709C-37X-1 and 115-709C-37X-4 (a total of four, possibly five). The ash layers in Core 115-709C-37X appear to be altered; the alteration minerals, however, have only been tentatively identified.

Visual core descriptions revealed no evidence of natural disturbance (i.e., slumping, turbidites, or reworking in Subunit IC). However, biostratigraphic evidence suggests an interval of disturbed sediment between Sections 115-709C-15H-3 and 115-709C-18H-4 (see "Biostratigraphy" section, this chapter).

A number of lithostratigraphic markers have been identified at Site 709, most of which have been discussed above. These horizons can be used for physical correlation between Holes 709A, 709B, and 709C, as shown in Figure 5.

BIOSTRATIGRAPHY

Introduction

The three holes drilled at Site 709 in water depths of 3038.2 m penetrated a 354-m-thick sedimentary sequence of calcareous ooze which is continuous from the Pleistocene to middle Eocene, with a condensed section in the middle Miocene. The calcareous plankton show evidence of displaced sediments in the lower middle Miocene, probably reflecting deposition of cryptoturbidites.

Calcareous nannofossils are abundant throughout the entire sequence, with a generally good to moderately good level of preservation. Significant nannofossil dissolution is observed in the condensed upper middle Miocene sequence. Planktonic foraminifers are abundant throughout the entire sequence. Their preservation is good in the Pleistocene, gradually degrading downward through the Pliocene, becoming poor in the Miocene, and improving in the Paleogene.

Benthic foraminifer abundance varies. They are generally common in Pleistocene to middle Miocene sediments, with significant increases in numbers in the upper Miocene and upper middle Miocene where calcareous fossils are dissolved and are generally rare from the lower Miocene downward. Their preservation is generally good throughout the entire sequence except in the middle Eocene, in which preservation is only fair.

Radiolarians are common in the Pleistocene to upper Miocene sequence and in the Paleogene, but they are absent in lower and middle Miocene sediments. Their preservation is good to

moderately good in the Neogene, generally poor in the Oligocene, and good to moderate in the Eocene.

Diatoms are fairly well preserved and abundant in the Pleistocene and are generally rare and poorly preserved in the Pliocene through the upper upper Miocene interval. Below that level, sediments are barren of diatoms except for a few fragments in the lower Oligocene and in the Eocene.

A biostratigraphic summary for Site 709 is presented in Figure 6.

Calcareous Nannofossils

Pleistocene to middle Eocene nannofossils were recovered from the three holes drilled at Site 709. Fossil preservation is generally good to moderate throughout the sequence. Pliocene-Pleistocene fossils are well preserved, but overgrown discoasters are commonly found in the lower cores. In the middle to lower Miocene sequences, recrystallization is moderate but discoasters are overgrown beyond species recognition. As at Site 708, significant dissolution was observed in the middle Miocene sequence.

Although the three holes drilled at Site 709 penetrated to different depths, a complete Neogene sequence was recovered from all holes. Samples from all core catchers and from most of the core sections were examined from the three holes. In this report we will summarize the nannofossil biostratigraphy for Hole 709C.

Pleistocene

We can place the first occurrence (FO) of *Emiliania huxleyi* (base of Zone CN15) between Samples 115-709C-1H-2, 82–83 cm, and 115-709C-1H-2, 102–103 cm. The last occurrence (LO) of *Pseudoemiliania lacunosa* (0.46 Ma) was placed between Samples 115-709C-1H-4, 82–83 cm, and 115-709C-1H-4, 102–103 cm.

The top of the small *Gephyrocapsa* Zone of Gartner (1977; 0.90 Ma) was identified between Samples 115-709C-2H-3, 42–43 cm, and 115-709C-2H-3, 82–83 cm. The LOs of *Helicosphaera sellii* (1.37 Ma) and *Calcidiscus macintyreii* (1.45 Ma) were recognized in Samples 115-709C-2H-6, 62–63 cm, and 115-709C-2H-6, 82–83 cm, respectively. Sample 115-709C-3H-1, 62–63 cm, yielded a few specimens of *Gephyrocapsa oceanica*, but the underlying Sample 115-709C-3H-1, 82–83 cm, did not contain *G. oceanica*. The base of Subzone CN14a (1.6 Ma) was placed, therefore, at the center of Core 115-709C-3H.

Pliocene

The LO of *Discoaster brouweri* (top of Zone CN12) occurs in Sample 115-709C-3H-2, 102 cm. The LOs of the subzonal marker discoasters for Zone CN12 were recognized within Cores 115-709C-3H and -4H. The LO of *Discoaster pentaradiatus*, for example, occurs within the lower part of Core 115-709C-3H, and the LO of *Discoaster tamalis* occurs either in Sample 115-709C-4H-3, 60 cm, or in Sample 115-709C-4H-4, 150 cm.

The LO of *Reticulofenestra pseudoumbilica* (top of CN11), which coincides approximately with the lower/upper Pliocene boundary, was placed in the interval between Samples 115-709C-5H-2, 60 cm, and 115-709C-5H-2, 60 cm. In Hole 709B, this event was placed between Samples 115-709B-5H-2, 60 cm, and 115-709B-5H-2, 100 cm.

Slightly overgrown *Ceratolithus acutus* were observed in Samples 115-709C-6H-6, 60 cm, and 115-709C-7H-3, 60 cm; this interval was assigned to the lower Pliocene Subzone CN10b. The assemblage observed in Sample 115-709C-7H-4, 60 cm, is assignable to Subzone CN10a. The LO of *Discoaster quinqueramus* (top of Zone CN9) was observed in Sample 115-709C-7H-6, 60 cm (64.7 mbsf). Because the Pliocene/Miocene boundary is correlated to the middle of Subzone CN10a, it can be placed within Section 115-709C-7H-5 (at about 61 mbsf). The Pliocene sequence is estimated to be about 43 m thick at Site 709.

Miocene

The FO of *Amaurolithus primus* (base of Zone CN9b) and the FO of *Discoaster quinqueramus* (base of Zone CN9a) were observed in Samples 115-709C-10H-5, 90 cm, and 115-709C-12-3, 60 cm, respectively.

We placed the LO of *Discoaster hamatus* (top of Zone CN7) in Sample 115-709C-13H-2, 30 cm. *Catinaster calyculus* and *Discoaster hamatus* occur together in Sample 115-709C-13H-2, 30 cm; this assemblage is assignable to the lower upper Miocene Subzone CN7b. The assemblage containing abundant *Catinaster coalitus* and rare *D. hamatus* in Sample 115-709C-13H-2, 90 cm, can be assigned to Subzone CN7a. The sequence assignable to Zone CN7 is represented by only about 1.5 m of sediment. As was observed at Site 708, nannofossils in the Zone CN7 assemblage show signs of advanced dissolution.

In Section 115-709C-13H-4, assigned to Zone CN5b, the grey color of the upper sediment gradually changes to brownish, and the degree of dissolution significantly increases in the upper three sections of Core 115-709C-14H (assignable to the middle Miocene Subzones CN5b and CN5a).

The interval between Samples 115-709C-14H-5, 30–31 cm, and 115-709C-15H-2, 30–31 cm, can be assigned to the lower middle Miocene Zone CN4. The sequence of assemblage changes observed above the latter sample is normal. The interval between Sections 115-709C-15H-4 and 115-709C-18H-3, however, yields various Miocene assemblages corresponding to Zones CN1–CN4 in random order. The individual assemblages found in this interval are relatively coherent and contain little reworked material, although the series of assemblages is stratigraphically disordered.

Reworking in this interval must have occurred repeatedly in the form of discrete slump units. The redeposited sequences were formed during the early middle Miocene to late early Miocene. The lowest occurrence of the slumped sequence was observed in Core 115-709C-18H; the three samples taken from the 30–31-cm interval of the upper three sections each contain assemblages belonging to Zone CN2, whereas two samples collected from the equivalent sample interval in the underlying two sections yielded a Zone CN3 assemblage. We therefore assume that sedimentation (reworking) started during late early Miocene times. The resedimented sequence is estimated to be at least 28 m thick.

Sections 115-709C-18H-6 and 115-709C-19H-1 are assigned to Zone CN2 with well-preserved *Sphenolithus belemnus* abundant in the assemblage. Assemblages assignable to Zone CN1 were observed between Sections 115-709C-19H-2 and 115-709C-21X, CC (~199 mbsf). The Miocene sequence is represented by 136 m of sediment.

Oligocene

Oligocene assemblages were observed in the interval between Sections 115-709C-22X-2 and 115-709C-30X-5. These Oligocene assemblages are similar to those observed at Sites 707 and 708. Nannofossils are moderately well preserved with slight to moderate overgrowths.

Sphenolithus ciperoensis occurs between Sections 115-709C-22X-2 and 115-709C-25X, CC, indicating upper Oligocene Zone CP19. Because of the tropical nature of the assemblage, *S. ciperoensis* is common, especially in the upper portion of this sequence. The LO of *Sphenolithus distentus* was identified in Section 115-709C-23X, CC, and the base of Subzone CP19b can be placed in between Sections 115-709C-23X-3 and 115-709C-23X, CC.

Sphenolithus distentus occurs continuously above Section 115-709C-26X, CC, and is absent in all sections of Core 115-709C-27X. Since the FO of *S. distentus* is the marker event for the base of Zone CP18, Cores 115-709C-25X and -26X seem

referable to the upper Oligocene Zone CP18, although sphenoliths (*S. distentus*) occur consistently but in very reduced numbers in the deeper Cores 115-709C-28X and -29X. On the other hand, *Reticulofenestra umbilica* occurs continuously below Section 115-709C-29X-2.

According to the biostratigraphic scheme we are using, the ranges of *S. distentus* and *R. umbilica* do not overlap (see Table 3 in "Explanatory Notes" chapter, this volume). They actually do co-occur in the lower portion of Core 115-709C-29X. This seemingly contradictory coexistence can be explained either by misidentification of *S. distentus* or diachroneity of the FO of *S. distentus*, which has an earlier appearance in this region compared with other world regions. If the former is true, two explanations are likely: (1) either overgrown *Sphenolithus predistentus* was recognized as *S. distentus*, or (2) a new species which has hitherto not been described occurs here. A "too early" appearance of *S. distentus* was also observed in Site 707. In any case, this matter needs further investigation.

We tentatively assigned the interval between Sections 115-709C-27X-1 and 115-709C-29X-2 to Zones CP18-CP17, and placed the interval between Sections 115-709C-29X-3 and 115-709C-30X-5 in Zone CP16. The LO of *Ericsonia formosa* (base of Subzone CP16c) and the end of the acme of *Ericsonia subdisticha* (base of Subzone CP16b) were detected in Sections 115-709C-29X, CC, and 115-709C-30X-2, respectively. *Hayella situiformis* is absent in the CP16b assemblage, but it is a common member of the CP16a flora.

Eocene

The LO of *Discoaster saipanensis* was recognized in Sample 115-709C-30X-6, 43-44 cm, and the LO of *Discoaster barbadiensis* was observed in the underlying Sample 115-709C-30X-7, 43-44 cm. Since these events are 0.5 m.y. older than the Eocene/Oligocene boundary, this boundary is assumed to be located within the upper part of Core 115-709C-30X or in the lower part of Core 115-709C-29X.

The interval between Sections 115-709C-30X-6 and 115-709C-33X-3 is assigned to the upper Eocene Zone CP15. Since *Isthmolithus recurvus* was not observed at this site, a subdivision of Zone CP15 was impossible. *Coccolithus pelagicus*, *Cyclicargolithus floridanus*, and *Dictyococcites bisectus* are abundant members of the CP15 flora. *Criboecentrum reticulatum* was rare in Section 115-709C-30X, CC, but was abundant throughout Core 115-709C-31X as well as in the upper sections of Core 115-709C-32X.

We observed the LO of *Chiasmolithus solitus* (base of Subzone CP14b) in Sample 115-709C-35X-3, 43-44 cm. The FO of *Reticulofenestra umbilica* (base of Zone CP14) also occurs in this same sample, which seemingly implies a short hiatus. However, the relationship between datums for these two taxa in the tropical Indian Ocean is considered far from clear.

The interval between Sections 115-709C-35X-4 and 115-709C-37X-4 are assigned to Subzone CP13c. *Coccolithus pelagicus*, *Cyclicargolithus floridanus*, and *Ericsonia formosa* are abundant in this interval, while *Discoaster barbadiensis*, *D. saipanensis*, *Pseudotriquetrorhabdulus inversus*, *Sphenolithus furcatorolithoides*, *S. moriformis*, *S. spiniger*, and *Zygrhablithus bijugatus* are common. Severely overgrown *Nannotetrina* spp. occur in low abundance.

The LO of *Chiasmolithus gigas* was recognized in Sample 115-709C-37X-5, 43-44 cm. This species also occurs in Section 115-709C-37X, CC. Thus, the lower two sections of Core 115-709C-37X were assigned to the middle Eocene Subzone CP13b. The Eocene sequence drilled at Hole 709C is about 72 m thick.

Planktonic Foraminifers

Neogene

The Neogene planktonic biostratigraphy of Hole 709A was established from core catchers for the upper 11 cores and from core catchers and additional samples between Cores 115-709A-12H and -21H. Planktonic foraminifers are abundant throughout the Neogene sequence. They are well preserved in the Pleistocene, moderately well to poorly preserved in the Pliocene, and poorly preserved in the Miocene. Intervals with better preservation and intervals with increased dissolution alternate throughout the Pliocene-Miocene, probably reflecting dissolution cycles.

Sections 115-709A-1H, CC, and 115-709A-2H, CC, are assigned to Pleistocene Zone N22 based on the rare occurrence of *Globorotalia truncatulinoides*. Assemblages are dominated by *Globorotalia tumida*, *G. menardii*, *Globigerinoides sacculifer*, *G. ruber*, and *Neogloboquadrina dutertrei*.

We assigned Section 115-709A-3H, CC, which contains common *Globorotalia limbata* and *Globigerinoides fistulosus*, to the upper Pliocene Zone N21. The presence of the latter species indicates an age younger than 2.9 Ma. The assemblage is dominated by *G. menardii* (whole specimens and abundant fragments). Sections 115-709A-4H, CC, through 115-709A-6H, CC, whose assemblages are dominated by *G. tumida* (including flexuous forms), are assigned to the lower Pliocene zonal interval N19-N18. The LOs of *Dentoglobigerina altispira* and *Sphaeroidinellopsis* spp. in Section 115-709A-4H, CC, date this sample at approximately 3.0 Ma.

Sections 115-709A-7H, CC, through 115-709A-11H, CC, are assigned to the upper Miocene Zone N17. The fauna is dominated by *Globorotalia limbata*, *G. plesiotumida*, *Dentoglobigerina altispira*, *Sphaeroidinellopsis* spp., and *Globoquadrina venezuelana*. The FO of *Pulleniatina primalis* occurs in Section 115-709A-7H, CC, marking the subzonal boundary N17b/N17a. The rarity of this species here, however, probably as a result of dissolution, does not make it a reliable marker.

Samples in Core 115-709A-12H are poorly preserved with abundant foraminifer fragments and common radiolarians and sponge spicules. The fauna is composed mainly of the two resistant species, *Sphaeroidinellopsis* and *G. venezuelana*. Rare *Neogloboquadrina acostaensis* (whose FO defines the base of Zone N16) and *Globorotalia siakensis* (whose LO defines the base of Zone N15) co-occur in these samples, which are therefore assigned to zonal interval N15-N16.

In the interval between Cores 115-709A-13H and 115-709A-17H, the lower to middle Miocene fauna are dominated by *G. venezuelana*, *D. altispira*, and *Globorotalia mayeri*. The base of Zone N13 is placed in Section 115-709A-13H-2 at the FO of *Sphaeroidinellopsis subdehiscens*, the base of N9 in Section 115-709A-15H-4 at the FO of *Orbulina*, and the base of N7 in Section 115-709A-17H, CC, at the LO of *Catapsydrax dissimilis*.

Samples in Core 115-709A-14H appear to be derived from older sediments. They contain a fauna similar to that of Cores 115-709A-17H through -20H, which is composed mainly of a dwarfed fauna. This interval is assigned to the lower Miocene zonal interval N4-N6, based on the presence of *Globoquadrina binaiensis* and *G. praedeheiscens*. Rare forms referable to *Globorotalia kugleri* were found in Section 115-709A-20X, CC.

Paleogene

Paleogene planktonic foraminifers in Hole 709C are only fairly well preserved throughout the late Oligocene to middle

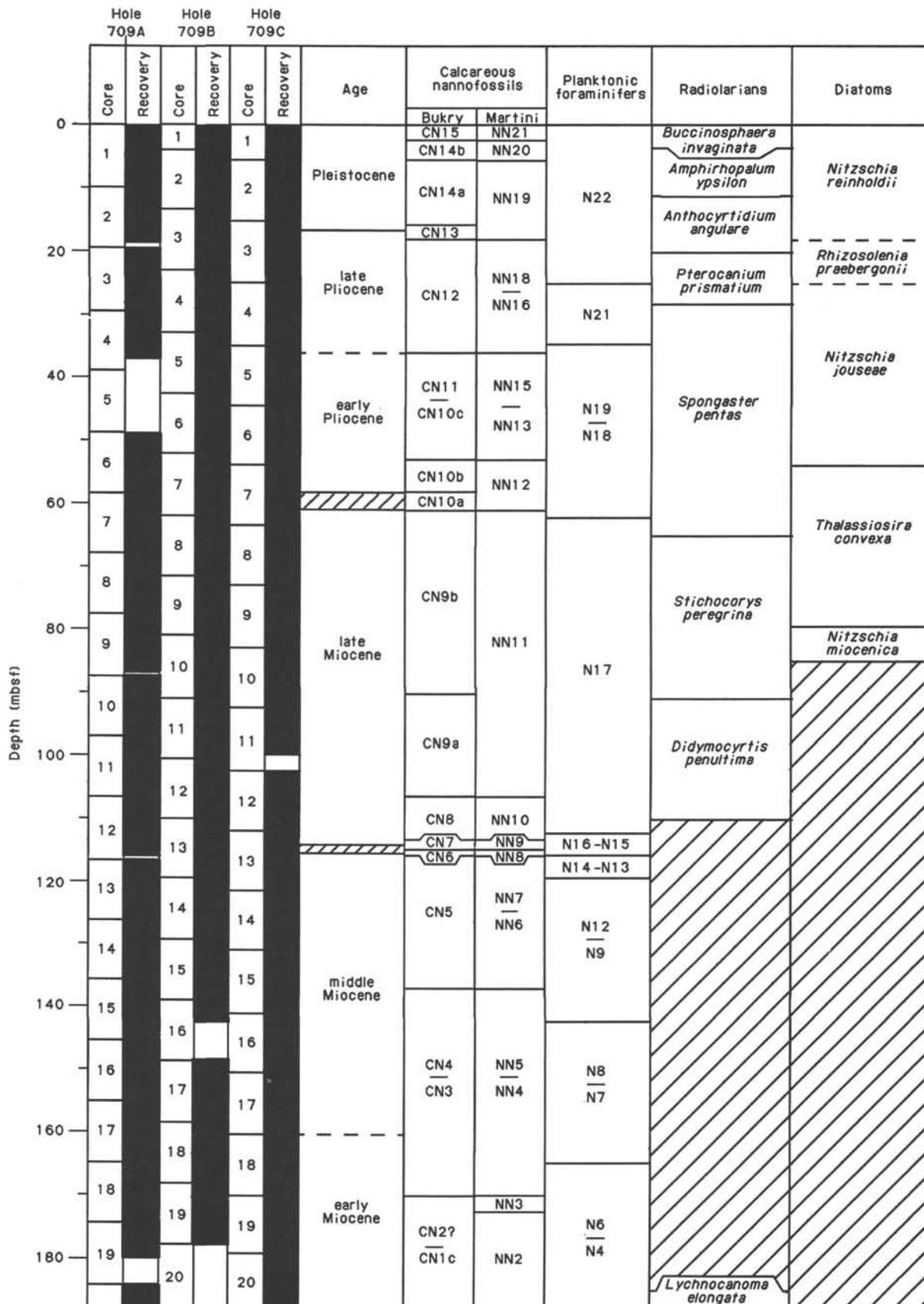


Figure 6. Biostratigraphic summary of Holes 709A, 709B, and 709C. Radiolarian zonal assignments are based on studies of Holes 709A, 709B, and 709C. Neogene planktonic foraminiferal zonal assignments are based on samples from Hole 709A. Zonal assignments from nannofossils, diatoms, and Paleogene planktonic foraminifers are based on studies of Hole 709C. Recovery in each hole is indicated by black bars.

Depth (mbsf)	Hole 709A		Hole 709B		Hole 709C		Age	Calcareous nannofossils		Planktonic foraminifers	Radiolarians	Diatoms
	Core	Recovery	Core	Recovery	Core	Recovery		Bukry	Martini			
	190	20X		21		21			early Miocene			
	21X		22		22							
210			23		23		late Oligocene	CP19b	NP25	P22	<i>Dorcadospyris atuechus</i>	
			24		24					P21b		
230			25		25			CP19a	NP24			
			26		26					P20		
250			27		27		early Oligocene	CP18	NP23		<i>Theocyrtis tuberosa</i>	
			28		28					P18-P19		early Oligocene
270			29		29			CP16c	NP22	P18		
			30		30			CP16b CP16a	NP21	P17		
290			31		31		late Eocene	CP15	NP20	P16	<i>Thyrsocyrtis bromia</i>	
			32		32				NP18			
310			33		33				NP17	P14	<i>Podocyrtis goetheana</i>	
			34		34			CP14	NP16		<i>Podocyrtis chalara</i>	
330			35		35		middle Eocene			P11	<i>Podocyrtis mitra</i>	
			36		36			CP13c	NP15		<i>Podocyrtis ampla</i>	Eocene
350			37		37			CP13b			<i>Thyrsocyrtis triacantha</i>	

Figure 6 (continued).

Eocene sequence. In the late Oligocene, diagenetic alteration of carbonate to chalk has dissolved many of the planktonic adults. Preservation improves slightly in middle Eocene Zone P11 (Section 115-709C-35X, CC), but it is poor in Cores 115-709C-36X and -37X. Because of this poor preservation, the tropical character of numerous faunas is distorted since only solution-resistant species remain.

The Oligocene sequence (Section 115-709C-22X, CC, through 115-709C-29X-7, 19 cm) can be subdivided as follows:

1. Zone P22 (Sample 115-709C-22X-4, 38 cm, and Section 115-709C-23X, CC), based on the presence of *Catapsydrax dissimilis* and one juvenile specimen of the nominate taxon, *Globigerina ciperoensis*.

2. Zone P21b (Section 115-709C-24X, CC), identified by the presence of *Globorotalia opima* and the absence of *Streptochilus*.

3. Zone P20 (Section 115-709C-26X, CC, through Sample 115-709C-27X-6, 4 cm), identified by the overlap of *Turborotalia pseudoampliapertura* and *P. opima* which occurs in the upper portion of Zone P20.

4. Zone P18 (Samples 115-709C-29X-6, 120 cm, to 115-709C-29X-7, 19 cm), determined by the presence of *Turborotalia centralis*, *Subbotina gortanii*, and *Globigerina tapuriensis*, but the absence of Eocene forms or the index species for the overlying zone, *Globoquadrina sellii*.

The Eocene/Oligocene boundary is located approximately at Sample 115-709C-29X-7, 19 cm, on the basis of the loss of hantkeninid spines and all *Globigerinatheka*, but the dominance of the fine fraction by *Streptochilus* and *Pseudohastigerina*. The uppermost Eocene is present in Section 115-709C-29X, CC, as indicated by the presence of very rare *Globigerinatheka* and the fine fraction dominance of streptochilids and pseudohastigerinids.

Eocene zones were identified as follows:

1. Zone P17 (Section 115-709C-29X, CC), indicated by the proliferation of streptochilids and pseudohastigerinids, despite extensive dissolution and the lack of other markers.

2. Zone P16 (Sections 115-709C-30X, CC, to 115-709C-31X, CC, and possibly Section 115-709C-32X, CC), located by the presence of turborotaliids, especially *Turborotalia cunialensis* in Section 115-709C-30X, CC, and the lack of *Globigerinatheka semiinvoluta*. The assignment of Section 115-709C-30X, CC, to the upper part of Zone P16 is indicated by the rare occurrence of the globigerinathekids and by the presence of *T. cunialensis*. Section 115-709C-32X, CC, is poorly preserved and lacks most diagnostic species. However, the presence of large-sized *Pseudohastigerina micra* suggests placement in Zone P16.

3. Zone P14 (Section 115-709C-33X, CC), determined by an abundance of the nominate taxon, *Acarinina rohri*, and the absence of *Orbulinoides beckmanni*. This is a tentative assignment because of the poor preservation.

4. Zone P11 (Sections 115-709C-34X, CC, to 115-709C-37X, CC), based on the overlap of *Morozovella aragonensis* with *Acarinina pentacamerata*, *Globigerinatheka mexicana*, *Turborotalia possagnoensis*, and *T. possagnoensis* trans. *pomeroli*.

Benthic Foraminifers

We recovered benthic foraminifers from all cores in Hole 709A and in Core 115-709C-22X and deeper cores in Hole 709C. Benthic foraminifers are moderately well preserved throughout the Neogene and Paleogene, except in the middle Eocene (Cores 115-709C-34X to -37X) where their preservation is only fair. They are common in most samples below the Pleistocene, and abundant in both the dissolved late Miocene interval (Core 115-709A-9H) and the late middle Miocene (Core 115-709A-12H). Benthic foraminifers are very rare and small in size in most of the early Miocene (Cores 115-709A-13H to -20H) and are rare throughout the middle Eocene (Cores 115-709C-34X to -37X).

Neogene

Two distinctive Pleistocene associations were present. The first, a gyroidinid-miliolid association, also contained moderate numbers of pullenids and *Uvigerina auberiana*. There are numerous individuals of few species, including *Triloculina lucernula*, *Epistominella exigua*, *Pyrgo murrhina*, *Gyroidinoides nitidus*, and *Pullenia quinqueloba*. The uvigerinids are hispid and elongate, a feature typical of subantarctic forms and in many species that live beneath upwellings. Most of the species in this fauna are cosmopolitan, occur in deep water, and predominate in as-

semblages found in corrosive environments. The presence of hispid uvigerinids suggests moderately oxygenated bottom conditions.

The second Pleistocene fauna, a *Uvigerina hispidocostata*-*Globocassidulina subglobosa* association, lacks the gyroidinids and pullenids typical above. An increase in uvigerinid abundance signals increased sediment accumulation or organic carbon content in the bottom environment.

Late Pliocene to late Miocene assemblages contain typical deep-water forms as well as species first named from Car Nicobar (Schwager, 1866). Usually an intermediate-depth fauna, the Car Nicobar element at Site 709 includes *Nodosaria skobrina*, *N. crassitesta*, *Osangularia bengalensis*, *Orthomorphina koina*, *Orthomorphina setosa*, *Martinottiella variabilis*, and *Cibicidoides cicatricosus*. In the Pliocene (Cores 115-709A-3H to -6H), this fauna is diluted with equal proportions of cosmopolitan species typical of deep water, including *Favocassidulina favus*, *Gyroidinoides soldanii*, *Globocassidulina subglobosa*, and the melonids. Late Miocene faunas include the Car Nicobar element, numerous miliolids, and are intruded by bottom-water forms such as the thick morphotype of *Melonis pompilioides*, *Nuttalides umbonifera*, and *Pullenia quinqueloba*.

The Car Nicobar fauna is usually restricted to intermediate depths, especially forms such as *Cibicidoides cicatricosus* and *Triloculina lucernula*. The fauna appears to be in place at the deep-water Site 709, however, because (1) seismic profiles suggest that this site is not located in an area of active sediment erosion and deposition, (2) physical properties data suggest no sediment disturbance, and (3) sedimentologic studies indicate the presence of numerous layers that correlate among the three holes at Site 709, suggesting that the sequences are complete and undisturbed. The presence of this particular faunal element thus suggests anomalous deep-water conditions at Site 709 from the later Miocene into the late Pliocene.

Several events discernible in the benthic faunas can be correlated to the South Atlantic and the southwest Pacific where they have been linked with ecologic events at the closing of the Miocene. An influx of miliolids and an abundance peak in the spinose uvigerinids (Core 115-709A-9H), accompanied by deteriorating preservation, is a signal for the late Miocene carbon excursion documented in all oceans (Lutze, 1977; Vincent et al., 1980; Boersma, 1984). Following this event, the poorly preserved levels with miliolids, hispidocostate uvigerinids, and an influx of bottom-water benthic foraminifers (Core 115-709A-7H) may indicate the latest Miocene episode of glacial accumulation in polar regions (Elmstrom and Kennett, 1986). As at Site 707, these events occur slightly below the Miocene-Pliocene boundary at Site 709, between Cores 115-709A-6H and -7H. The timing of this latter event is also in accord with the bottom-water cooling at about 6 Ma recorded at Site 253 (Oberhänsli, 1986).

The late middle Miocene proliferation of benthic foraminifers identified at Site 707 can be found in Core 115-709A-12H. Not only do benthic foraminifers become abundant, they increase in size. The most common species, also very large in size, is *Globocassidulina subglobosa*. Typical, too, are the large planulinids such as *Planulina marialana* and *P. renzi*, and a large flat species resembling *Planulina mexicana*. The most diverse group in this fauna are the pleurostomellids, represented by, inter alia, *Pleurostomella alternans*, *P. dominicana*, *P. bierigi*, and *P. subcylindrica*.

Despite slumping and repeated sections in the early Miocene (Cores 115-709A-13H to -16H), the consistency of the benthic faunas indicates that the repeated levels must be derived from nearly equivalent paleodepths. These faunas are dominated by small-sized pullenids, elongated pleurostomellids, and osangularids. Gyroidinids are also frequent. The stilostomellid is *Stilo-*

stomella subspinosa, and the uvigerinid is *Uvigerina auberiana*, a form correlated with oxidizing conditions in the bottom environment (Boersma, 1984). The fact that a large number of these forms are dissolution resistant suggests that these small-sized faunas and individuals may be the result of corrosive conditions on the seafloor. These conditions have also removed many of the larger planktonic foraminifers.

Paleogene

Most Paleogene benthic faunas are dissolution residues, remaining after carbonate diagenesis. Such faunas contain large numbers of only a few species, primarily *Globocassidulina subglobosa*, *Oridorsalis umbonatus*, *Gyroidinoides girardana*, *Stilostomella nuttalli*, and *S. subspinosa*. Buliminids and uvigerinids are very rare; brizalinids, tracers for low-oxygen conditions at the bottom, are absent.

The Oligocene fauna, containing numerous species originally described from Barbados (Beckmann, 1953), first appears just below the Eocene-Oligocene boundary (Core 115-709C-29X) and continues upward through the top of the Oligocene section (Core 115-709C-22X). This *Stilostomella subspinosa*-*Globocassidulina subglobosa*-dominated association is characterized by a short-lived pulse of *Plectofrondicularia lirata* into the fauna near its base. This late Eocene pulse of *P. lirata* has been identified in several Atlantic deep- and bottom-water sites, such as at Site 522 in the Angola Basin and in a piston core from the southern Brazil Basin, where its presence has been attributed to erosion during a deep-circulation event just prior to the Eocene-Oligocene boundary (Boersma, 1986). The *P. lirata* pulse at Site 709 may also reflect intensified erosion in the Mascarene Basin just before the Eocene-Oligocene boundary.

The pulse of *P. lirata* and the inception of the so-called Barbados fauna co-occur in Section 115-709C-29X, CC, immediately above the disappearance level of *Nuttalides truempyi* (Section 115-709C-30X, CC) in the upper part of Zone P16. *Nuttalides truempyi* is currently considered an indicator of corrosive bottom waters, possibly indicating a sluggish circulation and older, corrosive deep-water masses (Tjalsma and Lohmann, 1983). The disappearance of *N. truempyi*, followed by the incursion of the Barbados fauna and the *P. lirata* episode, suggests the transition from a sluggish, corrosive bottom circulation to a more vigorous circulation just prior to the Eocene-Oligocene boundary at this site.

A *Nuttalides truempyi*-*Bulimina semicostata* association containing *Alabamina dissonata*, *Globocassidulina subglobosa*, *Bulimina consanguinea*, *Hanzawaia grimsdalei*, and *Stilostomella subspinosa* persists through the early late and middle Eocene (Cores 115-709C-30X to -37X). All of these species are typical of deep-water paleodepths through at least the later portion of middle Eocene Zone P11.

Radiolarians

Well-preserved radiolarians were recovered in each of the three holes drilled at Site 709. Because of the prospects of establishing a high-resolution, magnetobiostratigraphic reference section at this site, radiolarian samples were prepared at intervals of four samples per core, or at approximately 2.5 m between samples. The intervals which were closely sampled may be summarized as follows:

Hole no.	Core nos.	Depth (mbsf)	Age range
709A	1H-21H	0-203.1	Quaternary-late Oligocene
709B	4H-6H	23.1-52.0	middle Pliocene
709B	21X-27X	187-254.8	early Miocene-early Oligocene
709C	27X-37X	247-353.7	early Oligocene-middle Eocene

This composite stratigraphic section was recovered with >95% core recovery. Thus, we are confident of the continuity of the recovered material and of the reported sub-bottom depths of each sample. The presence of discrete ash layers at several horizons will allow for an even more precise correlation (5-cm intervals using magnetic susceptibility profiles) of stratigraphic levels between the three parallel holes.

Because of the overlapping nature of the three holes at Site 709, we have written this summary for each epoch of the Cenozoic and have combined results from the parallel holes where appropriate.

Quaternary

The Quaternary radiolarian assemblages are well preserved in Sample 115-709A-1H-2, 75 cm, through Section 115-709A-2H, CC, which contain the *Buccinosphaera invaginata*, *Amphirhopalum ypsilon*, and *Anthocyrtdium angulare* Zones. Diagnostic taxa include *Theocorythium trachelium*, *Lamprocyrtis nigrinae*, *Stylatractus universus*, *Anthocyrtdium ophirensae*, *A. euryclathrum*, and *Spongaster tetras*.

Pliocene

Late Pliocene radiolarian assemblages of the *Pterocanium prismatium* Zone are common and well preserved in Samples 115-709A-3H-2, 65 cm, through 115-709A-3H-6, 65 cm. Section 115-709A-3H, CC, through Sample 115-709A-7H-4, 65 cm, belong to the early Pliocene *Spongaster pentas* Zone (>2.5 Ma), based on the common occurrence of *Stichocorys peregrina*. Other diagnostic taxa of the *S. pentas* Zone, which are commonly represented, include *Pterocanium prismatium*, *Anthocyrtdium jenghisi*, *A. nosicae*, *A. michelinae*, *Lychnodyctium audax*, *Phormostichoartus fistula*, and *P. doliolum*.

Miocene

Radiolarians are common and well preserved in part of the upper Miocene interval (Samples 115-709A-7H-6, 65 cm, through 115-709A-12H-2, 65 cm). However, radiolarian abundance and preservation decreases abruptly below Sample 115-709A-12H-4, 65 cm, at 111.8 mbsf, near the upper/middle Miocene boundary. This transition occurs at a stratigraphic level which is identical with that identified in DSDP Site 237 and Site 707 on the Seychelles-Mascarene Ridge nearby.

Samples 115-709A-7H-6, 65 cm, through 115-709A-10H-2, 65 cm, belong to the *Stichocorys peregrina* Zone of late Miocene age. Diagnostic taxa include *Didymocyrtis penultima*, *Solenosphaera omnitubus*, *Stichocorys peregrina*, *Acrobotrys tribubus*, and *Siphostichartus corona*. The genus *Spongaster* is notably rare, and thus the members of this genus, which have been characteristically chosen as zonal boundary markers (*S. berminghami* and *S. pentas*), appear to be unsuitable as criteria for zonal age assignment in this particular geographic region.

Samples 115-709A-10H-4, 65 cm, through 115-709A-12H-2, 65 cm, have been assigned to the *Didymocyrtis penultima* Zone of late Miocene age, based on common and well-preserved specimens of *Stichocorys delmontensis*, *Didymocyrtis penultima*, *Dendrosphyris bursa*, and *Lychnodyctium audax*.

The middle and early Miocene is barren of radiolarians in all samples examined between Sample 115-709A-12H-4, 65 cm, and Section 115-709A-19H, CC (111.8-183.9 mbsf).

Oligocene

The Oligocene is represented in all three holes drilled at Site 709. Radiolarian assemblages, however, are generally poorly preserved throughout the Oligocene and allow only an approximate zonal age assignment. Sample preservation improves downward within the Oligocene and becomes good in the lowermost Oligocene and in the underlying Eocene material.

In this discussion we will make reference only to the Oligocene material recovered in Holes 709B and 709C, since these holes contain the longest and most consistently preserved sequence of Oligocene age sediments.

Samples 115-709B-21X-2, 65 cm, through 115-709B-22X-2, 65 cm, are tentatively placed in the *Lychnocanoma elongata* Zone, which spans the Oligocene/Miocene boundary. Radiolarians in these samples are few and moderately to poorly preserved. Diagnostic taxa include *Dorcadospyrus ateuchus*, *D. papilio*, *Calocyclus robusta*, and *Lychnocanoma elongata*.

We assigned Sample 115-709B-22X-4, 65 cm, through Section 115-709B-25X, CC, to the *Dorcadospyrus ateuchus* Zone of late Oligocene age. Diagnostic taxa in these samples, all of which are poorly preserved, include *Dorcadospyrus ateuchus*, *D. papilio*, *Cyclampterium pegetrum*, and *Didymocyrtis prismatica*.

Sample 115-709B-26X-2, 65 cm, through Section 115-709C-29X, CC (237.7–276.1 mbsf) may be assigned to the *Theocyrtis tuberosa* Zone of early Oligocene age. Samples are poorly preserved in the upper part of the zone and improve in preservation downward. Diagnostic taxa include *Lithocyclus angusta*, *L. crux*, *Cyclampterium pegetrum*, *Tristylospyrus tricerus*, *Theocyrtis tuberosa*, *Artophormis gracilis*, and *Didymocyrtis prismatica*.

Eocene

Samples 115-709C-30X-2, 70 cm, through 115-709C-33X-2, 70 cm, are placed in the *Thyrsoyrtis bromia* Zone of late Eocene age. Radiolarians are common and moderately to well preserved within this stratigraphic interval. Diagnostic taxa include *Dictyoprora mongolfieri*, *D. armadillo*, *Sethochytris babylonis*, *Lithocyclus aristotelis*, *Tristylospyrus tricerus*, *Carpocanistrum azyx*, *Calocyclus turris*, and *Thyrsoyrtis tetracantha*.

Sample 115-709C-33X-4, 70 cm, through Section 115-709C-33X, CC, are assigned to the *Podocyrtis goetheana* Zone of late Eocene age. Radiolarians are common and moderately preserved. Diagnostic taxa include *Calocyclus hispida*, *Thyrsoyrtis triacantha*, *T. rhizodon*, *T. robusta*, *Podocyrtis trachodes*, and *Eusyringium fistuligerum*.

Samples 115-709C-34X-2, 70 cm, through 115-709C-34X-4, 70 cm, are assigned to the *Podocyrtis chalara* Zone, based on the presence of *P. chalara*. Samples 115-709C-34X-6, 70 cm, through 115-709C-35X-6, 70 cm, are assigned to the *Podocyrtis mitra* Zone of middle Eocene age. Radiolarians are common and moderately to well preserved. Diagnostic taxa include *Calocyclus hispida*, *Thyrsoyrtis triacantha*, *T. rhizodon*, *Podocyrtis papalis*, *P. mitra*, *P. trachodes*, *Lithocyclus ocellus*, and *Theocotyle ficus*.

We placed Section 115-709C-35X, CC, through Sample 115-709C-37X-6, 70 cm, in the *Podocyrtis ampla* Zone of middle Eocene age. Radiolarians are common and moderately to well preserved. Diagnostic taxa include *Podocyrtis fasciolata*, *P. dorus*, *P. papalis*, *Calocyclus hispida*, *Thyrsoyrtis triacantha*, *Dictyoprora mongolfieri*, and *Lithocyclus ocellus*.

Section 115-709C-37X, CC, is tentatively assigned to the *Thyrsoyrtis triacantha* Zone of middle Eocene age. Radiolarians are common and moderately preserved. Diagnostic taxa include early forms of *Thyrsoyrtis triacantha*, as well as *Podocyrtis sinuosa*, *P. dorus*, *P. phyxis*, *P. papalis*, *P. trachodes*, *Dictyoprora mongolfieri*, and *Lithochytris vespertilio*.

Summary

Radiolarians are common and well to moderately preserved in two stratigraphic intervals at Site 709: (1) from the Recent through the upper Miocene and (2) from the lowermost Oligocene down to the middle Eocene. For each of these stratigraphic intervals, it is very likely that we will be able to establish precise calibrations between radiolarian events and the standard calcareous microfossil datum levels, and also perhaps with the magnetic polarity time scale.

Diatoms

All core-catcher samples from the three holes of site 709 have been processed. Diatoms are consistently present in the Pleistocene through the uppermost Miocene interval. They are rare and poorly preserved in all of the diatom-bearing samples, except for the Pleistocene where they are well preserved. A few diatoms are present in the lower Oligocene interval of Holes 709B and 709C. The general absence of diatoms in sequences of early late Miocene through late Oligocene and Eocene ages is consistent with observations made at Sites 707 and 708.

Neogene

Section 115-709B-1H, CC, is placed at the boundary between the *Pseudoenotia doliolus* and *Nitzschia reinholdii* Zones, based on a fairly well-preserved assemblage which includes *P. doliolus* and some rare fragments of *N. reinholdii*. The preservation of diatoms deteriorates rapidly downhole in all three holes. The assemblages of the late Pliocene–Pleistocene *N. reinholdii* Zone are poorly preserved and are affected by strong silica dissolution, but age-diagnostic species such as *P. doliolus*, *N. reinholdii*, and *Thalassiosira oestrupii* have been identified in Sections 115-709A-1H, CC, 115-709B-2H, CC, 115-709C-1H, CC, and 115-709C-2H, CC.

The poorly preserved assemblages of Sections 115-709B-3H, CC, and 115-709C-3H, CC, are tentatively referred to the *Rhizosolenia praebergonii* Zone based on the presence of *R. praebergonii* and *Thalassiosira convexa* var. *aspinosa*.

We identified the *Nitzschia jouseae* Zone in the following sections: 115-709A-3H, CC, 115-709B-5H, CC, and 115-709C-4H, CC, through 115-709C-6H, CC. The zonal assignment is based on very poorly preserved assemblages in which *N. jouseae* and *T. convexa* var. *aspinosa* have been identified.

Sections 115-709A-4H, CC, 115-709A-7H, CC, and 115-709B-4H, CC, are all barren of diatoms.

The late Miocene–late Pliocene *Thalassiosira convexa* Zone has been identified in core-catcher samples from all three holes of Site 709 (Sections 115-709A-6H, CC, 115-709A-8H, CC, 115-709B-6H, CC, through 115-709B-9H, CC, 115-709C-7H, CC, and 115-709C-8H, CC). The preservation and abundance of the diatoms is slightly better than in the younger *N. jouseae* Zone, with assemblages including such age-diagnostic species as *Thalassiosira convexa* var. *aspinosa*, *T. miocenica*, and *Nitzschia cylindrica*.

The late Miocene *Nitzschia miocenica* Zone has only been identified in Hole 709C (Section 115-709C-9H, CC) based on the presence of *Thalassiosira praeconvexa* and *Nitzschia miocenica*.

The remaining Neogene core-catcher samples of Holes 709A, 709B, and 709C are all barren of diatoms.

Paleogene

The Paleogene is barren of diatoms except for a few diatoms of early Oligocene age in Section 115-709B-27X, CC, and Sections 115-709C-27X, CC, through 115-709C-29X, CC. The poorly preserved assemblages include species of the genera *Cestodiscus* sp. and *Coscinodiscus* sp.

PALEOMAGNETICS

Introduction

Pass-through magnetometer measurements of the 21 APC cores from Hole 709A provided only erratic paleomagnetic data. We also took measurements on 9 cores from Hole 709B and 13 cores from Hole 709C, which yielded similar results. Thus, it is impossible to determine from shipboard measurements the reversal stratigraphy of the sedimentary column examined at this site. However, the results from Site 709 do highlight the source for what may be an inherent difficulty in obtaining reliable pa-

leomagnetic measurements from many such sediment cores. Below we discuss evidence which indicates that the cores at this site were remagnetized by the remanent field of the core barrels.

Results

Highly erratic paleomagnetic directions were measured with the pass-through magnetometer; thus, these data will not be discussed in any detail. Pass-through measurement of intensity, however, does appear to reflect the magnetic character of the sediment and will be discussed briefly here.

The average natural-remanent-magnetization (NRM) intensity seen in Hole 709A (Fig. 7) suggests that sediments recovered from 20 to 120 mbsf are very weakly magnetized. This was also observed in the cores from Holes 709B and 709C. (Measurements were suspended for many of these weakly magnetized cores.) In some cases the intensity pattern within a single core taken from within this weakly magnetized zone shows a decrease of over two orders of magnitude from the top of the core to the bottom (an example of this behavior is shown in Fig. 8).

Discussion

The variation in NRM intensity is consistent among all three holes and also parallels the variation seen in the susceptibility measurements as discussed below. It seems, therefore, that the prospects for obtaining a reliable magnetic stratigraphy in the weakly magnetized zone (20–120 mbsf) is poor. The sharp decrease in intensity from the top of a core downward that we observed suggests that some rust contamination may have occurred. This problem appears to be much less consistent than was the case at Site 707; however, several such intensity profiles

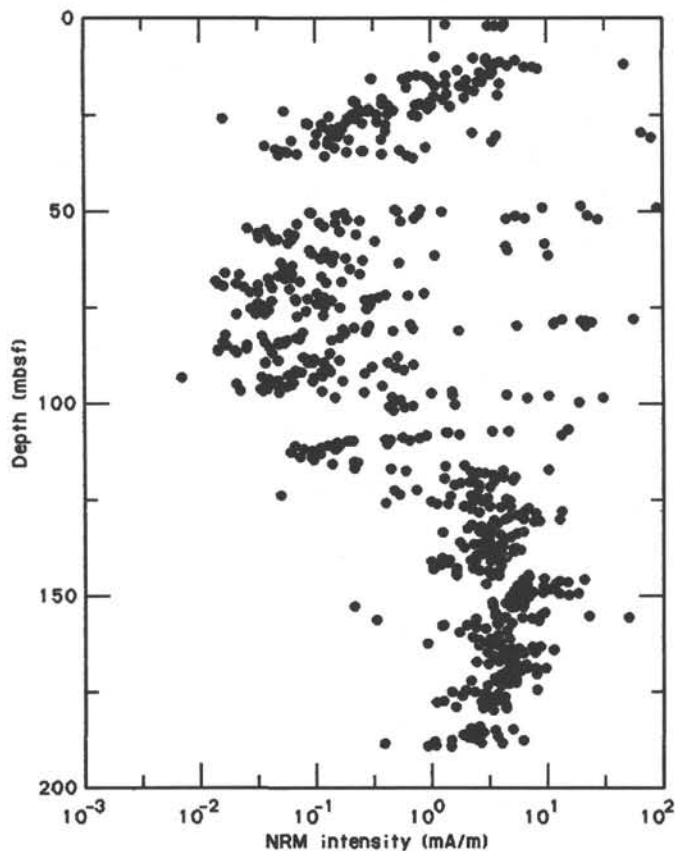


Figure 7. Natural-remanent-magnetization (NRM) intensity vs. sub-bottom depth in cores from Hole 709A showing a weakly magnetized zone between 20 and 120 mbsf.

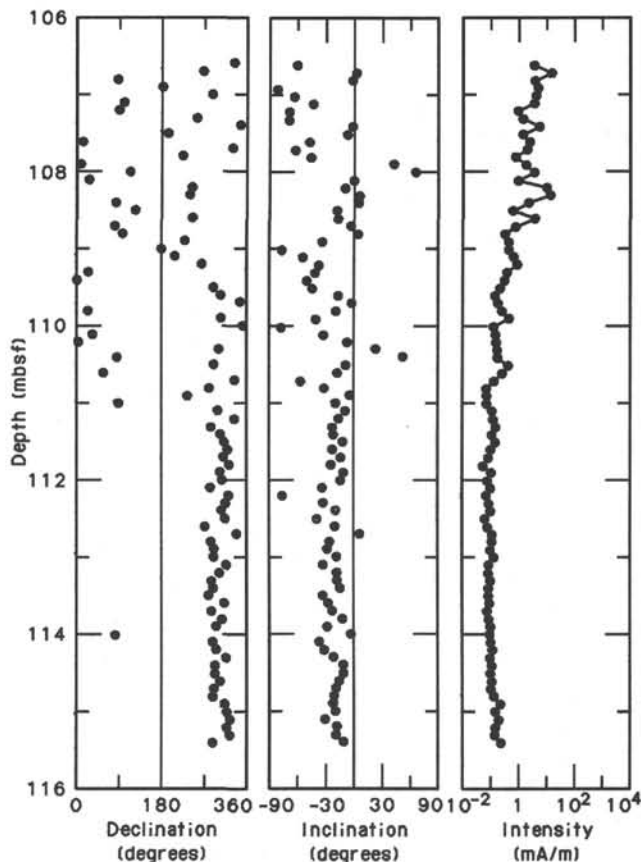


Figure 8. Results of pass-through magnetometer measurement of Core 115-709A-12H showing intensity decreasing from the top of the core downward, which suggests the presence of rust contamination.

were measured and some rust contamination of these cores may be suspected. A small amount of rust may explain some of the erratic background fluctuation in susceptibility measured at this site.

The Core Barrel Remagnetization Effect

The purpose of this discussion is to describe a remagnetization effect observed in many of the sediments recovered on Leg 115. Anomalous steep paleomagnetic inclinations in sediments obtained from ocean drilling have been previously noted. Several sources for these spurious magnetizations have been suggested, including exposure to large magnetic fields on the rig floor (Keating, 1984) or perhaps in the laboratory (Sager and Hutton, 1986). The discussion below presents observations which demonstrate that at least one type of remagnetization is caused by the remanent field of the steel core barrels used to take these cores.

Observations of Remagnetization

Any remagnetization effect is likely to vary considerably with sediment type, magnetic mineralogy, and physical properties. The factors controlling the paleomagnetic behavior of deep-sea sediments are little understood and may be quite subtle. Nevertheless, the highly variable results obtained at Site 709 are surprising given the striking homogeneity of the recovered sediments (see "Lithostratigraphy" section, this chapter). Thus, the paleomagnetic results from this site provide a valuable opportunity to study spurious remagnetization effects. In particular, the uniform, light brown nannofossil ooze recovered in 21 APC cores at Hole 709A show paleomagnetic inclinations which can

vary from steeply upward to steeply downward over the length of a few tens of centimeters. These APC cores show no evidence of being physically disturbed during drilling, yet such steep inclinations cannot reasonably be considered primary in these equatorial (4°S) Neogene sediments.

A clue to the source of this variation emerges from an examination of the average inclination of each of these cores as determined by pass-through magnetometer measurements (Fig. 9). In general, the odd-numbered cores display inclinations which are more positive than the even-numbered cores. This alteration is most conspicuous in Cores 115-709A-12H through -21H, but the pattern also appears higher in the section.

In addition, some of the cores taken at Site 709 show striking similarities in their seemingly erratic inclination patterns. For example, the pass-through magnetometer record from Core 115-709C-18H shows a highly variable inclination record which is nearly identical with that obtained from Core 115-709C-20H (Fig. 10), though it is quite different from that of the intervening core.

The effect of alternating-field (AF) demagnetization on such anomalous directions often appears to be systematic. Rather than being reduced, however, steep inclinations of NRM frequently become steeper upon demagnetization. The section shown in Figure 11 is typical of the core and clearly shows that, though AF treatment reduces the intensity, both positive and negative directions become more steeply inclined.

Discussion

The alternation of the paleomagnetic results in consecutive cores points directly to the core barrels as the source of the obvious remagnetization. In normal APC-drilling operations, two core barrels are used, one which is prepared on the rig floor while the other makes a round-trip through the drill string. Thus, alternate numbered cores are obtained with alternate core barrels. This then could account for the differences seen, since the processing of alternate cores is otherwise identical.

Behavior under AF demagnetization suggests that the effect is not a simple isothermal remanent magnetization (IRM) imparted by the remanent field of the core barrel, since it appears that the higher coercivity grains are affected the most by remagnetization. Perhaps a mechanical reorientation of the magnetic grains occurs, with the smaller (presumably higher coercivity) grains being rotated most readily. Though the coring drive itself might be the source of this mechanical energy, it seems more likely that the remagnetization occurs as the core travels up the

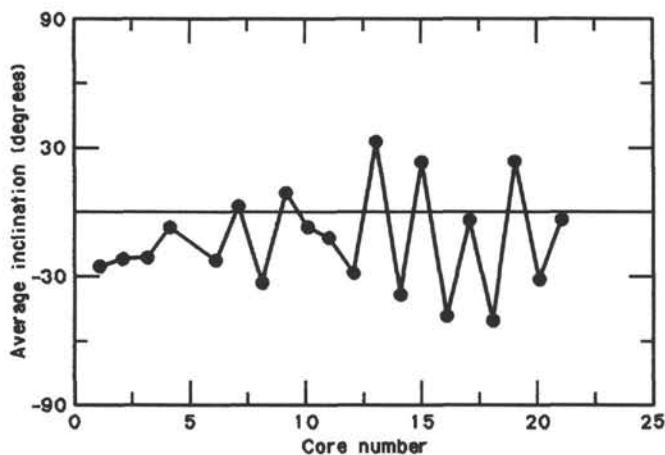


Figure 9. Alternation in the average inclination obtained from 21 APC cores from Hole 709A. Measurements by pass-through cryogenic magnetometer after 5-mT demagnetization.

drill string, presumably being subjected to repeated shock and vibration.

The proposed remagnetization mechanism may at least partially explain the frequent disagreement between paleomagnetic results obtained from pass-through and discrete measurements. A "profile" of paleomagnetic directions obtained across the diameter of one of these cores (Core 115-709C-15H in Fig. 12) suggests that the outermost sections of sediment can show unreasonably high inclinations (i.e., be remagnetized) while the center remains less affected. Apparently, exterior portions of the sediment cores are most apt to become remagnetized (perhaps because the field of the barrel drops off substantially near the center of the core). Discrete samples from the center of the core may be less likely to show erratic directions, so that an analysis of such samples may be warranted even where pass-through results show pervasive remagnetization.

Conclusion

Sediments obtained through APC coring, though physically undisturbed, often show erratic paleomagnetic directions, presumably from remagnetization during drilling. One particular source of remagnetization appears to be the remanent field of the core barrel which is impressed on the sediments during drilling operations. This remagnetization might be termed a "core-barrel" effect. The exact acquisition mechanism is unclear, but it may involve the physical rotation of magnetic grains. Such a remagnetization may be difficult, if not impossible, to remove with AF demagnetization; however, it appears that the measurement of discrete samples may be less prone to this effect than are pass-through measurements.

Magnetic Susceptibility

Whole-core magnetic susceptibility measurements were made at intervals of 6 cm on all sections of cores recovered from Hole 709A (Cores 115-709A-1H through -21H), on all sections of cores recovered from below 129 mbsf in Hole 709B (Cores 115-709B-15H through -27X), and on all sections of cores recovered from Hole 709C to a depth of 140 mbsf (Cores 115-709C-1H through -15H). Susceptibility measurements were made with a Bartington Susceptibility Meter (Model MS1) and whole-core, pass-through sensor coil of 80-mm inner diameter (Model MS2C). The results of these measurements are shown in Figures 13 and 14, in which possible correlations between Holes 709A and 709C are suggested.

In general, susceptibility values are low (mostly between 1 and 15×10^{-6} cgs), with the exception of volcanic-ash-rich horizons which yielded susceptibility values in excess of 5×10^{-5} cgs. Susceptibility values of less than 2×10^{-6} cgs are close to the limit of detection of the whole-core sensor coil. Therefore, erratic fluctuations in background noise tend to interfere with the susceptibility signal in response to lithologic variations in certain intervals of the sequence at Site 709 (i.e., between 22 and 100 mbsf in particular).

The generally lower susceptibility values at this site, compared with those of Site 708, are most likely due to its shallower position, and thus the higher degree of preservation of carbonate constituents in the sediment. The higher accumulation rate of carbonate at Site 709, relative to Site 708 (where bulk sediment accumulation rates were exaggerated by the large number of turbidites in the sequence), effectively dilutes the concentration of magnetizable material in the sediment, which resides principally in its nonbiogenic fraction (see "Explanatory Notes" and "Paleomagnetism" section, "Site 705 and 706" chapter, this volume).

The low concentration of magnetizable material in the sediment throughout Hole 709 is further depleted within the interval between sub-bottom depths of around 22 and 110 mbsf in

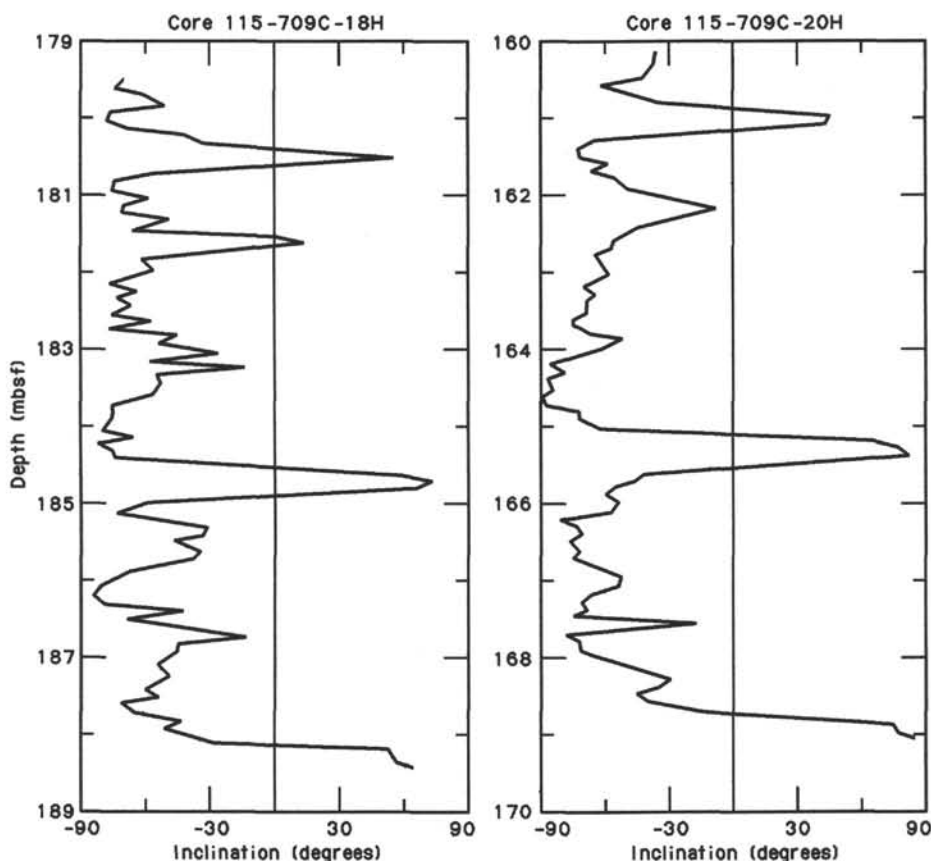


Figure 10. Repetition of anomalous inclination pattern seen after 5-mT demagnetization in Cores 115-709C-18H and 115-709C-20H taken with the same core barrel.

Holes 709A and 709C (Fig. 13). This interval corresponds to a section of gray or greenish gray sediment (nannofossil oozes with occasional degraded volcanic-ash bands) of late Miocene to late Pliocene age. The colors of this interval suggest that ferric-iron compounds in the sediment have undergone postdepositional reduction, possibly due to suboxic diagenesis of organic matter (cf. Karlin et al., 1987). Within this interval, therefore, most of the more strongly magnetic (NRM-carrying) forms of iron originally in the sediment, such as Fe(II)/Fe(III) oxides and Fe(III) oxyhydroxides, are likely to have been dissolved (i.e., bacterially dissociated), leaving only the non-NRM-carrying, paramagnetic forms of ferrous iron, such as clay minerals, ferromagnesian silicates, pyrite, etc., to contribute to susceptibility values.

Above and below this interval in Holes 709A and 709C, however, the sediments appear to be normally oxidized (i.e., they exhibit white, light yellowish brown, or buff colors) and consist of nannofossil oozes and clay-bearing nannofossil oozes. In these intervals, iron oxide and oxyhydroxide minerals originally present in the sediment are likely to have been preserved unaltered (or to have been further oxidized, but not magnetically disordered) since deposition. Hence, those horizons which have remained in an oxidized state since deposition exhibit magnetic susceptibility values which are generally higher than those of reduced horizons, variations in lithology notwithstanding.

Susceptibility values in the oxidized nannofossil ooze horizons of the sequence tend to covary with fluctuations in carbonate content of the sediment (see Figs. 20 and 21, "Geochemistry" section, this chapter); hence, they also reflect changes in lithology. This covariance is particularly clear in the intervals from 127 to 188 mbsf in Hole 709A, and from 132 to 190 mbsf

in Hole 709B, which are characterized by a generally lower proportion of carbonate in the sediment, and thus higher susceptibility values (both peak and background values) than elsewhere in the sequence, with the exception of volcanic-ash-rich horizons. The increase in susceptibility values and decrease in carbonate content in these horizons is possibly due to a period of intensified dissolution of biogenic constituents (both carbonate and silica (see "Biostratigraphy" section, this chapter) of the sediment during the early and middle Miocene. This effect was also identified at Site 708A for the same stratigraphic interval (see "Paleomagnetism" section, Site 708 chapter).

The strong lithologic control of magnetic susceptibility variations at Site 709 provides a reliable basis for interhole correlation (see Figs. 13 and 14). Figure 15 shows the correlation suggested in Figure 13 for the interval between 110 and 140 mbsf, plotted on an expanded scale in order to illuminate the decrease in susceptibility values (1) at the beginning of the phase of postdepositional reduction of sediment in the late Miocene (at 117 mbsf), and (2) at the end of the interval of lower carbonate content (possibly related to increased dissolution) during the beginning of the late Miocene (at 127 mbsf in Hole 709A and 129 mbsf in Hole 709C). Figure 15 also shows that the correlation based on high-resolution susceptibility profiles of Holes 709A and 709C has revealed the presence of two small hiatuses: one in Hole 709A at around 123.5 mbsf, and one in Hole 709C at around 129 mbsf.

Figure 16 shows the correlation suggested in Figure 14 for the interval between 148.5 and 178.5 mbsf, plotted on an expanded scale in order to illustrate, more clearly, the differences between the susceptibility profiles of Holes 709A and 709B in this interval, which mainly result from coring irregularities. These in-

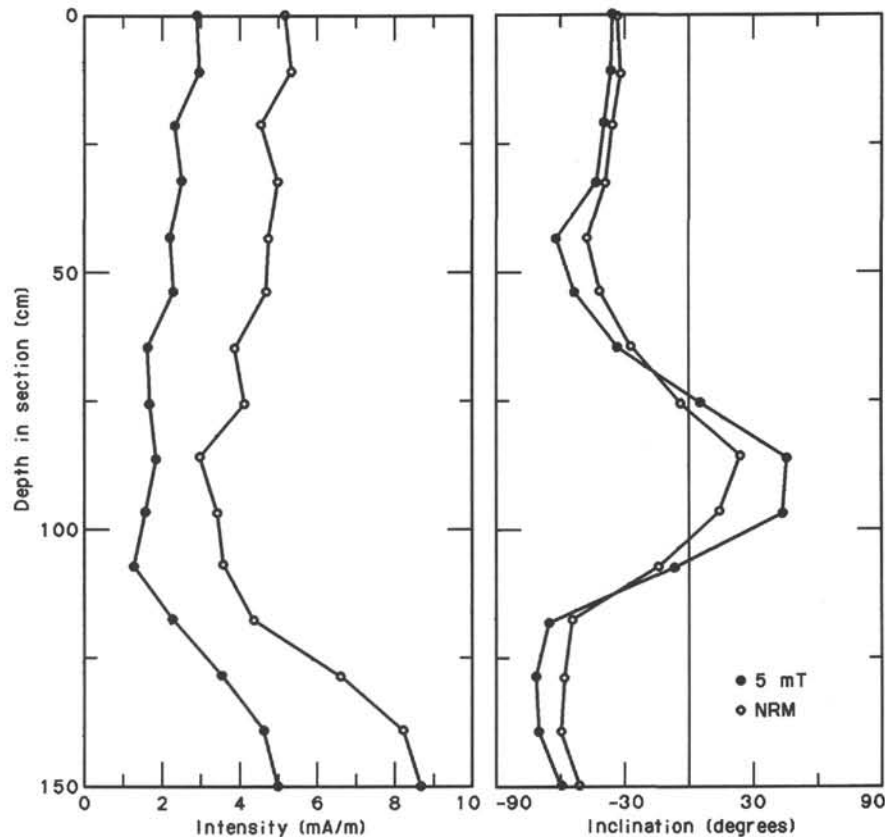


Figure 11. Steepening of anomalous inclinations with alternating-field (AF) demagnetization in Section 115-709C-18H-1. Results are from pass-through magnetometer measurements.

clude (1) loss of sediment between cores and (2) the presence of a repeated sequence, both of which occur in Hole 709B. Loss of material, and thus the stratigraphic record, occurs at the junction between Cores 115-709B-17H and -18H, and, in particular, between Cores 115-709B-18H and -19H. This effect is very likely to be related to the repetition of a sequence in this hole that occurs within Core 115-709B-18H. The repeated sequence in Hole 709B occurs between 163.3 and 168.0 mbsf and corresponds stratigraphically to the immediately overlying sequence in the same hole, between 158.3 and 163.3 mbsf. It is possible that the upper sequence represents a sediment slump or slide (lateral sediment translation) in which the dislocated material has been redeposited en masse, thus retaining its internal stratigraphy undeformed. It is much more likely, however, that the repetition of sequence in Hole 709B is attributable to repenetration of the corer.

The top of the uppermost of the two stratigraphically equivalent sequences occurs at 158.3 mbsf, while the base of the lower sequence occurs at 168.0 mbsf. This interval (158.3–168.0 mbsf) corresponds exactly to that of Core 115-709B-18H, and the loss of sediment between cores alluded to above occurs at the upper and lower boundaries of this core. It is therefore conceivable that, following initial penetration to only half that of the intended run length, the core barrel was temporarily withdrawn from the hole by accident (possibly due to inadequate heave compensation during the swell) and then reinserted at an immediately adjacent location to the previously cored interval, thus recovering the same sequence captured by the first penetration of the corer. A more detailed discussion of the causes and effects of repenetration during HPC coring, based on an analysis of DSDP Leg 94 sediments, is given by Ruddiman et al. (1987).

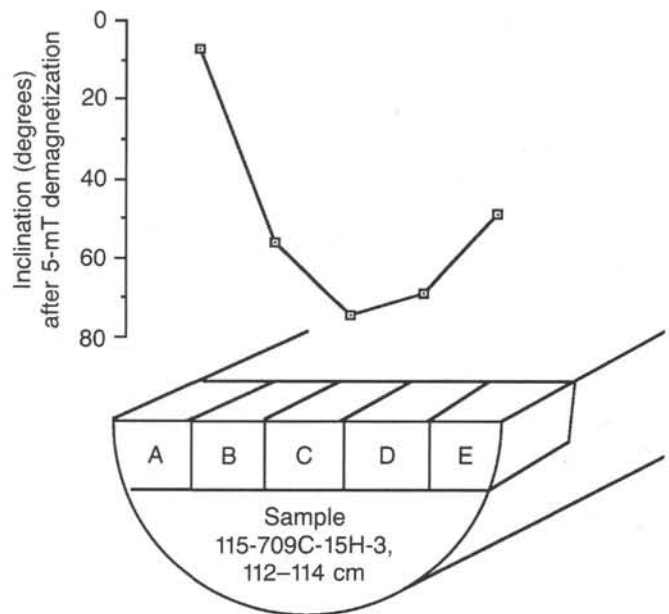


Figure 12. Remagnetization profile obtained from the measurement of five discrete samples cut transverse to the core axis.

SEDIMENTATION RATES

The datum events identified on the basis of the four fossil groups (calcareous nannofossils, planktonic foraminifers, radiolarians, and diatoms) are illustrated in Figure 17 and are listed in Table 3.

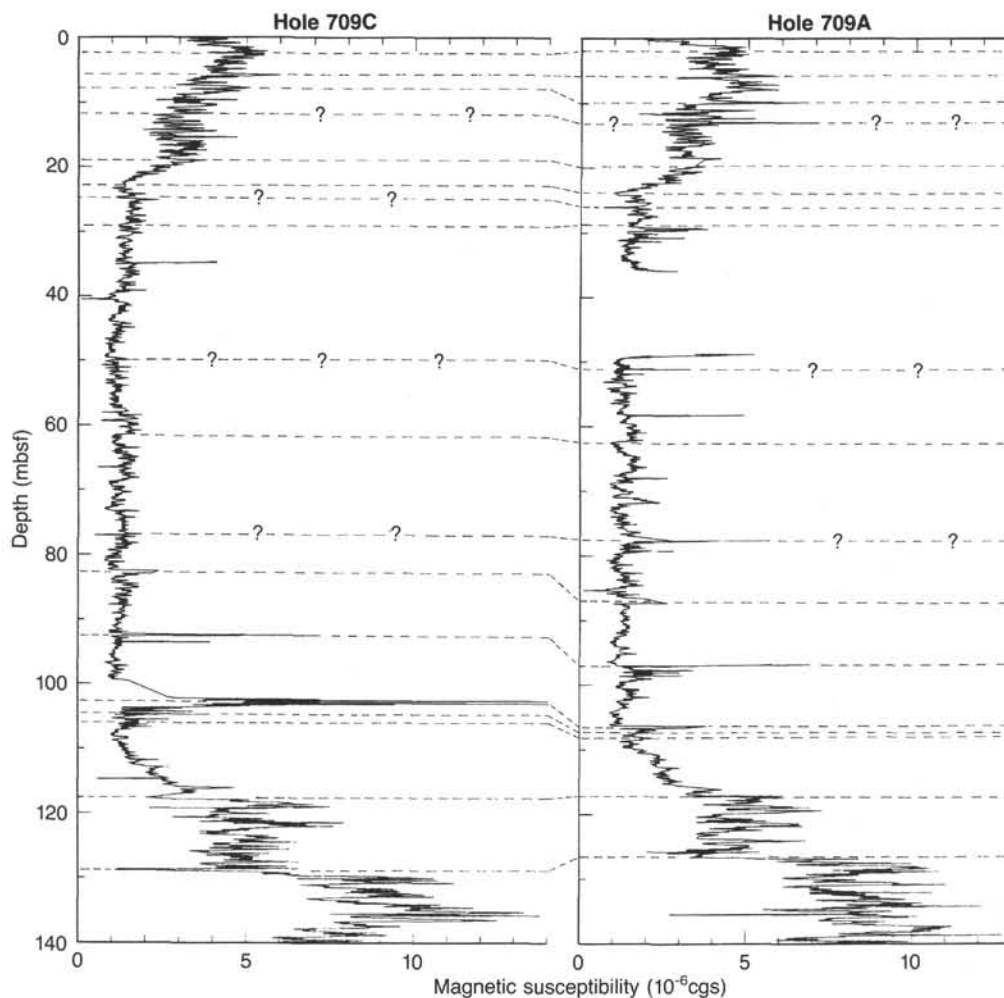


Figure 13. Suggested correlation between whole-core magnetic susceptibility profiles of Holes 709A and 709C for the interval from 0 to 140 mbsf.

The sedimentation rates of Site 709 display three major rate regimes: (1) a late Miocene through Pleistocene interval (0–9 Ma) of high rates, averaging around 13 m/m.y.; (2) a middle Miocene (9–13 Ma) condensed interval showing rates of about 3 m/m.y.; and (3) a middle Eocene to middle Miocene interval (13–47 Ma) with generally slow rates (~6 m/m.y.). Based on the plot in Figure 17, the rates can be determined more specifically for shorter time increments.

Age interval	Rate (m/m.y.)
0–0.46	11.3
0.46–3.56	9.8
3.56–6.5	18.5
6.5–8.9	9.8
8.9–10.8	1.2
10.8–13.2	4.8
13.2–18.6	7.9
18.6–24.1	4.2
24.1–40.0	7.4
40.0–47.0	5.7

The largest uncertainties occur in the middle Eocene, probably due to poor intercalibration between nannofossil, radiolarian, and foraminifer datum events.

GEOCHEMISTRY

Interstitial Water Studies

Data from interstitial water analyses and the Barnes down-hole water sampler are shown in Table 4 and Figure 18. Samples were taken from all three holes drilled at Site 709.

Calcium and Magnesium

Calcium and magnesium concentrations exhibit very weak, but nevertheless predictable, downhole gradients. Except for the first two cores, which exhibit sharp changes in Ca^{2+} and Mg^{2+} from their surface seawater values, the downhole Ca^{2+} and Mg^{2+} gradients of 0.0061 and -0.011 mmol/L/m are the lowest observed in any of the sites studied thus far. The larger changes in Ca^{2+} and Mg^{2+} in the upper portion of the core may reflect shallow subsurface diagenetic reactions, influenced either by sulfate reduction or by squeezing and then comparing the uppermost core samples with surface seawater.

Calcium concentrations from the two samples from Hole 709B were consistently lower than those from Hole 709A, perhaps as a result of contamination from the first hole which was drilled only several meters away. However, since the concentration of Mg^{2+} is essentially identical to that of Hole 709A, it suggests that subtle differences exist in the calcium gradient over short spatial distances. Lower than expected Ca^{2+} gradients were also measured in Hole 709C, but *in-situ* water samples

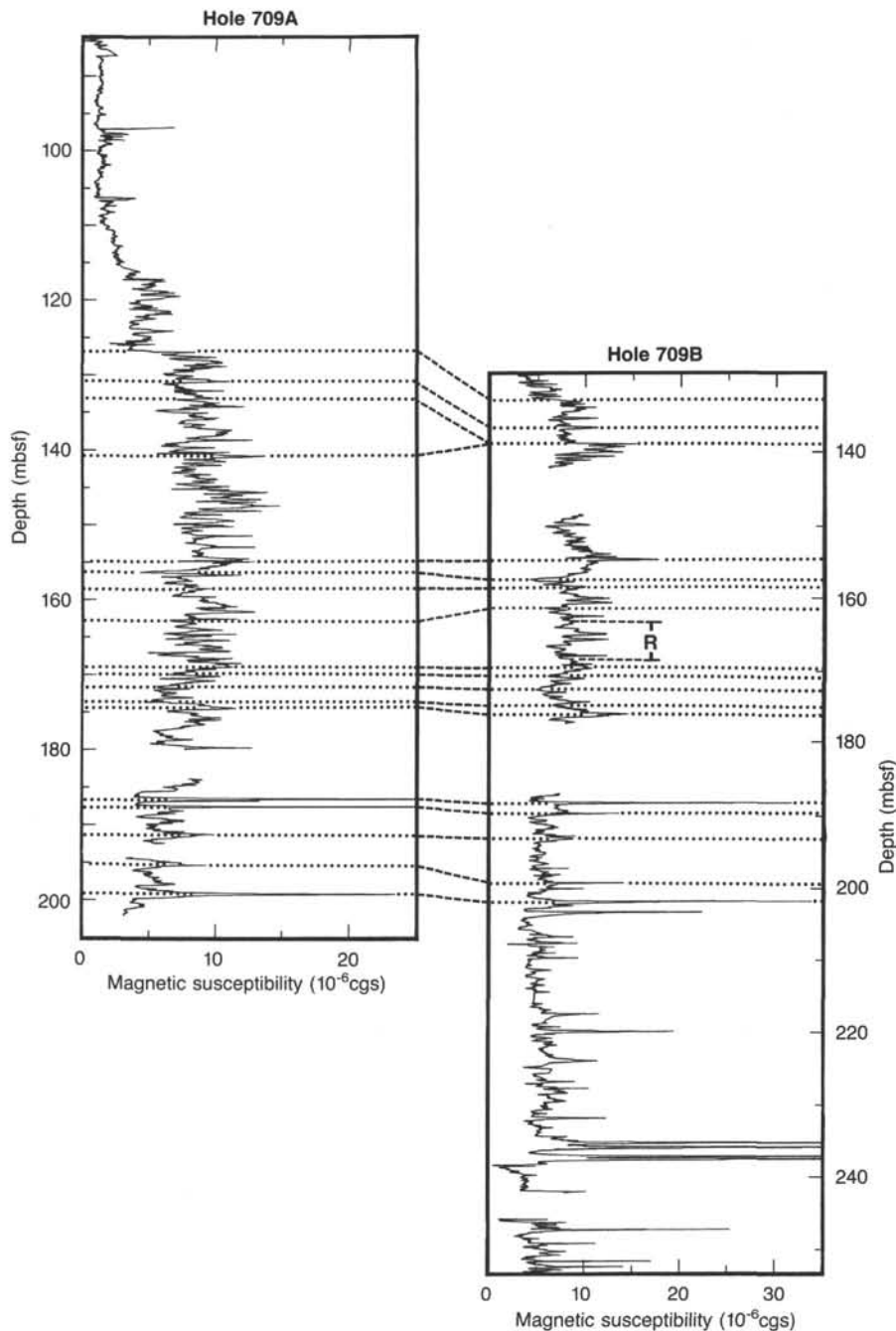


Figure 14. Whole-core magnetic susceptibility profiles of Holes 709A and 709B, showing suggested correlation between holes for the interval of overlap between 129 and 202 mbsf. Note the identification of a small hiatus in the stratigraphic record of Hole 709B at about 139 mbsf, and the presence of a repeated sequence (R) in Hole 709B between 163.3 mbsf and 168 mbsf.

taken using the Barnes water sampler showed that Ca^{2+} concentrations in the pore fluids were higher than in the squeezed samples by as much as 1 mmol/L. The data obtained from all three holes and the *in-situ* water sampler are compared in Figure 19.

Alkalinity values were higher by as much as 0.5 mmol/L, but magnesium concentrations were unchanged. Such values are not likely the result of contamination by seawater. The results clearly indicate that calcium and alkalinity values are depressed in squeezed sediment samples as a result of the precipitation of CaCO_3 , due to the loss of CO_2 (i.e., CO_3^{-2} increases) as the core is retrieved from great depths and pressures.

Sulfate, Ammonia, and Alkalinity

Sulfate concentrations exhibit a large decrease in the uppermost core, reaching a value as low as 21.12 mmol/L at a depth of 5.95 mbsf. Below this depth, values gradually increase to approximately seawater concentrations. In Core 115-709A-1H, alkalinity increases rapidly with depth, compared with surface seawater values, then gradually increases to a maximum value of 4.5 mmol/L at 220 mbsf. Concentrations of ammonia (NH_4^+) gradually increase with depth, in accordance with processes that cause the oxidation of organic material.

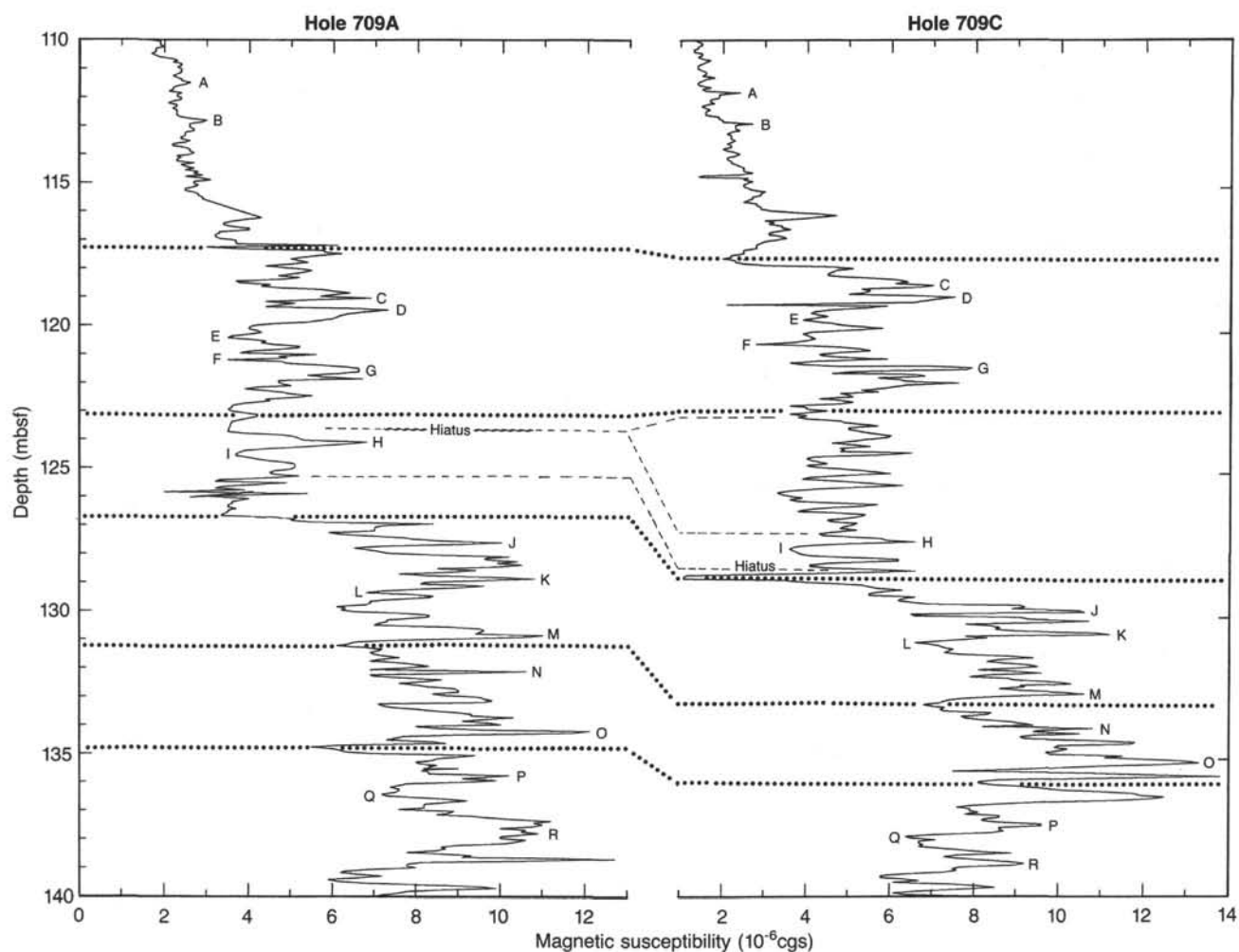


Figure 15. Suggested correlation between whole-core magnetic susceptibility profiles of Holes 709A and 709C for the interval from 110 to 140 mbsf. Note the identification of a small hiatus in the record of Hole 709A at around 123.5 mbsf, and a small hiatus in Hole 709C at around 129 mbsf.

Salinity and Chlorinity

Chlorinity shows a slight decrease with increasing depth. There is some variation in the uppermost five cores which is apparently mirrored in the salinity measurements.

Silica

Silica shows a rapid increase in concentration in the first core (Core 115-709A-1H) to 610 $\mu\text{mol/L}$ at 5.95 mbsf. A slight decrease occurs between 152.40 and 177.20 mbsf to a value of 402 $\mu\text{mol/L}$; this change was also observed using the Barnes down-hole water sampler. The observed decrease in silica concentration may be related to a silica precipitation front.

X-ray, Carbonate, and Organic Carbon Analyses

Mineralogy and Carbonate Content

The dominant mineralogy, determined by X-ray analysis, of the sediments in Holes 709A, 709B, and 709C is low-magnesium calcite, with quartz forming a ubiquitous background component with concentrations ranging from 1% to 2%.

The carbonate content of sediments in all holes from Site 709 varies from 76 wt% to 97 wt% (Fig. 20 and Table 5), with an overall average of 89.72 wt% (± 3.56 wt%). Based on a 10-sample running mean (Fig. 21), numerous cyclic intervals of high- and low-carbonate content can be seen. As in Site 707, a

low value in the carbonate content can be identified in the upper Miocene/Messinian. This "low" has a mean carbonate content of 90 wt%, approximately 1 wt%–1.5 wt% lower than at Site 707.

Three cycles can be identified in the upper Miocene which approximately correlate with fluctuations seen at Site 707. The three maxima in the upper Miocene are preceded by a low of 85% in the upper middle Miocene lasting for approximately 4 m.y. The concentration of carbonate rises irregularly toward the Miocene-Oligocene boundary in a series of four cycles. The boundary is characterized by a sudden drop from 92 wt% to 84 wt%. The percent carbonate, however, rises again during the middle Oligocene and then gradually decreases toward middle Eocene times.

Organic Carbon

The organic carbon content of the sediments is extremely low throughout both Holes 709A and 709C, ranging from 0.01% at 91.70 mbsf to one analysis of 0.66% at 318.05 mbsf (Table 6).

PHYSICAL PROPERTIES

Introduction

Site 709 is located north of the Mascarene Plateau in a small basin on the Madingley Rise. Three holes were drilled, recover-

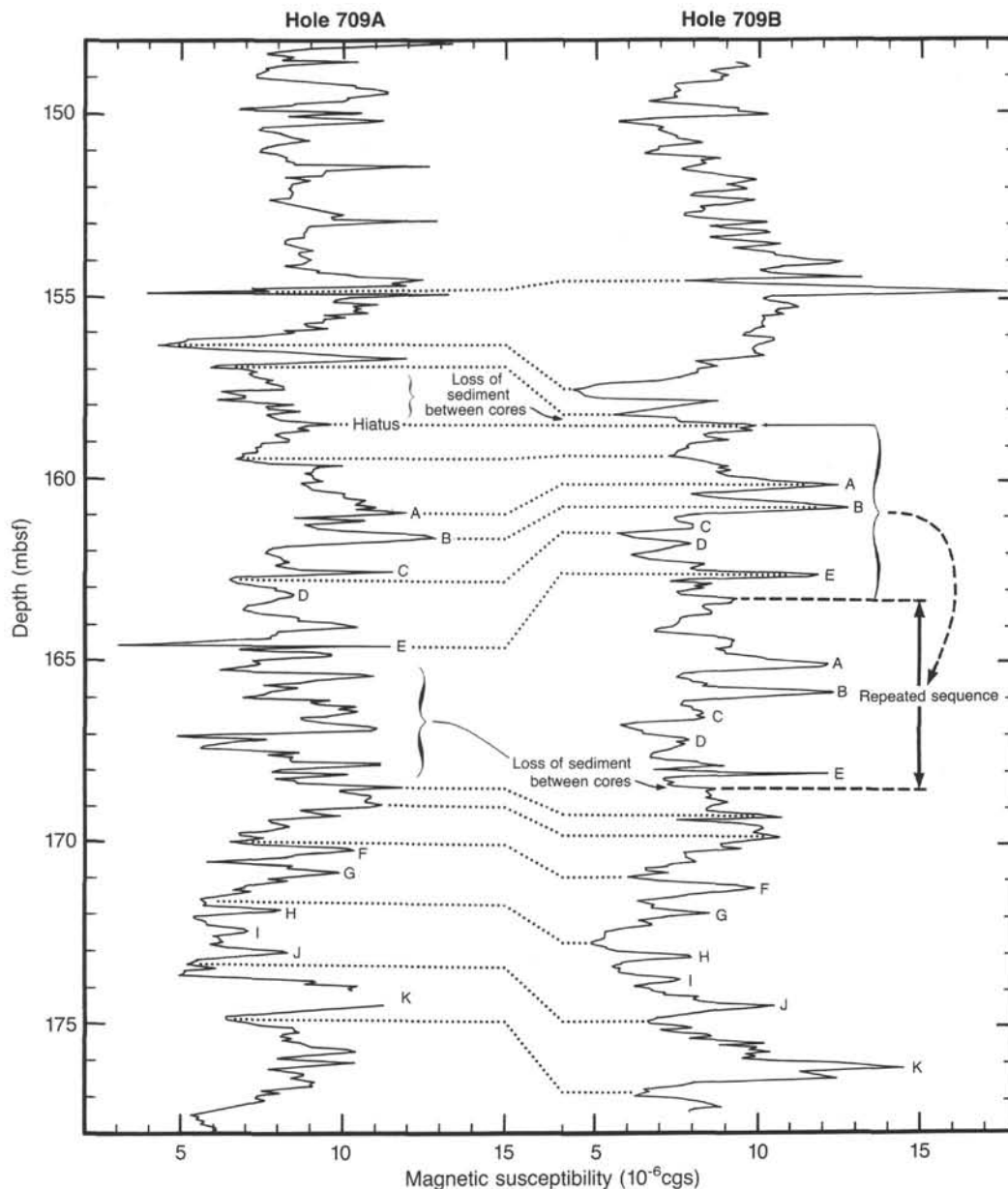


Figure 16. Suggested correlation between the whole-core magnetic susceptibility profiles of Holes 709A and 709B for the interval from 148.5 to 178 mbsf. Note the occurrence of stratigraphic discontinuities due to loss of sediment between cores in Hole 709B, at approximately 158.7 mbsf and 169 ± 0.2 mbsf, as well as the presence of a repeated sequence in Hole 709B between 163.3 mbsf and 168.0 mbsf which corresponds to the immediately overlying sequence between 158.3 mbsf and 163.3 mbsf. The apparent lack of correlation between the two holes above 154.5 mbsf may possibly be explained by the presence of an hiatus in the stratigraphic record of Hole 709B at this depth (see Fig. 14). Letters indicate points of correlation.

ing a 353.7-m-thick sequence of nannofossil ooze using APC- and XCB-coring techniques. Hole 709A was drilled using the APC; in Holes 709B and 709C the coring system was changed to the XCB at sub-bottom depths of 187.2 and 189.1 m, respectively.

The nannofossil ooze is homogeneous, varying only in degree of consolidation and disturbance downhole. The ooze increases in hardness and cohesion with depth; chalk "chunks" were observed at depths greater than 100 mbsf. The following physical properties were evaluated at Site 709: index properties, GRAPE wet-bulk density, compressional- and shear-wave velocities, shear strength, and thermal conductivity. The number of

measurements performed at each of the three holes varied, partly due to equipment failure.

Index Properties

The lack of downhole variation in the index properties illustrates the homogeneous character of the nannofossil ooze (Table 7). A transition from pure nannofossil ooze to ooze with interbedded nannofossil chalk "chunks" occurs at a sub-bottom depth of 160 m (Hole 709A). The same gradual transition was seen at 132 mbsf in Holes 709B and 709C. This transition can be related to the onset of fluctuations in the bulk densities (Figs. 22, 23, and 24). In all three holes of Site 709, cyclic fluctu-

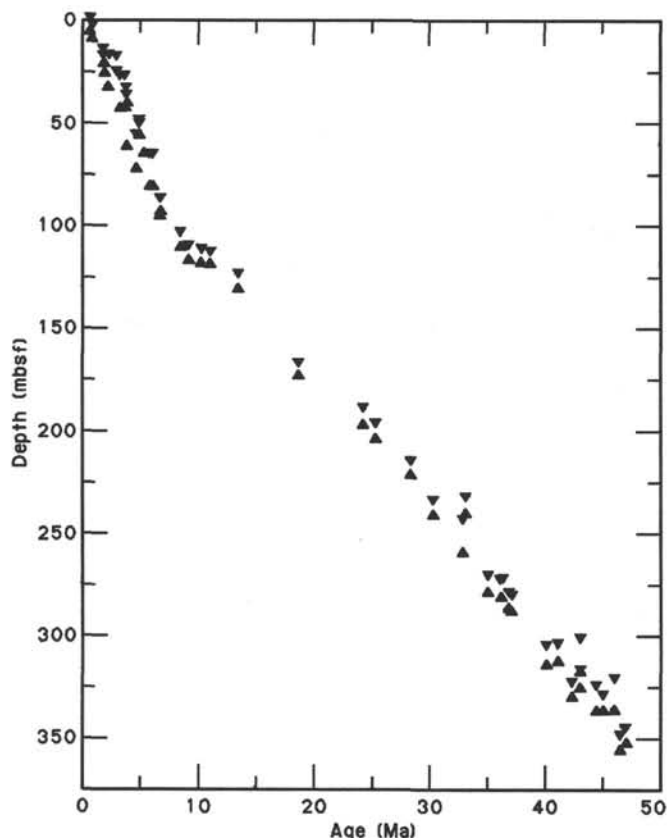


Figure 17. Age-depth plot showing sedimentation rates at Site 709.

tuations in the wet-bulk densities have a wavelength of about 25–30 m. In Hole 709B, porosity is correlated inversely with wet-bulk density: high porosities appear in sections of low density, and high densities are associated with low porosities. There is no obvious correlation between these results and the visual core descriptions (see “Lithostratigraphy” section, this chapter).

The wet-bulk densities of the three holes range from 1.55 to 1.73 g/cm³ and increase with depth. Both porosity and water content decrease downhole.

The grain density at this site is again mainly controlled by the carbonate content. Little variation in grain density is expected in sediments where the carbonate content only fluctuates between 80% and 95% (Fig. 25 and Table 8).

There is very good agreement between the density measurements on the discrete samples and the continuous density record of the GRAPE (Fig. 28). The low-frequency fluctuations in the bulk density mentioned above also find their expression in the continuous record, although it is partly disturbed by the high-frequency variation of density detected by the GRAPE.

Compressional-Wave Velocity and Acoustic Impedance

Compressional-wave velocity (V_p) was determined on discrete samples using the Hamilton Frame, and a continuous velocity profile was obtained from the P -wave logger.

Discrete V_p results for Site 709 are listed in Table 8 and shown in Figure 26. Velocities are constant with depth within the nanofossil ooze in Hole 709A, gradually increasing with depth in Holes 709B and 709C. There is an experimental scatter of less than $\pm 2\%$ from the mean value of 1525 m/s. Three V_p measurements were taken in the brittle chalk from the deepest core of Hole 709C. Measurements in the chalk for V_p give an

Table 3. Biostratigraphic datum levels, Site 709.

	Species event	Depth (mbsf)	Age (Ma)
FO	<i>E. huxleyi</i> (N)	1.4–1.9	0.27
LO	<i>P. lacunosa</i> (N)	4.9–5.4	0.46
LO	<i>C. macintyreii</i> (N)	16.7–17.2	1.45
LO	<i>P. prismatium</i> (R)	19.7–21.9	1.55
FO	<i>P. doliolus</i> (D)	19.7–29.4	1.8
LO	<i>D. brouweri</i> (N)	19.2–19.7	1.89
FO	<i>G. truncatulinoides</i> (F)	19.7–29.4	1.9
LO	<i>S. peregrina</i> (R)	27.9–29.4	2.6
LO	<i>N. jouseae</i> (D)	19.7–29.4	2.6
LO	<i>D. tamalis</i> (N)	27.2–28.7	2.65
FO	<i>G. fistulosus</i> (F)	29.4–39.1	2.9
LO	<i>D. altispira</i> (F)	29.4–39.1	2.9
LO	<i>Sphaeroidinellopsis</i> spp. (F)	29.4–39.1	3.0
LO	<i>L. audax</i> (R)	29.4–39.1	3.35
LO	<i>P. doliolum</i> (R)	39.1–58.3	3.53
LO	<i>R. pseudoumbilica</i> (N)	35.3–36.8	3.56
LO	<i>S. omnibus</i> (R)	58.3–69.0	4.3
FO	<i>C. rugosus</i> (N)	52.4–53.9	4.6
LO	<i>C. acutus</i> (N)	50.9–52.4	4.6
LO	<i>A. tritubus</i> (R)	68.0–77.6	5.5
LO	<i>D. quinquerramus</i> (N)	60.5–62.0	5.0
FO	<i>P. primalis</i> (F)	68.0–77.6	5.8
	<i>S. delmontensis</i> – <i>S. peregrina</i> (R)	87.3–96.9	6.4
FO	<i>C. primus</i> (N)	89.3–90.2	6.5
FO	<i>D. quinquerramus</i> (N)	105.8–107.3	8.2
LO	<i>D. hamatus</i> (N)	112.7–113.9	8.9
FO	<i>D. hamatus</i> (N)	114.2–115.1	10.0
FO	<i>C. coalitus</i> (N)	115.4–115.7	10.8
LO	<i>S. heteromorphus</i> (N)	126.5–127.7	13.2
FO	<i>S. heteromorphus</i> (N)	169.8–169.9	18.6
FO	<i>L. elongata</i> (R)	192.2–193.5	24.1
LO	<i>S. ciperoensis</i> (N)	199.3–200.8	25.2
LO	<i>S. distentus</i> (N)	218.0–218.6	28.2
FO	<i>S. ciperoensis</i> (N)	237.4–238.7	30.2
FO	<i>G. opima</i> (F)	247.0–256.7	32.7
	<i>D. triceros</i> – <i>D. atechus</i> (R)	235.5–237.7	33.0
LO	<i>E. formosa</i> (N)	274.3–276.1	34.9
	<i>L. aristotelis</i> – <i>L. angusta</i> (R)	276.1–278.3	36.0
LO	<i>Hantkenina</i> spp. (F)	275.8–276.2	36.2
LO	<i>D. saipanensis</i> (N)	282.5–284.0	36.7
LO	<i>D. barbadiensis</i> (N)	284.0–285.8	37.0
LO	<i>C. grandis</i> (N)	308.5–311.5	40.0
FO	<i>C. azyx</i> (R)	307.3–310.3	41.0
LO	<i>C. solitus</i> (N)	326.3–327.8	42.3
LO	<i>Acarinina</i> spp. (F)	305.1–314.8	43.0
	<i>P. mitra</i> – <i>P. chalara</i> (R)	320.0–323.0	43.0
FO	<i>R. umbilica</i> (N)	327.8–334.1	44.4
	<i>P. sinuosa</i> – <i>P. mitra</i> (R)	332.6–334.1	45.0
LO	<i>M. aragonensis</i> (F)	324.4–334.1	46.0
	<i>P. phyxis</i> – <i>P. ampla</i> (R)	352.1–353.7	46.5
LO	<i>C. gigas</i> (N)	348.8–350.3	47.0

Note: FO = first occurrence, LO = last occurrence, N = nanofossil, F = foraminifer, R = radiolarian, and D = diatom.

average velocity of 1645 m/s due to their greater degree of consolidation.

A comparison of Figure 26 with Figure 22 shows that changes in discrete V_p measurements correlate remarkably well with the sinuous variations in discrete density measurements for Site 709. This agreement, along with the good correlation of discrete V_p measurements between Holes 709A, 709B, and 709C, suggests that the variation of V_p with depth is a function of physical changes in the oozes and is not due to experimental scatter.

The impedances calculated from the discrete data for Holes 709A, 709B, and 709C are shown in Figure 27 and are listed in Table 8. These data show a linear increase of impedance with depth from 2.4 g/cm²·s·10⁵ near the surface to 2.8 g/cm²·s·10⁵ at 180 mbsf. The sinuous fluctuations in the discrete impedance profile are a result of the combination of changes in the wet-bulk density and velocity profiles. The close match in the velocity and wet-bulk density data increases the amplitude of the peaks observed in the discrete impedance plot.

Table 4. Interstitial water analyses and analyses from samples collected using the downhole water sampler at Site 709.

Sample interval (cm)	Depth (mbsf)	Ca (mmol/L)	Mg (mmol/L)	Cl (mmol/L)	Al (mmol/L)	pH	Salinity (‰)	Si ($\mu\text{mol/L}$)	SO ₄ (mmol/L)	NH ₄ ($\mu\text{mol/L}$)
Seawater	0	10.47	55.54	574.63	2.52	8.43	35.0	0	28.98	0
115-709A-										
1H-4, 145-150	5.95	10.71	54.81	554.38	3.42	7.65	34.5	610	21.12	0
2H-4, 145-150	16.05	11.57	53.54	568.24	3.66	7.37	35.0	710	25.12	4.28
3H-4, 145-150	25.65	11.64	53.31	549.76	3.82	7.33	34.9	753	25.82	12.15
4H-3, 145-150	33.85	11.77	52.01	570.07	3.78	7.53	35.2	683	27.22	5.82
6H-4, 145-150	54.65	11.85	52.94	546.06	3.96	7.49	35.1	764	26.94	7.36
7H-4, 145-150	64.25	12.02	52.93	546.06	4.03	7.70	35.1	784	27.50	32.00
10H-2, 120-125	90.00	12.28	52.42	546.99	4.25	7.50	35.2	822	27.92	11.20
13H-5, 120-125	123.40	12.51	51.36	549.76	4.31	7.40	35.2	574	25.20	18.90
16H-5, 120-125	152.40	12.73	51.41	546.06	4.42	7.50	35.0	402	26.94	18.13
19H-2, 120-125	177.20	13.05	51.17	542.37	4.53	7.50	34.8	562	29.13	11.97
115-709B-										
22X-5, 120-125	204.00	12.47	51.58	545.14	4.09	7.59	34.4	687	29.44	22.70
25X-4, 145-150	231.75	12.99	50.82	548.84	4.29	7.33	34.4	835	28.50	37.00
115-709C-										
28X-2, 145-150	259.65	13.02	50.82	540.52	4.59	7.56	34.4	845	27.02	38.90
31X-4, 145-150	291.75	13.31	50.41	550.68	4.50	7.55	34.5	942	27.15	29.70
34X-4, 145-150	320.75	13.49	50.07	547.91	4.50	7.52	34.8	849	27.36	38.10
37X-4, 145-150	349.85	13.14	50.26	546.99	4.22	7.45	34.9	759	26.59	26.59

Figure 28 shows the continuous velocity profile obtained from the *P*-wave logger plotted next to the GRAPE wet-bulk density and impedance profiles for Site 709. The velocity has an average value of 1540 m/s and is constant with depth, from the seafloor to 260 mbsf. At depths greater than 260 mbsf, V_p increases steadily, except for a discontinuity at 310 mbsf. The continuous velocity results show a similar long-wavelength, sinuous variation of V_p with depth (on the order of 30 m) as observed in the discrete V_p data. A comparison of Figures 26 and 29 shows that the continuous V_p profile is similar to the data obtained from the discrete samples, except for an offset of 15 m/s and the resolution of short-wavelength (high-frequency) variations. The 1% discrepancy between the continuous and discrete V_p measurements is within the experimental inaccuracies of both techniques and is due most likely to the lack of temperature corrections for the discrete data.

It can be seen that the continuous impedance profile closely matches the GRAPE wet-bulk density profile in Figure 28. There is as much as a 10% deviation in wet-bulk density from a mean of 1.6 g/cm³, and a 3% deviation in velocity from a mean of 1540 m/s. The variability in the GRAPE data—and therefore in the impedance profile—below 195 mbsf may be partially the result of drilling disturbance caused by XCB coring, which took over from APC coring at this depth.

Shear-Wave Velocity and Shear Strength

Shear-wave velocity (V_s) data collected at Holes 709A and 709B are shown in Figure 29 and listed in Table 9. These data show a large amount of variability, and the correlation between holes is not good. The data from Hole 709A show that V_s increases with increasing depth, from 50 m/s at 20 mbsf to 130 m/s at 120 mbsf. This is followed by a gradual drop in V_s to 50 m/s at 160 mbsf, with V_s then increasing again with greater depth. The results from Hole 709B do not show the reduction in V_s between 120 and 160 mbsf, but they do illustrate a general trend of increasing V_s with depth, from 50 m/s at the seafloor to 170 m/s at 220 mbsf.

The correlation between the shear strength data of Holes 709A and 709B is good (Fig. 30 and Table 10). In both holes the sediment lithology is homogeneous to a depth of 150 m (see

“Lithostratigraphy” section, this chapter). At this depth the first appearance of chalk chunks within the homogeneous nanofossil ooze occurred. There was also an increase in the degree of consolidation at this depth, which is reflected in the rise of shear strength from 60 to 80 kPa. At depths greater than 150 m, fluctuations in the shear strength occurred due to variability in consolidation. Loss of cohesion in the lesser consolidated oozes in Holes 709A and 709B may be due to drilling disturbance. There was definite visual evidence for disturbance in the XCB cores of Hole 709C (see “Lithostratigraphy” section, this chapter).

Thermal Conductivity

The thermal conductivity data from Holes 709A, 709B, and 709C are shown in Figure 31 and listed in Table 11. The data were collected from overlapping intervals in the three holes in order to obtain a continuous depth record from this site. Only two functional thermal conductivity probes were available, so the task of obtaining one measurement per section for wet-bulk density data precluded making duplicate measurements in the upper parts of Holes 709B and 709C. The character of the thermal conductivity profile is quite different at this site than at Sites 707 and 708. The thermal conductivity at the surface is similar, about 1.1 W·m⁻¹·K⁻¹, but instead of varying considerably, it shows a smooth and steady increase from the surface to 100 mbsf. There is then a brief interval of variability (about 10 m), followed by a less variable increase. At 140 mbsf the higher local variability resumes, but the overall conductivity now shows a steady decrease to 0.8 W·m⁻¹·K⁻¹ at 180 mbsf.

There is no obvious gross correlation between any other physical property and this thermal conductivity decrease, although detailed examination of the data may yield a different conclusion. Conductivity shows little variability at this minimum, but it does exhibit considerable variability as it increases again with depth to 200 mbsf. The data from Hole 709B show very little small-scale variability, with a slow decrease in conductivity values with depth. The upper part of the Hole 709C data continue the trend of the Hole 709B data. Local variability suddenly increases at about 280 mbsf in Hole 709C and is related to

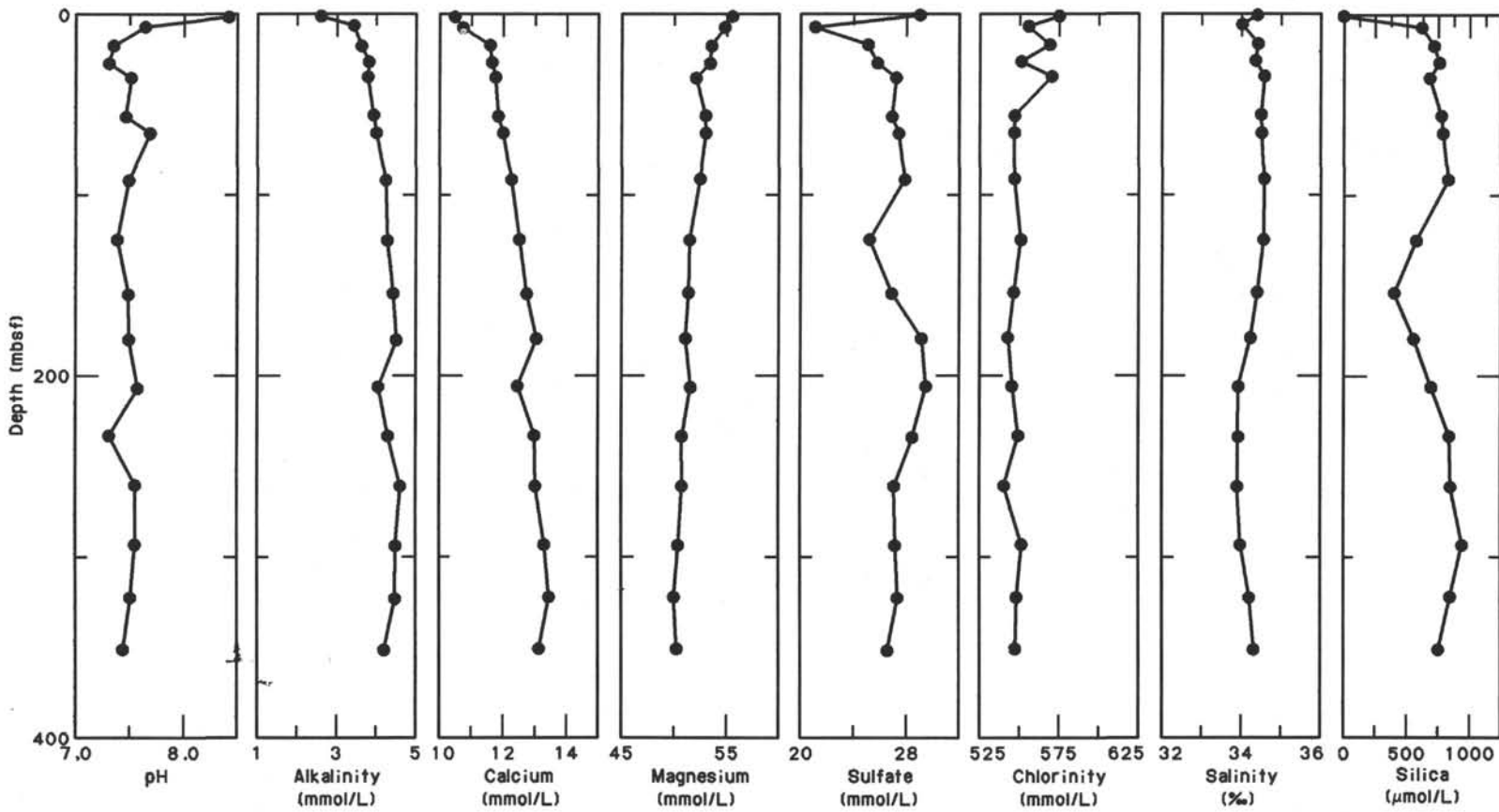


Figure 18. Summary of interstitial water analyses, Holes 709A, 709B, and 709C, as a function of sub-bottom depth. Surface seawater is plotted at 0 mbsf.

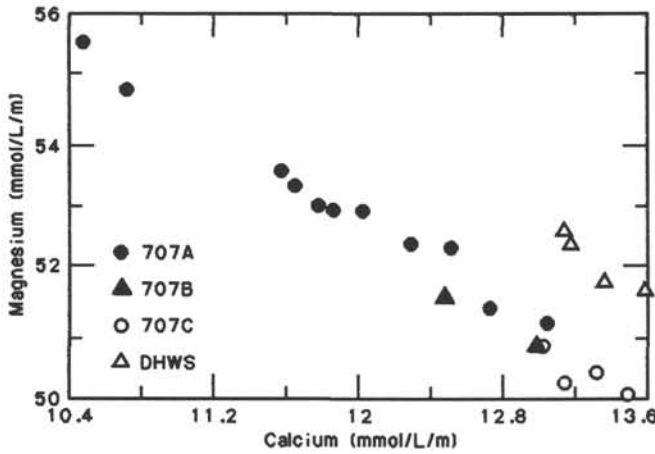


Figure 19. Comparison of calcium and magnesium gradients from Holes 709A, 709B, 709C, and samples obtained using the Barnes downhole water sampler.

an increase in the contrast between the harder semilithified carbonate layers and the softer layers in between. The thermal conductivity data are used in the calculation of integrated thermal resistivity, which is presented in the "Downhole Measurements" section, this chapter.

Summary

The homogeneous character of the nannofossil oozes at Site 709 is mirrored by a constant linear increase in wet-bulk density, a decrease in porosity, and a constant compressional-wave velocity. The presence of chalk intervals and differences in the degree of consolidation of the ooze are observed at depths greater than 150 mbsf. Between 130 and 180 mbsf, there is an inflection in the wet-bulk density and porosity curves, followed by fairly constant wet-bulk density and porosity values until 280 mbsf, where a further inflection occurs. At depths greater than 130 mbsf, a 30-m-wavelength cyclic variation is superimposed upon the linear trends in the index properties and compressional velocity. These fluctuations are amplified in the impedance profile.

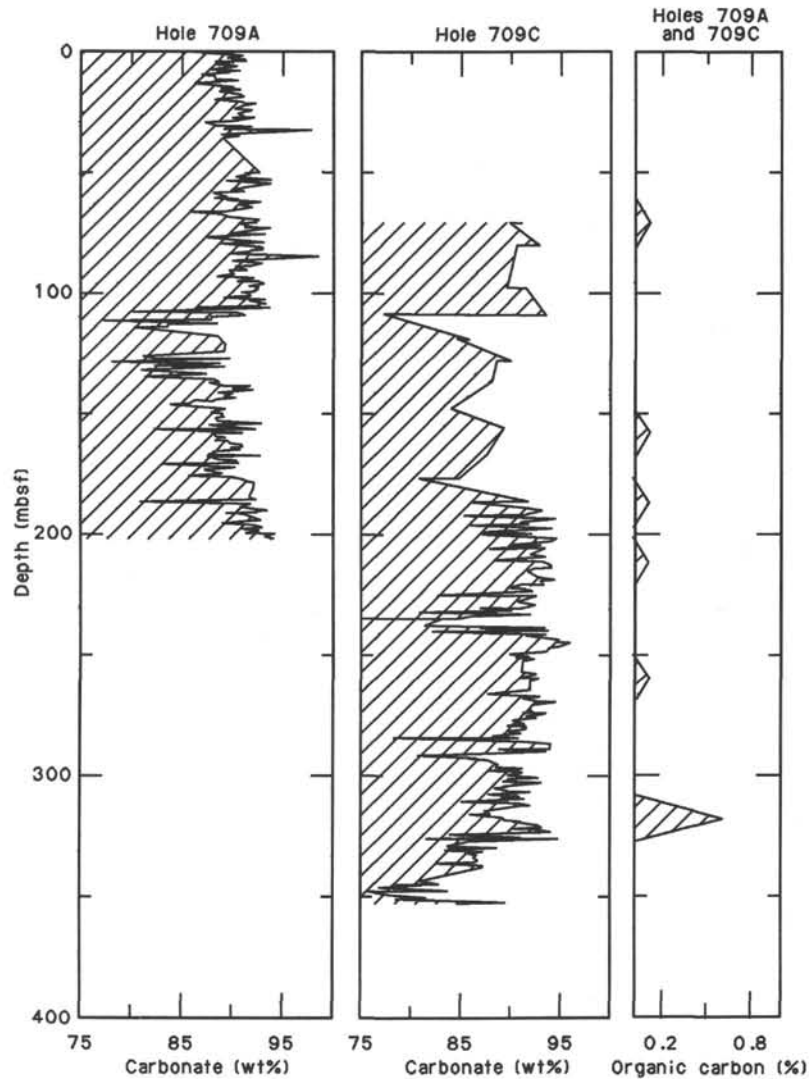


Figure 20. Carbonate and organic carbon content of samples from Holes 709A and 709C plotted against increasing sub-bottom depth.

Table 5. Carbonate content of samples from Holes 709A and 709C.

Sample interval (cm)	Depth (mbsf)	Carbonate (wt%)
115-709A-		
1H-1, 25-26	0.25	85.46
1H-1, 135-136	1.35	86.16
1H-2, 25-26	1.75	88.06
1H-2, 57-60	2.07	91.05
1H-2, 135-136	2.85	89.32
1H-3, 25-26	3.25	91.02
1H-3, 135-136	4.35	91.4
1H-4, 25-26	4.75	88.23
1H-4, 57-60	5.07	89.72
1H-4, 135-136	5.85	88.24
1H-5, 25-26	6.25	90.56
1H-5, 135-136	7.35	88.57
1H-6, 25-26	7.75	87.67
1H-6, 57-60	8.07	90.72
1H-6, 135-136	8.85	88.35
1H-7, 25-26	9.25	89.65
1H-7, 90-91	9.90	86.92
2H-1, 25-26	10.35	88.21
2H-1, 135-136	11.45	88.20
2H-2, 25-26	11.85	88.50
2H-2, 56-58	12.16	90.41
2H-2, 135-136	12.95	88.74
2H-3, 25-26	13.35	86.29
2H-3, 135-136	14.45	88.19
2H-4, 25-26	14.85	90.0
2H-4, 56-58	15.16	88.60
2H-4, 135-136	15.95	90.80
2H-5, 25-26	16.35	88.53
2H-5, 135-136	17.45	89.67
2H-6, 25-26	17.85	90.77
2H-6, 56-58	18.16	90.69
2H-6, 105-106	18.65	91.16
3H-1, 25-26	19.95	88.23
3H-1, 135-136	21.05	91.01
3H-2, 25-26	21.45	91.09
3H-2, 46-49	21.66	92.29
3H-2, 135-136	22.55	91.07
3H-3, 25-26	22.95	91.02
3H-3, 135-136	24.05	90.29
3H-4, 25-26	24.45	91.26
3H-4, 46-49	24.66	91.84
3H-5, 25-26	25.95	90.38
3H-5, 135-136	27.05	91.15
3H-6, 25-26	27.45	89.95
3H-6, 46-49	27.66	92.12
3H-6, 135-137	28.55	89.69
3H-7, 25-26	28.95	89.87
4H-1, 25-26	29.65	87.21
4H-1, 135-136	30.75	89.13
4H-2, 25-26	31.15	91.90
4H-2, 47-50	31.37	89.77
4H-2, 135-136	32.25	89.08
4H-3, 25-26	32.65	97.65
4H-3, 135-136	33.75	89.33
4H-4, 25-26	34.15	88.77
4H-4, 47-50	34.37	90.77
4H-4, 135-136	35.25	90.59
4H-5, 25-26	35.65	88.99
6H-1, 135-136	50.05	92.78
6H-2, 25-28	50.45	91.17
6H-2, 79-80	50.99	91.72
6H-2, 135-136	51.55	91.02
6H-3, 25-26	51.95	90.34
6H-3, 135-136	53.05	93.80
6H-4, 25-28	53.45	89.36
6H-4, 79-80	53.99	92.55
6H-4, 135-136	54.55	93.80
6H-5, 25-26	54.95	92.47
6H-5, 135-136	56.05	91.06
6H-6, 25-28	56.45	90.05
6H-6, 79-80	56.99	89.88
6H-6, 135-136	57.55	91.13
6H-7, 25-26	57.95	90.13
7H-1, 25-26	58.55	88.09
7H-1, 135-136	59.65	89.45
7H-2, 25-26	60.05	89.38

Table 5 (continued).

Sample interval (cm)	Depth (mbsf)	Carbonate (wt%)
7H-2, 56-58	60.36	88.14
7H-2, 135-136	61.15	90.53
7H-3, 25-26	61.55	89.32
7H-3, 135-136	62.65	92.73
7H-4, 25-26	63.05	91.47
7H-4, 56-58	63.36	90.55
7H-4, 135-136	64.15	91.21
7H-5, 25-26	64.55	91.92
7H-6, 25-26	66.05	89.22
7H-6, 56-58	66.36	85.65
7H-6, 135-136	67.15	88.95
8H-1, 25-26	68.25	89.71
8H-1, 135-136	69.35	92.22
8H-2, 25-26	69.75	92.72
8H-2, 57-60	70.07	91.85
8H-2, 135-136	70.85	92.39
8H-3, 25-26	71.25	90.57
8H-3, 135-136	72.35	91.8
8H-4, 25-26	72.75	91.18
8H-4, 57-60	73.07	93.67
8H-4, 135-136	73.85	92.30
8H-5, 25-26	74.25	92.09
8H-5, 135-136	75.35	89.73
8H-6, 25-26	75.75	93.27
8H-6, 57-60	76.07	89.33
8H-6, 135-136	76.85	87.21
9H-1, 25-26	77.85	90.00
9H-1, 135-136	78.95	93.14
9H-2, 25-26	79.35	92.94
9H-2, 57-60	79.67	88.88
9H-2, 135-136	80.45	91.85
9H-3, 25-26	80.85	92.94
9H-3, 135-136	81.95	92.91
9H-4, 25-26	82.35	91.79
9H-4, 70-73	82.80	91.56
9H-4, 135-136	83.45	89.68
9H-5, 25-26	83.85	90.42
9H-5, 135-136	84.95	98.51
9H-6, 25-26	85.35	93.92
9H-6, 57-60	85.67	92.76
9H-6, 135-136	86.45	89.97
10H-1, 20-21	87.50	92.90
10H-1, 140-141	88.70	91.85
10H-2, 20-21	89.00	90.27
10H-2, 140-141	90.20	91.47
10H-3, 20-21	90.50	89.69
10H-3, 68-70	90.98	90.39
10H-3, 140-141	91.70	89.88
10H-4, 20-21	92.00	90.17
10H-4, 140-141	93.20	88.50
10H-5, 20-21	93.50	92.05
10H-5, 80-81	94.10	91.07
10H-6, 20-21	95.00	90.41
10H-6, 52-54	95.32	92.58
10H-6, 140-141	96.20	93.2
10H-7, 12-13	96.42	92.94
10H-7, 80-81	97.10	91.64
11H-1, 25-26	97.15	92.51
11H-1, 135-136	98.25	92.42
11H-2, 25-26	98.65	92.13
11H-2, 86-88	99.26	92.24
11H-2, 135-136	99.75	90.82
11H-3, 25-26	100.15	91.59
11H-3, 135-136	101.25	91.83
11H-4, 25-26	101.65	91.08
11H-4, 53-55	101.93	89.11
11H-4, 135-136	102.75	93.27
11H-5, 25-26	103.15	91.64
11H-5, 135-136	104.25	93.33
11H-6, 25-26	104.65	92.5
11H-6, 135-136	105.75	92.75
11H-7, 11-13	106.01	86.69
11H-7, 25-26	106.15	93.62
12H-1, 25-26	106.85	85.04
12H-1, 135-136	107.95	80.2
12H-2, 25-26	108.35	90.56
12H-2, 135-136	109.45	91.25

Table 5 (continued).

Sample interval (cm)	Depth (mbsf)	Carbonate (wt%)
12H-3, 25-26	109.85	87.96
12H-3, 135-136	110.95	88.09
12H-4, 25-26	111.35	77.3
12H-4, 135-136	112.45	88.44
12H-5, 25-26	112.85	83.66
12H-5, 135-136	113.95	83.65
12H-6, 25-26	114.35	80.42
13H-2, 20-22	117.90	88.65
13H-4, 13-15	120.83	89.3
13H-6, 20-22	123.90	89.12
14H-1, 25-26	126.05	81.27
14H-1, 135-136	127.15	82.64
14H-2, 7-9	127.37	89.70
14H-2, 25-26	127.55	84.67
14H-2, 135-136	128.65	78.13
14H-3, 25-26	129.05	88.91
14H-3, 135-136	130.15	82.39
14H-4, 12-14	130.42	89.20
14H-4, 25-26	130.55	87.92
14H-4, 135-136	131.65	83.61
14H-5, 25-26	132.05	81.01
14H-5, 135-136	133.15	86.1
14H-6, 8-10	133.38	86.58
14H-6, 25-26	133.55	87.51
14H-6, 135-136	134.65	81.3
14H-7, 25-26	135.05	84.01
15H-1, 25-26	135.75	88.27
15H-1, 135-136	136.85	88.80
15H-2, 25-26	137.25	87.77
15H-2, 135-136	138.35	89.23
15H-3, 25-26	138.75	91.86
15H-3, 53-55	139.03	91.39
15H-3, 135-136	139.85	90.08
15H-4, 25-26	140.25	92.06
15H-4, 135-136	141.35	88.50
15H-5, 25-26	141.75	90.09
15H-5, 135-136	142.85	89.17
15H-6, 25-26	143.25	90.43
15H-6, 135-136	144.35	87.90
15H-7, 25-26	144.75	88.13
15H-7, 28-30	144.78	86.14
16H-1, 25-26	145.45	85.79
16H-1, 135-136	146.55	83.96
16H-2, 25-26	146.95	86.93
16H-2, 135-136	148.05	89.32
16H-3, 25-26	148.45	88.72
16H-3, 86-88	149.06	87.88
16H-3, 135-136	149.55	87.92
16H-4, 25-26	149.95	89.15
16H-4, 135-136	151.05	88.65
16H-5, 25-26	151.45	89.26
16H-5, 51-53	151.71	88.43
16H-6, 25-26	152.95	88.65
16H-6, 135-136	154.05	92.91
16H-7, 25-26	154.45	87.72
17H-1, 25-26	155.15	88.85
17H-1, 135-136	156.25	92.28
17H-2, 25-26	156.65	82.36
17H-2, 50-53	156.90	90.66
17H-2, 135-136	157.75	90.95
17H-3, 25-26	158.15	88.18
17H-3, 135-136	159.25	88.44
17H-4, 25-26	159.65	89.35
17H-4, 50-53	159.90	88.68
17H-4, 135-136	160.75	88.22
17H-5, 25-26	161.15	89.65
17H-5, 135-136	162.25	89.82
17H-6, 25-26	162.65	90.31
17H-6, 50-53	162.90	91.05
17H-6, 135-136	163.75	91.06
17H-7, 25-26	164.15	89.89
18H-1, 25-26	164.85	90.81
18H-1, 135-136	165.95	88.06
18H-2, 25-26	166.35	88.32
18H-2, 80-83	166.90	87.68
18H-2, 135-136	167.45	92.82
18H-3, 25-26	167.85	87.54

Table 5 (continued).

Sample interval (cm)	Depth (mbsf)	Carbonate (wt%)
18H-3, 135-136	168.95	88.87
18H-4, 25-26	169.35	90.43
18H-4, 80-83	169.90	90.09
18H-4, 135-136	170.45	90.70
18H-5, 25-26	170.85	83.04
18H-5, 135-136	171.95	88.12
18H-6, 25-26	172.35	90.33
18H-6, 80-83	172.90	88.92
18H-6, 135-136	173.45	87.22
19H-1, 25-26	174.75	89.12
19H-1, 135-136	175.85	85.60
19H-2, 25-26	176.25	89.97
19H-2, 111-112	177.11	90.84
19H-3, 25-26	177.75	91.25
19H-3, 50-53	178.00	90.82
19H-3, 135-136	178.85	92.28
19H-4, 25-26	179.25	92.13
19H-4, 85-86	179.85	92.13
20H-1, 25-26	184.15	91.73
20H-1, 135-136	185.25	91.72
20H-2, 25-26	185.65	92.41
20H-2, 57-60	185.97	91.17
20H-2, 135-136	186.75	80.92
20H-3, 25-26	187.15	91.88
20H-3, 135-136	188.25	90.6
20H-4, 25-26	188.65	91.54
20H-4, 135-136	189.75	93.47
20H-5, 25-26	190.15	91.32
20H-5, 60-63	190.50	92.51
20H-5, 135-136	191.25	89.37
20H-6, 25-26	191.65	91.12
21H-1, 25-26	193.75	92.87
21H-1, 135-136	194.85	90.5
21H-2, 25-26	195.25	89.01
21H-2, 135-136	196.35	92.13
21H-3, 25-26	196.75	92.68
21H-3, 57-60	197.07	93.09
21H-3, 135-136	197.85	90.99
21H-4, 25-26	198.25	92.7
21H-4, 135-136	199.35	91.33
21H-5, 25-26	199.75	94.29
21H-5, 135-136	200.85	93.07
21H-6, 25-26	201.25	93.8
21H-6, 57-60	201.57	94.25
115-709C-		
8H-5, 130-133	70.90	91.08
8H-5, 139-142	70.99	89.82
9H-5, 130-133	80.50	92.97
9H-5, 140-143	80.60	90.54
11H-4, 137-139	98.37	89.56
11H-4, 145-147	98.45	91.59
12H-5, 114-116	109.34	93.58
12H-5, 128-130	109.48	77.33
13H-5, 130-132	119.10	85.74
13H-5, 142-144	119.22	84.45
14H-5, 112-114	128.52	89.98
14H-5, 127-129	128.67	88.58
15H-4, 129-131	136.89	88.07
16H-5, 130-132	148.10	83.99
16H-5, 141-143	148.21	83.88
17H-4, 141-143	156.41	89.07
17H-4, 148-150	156.48	89.23
18H-5, 109-111	167.29	87.56
18H-5, 128-130	167.48	87.43
19H-5, 136-138	177.26	84.76
19H-5, 148-150	177.38	80.78
20H-5, 128-130	186.78	91.8
20H-5, 141-143	186.91	85.78
21X-1, 25-26	189.35	91.92
21X-1, 135-136	190.45	93.12
21X-2, 25-26	190.85	92.63
21X-2, 135-136	191.95	91.37
21X-3, 25-26	192.35	85.15
21X-3, 135-136	193.45	91.68
21X-4, 25-26	193.85	94.54

Table 5 (continued).

Sample interval (cm)	Depth (mbsf)	Carbonate (wt%)
21X-4, 135-136	194.95	90.96
21X-5, 25-26	195.35	92.72
21X-5, 130-133	196.40	90.57
21X-5, 135-136	196.45	91.86
21X-5, 140-143	196.50	85.78
21X-6, 25-26	196.85	90.12
21X-6, 135-136	197.95	94.11
22X-1, 27-28	198.97	87.11
22X-1, 137-138	200.07	92.10
22X-2, 27-28	200.47	87.11
22X-2, 137-138	201.57	94.18
22X-3, 27-28	201.97	94.66
22X-3, 137-138	203.07	94.09
22X-4, 27-28	203.47	93.55
22X-4, 137-138	204.57	90.07
22X-5, 27-28	204.97	93.07
22X-5, 137-138	206.07	87.76
22X-5, 140-143	206.10	93.06
22X-5, 145-148	206.15	93.43
23X-1, 25-26	208.65	92.05
23X-1, 135-136	209.75	93.57
23X-2, 25-26	210.15	91.88
23X-2, 135-136	211.25	88.19
23X-3, 25-26	211.65	93.32
23X-3, 135-136	212.75	93.98
23X-4, 25-26	213.15	94.09
23X-4, 135-136	214.25	94.15
23X-5, 25-26	214.65	92.27
23X-5, 135-136	215.75	91.66
24X-1, 25-26	218.25	92.90
24X-1, 135-136	219.35	94.40
24X-2, 25-26	219.75	92.95
24X-2, 135-136	220.85	93.20
24X-3, 25-26	221.25	91.24
24X-3, 135-136	222.35	89.58
24X-4, 25-26	222.75	91.38
24X-4, 135-136	223.85	92.22
24X-5, 25-26	224.25	91.06
24X-5, 135-136	225.35	82.51
24X-5, 139-142	225.39	91.18
24X-5, 144-146	225.44	90.77
24X-6, 25-26	225.75	92.68
25X-1, 25-26	227.95	90.67
25X-1, 135-136	229.05	92.12
25X-2, 25-26	229.45	92.52
25X-2, 135-136	230.55	91.18
25X-3, 25-26	230.95	86.91
25X-3, 135-136	232.05	90.16
25X-4, 25-26	232.45	80.73
25X-4, 135-136	233.55	91.9
25X-5, 25-26	233.95	86.13
25X-5, 133-136	235.03	84.59
25X-5, 135-136	235.05	72.66
25X-5, 140-143	235.10	83.15
26X-1, 25-26	237.65	81.38
26X-1, 135-136	238.75	93.59
26X-2, 25-26	239.15	86.85
26X-2, 135-136	240.25	93.86
26X-3, 25-26	240.65	82.01
26X-3, 86-89	241.26	92.11
26X-3, 135-136	241.75	93.60
26X-4, 25-26	242.15	91.61
26X-4, 135-136	243.25	94.33
26X-5, 25-26	243.65	94.94
26X-5, 135-136	244.75	94.64
26X-5, 138-140	244.78	95.94
26X-6, 25-26	245.15	95.94
26X-6, 135-136	246.25	95.25
27X-1, 25-26	247.25	93.75
27X-1, 135-136	248.35	93.82
27X-2, 25-26	248.75	93.18
27X-2, 135-136	249.85	89.97
27X-3, 25-26	250.25	91.84
27X-3, 60-63	250.60	91.89
27X-3, 135-136	251.35	90.45
27X-4, 25-26	251.75	92.42
27X-4, 135-136	252.85	91.21

Table 5 (continued).

Sample interval (cm)	Depth (mbsf)	Carbonate (wt%)
28X-1, 25-26	256.95	91.05
28X-1, 135-136	258.05	92.62
28X-2, 25-26	258.45	92.15
28X-2, 110-112	259.30	90.91
28X-3, 25-26	259.95	92.82
28X-3, 142-144	261.12	91.80
28X-3, 145-146	261.15	92.02
28X-4, 21-22	265.00	91.91
29X-1, 25-26	266.65	87.77
29X-1, 135-136	267.75	93.07
29X-2, 25-26	268.15	91.3
29X-2, 135-136	269.25	92.59
29X-3, 25-26	269.65	92.88
29X-3, 65-68	270.05	94.59
29X-3, 135-136	270.75	93.44
29X-4, 25-26	271.15	92.21
29X-4, 135-136	272.25	92.07
29X-5, 25-26	272.65	92.19
29X-5, 135-136	273.75	92.38
29X-6, 25-26	274.15	91.28
29X-6, 47-50	274.37	93.69
29X-6, 135-136	275.25	92.56
29X-7, 25-26	275.65	91.78
30X-1, 25-26	276.35	92.77
30X-1, 135-136	277.45	90.15
30X-2, 135-136	278.95	91.69
30X-3, 25-26	279.35	89.7
30X-3, 60-63	279.70	91.75
30X-3, 135-136	280.45	91.20
30X-4, 25-26	280.85	91.74
30X-4, 135-136	281.95	89.71
30X-5, 25-26	282.35	91.18
30X-5, 135-136	283.45	89.43
30X-6, 25-26	283.85	88.24
30X-6, 60-63	284.20	90.97
30X-7, 25-26	285.00	78.34
31X-1, 25-26	286.05	91.05
31X-1, 135-136	287.15	94.19
31X-2, 25-26	287.55	93.9
31X-2, 135-136	288.65	93.96
31X-3, 25-26	289.05	94.15
31X-3, 52-55	289.32	88.72
31X-3, 135-136	290.15	93.64
31X-4, 25-26	290.55	92.53
31X-5, 25-26	292.05	80.66
31X-5, 135-136	293.15	86.50
31X-6, 25-26	293.55	85.68
31X-6, 107-110	294.00	87.75
32X-1, 25-26	295.65	88.64
32X-1, 135-136	296.75	88.43
32X-2, 25-26	297.15	91.27
32X-2, 135-136	298.25	87.79
32X-3, 25-26	298.65	91.18
32X-3, 57-60	298.97	91.30
32X-3, 135-136	299.75	90.53
32X-4, 25-26	300.15	89.65
32X-4, 135-136	301.25	92.84
32X-5, 25-26	301.65	89.65
32X-5, 57-60	301.97	90.71
32X-5, 135-136	302.75	89.2
32X-6, 25-26	303.15	93.0
32X-6, 135-136	304.25	89.58
32X, CC, 25-26	304.95	89.74
33X-1, 25-26	305.35	88.34
33X-1, 135-136	306.45	89.88
33X-2, 25-26	306.85	92.06
33X-2, 135-136	307.95	87.74
33X-3, 25-26	308.35	90.59
33X-3, 63-66	308.73	91.00
33X-3, 135-136	309.45	88.95
33X-4, 25-26	309.85	91.5
33X-4, 135-136	310.95	84.91
33X-5, 25-26	311.35	89.22
33X-5, 63-66	311.73	90.92
33X-5, 135-136	312.45	92.01
33X-6, 25-26	312.85	90.47

Table 5 (continued).

Sample interval (cm)	Depth (mbsf)	Carbonate (wt%)
34X-1, 25-26	315.05	87.28
34X-1, 135-136	316.15	87.9
34X-2, 25-26	316.55	85.84
34X-2, 135-136	317.65	89.35
34X-3, 25-26	318.05	89.29
34X-3, 124-126	319.04	91.03
34X-3, 125-128	319.05	89.94
34X-3, 135-136	319.15	91.19
34X-4, 25-26	319.55	90.3
34X-4, 135-136	320.65	92.92
34X-5, 25-26	321.05	92.39
34X-5, 63-65	321.43	92.59
34X-5, 65-67	321.45	93.28
34X-5, 135-136	322.15	90.38
34X-6, 25-26	322.55	92.32
34X-6, 135-136	323.65	94.17
35X-1, 28-29	324.68	83.89
35X-1, 135-136	325.75	91.08
35X-2, 25-26	326.15	87.05
35X-2, 54-56	326.44	81.51
35X-2, 63-65	326.53	94.95
35X-2, 135-136	327.25	91.01
35X-3, 25-26	327.65	86.16
35X-3, 140-141	328.80	84.04
35X-4, 25-26	329.15	83.61
35X-4, 135-136	330.25	88.52
35X-5, 30-31	330.70	83.63
35X-5, 50-52	330.90	86.11
35X-5, 52-54	330.92	83.46
35X-5, 138-139	331.78	87.29
35X-6, 29-30	332.19	85.42
35X-6, 144-145	333.34	86.67
36X-1, 25-26	334.35	86.13
36X-1, 135-136	335.45	86.74
36X-2, 25-26	335.85	86.57
36X-2, 92-94	336.52	85.73
36X-2, 95-97	336.55	82.46
36X-2, 135-136	336.95	85.50
36X-3, 25-26	337.35	87.10
36X-3, 135-136	338.45	87.19
36X-4, 25-26	338.85	86.18
37X-1, 24-25	344.14	80.91
37X-1, 135-136	345.25	82.84
37X-2, 18-19	345.58	78.56
37X-2, 71-73	346.11	81.16
37X-2, 135-136	346.75	76.89
37X-3, 25-26	347.15	79.46
37X-3, 135-136	348.25	83.65
37X-4, 26-27	348.66	75.71
37X-5, 25-26	350.15	78.49
37X-5, 67-69	350.57	81.68
37X-5, 135-136	351.25	81.66
37X-6, 25-26	351.65	78.51
37X-6, 135-136	352.75	84.75
37X-7, 1-3	352.91	89.49
37X-7, 25-26	353.15	84.69

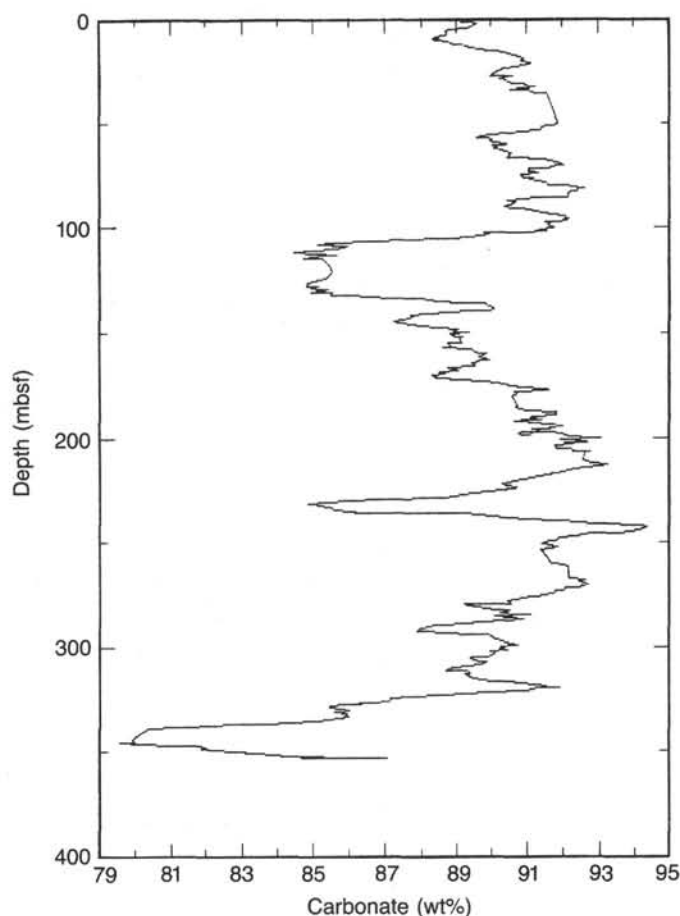


Figure 21. Ten-sample running mean of carbonate data shown in Figure 20 and Table 5, plotted as a function of sub-bottom depth.

The basement is extremely irregular and the east and west margins are aligned with transform faults, so it is probable that this feature was formed at the spreading ridge by somewhat excessive volcanism. For our purposes, the Madingley Rise provided a raised platform from which to sample pelagic sediments from several depths, largely protected from the disturbance of turbidites.

Site 709 is located in a small basin perched near the summit of the platform, at water depths of 3038.2 m. An initial site was selected from seismic reflection profile RC12-15 (Fig. 33), near the crossing with a Wilkes 921 profile. The *JOIDES Resolution* surveyed the area on 5 June 1987, and the new single-channel seismic (SCS) profile showed that sediments at the selected site were much more disturbed than previously realized. We continued our recording, therefore, to the east and north where the Wilkes 921 profile promised a better section. This we found 5 nmi north of the original site (Fig. 34).

Here, 0.40 s of flat-lying, parallel, weak reflectors overlie a strong basement surface. The topography falls away gently in all directions so this area seemed safe from turbidite problems. Drilling proved this to be the true. From shipboard measurements (see "Physical Properties" section, this chapter) on the cored material, we estimate *P*-wave velocities in the section to be around 1550 m/s. Hence, the total sediment thickness must not be very much thicker than the roughly 350 m drilled at Site 709.

DOWNHOLE MEASUREMENTS

Heat-flow measurements were made at Site 709 with thermal conductivity measurements in Holes 709A, 709B, and 709C,

The grain wet-bulk density and carbonate content are constant downhole. The discrete and continuous impedance profiles are in good agreement and exhibit no major contrasts. Weak seismic reflectors are predicted. Shear-wave velocity measurements are scattered over a great range and show no obvious correlation to the lithology, whereas the shear strength measurements allow a hole-to-hole correlation after the first occurrence of chalk in the ooze. Increases in shear strength indicate a gradual increase of consolidation with depth.

SEISMIC STRATIGRAPHY

The Madingley Rise is a $1^{\circ} \times 2^{\circ}$ trapezoidal block of ocean crust elevated as much as 1000 m above the surrounding abyssal plain, between the Seychelles Bank-Saya de Malha Bank ridge and the Carlsberg Ridge in the western Indian Ocean (Fig. 32).

Table 6. Percentage of organic carbon, Holes 709A and 709C.

Sample interval (cm)	Depth (mbsf)	Organic carbon (%)
115-709A-		
1H-2, 25-26	1.75	0
1H-5, 25-26	6.25	0
2H-2, 25-26	11.85	0
2H-5, 25-26	16.35	0.03
3H-2, 135-136	22.55	0
3H-5, 25-26	25.95	0.01
4H-2, 25-26	31.15	0
4H-5, 25-26	35.65	0
6H-3, 135-136	53.05	0
7H-3, 25-26	61.55	0.04
8H-3, 25-26	71.25	0.18
9H-3, 25-26	80.85	0
10H-3, 140-141	91.70	0.01
11H-3, 25-26	100.15	0.08
12H-3, 25-26	109.85	0
14H-3, 25-26	129.05	0
15H-3, 25-26	138.75	0.02
16H-3, 25-26	148.45	0.05
17H-3, 25-26	158.15	0.13
18H-3, 25-26	167.85	0.04
19H-3, 25-26	177.55	0.04
20H-3, 25-26	187.15	0.13
21H-3, 25-26	196.75	0
115-709C-		
21X-3, 25-26	192.35	0
22X-3, 27-28	201.97	0
23X-3, 25-26	211.65	0.13
24X-3, 25-26	221.25	0.05
25X-3, 25-26	230.95	0
26X-3, 25-26	240.65	0
27X-3, 25-26	250.25	0
28X-3, 25-26	259.95	0.13
29X-3, 25-26	269.65	0
30X-3, 25-26	279.35	0.02
31X-3, 25-26	289.05	0
32X-3, 25-26	298.65	0.06
33X-3, 25-26	308.35	0
34X-3, 25-26	318.05	0.66
35X-3, 24-25	327.64	0.07
36X-3, 25-26	337.35	0.07
37X-3, 25-26	347.15	0

and with downhole temperature measurements in Hole 709C. The thermal conductivity measurements were made with both the normal needle-probe apparatus for soft sediments (Von Herzen and Maxwell, 1959) and a needle probe embedded in the surface of a plate of known thermal conductivity, the "half-space" probe. This is similar to the "QTM" device used on the *Glomar Challenger* (Horai, 1981), except that here the probe is rigidly attached to the bottom of a small water bath in which the samples are immersed. The thermal conductivity measurements are discussed more fully in the "Physical Properties" section of this chapter.

Temperature measurements were made with two different temperature recorders. The first is the Yokota-Kinoshita-Uyeda (Y-K-U) probe (Yokota et al., 1980), which is mounted in the downhole pore-water/heat-flow probe. The second type of recorder is the Von Herzen miniature recorder which mounts within the cutting shoe of the APC core barrel (Horai and Von Herzen, 1985; Koehler and Von Herzen, 1986). Both recorders can be run together on a single measurement run, as is the normal practice. This provides redundancy in case one recorder malfunctions.

Three temperature measurement runs were made at Hole 709C at depths of 102.4, 140.8, and 189.1 mbsf. The Y-K-U probe worked well during all three runs, but the battery pack of

the Von Herzen probe failed during the third run, causing the loss of that run's data. The five good temperature measurement records are presented in the accompanying figures.

Figure 35 shows the Von Herzen instrument record for the first run, 102.4 mbsf. The initial part of the record, up to measurement #50, shows the temperatures in the shipboard lab and on deck as the tool is assembled and put into the drill pipe. The sharp but smooth decrease from measurement #50 to measurement #100 reflects the decrease in the surrounding water temperature as the tool descends through the drill pipe to the seafloor. The sharp temperature increase at measurement #105 shows the probe entering the sediments at the bottom of the hole. The steady, but slowly increasing, temperature record from measurement #105 to measurement #228 occurs as the temperature probe approaches equilibrium with the surrounding sediments.

The sharp increase at measurement #228 is caused by frictional heating as the probe is withdrawn from the sediments. The probe is then pulled up the pipe to the mud line and allowed to equilibrate there in order to obtain a bottom water temperature measurement (measurements #265 to #280). The probe is then brought to the surface.

Figure 36 shows the corresponding Y-K-U recorder record for the first temperature run. The essential points are the same, except that the Y-K-U probe, with a different sampling rate, records the return to the surface and temperatures on deck.

Figures 37 and 38 show the Von Herzen and Y-K-U records for the second temperature run, 140.8 mbsf. Note the increase of temperature at measurement #111 in the Von Herzen record. This represents a slight disturbance to the probe causing additional frictional heating; the temperature records are long enough that the data quality is not compromised. The other features of the record are similar to that of the first run.

Figure 39 shows the Y-K-U record for the third run, 189.1 mbsf. There is no Von Herzen instrument record for this run. Again, the features of the record are similar, although the temperature increase at measurement #36 appears to be an erroneous reading.

The five sediment temperature measurements made during these three runs are presented in Table 12. The records displayed in the accompanying figures are remarkable in that there is little evidence of frictional heating caused by initial entry into the sediments. This is sometimes observed in normal marine heat-flow measurements when a probe penetrates soft sediments, but it is quite rare in DSDP/ODP measurements. The cause, however, is the same: the sediments are so soft that there is no significant frictional heating when the probe is thrust into them.

Since these temperatures are so stable, we have not found it necessary at this time to apply the corrections developed by Horai and Von Herzen (1985) to the measurements. The Y-K-U temperatures reported in the table have been revised downward by 0.33°C in order to bring the bottom-water temperatures measured by the Y-K-U probe into agreement with the temperatures measured by the Von Herzen probe. It is felt that the Von Herzen probes are more accurately calibrated for absolute temperatures.

Heat flow is the product of the temperature gradient and the thermal conductivity. The thermal conductivity measurements at Site 709 (Fig. 40) show a fair amount of small-scale variability (especially at greater depths), but few gross changes aside from a pronounced decrease in the interval from 160 to 200 mbsf. When there is variability in the thermal conductivity with depth, it is more appropriate to determine the heat flow from a regression between temperature and integrated thermal resistivity (thermal resistivity is the inverse of thermal conductivity). Figure 41 shows the depth integral of thermal resistivity plotted vs. depth below the seafloor. It is easy to see the basic uniformity of the thermal resistivity (and conductivity) with depth, except for the interval mentioned above.

Table 7. Index-properties data, Site 709.

Sample interval (cm)	Depth (mbsf)	Water content (%)	Porosity (%)	Wet-bulk density (g/cm ³)	Dry-bulk density (g/cm ³)	Grain density (g/cm ³)	Carbonate content (wt%)
115-709A-							
1H-2, 57	2.07	45.39	68.72	1.56	0.85	2.67	91.05
1H-4, 57	5.07	46.99	70.71	1.55	0.82	2.75	89.72
1H-6, 57	8.07	46.65	70.98	1.58	0.84	2.83	90.72
2H-2, 56	12.16	45.56	69.16	1.59	0.86	2.71	90.41
2H-4, 56	15.16	46.41	69.85	1.55	0.83	2.70	88.60
2H-6, 54	18.14	41.92	65.46	1.66	0.96	2.66	90.69
3H-2, 46	21.66	41.71	65.94	1.62	0.94	2.74	92.25
3H-4, 46	24.66	50.18	73.30	1.52	0.76	2.75	91.84
3H-6, 46	27.66	42.48	66.37	1.61	0.92	2.70	92.12
4H-2, 47	31.37	43.83	67.51	1.61	0.91	2.69	89.77
4H-4, 47	34.37	42.69	66.24	1.61	0.92	2.66	90.77
6H-2, 25	50.45	41.48	65.89	1.66	0.97	2.76	91.17
6H-4, 25	53.45	41.68	65.65	1.64	0.95	2.71	89.36
6H-6, 25	56.45	43.48	67.89	1.61	0.91	2.78	90.55
7H-2, 56	60.36	43.98	67.97	1.59	0.89	2.73	88.14
7H-4, 56	63.36	39.08	63.71	1.54	0.94	2.77	90.55
7H-6, 56	66.36	41.66	65.49	1.65	0.96	2.69	85.65
8H-2, 57	70.07	39.91	63.94	1.65	0.99	2.70	91.89
8H-4, 57	73.07	39.10	62.86	1.68	1.02	2.67	93.67
8H-6, 57	76.07	42.93	68.08	1.68	0.96	2.87	89.33
9H-2, 57	79.67	40.52	65.26	1.68	1.00	2.79	88.88
9H-4, 70	82.80	39.37	62.95	1.67	1.01	2.65	91.56
9H-6, 57	85.67	38.47	63.28	1.70	1.05	2.79	92.76
10H-3, 68	90.98	39.17	63.99	1.68	1.02	2.80	90.39
10H-6, 52	95.32	39.83	64.13	1.68	1.01	2.73	92.58
11H-2, 86	99.26	49.01	72.15	1.65	0.84	2.72	92.24
11H-4, 53	101.93	47.87	70.62	1.70	0.88	2.64	89.11
11H-7, 11	106.01	34.57	58.74	1.69	1.11	2.73	86.69
13H-2, 20	117.90	38.66	64.21	1.74	1.06	2.88	88.65
13H-4, 13	120.83	50.83	73.47	1.75	1.01	2.70	89.30
13H-6, 86	124.56	35.64	59.87	1.71	1.10	2.73	89.12
14H-2, 7	127.37	37.60	61.54	1.68	1.05	2.69	89.70
14H-6, 8	133.38	37.15	62.14	1.72	1.08	2.81	86.58
15H-3, 53	139.03	36.23	60.77	1.72	1.09	2.76	91.38
15H-7, 28	144.78	35.94	60.33	1.76	1.13	2.75	86.14
16H-3, 86	149.06	36.16	61.11	1.73	1.10	2.81	87.88
16H-6, 51	153.21	35.34	59.95	1.72	1.11	2.77	88.43
17H-2, 50	156.90	39.11	63.88	1.66	1.01	2.79	90.66
17H-4, 50	159.90	34.52	58.57	1.71	1.12	2.72	88.68
18H-2, 80	166.90	35.38	59.62	1.73	1.12	2.73	87.68
18H-4, 80	169.90	33.72	58.00	1.78	1.18	2.75	90.09
18H-6, 80	172.90	36.08	64.23	1.75	1.12	2.61	88.92
19H-3, 50	178.00	34.71	59.12	1.78	1.16	2.76	90.82
20H-2, 57	185.97	38.73	62.85	1.71	1.05	2.71	91.17
20H-5, 60	190.50	40.56	65.26	1.67	0.99	2.79	92.51
21H-3, 57	197.07	38.37	62.17	1.70	1.05	2.67	93.09
21H-6, 57	201.57	37.42	61.83	1.71	1.07	2.74	94.25
115-709B-							
1H-2, 60	2.10	48.58	71.52	1.51	0.78	2.68	88.83
2H-1, 50	4.30	47.62	71.08	1.53	0.80	2.73	87.52
2H-5, 50	10.30	47.96	71.58	1.53	0.80	2.76	87.17
3H-3, 57	16.97	44.67	69.04	1.56	0.86	2.79	90.35
4H-3, 57	26.67	41.65	67.01	1.62	0.95	2.88	89.74
4H-6, 57	31.17	46.04	70.01	1.57	0.85	2.77	90.38
5H-3, 70	36.50	44.08	68.09	1.59	0.89	2.74	91.12
5H-3, 133	37.13	47.75	71.56	1.53	0.80	2.78	90.18
5H-5, 142	40.22	45.98	69.68	1.57	0.85	2.73	89.19
5H-6, 40	40.70	44.03	68.38	1.61	0.90	2.78	90.11
6H-3, 56	45.96	42.48	66.69	1.60	0.92	2.74	89.47
6H-6, 56	50.46	42.09	66.52	1.61	0.93	2.77	92.26
7H-3, 40	55.40	42.45	66.28	1.61	0.92	2.70	89.14
7H-6, 40	59.90	40.88	65.50	1.64	0.97	2.78	89.41
7H-6, 142	60.92	43.01	67.10	1.61	0.92	2.73	87.71
8H-3, 55	65.25	43.79	68.13	1.61	0.90	2.78	90.15
8H-6, 60	69.80	43.27	67.26	1.60	0.91	2.72	96.96
9H-3, 60	74.90	42.83	66.48	1.63	0.93	2.68	88.34
9H-6, 60	79.40	42.22	66.20	1.65	0.95	2.71	89.54
10H-6, 142	89.92	41.60	65.66	1.64	0.96	2.72	92.50
11H-3, 85	94.45	41.00	65.56	1.65	0.97	2.77	89.84
11H-6, 85	98.95	41.00	65.56	1.65	0.97	2.77	91.16
12H-3, 83	104.13	40.00	64.27	1.66	0.99	2.73	92.66
13H-3, 90	113.80	38.22	62.14	1.71	1.06	2.69	88.14
13H-6, 65	118.05	37.56	62.26	1.72	1.08	2.78	87.54
14H-3, 84	123.34	35.80	59.59	1.71	1.10	2.68	85.81
14H-6, 69	127.69	35.01	59.80	1.75	1.14	2.80	86.83
15H-3, 88	133.08	36.54	60.20	1.73	1.10	2.66	88.87
15H-6, 70	137.40	38.17	62.11	1.68	1.04	2.69	87.44
16H-2, 84	141.24	36.93	60.75	1.70	1.07	2.68	89.44

Table 7 (continued).

Sample interval (cm)	Depth (mbsf)	Water content (%)	Porosity (%)	Wet-bulk density (g/cm ³)	Dry-bulk density (g/cm ³)	Grain density (g/cm ³)	Carbonate content (wt%)
115-709B-							
17H-3, 85	152.45	36.64	62.29	1.75	1.11	2.89	86.26
17H-6, 58	156.68	36.01	60.40	1.73	1.11	2.73	87.06
18H-3, 81	162.11	38.07	62.41	1.68	1.04	2.74	89.90
18H-6, 63	166.43	35.95	60.01	1.73	1.11	2.71	88.49
19H-3, 77	171.77	33.90	58.40	1.76	1.16	2.78	91.41
19H-6, 70	176.20	32.35	55.68	1.79	1.21	2.66	82.57
21X-6, 47	195.17	40.19	64.41	1.66	0.99	2.73	92.04
22X-3, 75	200.55	43.27	67.07	1.61	0.91	2.70	90.50
22X-6, 120	205.50	37.51	61.64	1.70	1.06	2.71	93.14
23X-3, 56	210.06	39.17	63.27	1.68	1.02	2.71	93.77
23X-6, 56	214.56	46.94	66.61	1.71	0.91	2.68	90.83
24X-3, 57	219.67	38.75	63.30	1.70	1.04	2.76	92.19
24X-6, 57	224.17	41.61	65.73	1.63	0.95	2.72	88.99
25X-2, 57	227.87	41.70	65.55	1.65	0.96	2.69	91.79
25X-6, 57	233.87	40.68	64.66	1.65	0.98	2.70	91.35
26X-3, 57	239.07	40.16	64.86	1.67	1.00	2.78	91.76
26X-6, 74	243.64	41.75	66.20	1.63	0.95	2.76	92.66
27X-3, 67	248.77	38.08	62.30	1.72	1.07	2.72	92.95
115-709C-							
8H-5, 130	70.90	39.64	64.00	1.67	1.01	2.74	91.08
8H-5, 139	70.99	40.19	65.13	1.64	0.98	2.81	89.82
9H-5, 130	80.50	40.75	65.56	1.63	0.97	2.80	92.97
10H-5, 130	90.20	39.08	63.28	1.67	1.02	2.72	89.91
10H-5, 142	90.32	38.47	63.46	1.66	1.02	2.81	89.79
11H-4, 137	98.37	39.13	63.29	1.68	1.02	2.72	89.56
11H-4, 145	98.45	38.74	62.87	1.66	1.01	2.71	91.59
12H-5, 114	109.34	40.13	64.83	1.54	0.92	2.78	93.58
12H-5, 128	109.48	43.94	66.86	1.65	0.92	2.60	77.33
13H-5, 130	119.10	35.31	60.68	1.76	1.14	2.87	85.74
13H-5, 142	119.22	35.44	59.54	1.76	1.14	2.72	84.45
14H-5, 112	128.52	36.86	60.50	1.70	1.07	2.66	89.98
14H-5, 127	128.67	36.64	61.82	1.73	1.09	2.84	88.58
15H-4, 129	136.89	36.94	61.26	1.70	1.07	2.73	88.07
15H-4, 147	137.07	36.86	61.93	1.70	1.07	2.82	87.50
16H-5, 130	148.10	36.40	61.26	1.73	1.10	2.80	83.99
16H-5, 141	148.21	34.29	58.42	1.77	1.16	2.73	83.88
17H-4, 128	156.28	33.1	57.9	1.83	1.22	2.82	—
17H-4, 148	156.48	26.86	49.57	1.49	1.09	2.71	89.07
18H-5, 109	167.29	35.59	60.09	1.72	1.11	2.76	87.56
18H-5, 128	167.48	33.85	58.18	1.73	1.14	2.75	87.43
19H-5, 136	177.26	32.83	57.11	1.77	1.19	2.76	84.76
19H-5, 148	177.38	34.00	58.37	1.75	1.16	2.76	80.78
20H-3, 80	183.30	37.80	63.50	1.75	1.09	2.98	—
20H-5, 128	186.78	37.67	63.23	1.71	1.07	2.88	91.80
20H-4, 78	184.78	38.70	64.40	1.73	1.07	2.98	—
21X-1, 47	189.57	30.70	58.40	1.74	1.20	3.21	—
21X-5, 130	196.40	41.34	65.88	1.62	0.95	2.77	90.57
21X-5, 140	196.50	41.35	63.12	1.66	0.97	2.45	85.78
22X-5, 140	206.10	38.10	62.72	1.68	1.04	2.77	93.06
22X-5, 145	206.15	38.29	63.10	1.69	1.04	2.79	93.43
23X-5, 136	215.76	37.59	62.54	1.72	1.07	2.81	91.02
24X-5, 139	225.39	39.32	63.75	1.67	1.01	2.75	91.18
24X-5, 144	225.44	39.70	65.22	1.70	1.02	2.88	90.77
25X-5, 133	235.03	40.33	64.67	1.67	1.00	2.74	84.59
25X-5, 140	235.10	39.83	63.27	1.63	0.98	2.63	83.15
26X-5, 138	244.78	45.24	68.90	1.87	1.02	2.71	95.94
27X-3, 60	250.60	37.36	63.33	1.73	1.08	2.93	91.89
28X-3, 142	261.12	42.58	67.37	1.61	0.93	2.82	91.80
29X-3, 65	270.05	40.33	64.12	1.64	0.98	2.68	94.59
29X-6, 47	274.37	37.14	61.31	1.71	1.07	2.72	93.69
30X-3, 60	279.70	36.58	61.76	1.75	1.11	2.84	91.75
30X-6, 60	284.20	35.16	60.27	1.77	1.15	2.84	90.97
31X-3, 52	289.32	32.47	56.66	1.78	1.20	2.76	88.72
31X-6, 107	293.37	38.89	63.68	1.68	1.03	2.79	87.75
32X-3, 57	298.97	34.27	58.12	1.74	1.14	2.70	91.30
32X-5, 57	301.97	35.74	59.90	1.72	1.11	2.72	90.74
33X-3, 63	308.73	34.49	59.41	1.75	1.14	2.82	91.00
33X-5, 64	311.74	30.34	53.77	1.82	1.27	2.71	90.92
34X-3, 124	319.04	35.43	59.04	1.73	1.12	2.66	91.03
34X-3, 126	319.06	33.69	57.61	1.78	1.18	2.71	89.94
34X-5, 65	321.45	30.96	54.34	1.79	1.24	2.69	93.28
35X-2, 54	326.44	37.48	61.49	1.75	1.10	2.70	81.51
35X-5, 50	330.90	34.89	58.88	1.75	1.14	2.71	86.11
35X-5, 52	330.92	36.50	60.70	1.69	1.07	2.72	83.46
36X-2, 92	336.52	34.51	58.37	1.73	1.14	2.70	85.73
36X-2, 95	336.55	33.27	57.44	1.76	1.17	2.74	82.46
37X-2, 71	346.11	33.49	56.29	1.70	1.13	2.59	81.16
37X-5, 67	350.57	36.75	60.14	1.67	1.06	2.63	81.68
37X-7, 1	352.91	36.00	59.60	1.72	1.10	2.66	89.49

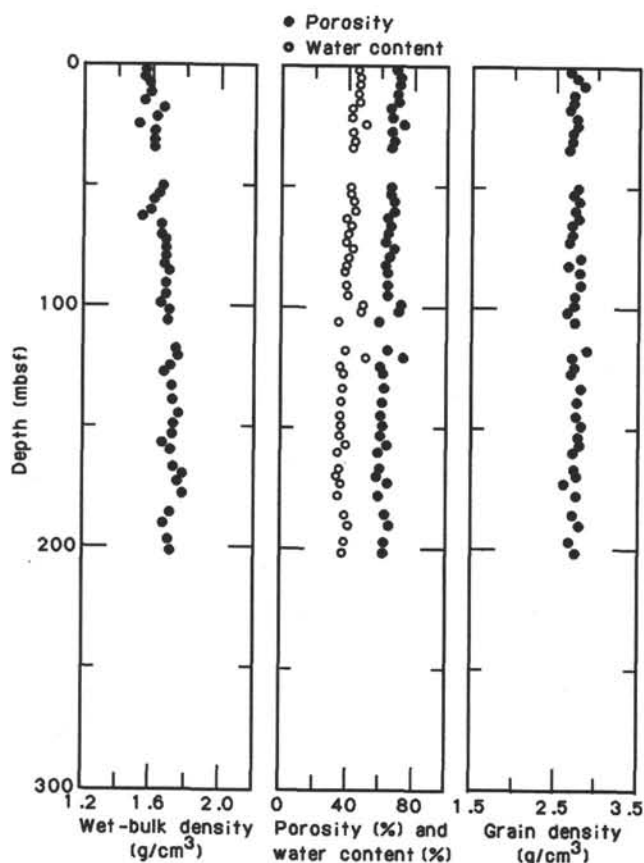


Figure 22. Index properties (wet-bulk density, water content, porosity, and grain density) for Hole 709A.

Temperature measurements are plotted vs. integrated thermal resistivity in Figure 42. The linear least-squares regression line through these measurements and the bottom-water temperature is shown; this regression gives a value for the heat flow of 32.4 mW/m², which is low for the estimated age of 55 Ma for the crust at this site. The "normal" heat flow for crust of this age should be about 70 mW/m². The sediments surrounding this site are fairly thick and uniform, so it is not apparent why this value is low, unless it reflects continuing fluid circulation within the basement underneath the sediments or possibly within the sediments themselves.

REFERENCES

Beckmann, J. P., 1953. Die Foraminiferen der Oceanic Formation (Eocæn-Oligocæn) von Barbadoes. *Eclogae Geol. Helv.*, 46:301-412.

Berger, W. H., 1971. Sedimentation of planktonic foraminifera. *Mar. Geol.*, 11:325-358.

Boersma, A., 1984. Pliocene planktonic and benthic foraminifera from the southeastern Atlantic Angolan margin: Leg 75, Site 532, Deep Sea Drilling Project. In Hay, W. W., Sibuet, J.-C., et al., *Init. Repts. DSDP*, 75, Pt. 2: Washington, D.C. (U.S. Govt. Printing Office), 657-669.

Boersma, A., 1986. Eocene-Oligocene Atlantic paleo-oceanography, using benthic foraminifera. In Pomeroy, C., and Premoli Silva, I. (Eds.), *Terminal Eocene Events: Amsterdam* (Elsevier), 225-236.

Broecker, W. S., and Peng, T.-H., 1982. *Tracers in the Sea*: Palisades, NY (Eldigio Press).

Elmstrom, K. M., and Kennett, J. P., 1986. Late Neogene paleoceanographic evolution of Site 590: southwest Pacific. In Kennett, J. P., von der Borch, C. C., et al., *Init. Repts. DSDP*, 90: Washington (U.S. Govt. Printing Office), 1361-1381.

Fisher, R. L., Bunce, E. T., et al., 1974. *Init. Repts. DSDP*, 24: Washington (U.S. Govt. Printing Office).

Fisher, R. L., Selater, J. G., and McKenzie, D. P., 1971. Evolution of the Central Indian Ridge, western Indian Ocean. *Geol. Soc. Am. Bull.*, 82:553-562.

Gardner, J. V., Nelson, C. S., and Baker, P., 1986. Distribution and character of pale green laminae in sediment from the Lord Howe Rise: a probable Late Neogene and Quaternary tephrstratigraphic record. In Kennett, J. P., von der Borch, C. C., et al., *Init. Repts. DSDP*, 90: Washington (U.S. Govt. Printing Office), 1145-1160.

Gartner, S., 1977. Calcareous nannofossil biostratigraphy and revised zonation of the Pleistocene. *Mar. Micropaleontol.*, 2:1-25.

Heath, G. R., and Culberson, C., 1970. Calcite: degree of saturation, rate of dissolution and the compensation depth in the deep oceans. *Geol. Soc. Am. Bull.*, 81:3157-3160.

Horai, K.-I., 1981. Thermal conductivity of sediments and igneous rocks recovered during Deep Sea Drilling Project Leg 60. In Husong, D. M., Uyeda, S., et al., *Init. Repts. DSDP*, 60: Washington (U.S. Govt. Printing Office), 807-834.

Horai, K.-I., and Von Herzen, R. P., 1985. Measurement of heat flow on Leg 86 of DSDP. In Heath, G. R., Burckle, L. H., et al., *Init. Repts. DSDP*, 86: Washington (U.S. Govt. Printing Office), 759-777.

Karlin, R., Lyle, M., and Heath, G. R., 1987. Authigenic magnetite formation in suboxic marine sediments. *Nature*, 326:490-493.

Keating, B. H., 1984. Magnetometer measurements on the drilling floor of the *Glomar Challenger*: possible causes of rock remagnetization. In Hay, W. W., Sibuet, J.-C., et al., *Init. Repts. DSDP*, 75: Washington (U.S. Govt. Printing Office), 1219-1226.

Kennett, J. P., von der Borch, C. C., et al., 1986. *Init. Repts. DSDP*, 90: Washington (U.S. Govt. Printing Office).

Koehler, R., and Von Herzen, R. P., 1986. *A Miniature Deep-Sea Temperature Data Recorder: Design, Construction, and Use*: Woods Hole, MA (Woods Hole Oceanographic Institution), Tech. Rept. WHOI-86-3.

Lutze, G. F., 1977. Neogene benthonic foraminifera from Site 369, Leg 41, Deep Sea Drilling Project. In Lancelot, Y., Seibold, E., et al., *Init. Repts. DSDP*, 41: Washington (U.S. Govt. Printing Office), 659-666.

Oberhänsli, H., 1986. Latest Cretaceous-early Neogene oxygen and carbon isotopic record at DSDP sites in the Indian Ocean. *Mar. Micropaleontol.*, 10:99-117.

Pisias, N. G., and Prell, W. L., 1985. Changes in calcium carbonate accumulation in the Equatorial Pacific during the late Cenozoic: evidence from HPC Site 572. In Sundquist, E. T., and Broecker, W. S. (Eds.), *The Carbon Cycle and Atmospheric CO₂: Natural Variations Archean to Present*: Washington (American Geophysical Union), 443-454.

Ruddiman, W. F., Cameron, D., and Clement, B. M., 1987. Sediment disturbance and correlation of offset holes drilled with the hydraulic piston corer: Leg 94. In Ruddiman, W. F., Kidd, R. B., Thomas, E., et al., *Init. Repts. DSDP*, 94, Pt. 2: Washington (U.S. Govt. Printing Office): 615-634.

Sager, W. W., and Hutton, H. H., 1986. Magnetic-field measurements aboard the *Joides Resolution* and implications for shipboard paleomagnetic studies. In Austin, J. A., Jr., Schlager, W., et al., *Proc. ODP, Init. Repts.*, 101: College Station, TX (Ocean Drilling Program), 33-37.

Schwager, C., 1966. Fossile foraminiferen von Kar Nikobar, Novara Expedition, 1857-1859 (Vol. 2): Wien (Geol. Theil), 187-286.

Tjalsma, R. C., and Lohmann, G. P., 1983. *Paleocene-Eocene Bathyal and Abyssal Benthic Foraminifera from the Atlantic Ocean*, Spec. Pub. 4: New York (Micropaleontology Press).

van Andel, T. H., 1975. Mesozoic-Cenozoic calcite compensation depth and the global distribution of calcareous sediments. *Earth Planet. Sci. Lett.*, 26:187-194.

Vincent, E., Killingley, J. S., and Berger, W. H., 1980. The Magnetic Epoch-6 carbon shift: a change in the ocean's ¹³C/¹²C ratio 6.2 million years ago. *Mar. Micropaleontol.*, 5:185-203.

Von Herzen, R. P., and Maxwell, A. E., 1959. The measurement of thermal conductivity of deep-sea sediments by a needle-probe method. *J. Geophys. Res.*, 64:1557-1563.

Yokota, T., Kinoshita, H., and Uyeda, S., 1980. New DSDP (Deep Sea Drilling Project) downhole temperature probe utilizing IC RAM (Memory) elements. *Bull. Earthquake Res. Inst. Univ. Tokyo*, 55:77-88.

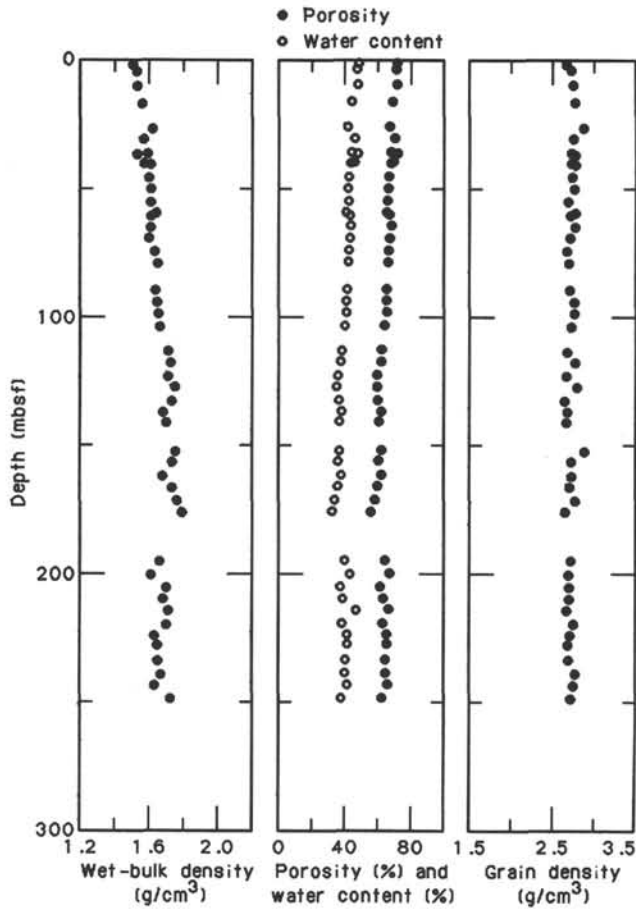


Figure 23. Index properties (wet-bulk density, water content, porosity, and grain density) for Hole 709B.

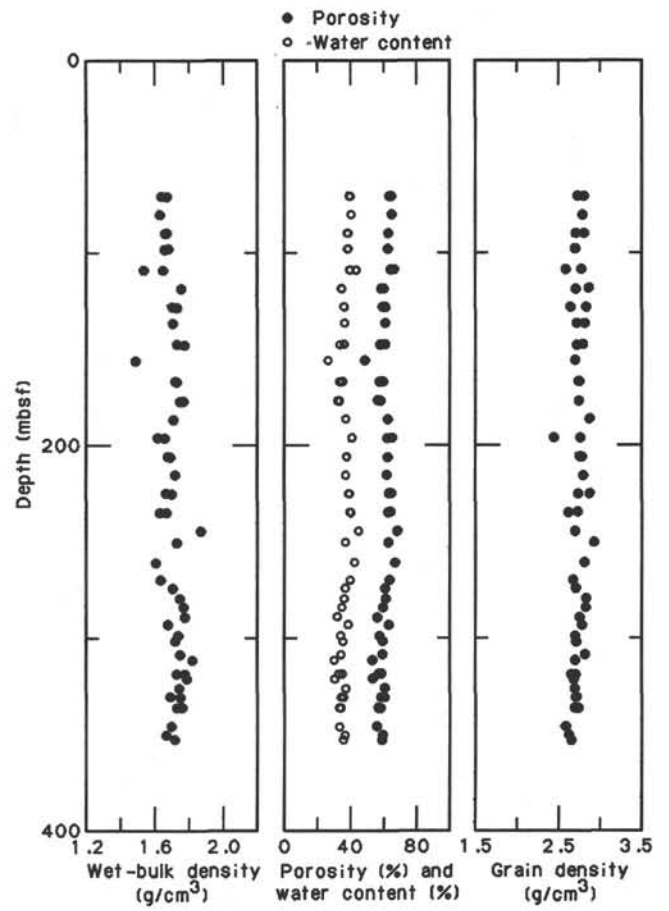


Figure 24. Index properties (wet-bulk density, water content, porosity, and grain density) for Hole 709C.

Table 8. Compressional-wave velocity and acoustic impedance data, Site 709.

Section interval (cm)	Depth (mbsf)	V _p (m/s)	Acoustic impedance (g/cm ² ·s·10 ⁴)
115-709A-			
1H-2, 57	2.07	1531	23.88
1H-4, 57	5.07	1541	23.88
1H-6, 57	8.07	1558	24.61
2H-2, 56	12.16	1549	24.63
2H-4, 56	15.16	1519	23.55
2H-6, 54	18.14	1513	25.11
3H-2, 46	21.66	1510	24.46
3H-4, 46	24.66	1517	23.05
3H-6, 46	27.66	1530	24.63
4H-2, 47	31.37	1526	24.56
4H-4, 47	34.37	1500	24.15
6H-2, 25	50.45	1551	25.74
6H-4, 25	53.45	1526	25.02
6H-6, 25	56.45	1514	24.37
7H-2, 56	60.36	1530	24.32
7H-4, 56	63.36	1473	22.68
7H-6, 56	66.36	1516	25.01
8H-2, 57	70.07	1515	24.99
8H-4, 57	73.07	1518	25.50
8H-6, 57	76.07	1510	25.36
9H-2, 57	79.67	1524	25.60
9H-4, 70	82.80	1506	25.15
9H-6, 57	85.67	1519	25.82
10H-3, 68	90.98	1553	26.09
10H-6, 52	95.32	1540	25.87
11H-2, 86	99.26	1544	25.47
11H-4, 53	101.93	1533	26.06
11H-7, 11	106.01	1539	26.00
13H-2, 20	117.90	1521	26.43
13H-6, 20	123.90	1531	26.01
14H-2, 7	127.37	1522	25.57
14H-6, 8	133.38	1537	26.43
15H-3, 53	139.03	1530	26.31
15H-7, 28	144.78	1539	27.08
16H-3, 86	149.06	1548	26.78
16H-6, 51	153.21	1523	26.19
17H-2, 50	156.90	1519	25.21
17H-4, 50	159.90	1544	26.40
18H-1, 80	165.40	1522	26.33
18H-4, 80	169.90	1562	27.80
18H-6, 80	172.90	1538	26.91
19H-3, 50	178.00	1533	27.28
20H-2, 57	185.97	1535	26.25
20H-5, 60	190.50	1523	25.43
21H-6, 57	201.57	1518	25.95
115-709B-			
1H-2, 60	2.10	1509	22.78
2H-2, 50	5.80	1505	23.02
2H-5, 50	10.30	1522	23.28
3H-3, 57	16.97	1511	23.57
4H-3, 57	26.67	1501	24.31
4H-6, 57	31.17	1514	23.76
5H-3, 70	36.50	1500	23.85
5H-5, 142	40.22	1524	23.92
5H-6, 40	40.70	1507	24.26
6H-3, 56	45.96	1533	24.52
6H-6, 56	50.46	1509	24.29
7H-3, 40	55.40	1503	24.19
7H-6, 40	59.90	1495	24.51
7H-6, 136	60.86	1500	24.15
8H-3, 55	65.25	1525	24.55
8H-6, 60	69.80	1517	24.27
9H-3, 60	74.90	1515	24.69
9H-6, 60	79.40	1511	24.93
9H-6, 142	80.22	1512	24.79
11H-3, 85	94.45	1536	25.34
11H-6, 78	98.88	1512	26.38
12H-3, 83	104.13	1527	25.34
13H-3, 90	113.80	1543	26.38
14H-3, 84	123.34	1542	26.36
14H-6, 69	127.69	1551	27.14
15H-3, 88	133.08	1555	26.90

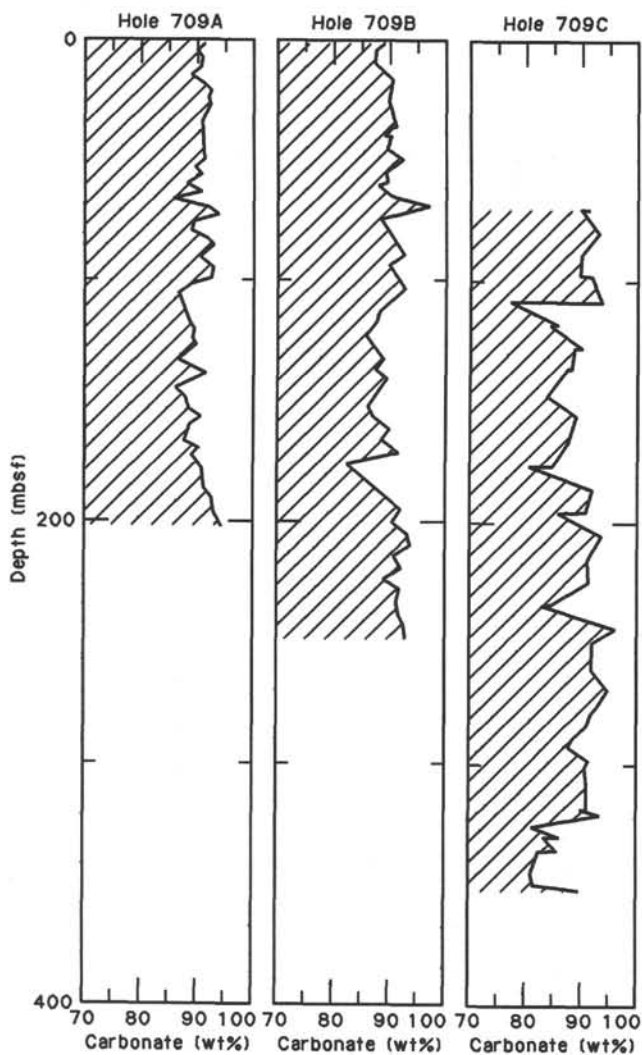


Figure 25. Carbonate content of samples for which the index properties were measured in Holes 709A, 709B, and 709C.

Table 8 (continued).

Section interval (cm)	Depth (mbsf)	V_p (m/s)	Acoustic impedance ($\text{g}/\text{cm}^2 \cdot \text{s} \cdot 10^4$)
115-709B-			
15H-6, 70	137.40	1529	25.68
16H-2, 84	141.24	1531	26.02
17H-3, 85	152.45	1544	27.02
17H-6, 58	156.68	1554	26.88
18H-3, 81	162.11	1548	26.00
18H-6, 63	166.43	1537	26.59
19H-3, 77	171.77	1559	27.43
19H-6, 70	176.20	1575	28.19
23X-3, 56	210.06	1517	25.48
115-709C-			
8H-5, 130	70.90	1576	26.31
8H-5, 138	70.98	1514	24.82
9H-5, 140	80.60	1516	24.71
10H-5, 130	90.20	1516	25.31
10H-5, 142	90.32	1510	25.06
11H-4, 137	98.37	1516	25.46
11H-4, 145	98.45	1536	25.49
12H-5, 128	109.48	1532	25.27
13H-5, 130	119.10	1548	27.24
14H-5, 112	128.52	1534	26.07
14H-5, 127	128.67	1543	26.69
15H-4, 129	136.89	1523	25.89
15H-4, 147	137.07	1541	26.19
17H-4, 148	156.48	1522	22.67
18H-5, 109	167.29	1548	26.62
18H-5, 128	167.48	1570	27.16
21X-5, 130	196.40	1515	24.54
26X-5, 138	244.78	1584	29.62
29X-6, 47	274.37	1537	26.89
31X-3, 52	289.32	1563	27.82
37X-2, 71	346.11	1684	32.66
37X-5, 67	350.57	1605	27.12
37X-7, 1	352.91	1647	28.32

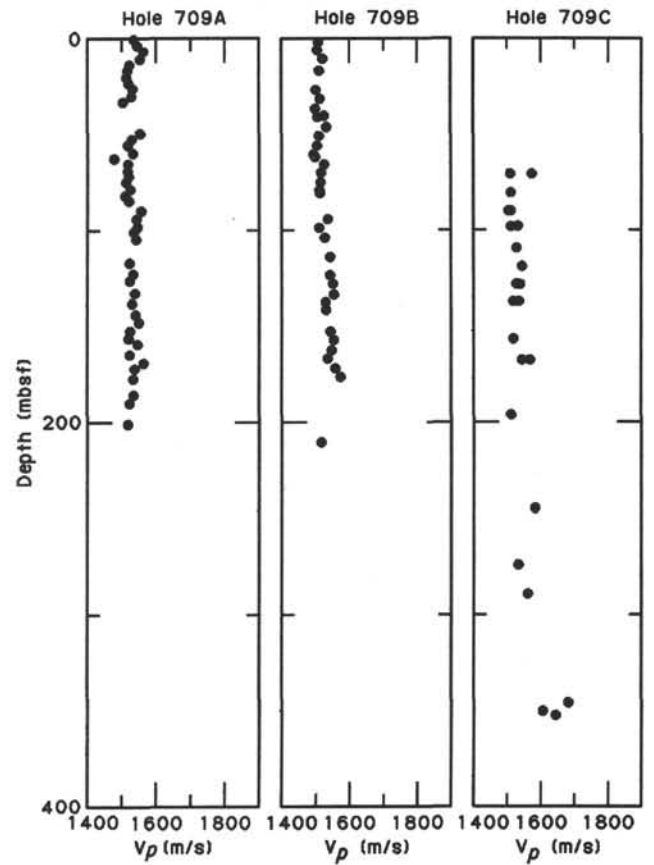


Figure 26. Compressional-wave velocity (V_p) for Holes 709A, 709B, and 709C.

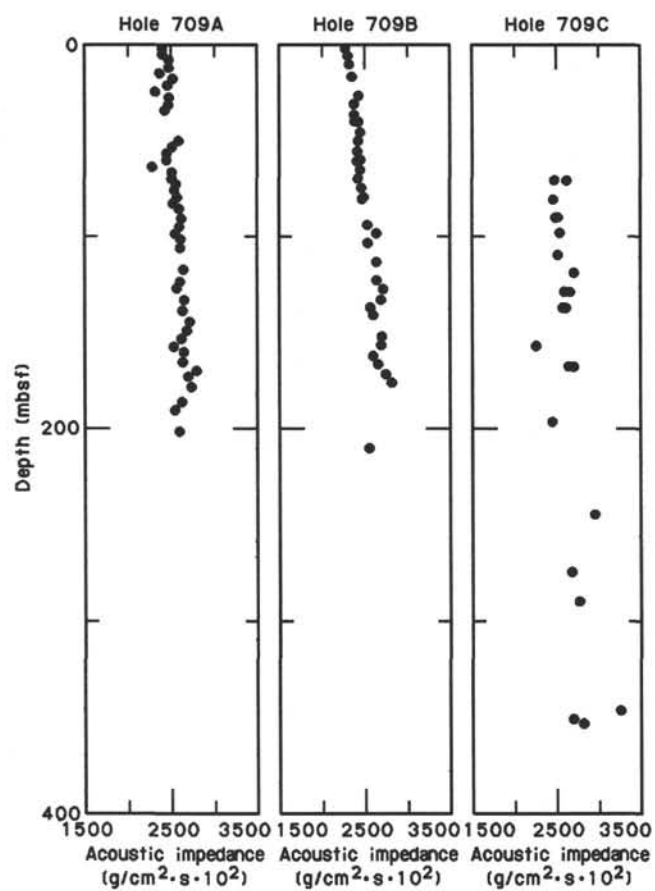


Figure 27. Acoustic impedance calculated from the wet-bulk density and compressional-wave velocity of discrete samples from Holes 709A, 709B, and 709C.

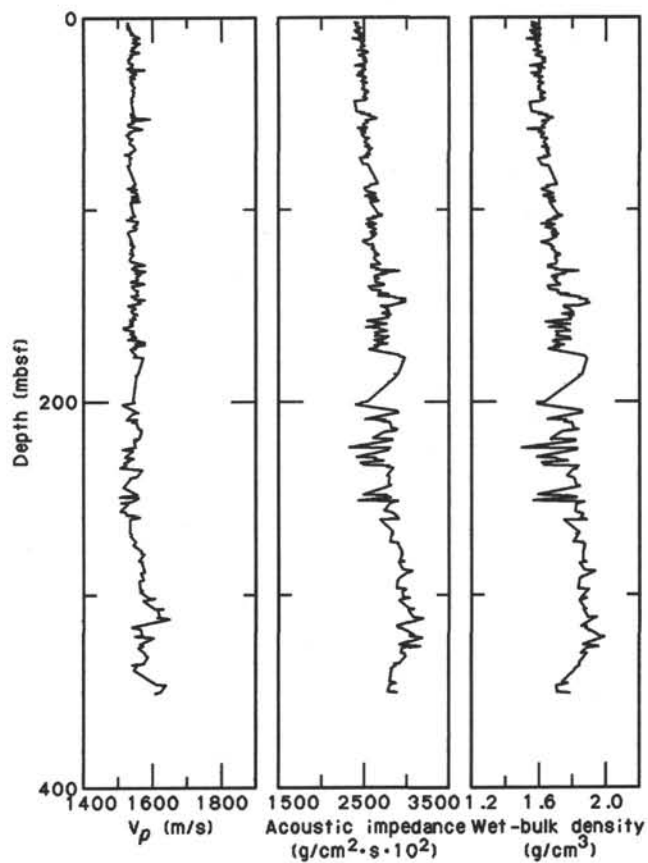


Figure 28. Continuous V_p record (P -wave logger), the calculated acoustic impedance profile, and the wet-bulk density record (GRAPE) at Site 709.

Table 9. Shear-wave velocity data, Site 709.

Section interval (cm)	Depth (mbsf)	V_s (m/s)	Section interval (cm)	Depth (mbsf)	V_s (m/s)
115-709A-			115-709B-		
3H-2, 84	22.04	56	1H-2, 48	1.98	116
3H-4, 85	25.05	57	2H-3, 45	7.25	54
3H-6, 56	27.76	79	2H-6, 44	11.74	65
4H-2, 57	31.47	79	3H-3, 71	17.11	44
6H-2, 56	50.76	77	3H-5, 133	20.73	70
6H-4, 55	53.75	106	4H-4, 48	28.08	103
7H-2, 85	60.65	88	4H-6, 44	31.04	94
7H-4, 86	63.66	115	5H-3, 60	36.40	91
8H-2, 86	70.36	74	5H-5, 142	40.22	113
8H-4, 89	73.39	71	6H-4, 46	47.36	63
8H-6, 86	76.36	87	6H-6, 45	50.35	70
9H-2, 51	79.61	126	7H-2, 50	54.00	81
10H-3, 60	90.90	263	7H-6, 56	60.06	67
10H-6, 55	95.35	347	7H-6, 140	60.90	67
11H-2, 87	99.27	188	8H-3, 60	65.30	68
11H-4, 54	101.94	121	8H-6, 48	69.68	92
11H-7, 12	106.02	113	9H-3, 92	75.22	129
12H-2, 87	108.97	110	9H-6, 46	79.26	35
12H-4, 54	111.64	105	9H-6, 142	80.22	85
12H-6, 58	114.68	123	10H-6, 140	89.90	58
13H-2, 21	117.91	145	11H-3, 92	94.52	86
13H-4, 13	120.83	122	11H-6, 84	98.94	82
13H-6, 21	123.91	104	12H-3, 89	104.19	87
14H-2, 13	127.43	86	12H-6, 70	108.50	89
14H-4, 22	130.52	86	13H-3, 94	113.84	130
14H-6, 14	133.44	78	13H-6, 68	118.08	95
15H-3, 55	139.05	76	14H-3, 91	123.41	88
15H-7, 22	144.72	72	14H-6, 75	127.75	78
16H-3, 92	149.12	54	15H-3, 94	133.14	121
16H-6, 52	153.22	51	15H-6, 76	137.46	157
17H-2, 57	156.97	65	16H-2, 91	141.31	78
17H-6, 84	163.24	78	17H-3, 92	152.52	99
18H-3, 60	168.20	49	17H-6, 70	156.80	87
18H-6, 54	172.64	42	18H-3, 81	162.11	90
19H-3, 58	178.08	77	18H-6, 63	166.43	82
20H-3, 53	187.43	37	19H-3, 85	171.85	99
21H-3, 63	197.13	107	19H-6, 77	176.27	134
21H-6, 49	201.49	104	21X-3, 67	190.87	110
			21X-6, 52	195.22	182
			22X-3, 64	200.44	179
			22X-6, 53	204.83	92
			23X-6, 24	214.24	108
			24X-3, 70	219.80	126
			24X-6, 50	224.10	192
			25X-3, 67	229.47	174
			25X-6, 76	234.06	153

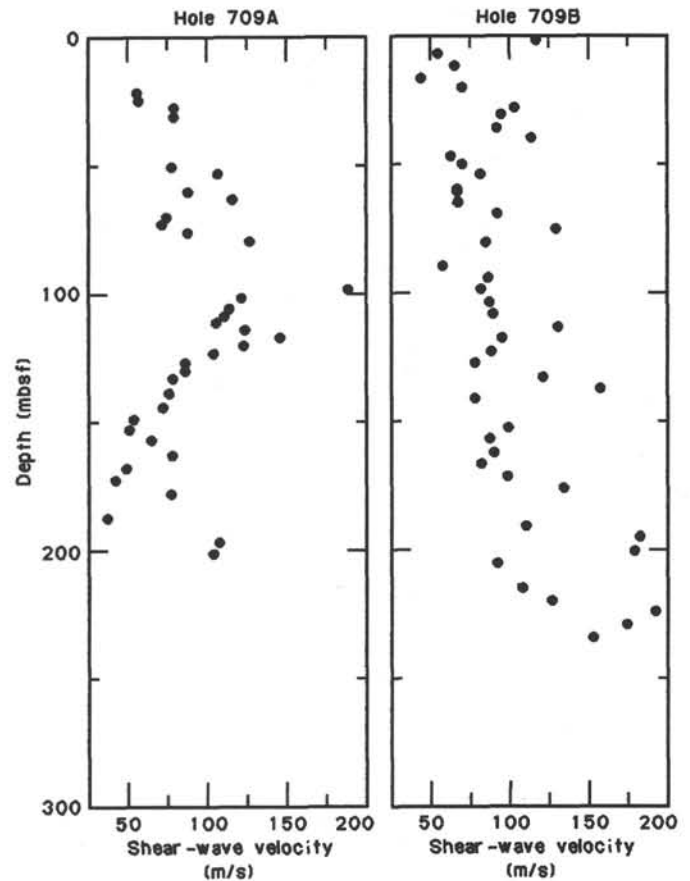


Figure 29. Shear-wave velocity in Holes 709A and 709B.

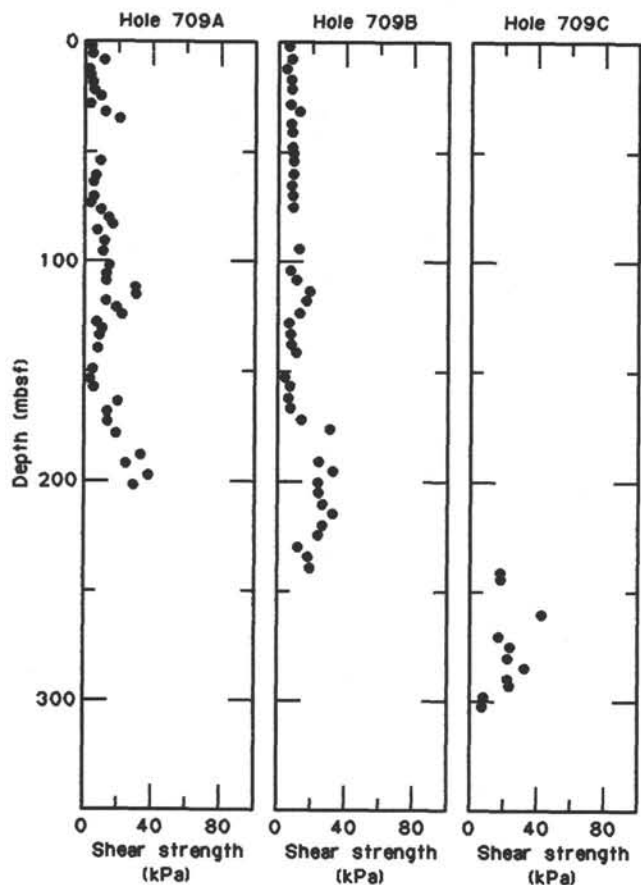


Table 10. Motorized shear strength data, Site 709.

Section interval (cm)	Depth (mbsf)	Peak (kPa)	Section interval (cm)	Depth (mbsf)	Peak (kPa)
115-709A-			115-709B-		
1H-2, 86	2.36	4.2	1H-2, 83	2.33	6.5
1H-4, 84	5.34	4.8	2H-3, 72	7.52	8.3
1H-6, 65	8.15	11.3	2H-6, 65	11.95	4.8
2H-2, 65	12.25	2.7	3H-3, 90	17.30	7.7
2H-4, 65	15.25	3.5	3H-6, 90	21.80	8.1
2H-6, 92	18.52	4.8	4H-4, 80	28.40	7.7
3H-2, 88	22.08	5.9	4H-6, 80	31.40	13.1
3H-4, 57	24.77	9.5	5H-3, 88	36.68	7.7
3H-6, 87	28.07	3.5	5H-6, 80	41.10	8.6
4H-2, 86	31.76	11.9	6H-4, 80	47.70	8.9
4H-4, 93	34.83	20.8	6H-6, 80	50.70	9.5
6H-4, 87	54.07	9.5	7H-2, 80	54.30	9.5
7H-2, 89	60.69	7.1	7H-6, 80	60.30	9.5
7H-4, 93	63.73	5.3	8H-3, 82	65.52	8.3
8H-2, 90	70.40	5.9	8H-6, 82	70.02	8.9
8H-4, 81	73.31	4.2	9H-3, 98	75.28	9.5
8H-6, 91	76.41	10.1	11H-3, 98	94.58	13.1
9H-2, 86	79.96	14.2	12H-3, 95	104.25	8.3
9H-4, 89	82.99	16.6	12H-6, 83	108.63	11.9
9H-6, 78	85.88	7.7	13H-3, 100	113.90	19.5
10H-3, 89	91.19	11.9	13H-6, 76	118.16	17.8
10H-6, 60	95.40	10.6	14H-3, 97	123.47	13.6
11H-2, 93	99.33	13.1	14H-6, 81	127.81	7.1
11H-4, 60	102.00	14.8	15H-3, 100	133.20	8.3
11H-7, 20	106.10	13.1	15H-6, 100	137.70	8.9
12H-2, 93	109.03	13.1	16H-2, 97	141.37	11.8
12H-4, 61	111.71	30.8	17H-3, 98	152.58	4.8
12H-6, 94	115.05	30.8	17H-6, 76	156.86	7.7
13H-2, 28	117.98	13.1	18H-3, 94	162.24	7.1
13H-4, 26	120.96	19.0	18H-6, 76	166.56	8.3
13H-6, 29	123.99	22.5	19H-3, 92	171.92	14.8
14H-2, 20	127.50	7.7	19H-6, 84	176.34	31.4
14H-4, 20	130.50	10.6	21X-3, 74	190.94	25.5
14H-6, 20	133.50	9.5	21X-6, 57	195.27	33.2
15H-3, 63	139.13	8.3	22X-3, 90	200.70	24.9
16H-3, 66	148.86	5.3	22X-6, 75	205.05	24.9
16H-6, 54	153.24	3.5	23X-3, 90	210.40	27.3
17H-2, 85	157.25	5.9	23X-6, 50	214.50	33.2
17H-6, 100	163.40	20.1	24X-3, 95	220.05	27.3
18H-3, 86	168.46	13.6	24X-6, 75	224.35	24.9
18H-6, 89	172.99	13.9	25X-3, 90	229.70	13.1
19H-3, 85	178.35	19.0	25X-6, 93	234.23	19.0
20H-3, 84	187.74	33.8	26X-3, 94	239.44	20.1
20H-6, 60	192.00	24.9			
21H-3, 85	197.35	38.0			
21H-6, 89	201.89	29.6			

Figure 30. Shear strength in Holes 709A, 709B, and 709C.

Table 11. Thermal conductivity data, Site 709.

Sample interval (cm)	Depth (mbsf)	Thermal conductivity ($W \cdot m^{-1} \cdot K^{-1}$)
115-709A-		
1H-1, 92	0.92	1.147
1H-2, 80	2.30	1.140
1H-3, 80	3.80	1.134
1H-4, 80	5.30	1.131
1H-5, 80	6.80	1.426
1H-6, 80	8.30	1.233
1H-7, 40	9.40	1.216
2H-1, 80	10.90	1.241
2H-2, 80	12.40	1.177
2H-3, 80	13.90	1.221
2H-4, 80	15.40	1.220
2H-5, 80	16.90	1.305
2H-6, 80	18.40	1.245
3H-1, 80	20.50	1.109
3H-2, 80	22.00	1.311
3H-3, 80	23.50	1.352
3H-4, 80	25.00	1.215
3H-5, 80	26.50	1.198
3H-6, 80	28.00	1.272
3H-7, 80	29.50	1.251
4H-1, 80	30.20	1.262
4H-2, 80	31.70	1.214
4H-3, 80	33.20	1.298
4H-4, 80	34.70	1.269
4H-5, 40	35.80	1.238
6H-1, 80	49.50	1.270
6H-2, 80	51.00	1.259
6H-3, 80	52.50	1.308
6H-4, 80	54.00	1.371
6H-5, 80	55.50	1.298
6H-6, 80	57.00	1.305
6H-7, 40	58.10	1.259
7H-1, 80	59.10	1.314
7H-2, 80	60.60	1.265
7H-3, 80	62.10	1.299
7H-4, 80	63.60	1.298
7H-5, 80	65.10	1.293
7H-6, 80	66.60	1.342
7H-7, 40	67.70	1.349
8H-1, 80	68.80	1.354
8H-2, 80	70.30	1.282
8H-3, 80	71.80	1.291
8H-4, 80	73.30	1.285
8H-5, 80	74.80	1.312
8H-6, 80	76.30	1.333
8H-7, 40	77.40	1.307
9H-1, 80	78.40	1.394
9H-2, 80	79.90	1.283
9H-3, 80	81.40	1.099
9H-4, 80	82.90	1.355
9H-5, 80	84.40	1.346
9H-6, 80	85.90	1.427
10H-1, 85	88.15	1.361
10H-2, 80	89.60	1.353
10H-3, 80	91.10	1.334
10H-4, 80	92.60	1.336
10H-6, 80	95.60	1.333
10H-7, 40	96.70	1.134
11H-1, 80	97.70	1.397
11H-2, 80	99.20	1.111
11H-3, 80	100.70	1.443
11H-5, 80	103.70	0.977
11H-7, 30	106.20	1.381
12H-1, 80	107.40	1.191
12H-2, 80	108.90	1.354
12H-3, 80	110.40	1.038
12H-4, 80	111.90	1.410
12H-5, 80	113.40	1.296
12H-6, 80	114.90	1.381
13H-2, 110	118.80	1.432
13H-4, 80	121.50	1.506
13H-6, 80	124.50	1.358
14H-1, 80	126.60	1.337
14H-3, 80	129.60	1.446

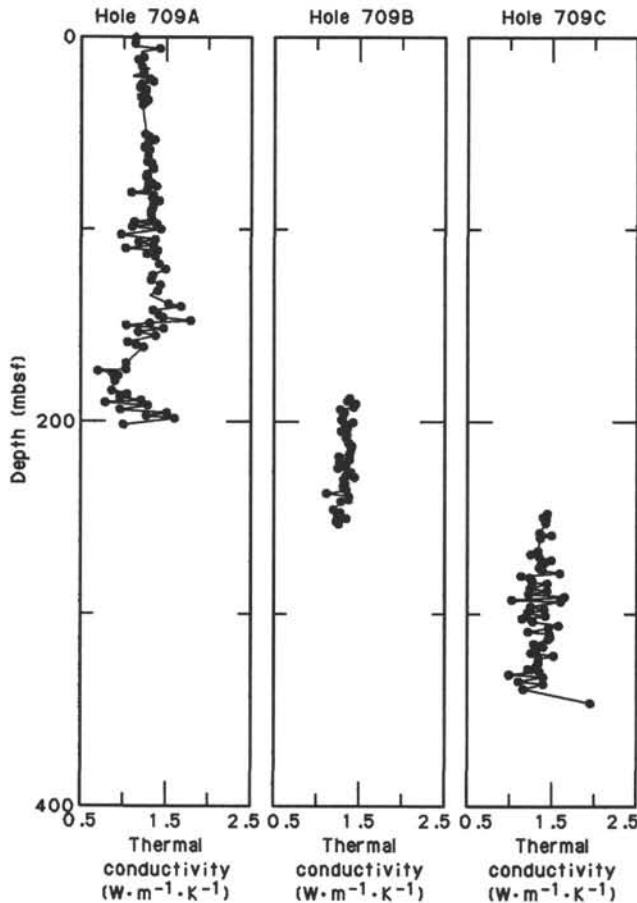


Figure 31. Thermal conductivity in Holes 709A, 709B, and 709C.

Table 11 (continued).

Sample interval (cm)	Depth (mbsf)	Thermal conductivity ($W \cdot m^{-1} \cdot K^{-1}$)
115-709A-		
14H-5, 80	132.60	1.415
14H-7, 30	135.10	1.325
15H-3, 80	139.30	1.543
15H-4, 80	140.80	1.689
15H-5, 80	142.30	1.369
15H-7, 40	144.90	1.432
16H-1, 80	146.00	1.477
16H-2, 80	147.50	1.806
16H-3, 80	149.00	1.329
16H-4, 80	150.50	1.039
16H-5, 60	151.80	1.481
16H-6, 80	153.50	1.191
17H-1, 80	155.70	1.392
17H-3, 80	158.70	1.063
17H-4, 80	160.20	1.163
17H-5, 80	161.70	1.251
18H-4, 80	169.90	1.039
18H-6, 80	172.90	1.033
18H-7, 19	173.79	0.719
19H-1, 80	175.10	0.876
19H-2, 60	176.40	0.949
19H-3, 80	178.10	0.913
19H-4, 50	179.30	0.910
20H-1, 80	184.70	0.876
20H-2, 80	186.20	1.049
20H-3, 80	187.70	0.972
20H-4, 80	189.20	1.229
20H-5, 80	190.70	0.806
20H-6, 60	192.00	1.302
21H-1, 80	194.30	0.974
21H-2, 80	195.80	1.520
21H-3, 80	197.30	1.286
21H-4, 80	198.80	1.609
21H-6, 80	201.80	1.015
115-709B-		
21X-1, 80	188.00	1.395
21X-2, 80	189.50	1.370
21X-3, 80	191.00	1.469
21X-4, 80	192.50	1.444
21X-5, 80	194.00	1.287
21X-6, 80	195.50	1.329
22X-1, 80	197.60	1.315
22X-2, 80	199.10	1.301
22X-3, 80	200.60	1.433
22X-4, 80	202.10	1.340
22X-5, 80	203.60	1.366
22X-6, 80	205.10	1.298
23X-1, 80	207.30	1.357
23X-2, 80	208.80	1.351
23X-3, 80	210.30	1.426
23X-4, 80	211.80	1.387
23X-5, 80	213.30	1.418
23X-6, 80	214.80	1.412
24X-1, 80	216.90	1.392
24X-2, 80	218.40	1.271
24X-3, 80	219.90	1.394
24X-4, 80	221.40	1.277
24X-5, 80	222.90	1.351
24X-6, 80	224.40	1.269
25X-1, 80	226.60	1.411
25X-2, 80	228.10	1.355
25X-3, 65	229.45	1.452
25X-4, 65	230.95	1.323
25X-5, 80	232.60	1.342
25X-6, 80	234.10	1.317
26X-1, 80	236.30	1.353
26X-2, 80	237.80	1.130
26X-3, 82	239.32	1.386
26X-4, 80	240.80	1.391
26X-5, 30	241.80	1.299
27X-1, 80	245.90	1.208
27X-2, 80	247.40	1.287
27X-3, 80	248.90	1.258
27X-4, 80	250.40	1.358
27X-5, 80	251.90	1.256
27X-6, 40	253.00	1.266

Table 11 (continued).

Sample interval (cm)	Depth (mbsf)	Thermal conductivity ($W \cdot m^{-1} \cdot K^{-1}$)
115-709C-		
27X-1, 80	247.80	1.453
27X-2, 80	249.30	1.407
27X-3, 80	250.80	1.440
27X-4, 80	252.30	1.433
28X-1, 90	257.60	1.366
28X-2, 80	259.00	1.501
28X-3, 80	260.50	1.379
29X-1, 80	267.20	1.338
29X-2, 80	268.70	1.262
29X-3, 80	270.20	1.366
29X-4, 80	271.70	1.496
29X-5, 80	273.20	1.421
29X-6, 80	274.70	1.383
29X-7, 15	275.55	1.373
30X-1, 80	276.90	1.400
30X-2, 80	278.40	1.597
30X-3, 80	279.90	1.144
30X-4, 80	281.40	1.249
30X-5, 80	282.90	1.285
30X-6, 40	284.00	1.450
31X-1, 80	286.60	1.253
31X-2, 80	288.10	1.452
31X-3, 80	289.60	1.237
31X-4, 80	291.10	1.650
31X-5, 80	292.60	1.030
31X-6, 40	293.70	1.605
32X-1, 80	296.20	1.255
32X-2, 80	297.70	1.410
32X-3, 80	299.20	1.219
32X-4, 80	300.70	1.433
32X-5, 80	302.20	1.153
32X-6, 80	303.70	1.281
33X-1, 80	305.90	1.579
33X-2, 80	307.40	1.464
33X-3, 90	309.00	1.227
33X-4, 80	310.40	1.476
33X-5, 80	311.90	1.487
33X-6, 40	313.00	1.468
34X-1, 80	315.60	1.303
34X-2, 80	317.10	1.403
34X-3, 80	318.60	1.320
34X-4, 80	320.10	1.271
34X-5, 80	321.60	1.522
34X-6, 80	323.10	1.358
35X-1, 80	325.20	1.353
35X-2, 80	326.70	1.333
35X-3, 80	328.20	1.226
35X-4, 80	329.70	1.360
35X-5, 80	331.20	0.997
35X-6, 80	332.70	1.398
36X-1, 80	334.90	1.110
36X-2, 80	336.40	1.399
36X-4, 40	339.00	1.166
37X-2, 70	346.10	1.950

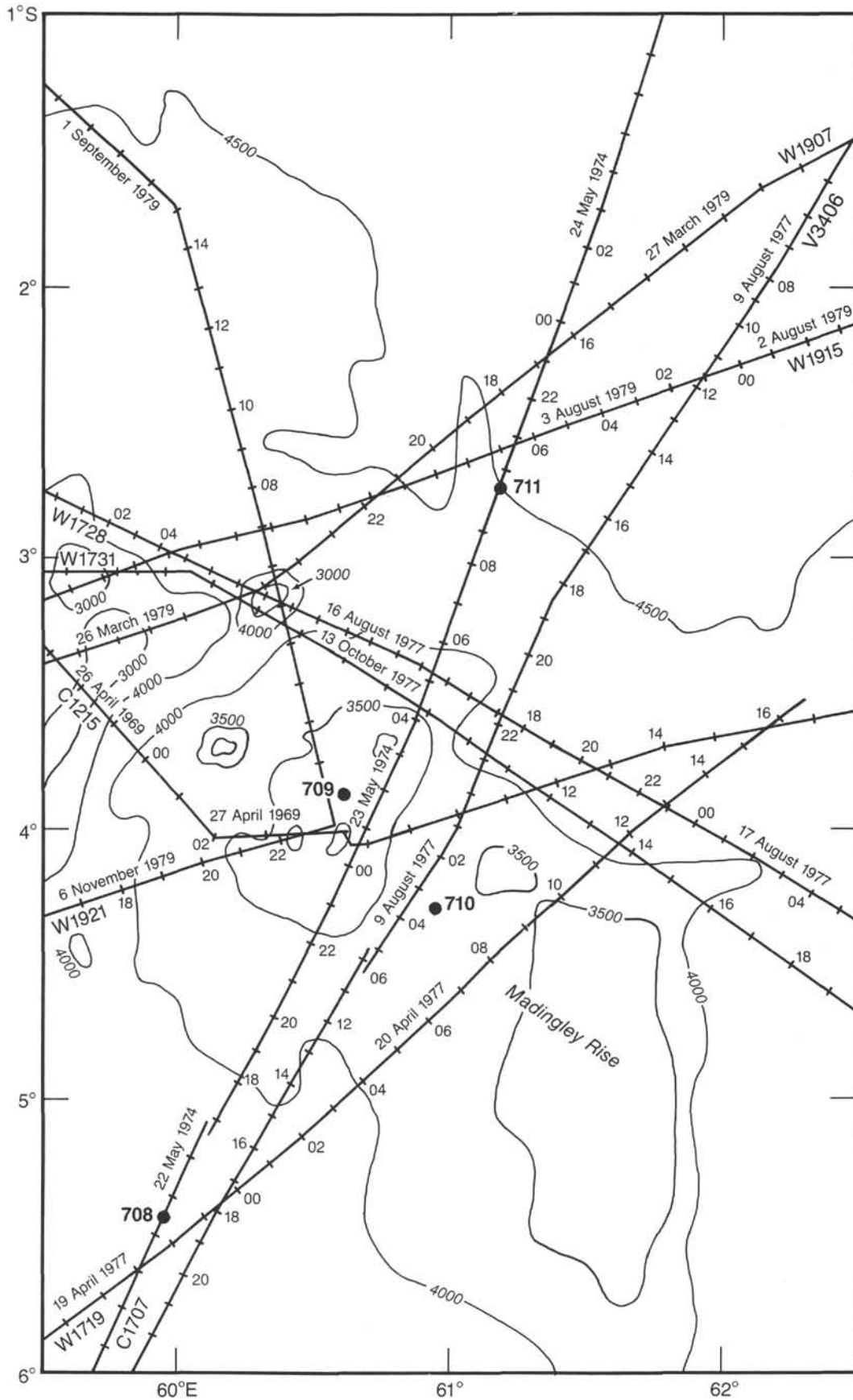


Figure 32. Bathymetric map of the seafloor near Site 709 showing the location of single-channel seismic (SCS) profiles used to select sites for the carbonate dissolution transect objective. Depth in meters.

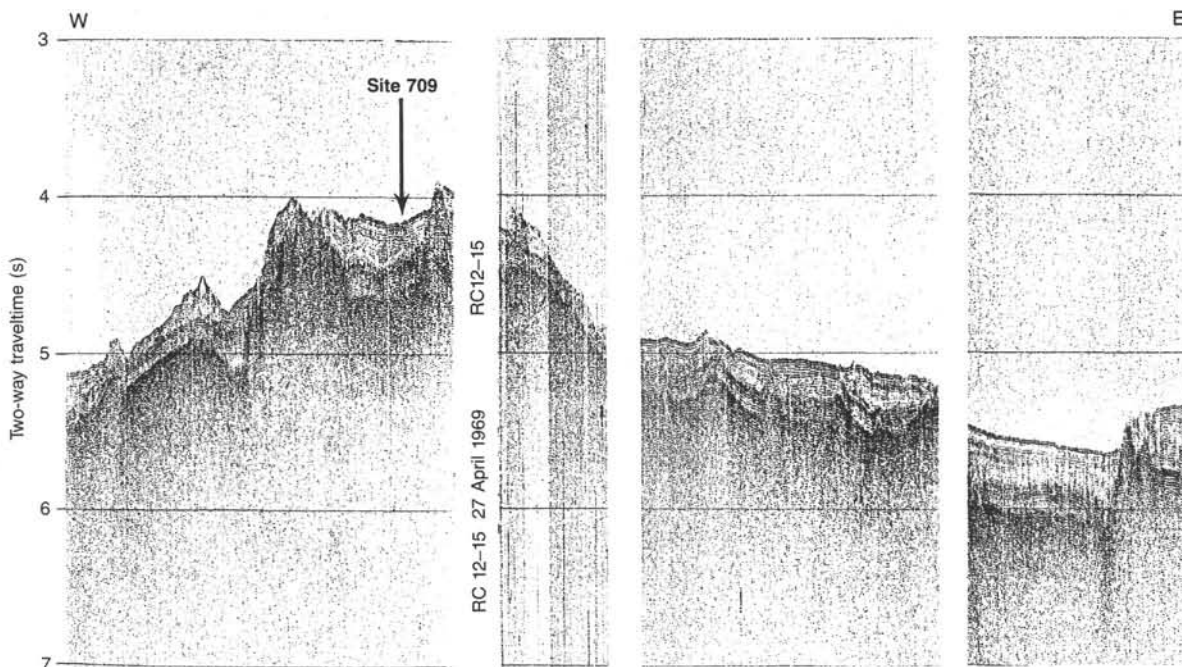


Figure 33. The RC12-15 cruise single-channel seismic (SCS), water-gun reflection profile (27 April 1969) in the vicinity of Site 709. The basement reflector is extremely irregular owing to the presumed volcanic origin of the Madingley Rise and forms the sides of a small perched basin.

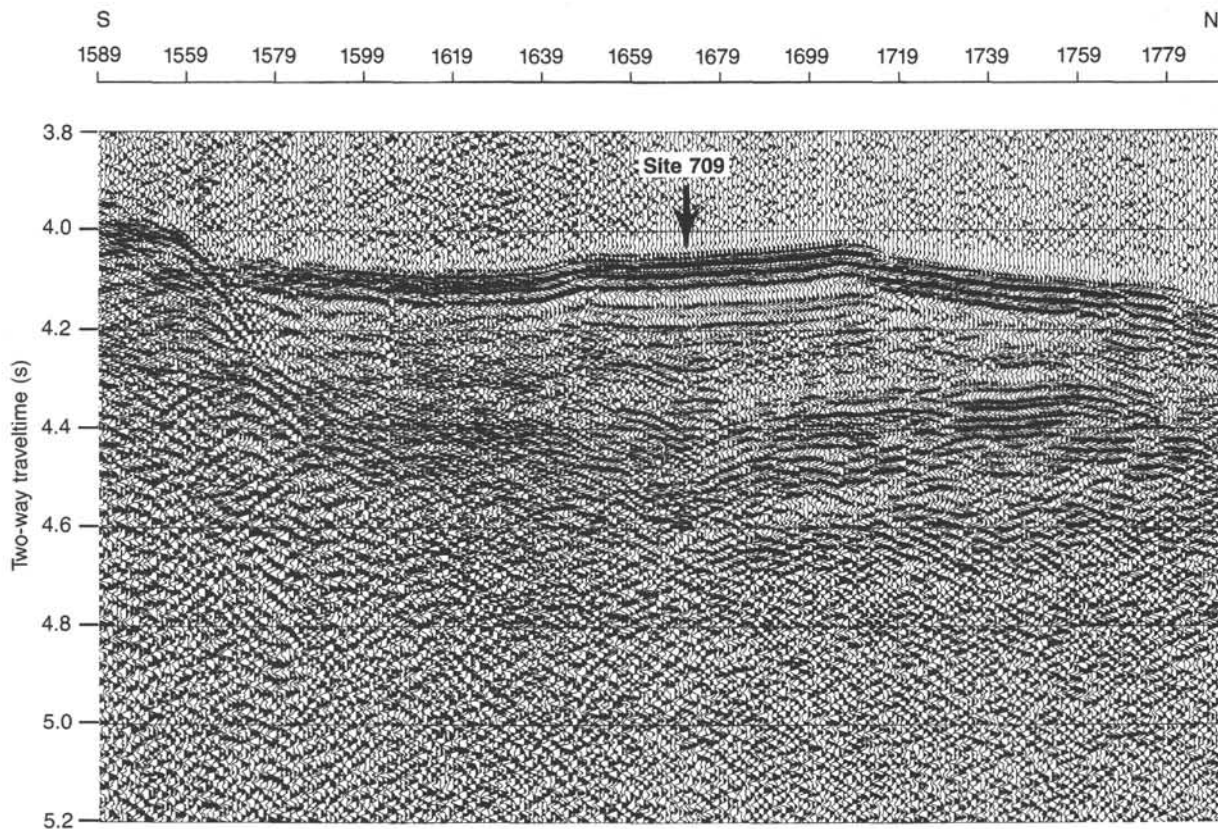


Figure 34. The *JOIDES Resolution* single-channel seismic (SCS), water-gun reflection profile over Site 709 shows rather transparent sediments on top of a faulted volcanic basement.

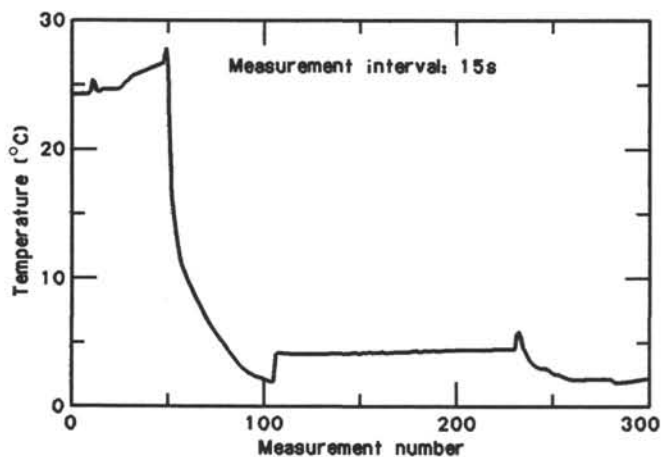


Figure 35. APC (Von Herzen) instrument downhole temperature run at 102.4 mbsf, Core 115-709C-12H.

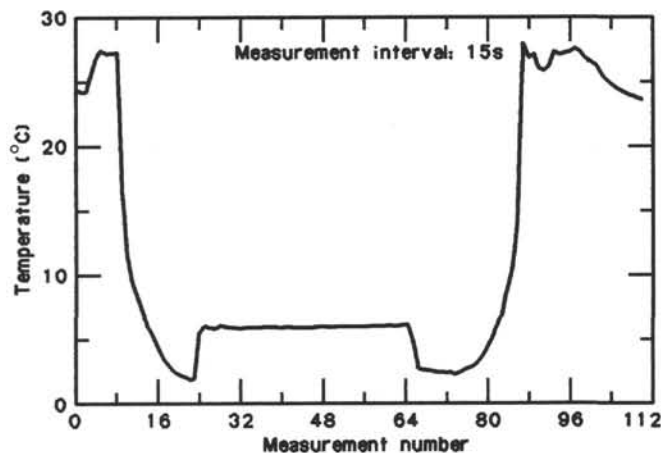


Figure 38. Uyeda (Y-K-U) instrument downhole temperature run at 140.8 mbsf, Core 115-709C-16H.

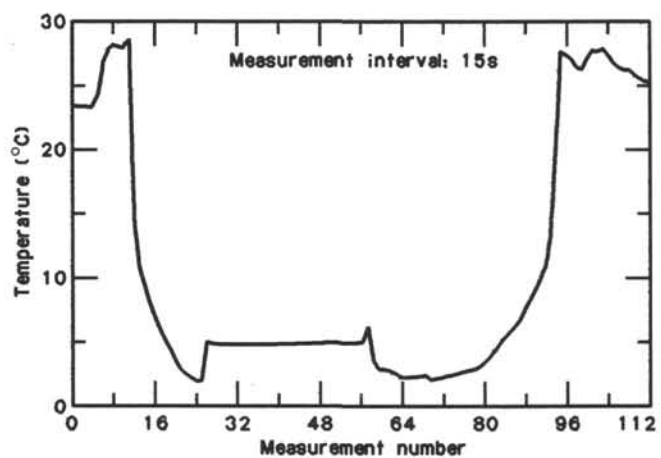


Figure 36. Uyeda (Y-K-U) instrument downhole temperature run at 102.4 mbsf, Core 115-709C-12H.

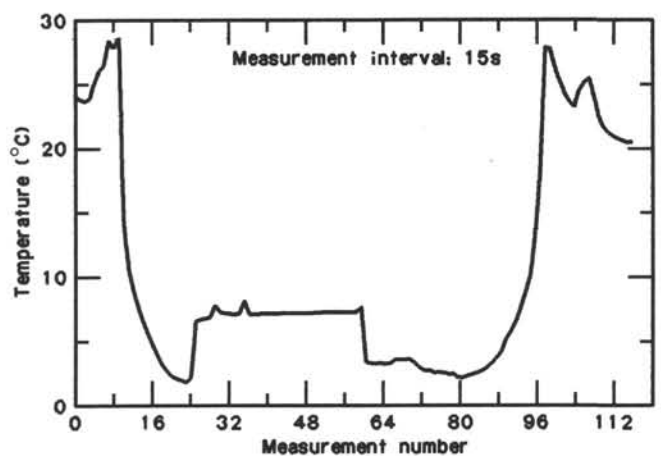


Figure 39. Uyeda (Y-K-U) instrument downhole temperature run at 189.1 mbsf, Core 115-709C-21X. Spike in temperature at measurement #36 is an erroneous point.

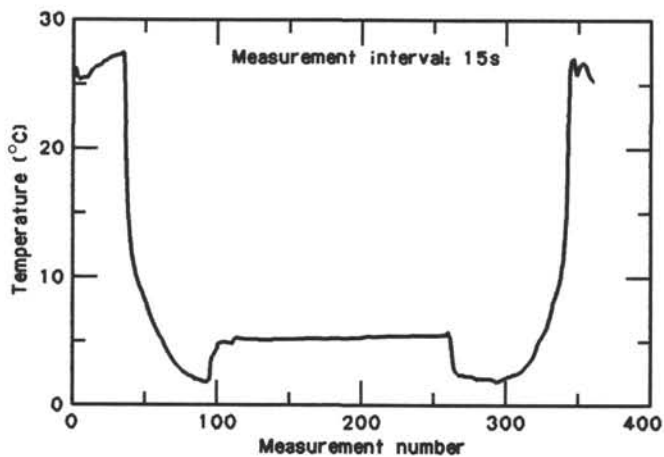


Figure 37. APC (Von Herzen) instrument downhole temperature run at 140.8 mbsf, Core 115-709C-16H.

Table 12. Temperature tool results for Site 709.

Depth (mbsf)	Temperature (°C)	Integrated thermal resistivity (m ² °K/W)	Instrument
0	2.14	0	VH, YKU
102.4	4.49	80.80	VH
102.4	4.74	80.80	YKU
140.8	5.62	109.22	VH
140.8	5.79	109.22	YKU
189.1	7.04	152.85	YKU

Note: VH = Von Herzen miniature temperature probe, and YKU = Yokota-Kinoshita-Uyeda temperature probe.

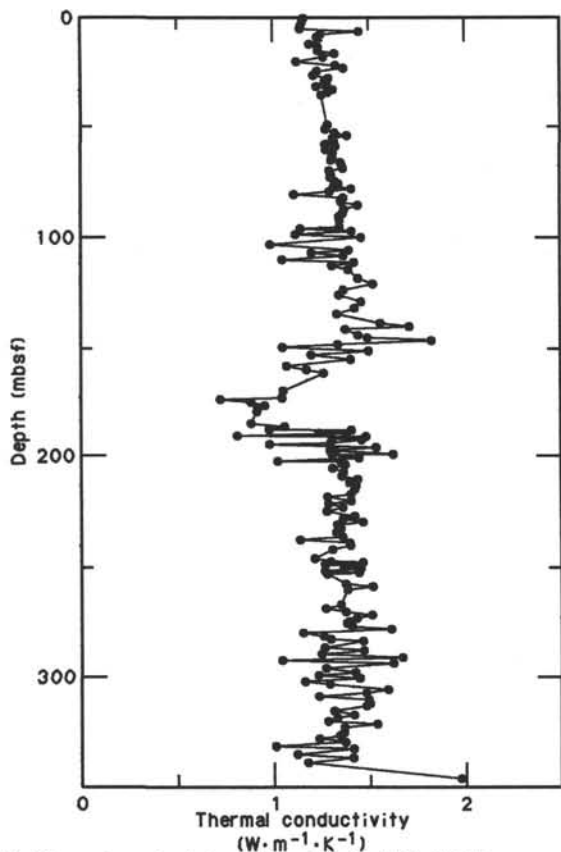


Figure 40. Thermal conductivity vs. depth at Site 709. This is a composite of all the measurements at Holes 709A, 709B, and 709C.

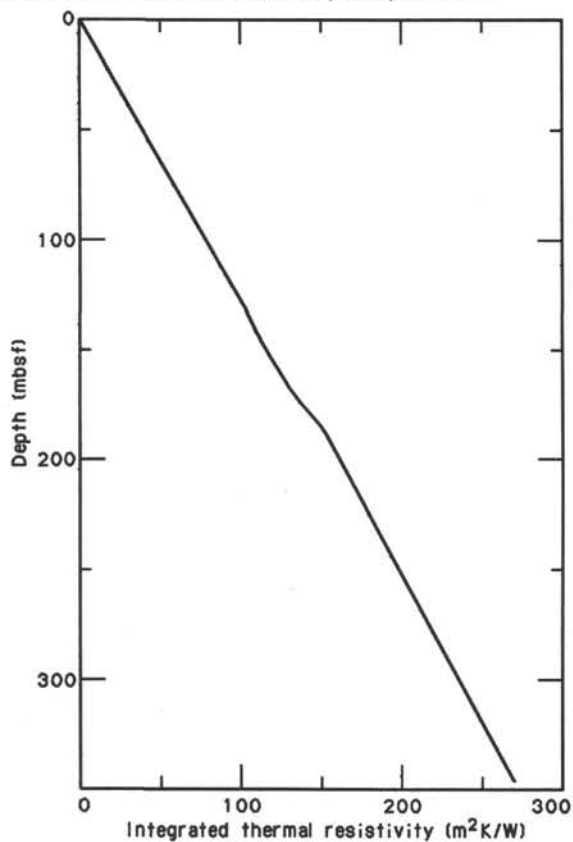


Figure 41. Integrated thermal resistivity vs. depth at Site 709. This is the integral over depth of the resistivity (1/conductivity).

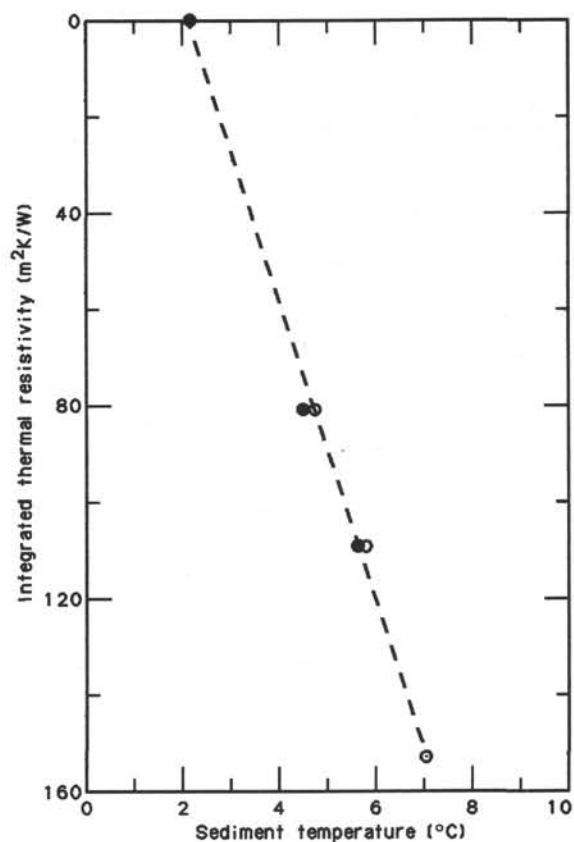
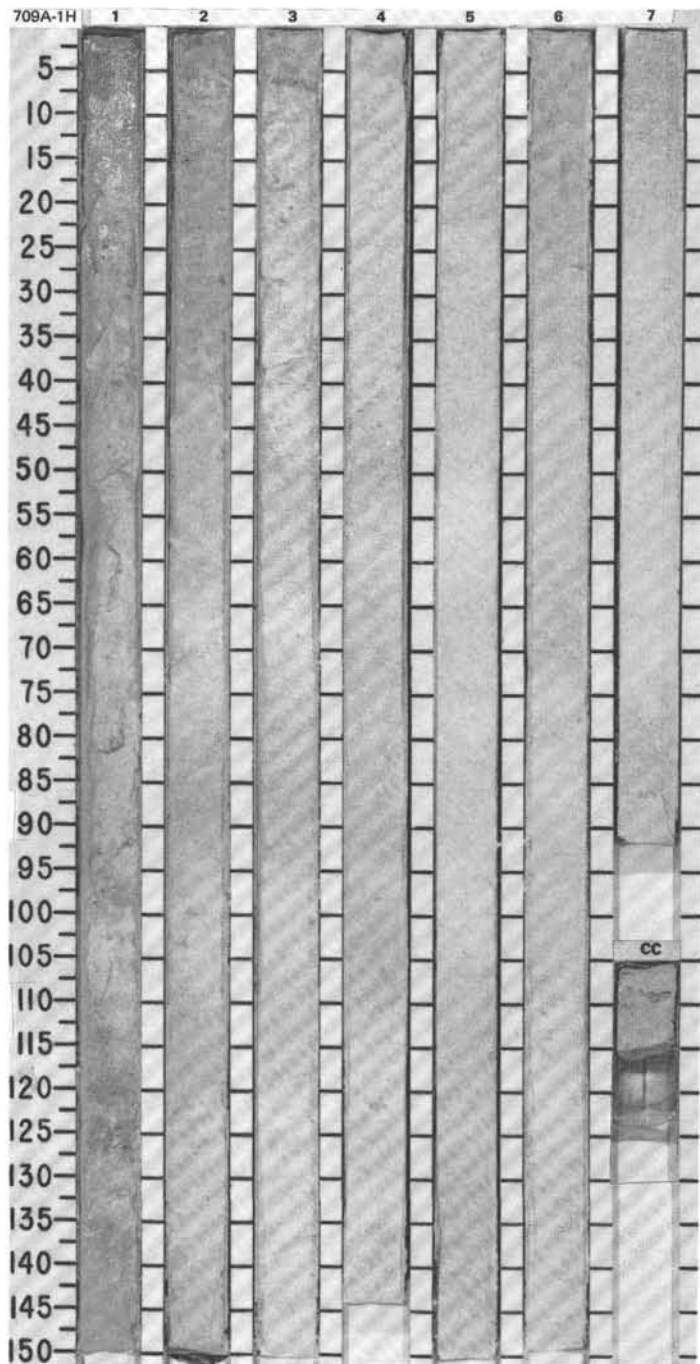


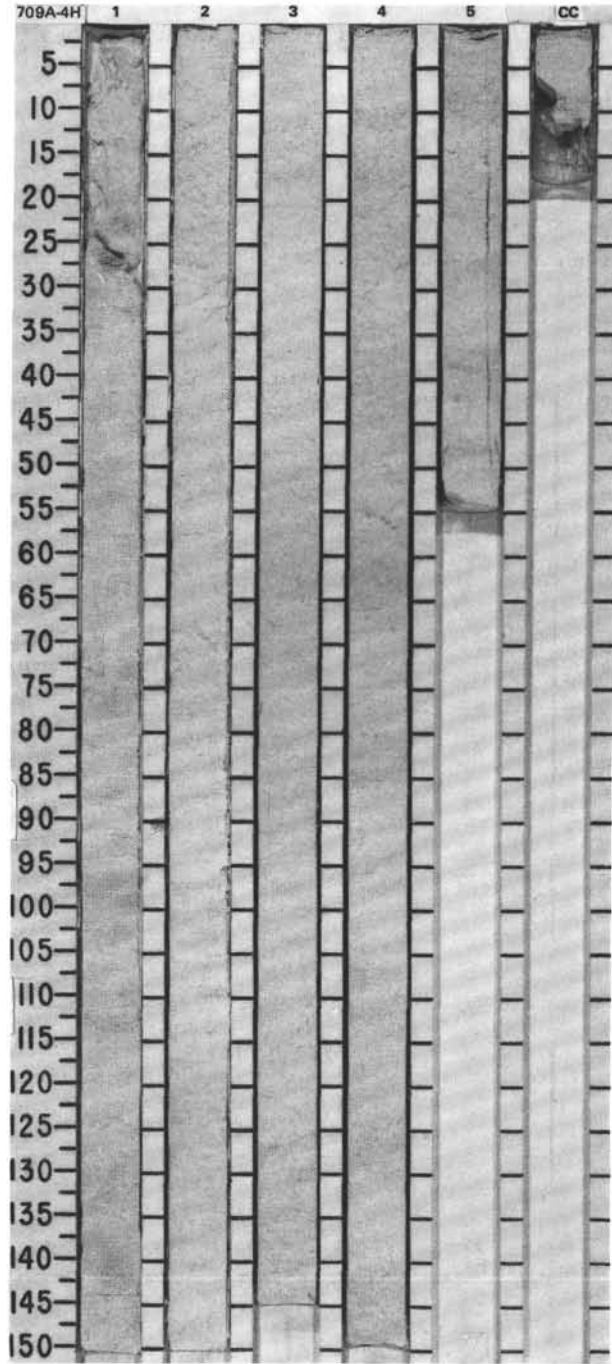
Figure 42. Temperature vs. integrated thermal resistivity at Site 709. Filled circles represent the Von Herzen tool temperature points, and open circles, the Y-K-U tool temperature points. The dashed line is the best-fitting linear, least-squares regression fit. The heat flow value is 32.4 mW/m².

SITE 709 HOLE A CORE 1H CORED INTERVAL 3036.4-3046.5 mbsl; 0.0-10.1 mbsf

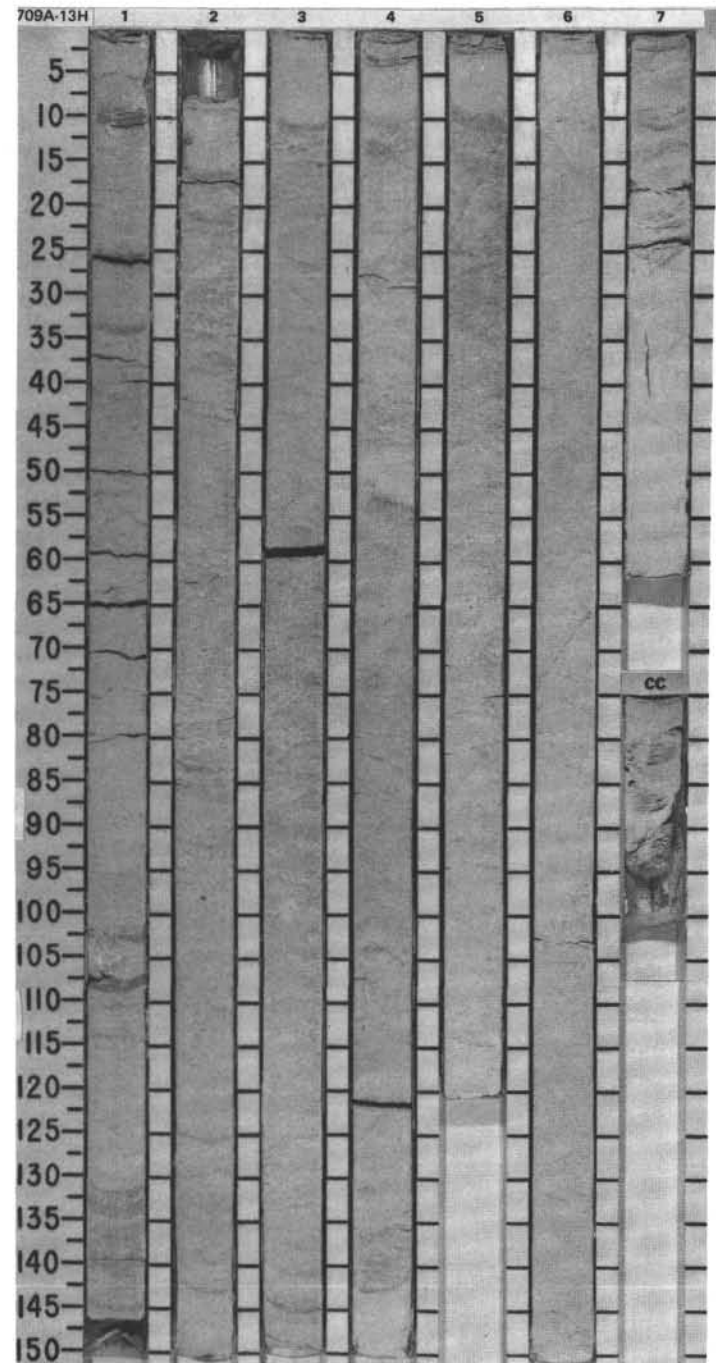
TIME-ROCK UNIT	BIOSTRAT. ZONE/ FOSSIL CHARACTER			PALEOMAGNETICS	PHYS. PROPERTIES	CHEMISTRY	SECTION	METERS	GRAPHIC LITHOLOGY	DRILLING DISTURB.	SED. STRUCTURES	SAMPLES	LITHOLOGIC DESCRIPTION																														
	FORAMINIFERS	NANNOFOSSILS	RADIOLARIANS											DIATOMS																													
AG	N 22												FORAMINIFER-BEARING NANNOFOSSIL OOZE and CLAY-BEARING FORAMINIFER-BEARING NANNOFOSSIL OOZE Major lithologies: Foraminifer-bearing nannofossil ooze and clay-bearing foraminifer-bearing nannofossil ooze, white (10YR 8/2, 8/1). Sections 1-4 weakly bioturbated. SMEAR SLIDE SUMMARY (%): <table style="margin-left: 20px;"> <tr> <td></td> <td>3, 2</td> <td>3, 20</td> </tr> <tr> <td></td> <td>D</td> <td>D</td> </tr> </table> TEXTURE: Silt 27 28 Clay 73 72 COMPOSITION: <table style="margin-left: 20px;"> <tr> <td>Quartz</td> <td>—</td> <td>Tr</td> </tr> <tr> <td>Volcanic glass</td> <td>—</td> <td>1</td> </tr> <tr> <td>Foraminifers</td> <td>25</td> <td>25</td> </tr> <tr> <td>Nannofossils</td> <td>71</td> <td>72</td> </tr> <tr> <td>Diatoms</td> <td>2</td> <td>Tr</td> </tr> <tr> <td>Radiolarians</td> <td>1</td> <td>1</td> </tr> <tr> <td>Sponge spicules</td> <td>Tr</td> <td>1</td> </tr> <tr> <td>Silicoflagellates</td> <td>1</td> <td>Tr</td> </tr> </table>		3, 2	3, 20		D	D	Quartz	—	Tr	Volcanic glass	—	1	Foraminifers	25	25	Nannofossils	71	72	Diatoms	2	Tr	Radiolarians	1	1	Sponge spicules	Tr	1	Silicoflagellates	1	Tr
	3, 2	3, 20																																									
	D	D																																									
Quartz	—	Tr																																									
Volcanic glass	—	1																																									
Foraminifers	25	25																																									
Nannofossils	71	72																																									
Diatoms	2	Tr																																									
Radiolarians	1	1																																									
Sponge spicules	Tr	1																																									
Silicoflagellates	1	Tr																																									
AG	CN 14a (NN 19)	CN 14b (NN 20)	CN 15 (NN 21)																																								
CG	<i>Amphiropalum ypsilon</i>																																										
RP	<i>N. reinholdii</i>																																										
CC																																											



TIME-ROCK UNIT		BIOSTRAT. ZONE/ FOSSIL CHARACTER		PALEOMAGNETICS	PHYS. PROPERTIES	CHEMISTRY	SECTION	METERS	GRAPHIC LITHOLOGY	DRILLING DISTURB.	SED. STRUCTURES	SAMPLES	LITHOLOGIC DESCRIPTION																																	
FORAMINIFERS	NANNOFOSSILS	RADIOLARIANS	DIAZONIS																																											
UPPER PLIOCENE		AM CN 12a (NN 16)					1	0.5 1.0				*	<p>FORAMINIFER-BEARING NANNOFOSSIL OOZE and CLAY-BEARING FORAMINIFER-NANNOFOSSIL OOZE</p> <p>Major lithology: Foraminifer-bearing nannofossil ooze and clay-bearing foraminifer-bearing nannofossil ooze, very light gray (N8) to very light greenish gray (5G 8/1), with 10 thin interbedded horizons of light greenish gray (5G 7/1) in Sections 1 and 5. Pyrite-stained blebs at Section 4, 53-56 cm.</p> <p>SMEAR SLIDE SUMMARY (%):</p> <table border="1"> <tr> <td></td> <td>1, 80</td> <td>4, 80</td> </tr> <tr> <td>D</td> <td></td> <td>D</td> </tr> </table> <p>TEXTURE:</p> <table border="1"> <tr> <td>Sand</td> <td>10</td> <td>10</td> </tr> <tr> <td>Silt</td> <td>90</td> <td>90</td> </tr> </table> <p>COMPOSITION:</p> <table border="1"> <tr> <td>Feldspar</td> <td>Tr</td> <td>—</td> </tr> <tr> <td>Volcanic glass</td> <td>Tr</td> <td>Tr</td> </tr> <tr> <td>Dolomite</td> <td>Tr</td> <td>—</td> </tr> <tr> <td>Foraminifers</td> <td>10</td> <td>10</td> </tr> <tr> <td>Nannofossils</td> <td>90</td> <td>90</td> </tr> <tr> <td>Radiolarians</td> <td>Tr</td> <td>Tr</td> </tr> <tr> <td>Sponge spicules</td> <td>Tr</td> <td>Tr</td> </tr> </table>		1, 80	4, 80	D		D	Sand	10	10	Silt	90	90	Feldspar	Tr	—	Volcanic glass	Tr	Tr	Dolomite	Tr	—	Foraminifers	10	10	Nannofossils	90	90	Radiolarians	Tr	Tr	Sponge spicules	Tr	Tr
	1, 80	4, 80																																												
D		D																																												
Sand	10	10																																												
Silt	90	90																																												
Feldspar	Tr	—																																												
Volcanic glass	Tr	Tr																																												
Dolomite	Tr	—																																												
Foraminifers	10	10																																												
Nannofossils	90	90																																												
Radiolarians	Tr	Tr																																												
Sponge spicules	Tr	Tr																																												
LOWER PLIOCENE		AM N 19 - N 18					2																																							
		AM CN 11 (NN 15)					3																																							
		Fp <i>Spongaster pentas</i>					4																																							
		Barren					5																																							
							CC																																							

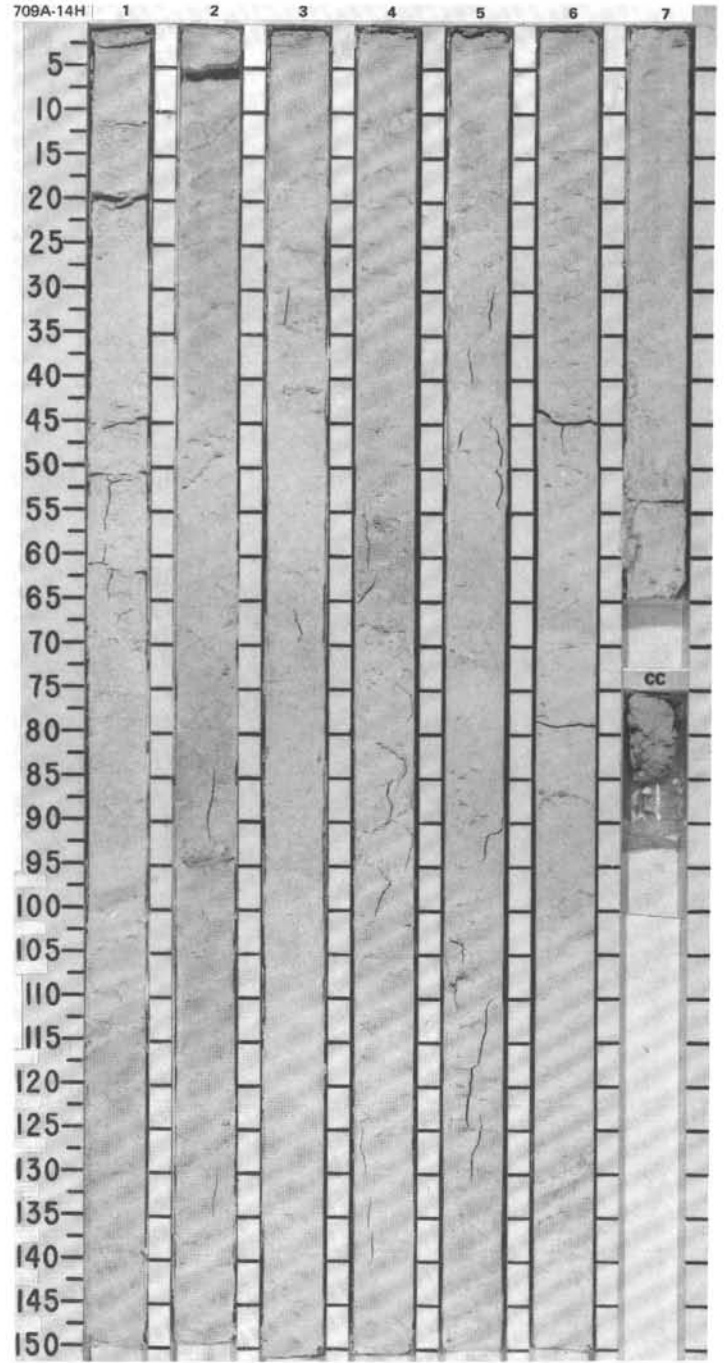


TIME-ROCK UNIT	BIOSTRAT. ZONE/ FOSSIL CHARACTER			PALEOMAGNETICS	PHYS. PROPERTIES	CHEMISTRY	SECTION	METERS	GRAPHIC LITHOLOGY	DRILLING DISTURB.	SEC. STRUCTURES	SAMPLES	LITHOLOGIC DESCRIPTION																																																
	FORAMINIFERS	NANNOFOSSILS	RADIOLARIANS																																																										
AM	MIDDLE MIOCENE												<p>NANNOFOSSIL OOZE and CLAY-BEARING NANNOFOSSIL OOZE</p> <p>Major lithologies: Nannofossil ooze and clay-bearing nannofossil ooze, homogeneous, featureless, very light greenish gray (5G 8/1, 5GY 8/1).</p> <p>SMEAR SLIDE SUMMARY (%):</p> <table border="1"> <tr> <td></td> <td>1, 90</td> <td>2, 70</td> <td>6, 70</td> </tr> <tr> <td></td> <td>D</td> <td>D</td> <td>D</td> </tr> </table> <p>TEXTURE:</p> <table border="1"> <tr> <td>Sand</td> <td>—</td> <td>—</td> <td>1</td> </tr> <tr> <td>Silt</td> <td>2</td> <td>2</td> <td>4</td> </tr> <tr> <td>Clay</td> <td>98</td> <td>98</td> <td>95</td> </tr> </table> <p>COMPOSITION:</p> <table border="1"> <tr> <td>Volcanic glass</td> <td>—</td> <td>Tr</td> <td>Tr</td> </tr> <tr> <td>Accessory minerals</td> <td>—</td> <td>Tr</td> <td>—</td> </tr> <tr> <td>Foraminifers</td> <td>2</td> <td>2</td> <td>5</td> </tr> <tr> <td>Nannofossils</td> <td>98</td> <td>98</td> <td>95</td> </tr> <tr> <td>Radiolarians</td> <td>Tr</td> <td>—</td> <td>—</td> </tr> <tr> <td>Sponge spicules</td> <td>—</td> <td>Tr</td> <td>Tr</td> </tr> <tr> <td>Silicoflagellates</td> <td>Tr</td> <td>Tr</td> <td>—</td> </tr> </table>		1, 90	2, 70	6, 70		D	D	D	Sand	—	—	1	Silt	2	2	4	Clay	98	98	95	Volcanic glass	—	Tr	Tr	Accessory minerals	—	Tr	—	Foraminifers	2	2	5	Nannofossils	98	98	95	Radiolarians	Tr	—	—	Sponge spicules	—	Tr	Tr	Silicoflagellates	Tr	Tr	—
	1, 90	2, 70	6, 70																																																										
	D	D	D																																																										
Sand	—	—	1																																																										
Silt	2	2	4																																																										
Clay	98	98	95																																																										
Volcanic glass	—	Tr	Tr																																																										
Accessory minerals	—	Tr	—																																																										
Foraminifers	2	2	5																																																										
Nannofossils	98	98	95																																																										
Radiolarians	Tr	—	—																																																										
Sponge spicules	—	Tr	Tr																																																										
Silicoflagellates	Tr	Tr	—																																																										
AM	N 9 - N 12	AM					0.5	VOID					<p>VOID</p> <p>VOID</p> <p>VOID</p> <p>VOID</p> <p>VOID</p> <p>VOID</p> <p>VOID</p>																																																
AM	CN 5a (NN 6)	CN 5b (NN 7)					1.0				*																																																		
	Barren						2				*																																																		
	Barren						3																																																						
							4																																																						
							5																																																						
							6																																																						
							7																																																						
CC																																																													

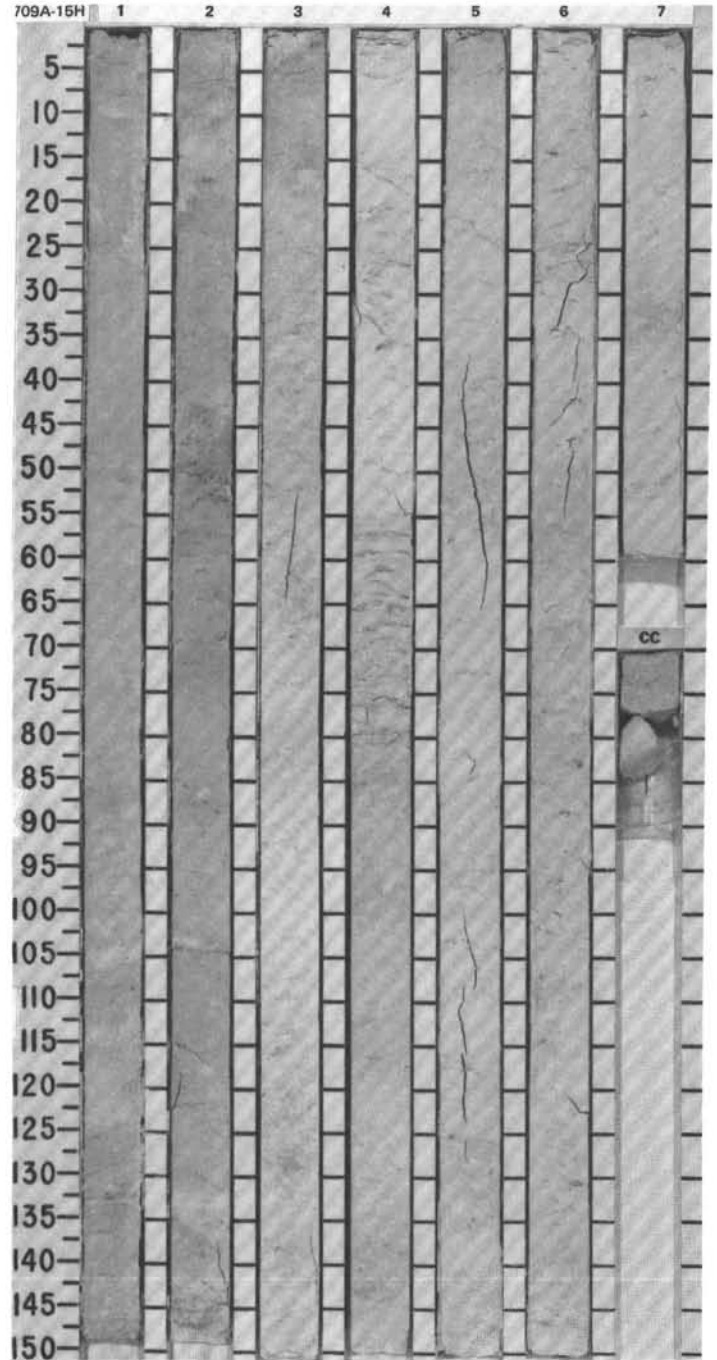


SITE 709 HOLE A CORE 14H CORED INTERVAL 3162.2-3171.9 mbsl; 125.8-135.5 mbsf

TIME-ROCK UNIT	BIOSTRAT. ZONE/ FOSSIL CHARACTER			PALEOMAGNETICS	PHYS. PROPERTIES	CHEMISTRY	SECTION METERS	GRAPHIC LITHOLOGY	DRILLING DISTURB. SED. STRUCTURES SAMPLES	LITHOLOGIC DESCRIPTION																																				
	FORAMINIFERS	NANNOFOSSILS	RADIOLARIANS DIATOMS																																											
MIDDLE MIOCENE	AM	CN 4 (NN 5)	Barten				0.5 1.0		*	<p>CLAY-BEARING NANNOFOSSIL OOZE</p> <p>Major lithology: Clay-bearing nannofossil ooze, white (10YR 8/1), faintly burrow-mottled.</p> <p>Minor lithologies:</p> <p>a. Clay-bearing nannofossil chalk, white (10YR 8/1), irregularly spaced, thin chalky intervals in Sections 3, 5, and 6.</p> <p>b. Clay-bearing foraminifer-bearing nannofossil ooze, Section 6, 70-150 cm, white (10YR 8/1).</p> <p>SMEAR SLIDE SUMMARY (%):</p> <table border="1"> <tr> <td></td> <td>1, 66</td> <td>3, 67</td> <td>6, 100</td> </tr> <tr> <td></td> <td>D</td> <td>D</td> <td>D</td> </tr> </table> <p>TEXTURE:</p> <table border="1"> <tr> <td>Sand</td> <td>10</td> <td>5</td> <td>10</td> </tr> <tr> <td>Silt</td> <td>20</td> <td>30</td> <td>20</td> </tr> <tr> <td>Clay</td> <td>70</td> <td>65</td> <td>70</td> </tr> </table> <p>COMPOSITION:</p> <table border="1"> <tr> <td>Accessory minerals</td> <td>Tr</td> <td>Tr</td> <td>—</td> </tr> <tr> <td>Foraminifers</td> <td>10</td> <td>5</td> <td>10</td> </tr> <tr> <td>Nannofossils</td> <td>90</td> <td>95</td> <td>90</td> </tr> <tr> <td>Sponge spicules</td> <td>—</td> <td>—</td> <td>Tr</td> </tr> </table>		1, 66	3, 67	6, 100		D	D	D	Sand	10	5	10	Silt	20	30	20	Clay	70	65	70	Accessory minerals	Tr	Tr	—	Foraminifers	10	5	10	Nannofossils	90	95	90	Sponge spicules	—	—	Tr
	1, 66	3, 67	6, 100																																											
	D	D	D																																											
Sand	10	5	10																																											
Silt	20	30	20																																											
Clay	70	65	70																																											
Accessory minerals	Tr	Tr	—																																											
Foraminifers	10	5	10																																											
Nannofossils	90	95	90																																											
Sponge spicules	—	—	Tr																																											
	AM	CN 4 (NN 3)	Barten				2		*																																					
	AM	CN 4 (NN 2 - NN 3)	Barten				3		*																																					
	AM	CN 4 (NN 2 - NN 3)	Barten				4		*																																					
	AM	CN 4 (NN 2 - NN 3)	Barten				5		*																																					
	AM	CN 4 (NN 2 - NN 3)	Barten				6		*																																					
	AM	CN 4 (NN 2 - NN 3)	Barten				7		*																																					

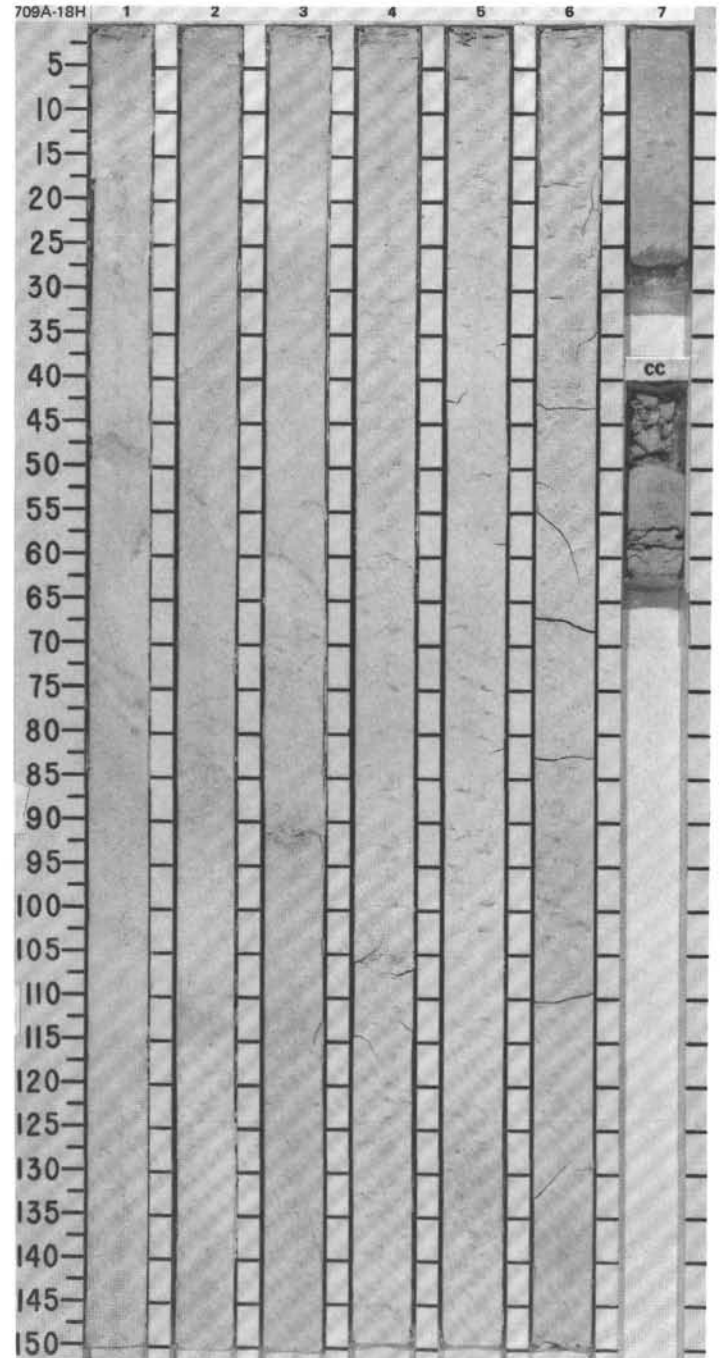


TIME-ROCK UNIT	BIOSTRAT. ZONE/ FOSSIL CHARACTER			PALEOMAGNETICS	PHYS. PROPERTIES	CHEMISTRY	SECTION	METERS	GRAPHIC LITHOLOGY	DRILLING DISTURB.	SED. STRUCTURES	SAMPLES	LITHOLOGIC DESCRIPTION																												
	FORAMINIFERS	NANNOFOSSILS	RADIOLARIANS																																						
LOWER MIOCENE																																									
AM	N 9 - N 12							0.5					<p>FORAMINIFER-BEARING NANNOFOSSIL OOZE and CLAY-BEARING FORAMINIFER-BEARING NANNOFOSSIL OOZE</p> <p>Major lithologies: Foraminifer-bearing nannofossil ooze and clay-bearing foraminifer-bearing nannofossil ooze, faintly burrow-mottled, white (10YR 8/2) to light gray (10YR 7/2).</p> <p>Minor lithologies: Foraminifer-bearing nannofossil chalk and clay-bearing foraminifer-bearing nannofossil chalk, white (10YR 8/2) to light gray (10YR 7/2), occurring in thin, irregularly spaced intervals.</p> <p>SMEAR SLIDE SUMMARY (%):</p> <table border="1"> <tr> <td></td> <td>1, 69</td> <td>3, 69</td> <td>6, 82</td> </tr> <tr> <td>D</td> <td></td> <td></td> <td></td> </tr> </table> <p>TEXTURE:</p> <table border="1"> <tr> <td>Sand</td> <td>10</td> <td>10</td> <td>10</td> </tr> <tr> <td>Silt</td> <td>20</td> <td>20</td> <td>20</td> </tr> <tr> <td>Clay</td> <td>70</td> <td>70</td> <td>70</td> </tr> </table> <p>COMPOSITION:</p> <table border="1"> <tr> <td>Foraminifers</td> <td>10</td> <td>10</td> <td>10</td> </tr> <tr> <td>Nannofossils</td> <td>90</td> <td>90</td> <td>90</td> </tr> </table>		1, 69	3, 69	6, 82	D				Sand	10	10	10	Silt	20	20	20	Clay	70	70	70	Foraminifers	10	10	10	Nannofossils	90	90	90
	1, 69	3, 69	6, 82																																						
D																																									
Sand	10	10	10																																						
Silt	20	20	20																																						
Clay	70	70	70																																						
Foraminifers	10	10	10																																						
Nannofossils	90	90	90																																						
AM	CN 3 (NN 4)						1.0																																		
	Barren																																								
	Barren																																								
CC																																									

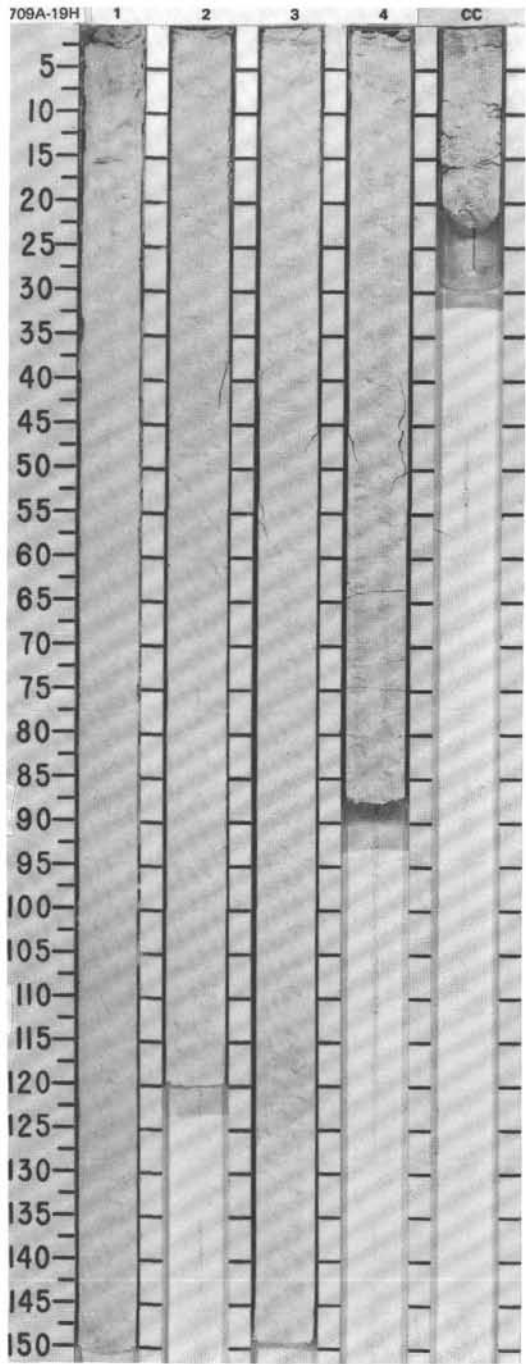


SITE 709 HOLE A CORE 18H CORED INTERVAL 3201.0-3210.7 mbsl; 164.6-174.3 mbsf

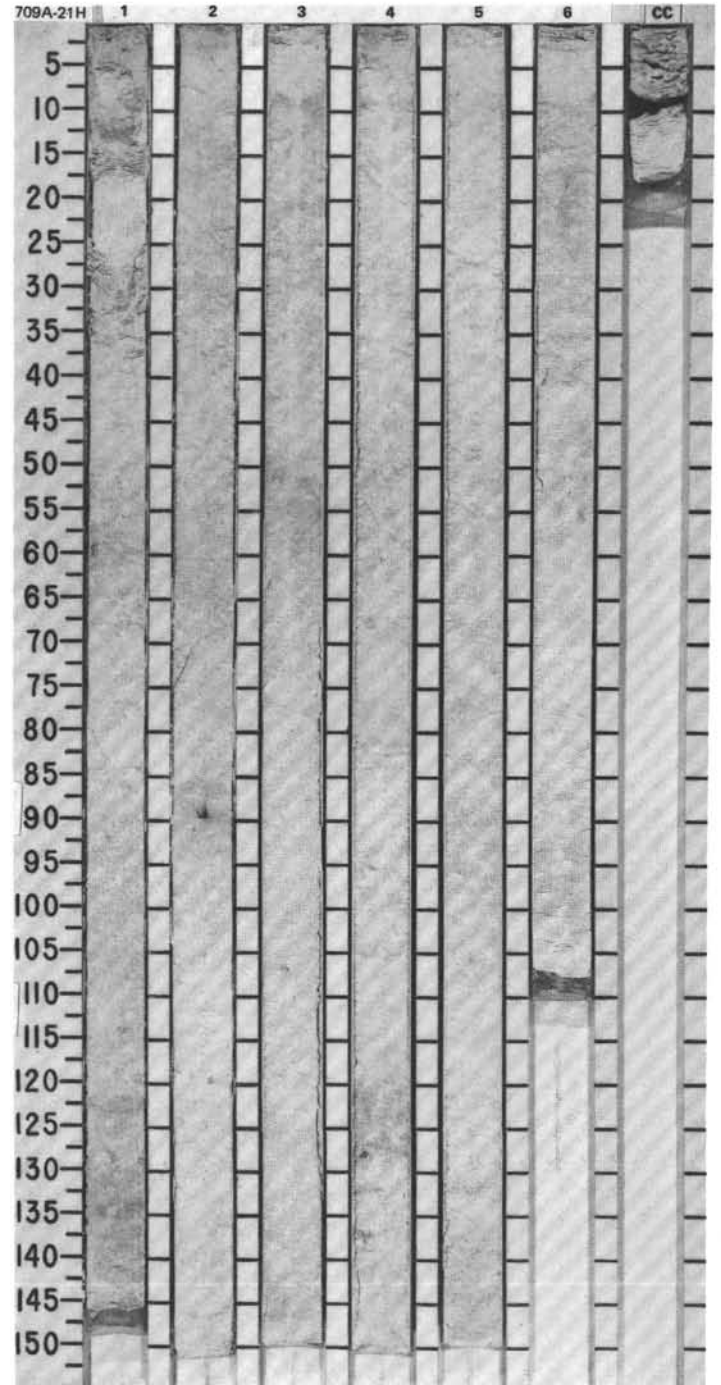
TIME-ROCK UNIT	BIOSTRAT. ZONE/ FOSSIL CHARACTER				PALEOMAGNETICS	PHYS. PROPERTIES	CHEMISTRY	SECTION	METERS	GRAPHIC LITHOLOGY	DRILLING DISTURB.	SED. STRUCTURES	SAMPLES	LITHOLOGIC DESCRIPTION
	FORAMINIFERS	NANNOFOSSILS	RADIOLARIANS	DIATOMS										
CP	LOWER MIOCENE													<p>NANNOFOSSIL OOZE and CLAY-BEARING NANNOFOSSIL OOZE, alternating with NANNOFOSSIL CHALK and CLAY-BEARING NANNOFOSSIL CHALK</p> <p>Major lithologies:</p> <ol style="list-style-type: none"> Nannofossil ooze and clay-bearing nannofossil ooze, white (10YR 8/2) to very pale brown (10YR 8/3). Nannofossil chalk and clay-bearing nannofossil chalk, white (10YR 8/2) to very pale brown (10YR 8/3), occurring as irregularly spaced nodules distributed throughout core. <p>SMEAR SLIDE SUMMARY (%):</p> <p style="margin-left: 40px;">3, 70 D</p> <p>TEXTURE:</p> <p>Sand 2 Silt 2 Clay 96</p> <p>COMPOSITION:</p> <p>Clay Tr Foraminifers 4 Nannofossils 96 Sponge spicules Tr</p>
AM	N 4-N 6 CN 1a and CN 1b (NN 1) Barren Barren							0.5 1.0						
								2						
								3						
								4						
								5						
								6						
								7						
								CC						



TIME-ROCK UNIT		BIOSTRAT. ZONE/ FOSSIL CHARACTER			PALEOMAGNETICS	PHYS. PROPERTIES	CHEMISTRY	SECTION	METERS	GRAPHIC LITHOLOGY	DRILLING DISTURB.	SED. STRUCTURES	SAMPLES	LITHOLOGIC DESCRIPTION
FORAMINIFERS	NANNOFOSSILS	RADIOLARIANS	DIATOMS											
AM	LOWER MIOCENE	N 4-N 6												<p>NANNOFOSSIL OOZE and CLAY-BEARING NANNOFOSSIL OOZE, alternating with NANNOFOSSIL CHALK and CLAY-BEARING NANNOFOSSIL CHALK</p> <p>Major lithologies:</p> <p>a. Nannofossil ooze and clay-bearing nannofossil ooze, homogeneous, white (10YR 8/2).</p> <p>b. Nannofossil chalk and clay-bearing nannofossil chalk, white (10YR 8/2), occurring as irregularly spaced nodules and biscuits in Sections 1 and 2.</p> <p>SMEAR SLIDE SUMMARY (%):</p> <p style="padding-left: 40px;">3, 80 D</p> <p>TEXTURE:</p> <p>Sand 5 Silt 2 Clay 93</p> <p>COMPOSITION:</p> <p>Quartz Tr Dolomite Tr Foraminifers 7 Nannofossils 93</p>
AM		CN 1 - CN 2(?) (NN 1 - NN 2)					1	0.5						
		Barren					2	1.0						
		Barren					3							
							4							
							CC							

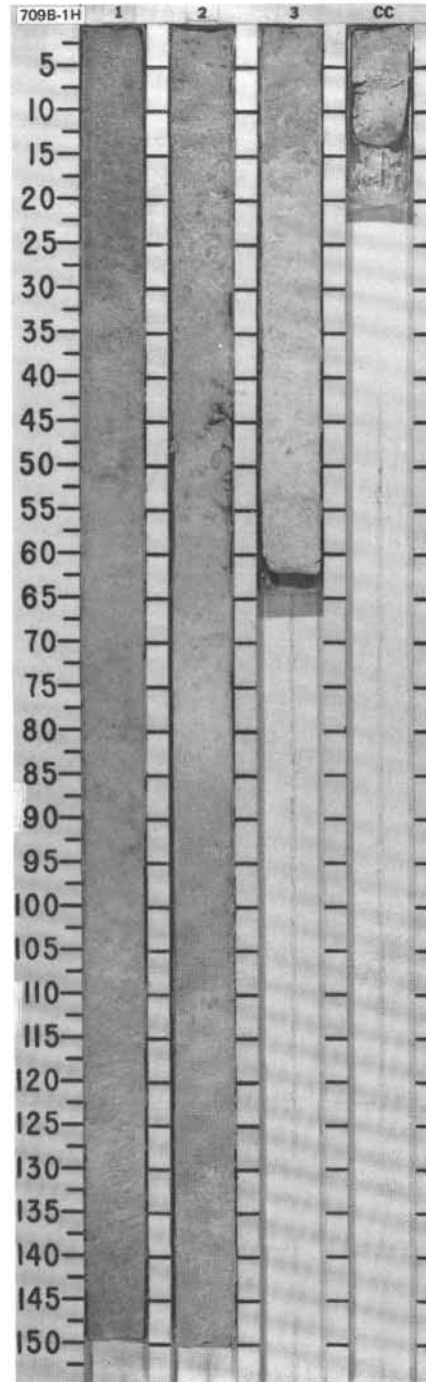


TIME-ROCK UNIT	BIOSTRAT. ZONE/ FOSSIL CHARACTER				PALEOMAGNETICS	PHYS. PROPERTIES	CHEMISTRY	SECTION	METERS	GRAPHIC LITHOLOGY	DRILLING DISTURB.	BED. STRUCTURES	SAMPLES	LITHOLOGIC DESCRIPTION
	FORAMINIFERS	NANNOFOSSILS	RADIOLARIANS	DIATOMS										
UPPER OLIGOCENE	AM	CP 19b (NP 25)	<i>Dorcadospirys atueuchus</i>											<p>NANNOFOSSIL OOZE</p> <p>Major lithology: Nannofossil ooze, homogeneous, white (10YR 8/2).</p> <p>Minor lithologies:</p> <p>a. Nannofossil chalk, white (10YR 8/2), thin, irregularly spaced lenses, sparsely distributed throughout core.</p> <p>b. Volcanic ash, Section 4, 120-130 cm, altered, bioturbated, white (10YR 8/2) mottled with light gray (10YR 7/2).</p> <p>SMEAR SLIDE SUMMARY (%):</p> <p style="margin-left: 40px;">3, 80 D</p> <p>TEXTURE:</p> <p>Sand 8 Silt 2 Clay 90</p> <p>COMPOSITION:</p> <p>Foraminifers 8 Nannofossils 91 Radiolarians Tr Sponge spicules Tr Calcareous spicules 1</p>
	RP		Barren											

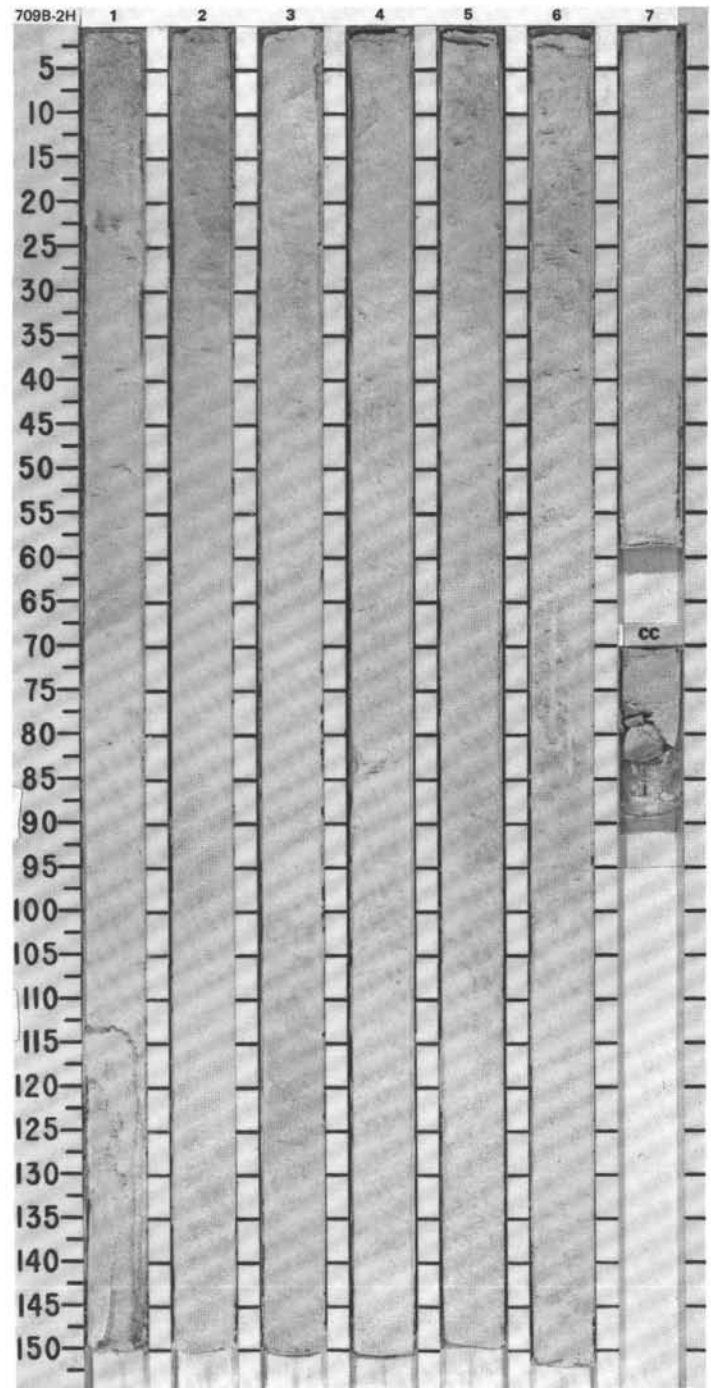


SITE 709 HOLE B CORE 1H CORED INTERVAL 3038.2-3042.0 mbsi; 0.0-3.8 mbsf

TIME-ROCK UNIT	BIOSTRAT. ZONE/ FOSSIL CHARACTER				PALEOMAGNETICS	PHYS. PROPERTIES	CHEMISTRY	SECTION METERS	GRAPHIC LITHOLOGY	DRILLING DISTURB.	SED. STRUCTURES	SAMPLES	LITHOLOGIC DESCRIPTION	
	FORAMINIFERS	NANNOFOSSILS	RADIOLARIANS	DIATOMS										
PLEISTOCENE								0.5					<p>NANNOFOSSIL-FORAMINIFER OOZE with CLAY-BEARING NANNOFOSSIL-FORAMINIFER OOZE and FORAMINIFER-NANNOFOSSIL OOZE with CLAY-BEARING FORAMINIFER-NANNOFOSSIL OOZE, alternating with FORAMINIFER-BEARING NANNOFOSSIL OOZE and CLAY-BEARING FORAMINIFER-BEARING NANNOFOSSIL OOZE</p> <p>Major lithologies:</p> <p>a. Nannofossil-foraminifer ooze and clay-bearing nannofossil-foraminifer ooze, very pale brown (10YR 8/3).</p> <p>b. Foraminifer-nannofossil ooze and clay-bearing foraminifer-nannofossil ooze, light gray (10YR 7/1) to white (10YR 8/2).</p> <p>c. Foraminifer-bearing nannofossil ooze and clay-bearing foraminifer-bearing nannofossil ooze, very pale brown (10YR 8/3) and light gray (10YR 7/2) to white (10YR 8/2).</p> <p>Faint burrow-mottling throughout core.</p> <p>SMEAR SLIDE SUMMARY (%):</p> <p>2, 80 D</p> <p>TEXTURE:</p> <p>Sand 15 Silt 5 Clay 80</p> <p>COMPOSITION:</p> <p>Foraminifers 15 Nannofossils 80 Diatoms 3 Radiolarians 2 Sponge spicules Tr Fish remains Tr</p>	
	AG CN 14b (NN 20)	CN 15 (NN 21)						1.0						
								2						
								3						
							CC							

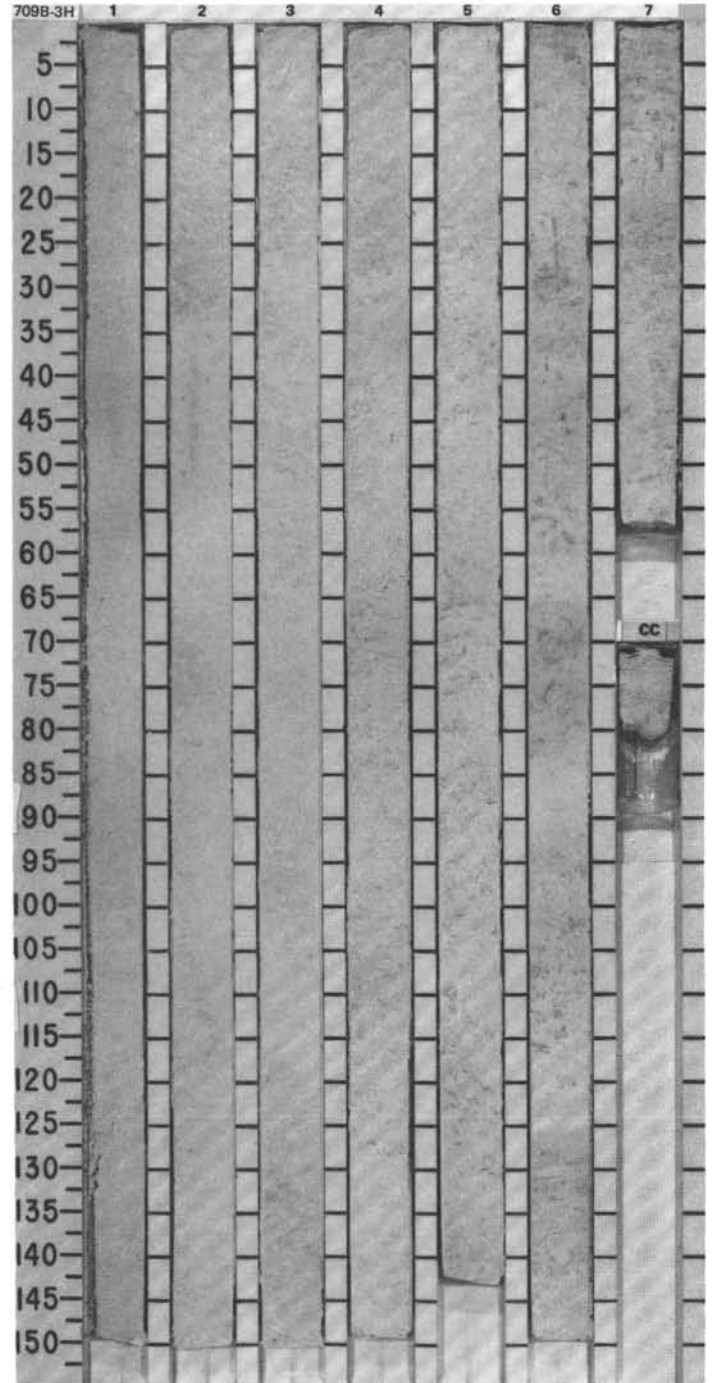


TIME-ROCK UNIT	BIOSTRAT. ZONE/ FOSSIL CHARACTER			PALEOMAGNETICS	PHYS. PROPERTIES	CHEMISTRY	SECTION	METERS	GRAPHIC LITHOLOGY	DRILLING DISTURB.	SEP. STRUCTURES	SAMPLES	LITHOLOGIC DESCRIPTION
	FORAMINIFERS	NANNOFOSSILS	RADIOLARIANS										
PLEISTOCENE	AG	CN 14a (NN 19)	<i>N. reinholdii</i>					0.5 1 1.0					<p>FORAMINIFER-BEARING NANNOFOSSIL OOZE and CLAY-BEARING FORAMINIFER-BEARING NANNOFOSSIL OOZE</p> <p>Major lithologies: Foraminifer-bearing nannofossil ooze and clay-bearing foraminifer-bearing nannofossil ooze, white (10YR 8/2, 8/1) to light gray (10YR 7/2), faintly burrow-mottled (intermittently).</p> <p>SMEAR SLIDE SUMMARY (%):</p> <p>1, 80 D</p> <p>TEXTURE:</p> <p>Silt 22 Clay 78</p> <p>COMPOSITION:</p> <p>Volcanic glass 1 Foraminifers 20 Nannofossils 78 Diatoms Tr Radiolarians 1 Sponge spicules Tr Silicoflagellates Tr</p>
	AG							2					
	CM							3					
								4					
								5					
								6					
								7					
								CC					

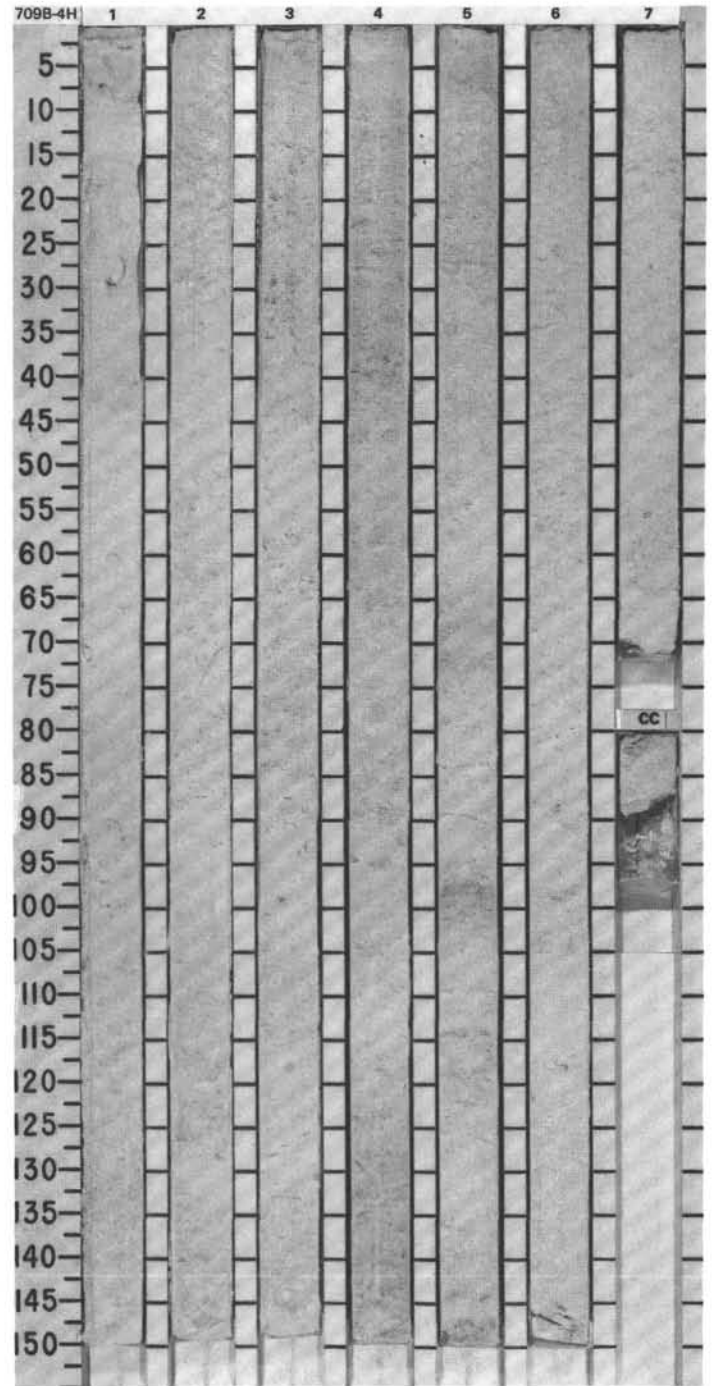


SITE 709 HOLE B CORE 3H CORED INTERVAL 3051.6-3061.3 mbsl: 13.4-23.1 mbsf

TIME-ROCK UNIT		BIOSTRAT. ZONE/ FOSSIL CHARACTER				PALEOMAGNETICS	PHYS. PROPERTIES	CHEMISTRY	SECTION	METERS	GRAPHIC LITHOLOGY	DRILLING DISTURB.	BED. STRUCTURES	SAMPLES	LITHOLOGIC DESCRIPTION																		
UPPER PLIOCENE	PLEISTOCENE	FORAMINIFERS	NANNOFOSSILS	RADIOLARIANS	DIATOMS																												
AM		CN 12d (NN 18)	CN 13 (NN 19)	CN 14b (NN 19)					0.5 1.0						<p>FORAMINIFER-BEARING NANNOFOSSIL OOZE and CLAY-BEARING FORAMINIFER-BEARING NANNOFOSSIL OOZE</p> <p>Major lithologies: Foraminifer-bearing nannofossil ooze and clay-bearing foraminifer-bearing nannofossil ooze, white (10YR 8/1), alternating with light gray (N7) and very light gray (N8). Burrow-mottling occurs in Sections 6, 7, and CC.</p> <p>SMEAR SLIDE SUMMARY (%):</p> <table border="0"> <tr> <td></td> <td>1, 80</td> </tr> <tr> <td>D</td> <td></td> </tr> </table> <p>TEXTURE:</p> <table border="0"> <tr> <td>Sand</td> <td>20</td> </tr> <tr> <td>Clay</td> <td>80</td> </tr> </table> <p>COMPOSITION:</p> <table border="0"> <tr> <td>Volcanic glass</td> <td>Tr</td> </tr> <tr> <td>Foraminifers</td> <td>20</td> </tr> <tr> <td>Nannofossils</td> <td>80</td> </tr> <tr> <td>Radiolarians</td> <td>Tr</td> </tr> <tr> <td>Sponge spicules</td> <td>Tr</td> </tr> </table>		1, 80	D		Sand	20	Clay	80	Volcanic glass	Tr	Foraminifers	20	Nannofossils	80	Radiolarians	Tr	Sponge spicules	Tr
	1, 80																																
D																																	
Sand	20																																
Clay	80																																
Volcanic glass	Tr																																
Foraminifers	20																																
Nannofossils	80																																
Radiolarians	Tr																																
Sponge spicules	Tr																																
RP		<i>R. praerbergonii</i>																															

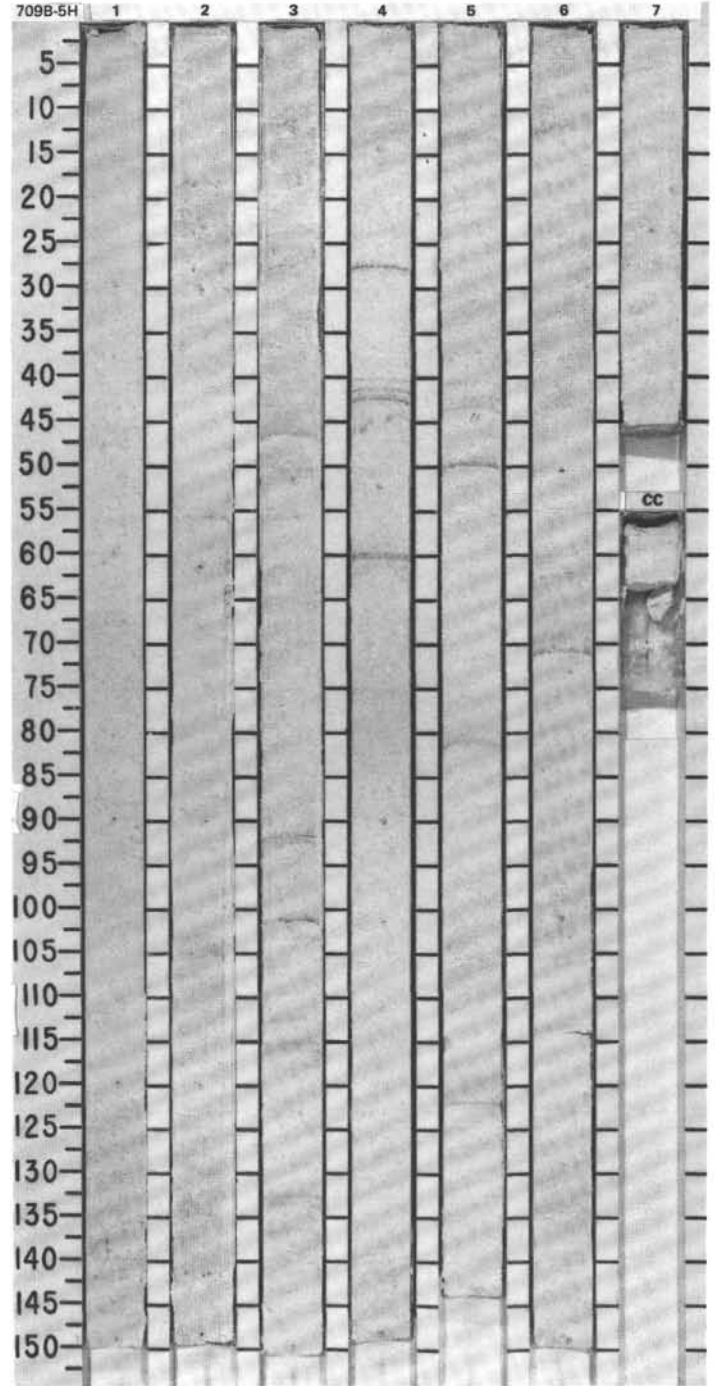


TIME-ROCK UNIT	BIOSTRAT. ZONE/ FOSSIL CHARACTER				PALEOMAGNETICS	PHYS. PROPERTIES	CHEMISTRY	SECTION	METERS	GRAPHIC LITHOLOGY	DRILLING DISTURB.	SED. STRUCTURES	SAMPLES	LITHOLOGIC DESCRIPTION	
	FORAMINIFERS	NANNOFOSSILS	RADIOLARIANS	DIATOMS											
UPPER PLIOCENE	AM	CN 12 (NN 16)	CN 12b (NN 16)	NN18				1	0.5 1.0					<p>FORAMINIFER-BEARING NANNOFOSSIL OOZE and CLAY-BEARING FORAMINIFER-BEARING NANNOFOSSIL OOZE</p> <p>Major lithologies: Foraminifer-bearing nannofossil ooze and clay-bearing foraminifer-bearing nannofossil ooze, homogeneous to slightly burrow-mottled, white (N9) and very light gray (N8) to very light greenish gray (5G 8/1), with 7 thin interbedded horizons of light greenish gray (5G 7/1) in Section 5.</p> <p>SMEAR SLIDE SUMMARY (%):</p> <p style="margin-left: 40px;">4, 100 D</p> <p>TEXTURE:</p> <p>Silt 20 Clay 80</p> <p>COMPOSITION:</p> <p>Volcanic glass Tr Foraminifers 20 Nannofossils 80 Radiolarians Tr Sponge spicules Tr Silicoflagellates Tr</p>	
	CM							2							
								3							
								4							
								5							
								6							
								7							

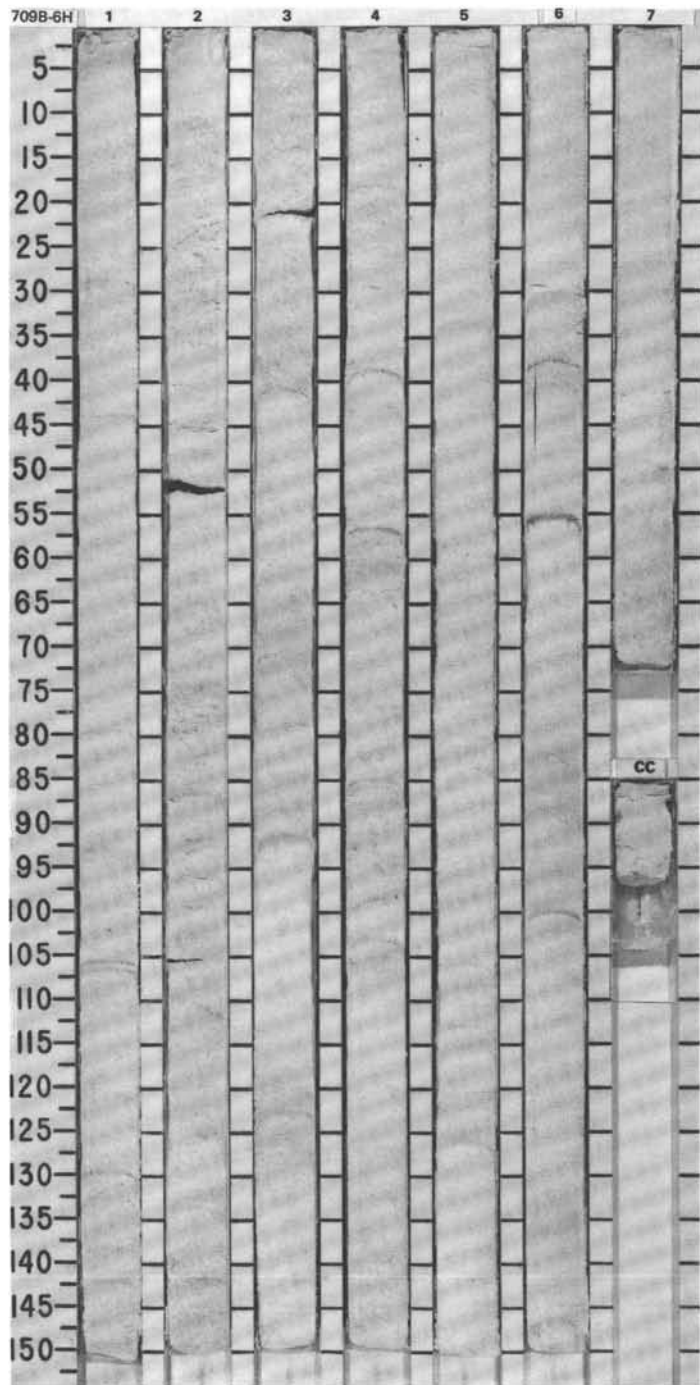


SITE 709 HOLE B CORE 5H CORED INTERVAL 3071.0-3080.6 mbsf; 32.8-42.4 mbsf

TIME-ROCK UNIT	BIOSTRAT. ZONE/ FOSSIL CHARACTER				PALEOMAGNETICS	PHYS. PROPERTIES	CHEMISTRY	SECTION	METERS	GRAPHIC LITHOLOGY	DRILLING DISTURB.	SED. STRUCTURES	SAMPLES	LITHOLOGIC DESCRIPTION
	FORAMINIFERS	NANNOFOSSILS	RADIOLARIANS	DIATOMS										
LOWER PLIOCENE	AM	CN 10c - CN 11 (NN 13 - NN 15)	CN 12b (NN 16)					0.5						<p>FORAMINIFER-BEARING NANNOFOSSIL OOZE and CLAY-BEARING FORAMINIFER-BEARING NANNOFOSSIL OOZE</p> <p>Major lithologies: Foraminifer-bearing nannofossil ooze and clay-bearing foraminifer-bearing nannofossil ooze, white (N9) and very light gray (N8) to very light greenish gray (5G 8/1), with 15 thin interbedded horizons of light gray (N7) and light greenish gray (5G 7/1) in Sections 2-6.</p> <p>SMEAR SLIDE SUMMARY (%):</p> <p>1, 80 D</p> <p>TEXTURE:</p> <p>Silt 22 Clay 78</p> <p>COMPOSITION:</p> <p>Accessory minerals: Zeolite(?) 2 Foraminifers 20 Nannofossils 78 Radiolarians Tr Sponge spicules Tr Silicoflagellates Tr</p>
	CG						1.0							
	RP							2						
								3						
								4						
								5						
								6						
							7							

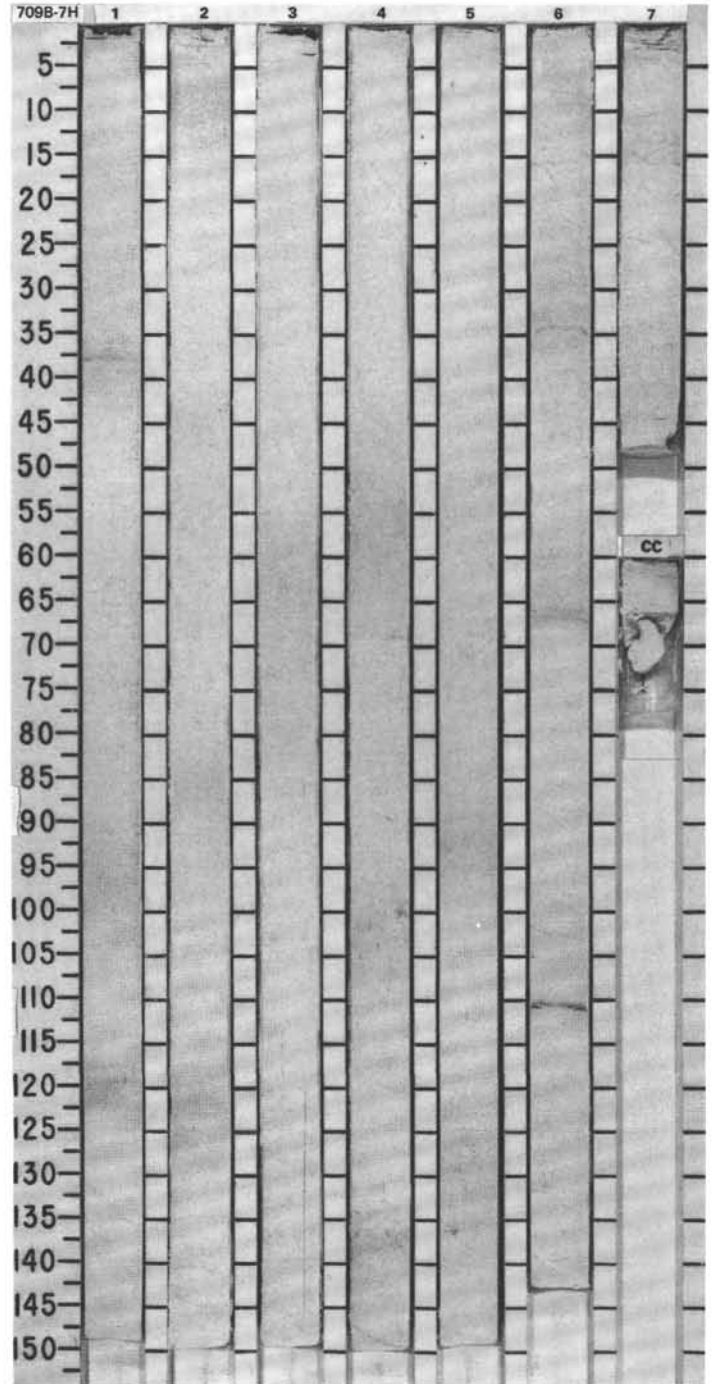


TIME-ROCK UNIT	BIOSTRAT. ZONE/ FOSSIL CHARACTER				PALEOMAGNETICS	PHYS. PROPERTIES	CHEMISTRY	SECTION	METERS	GRAPHIC LITHOLOGY	DRILLING DISTURB.	SED. STRUCTURES	SAMPLES	LITHOLOGIC DESCRIPTION														
	FORAMINIFERS	NANNOFOSSILS	RADIOLARIANS	DIATOMS																								
LOWER PLIOCENE	AM	CN 10c - CN 11 (NN 13 - NN 15)												<p>FORAMINIFER-BEARING NANNOFOSSIL OOZE and CLAY-BEARING FORAMINIFER-BEARING NANNOFOSSIL OOZE</p> <p>Major lithologies: Foraminifer-bearing nannofossil ooze and clay-bearing foraminifer-bearing nannofossil ooze, very light gray (N8) to very light greenish gray (5G 8/1), with 36 thin interbedded horizons of light greenish gray (5G 7/1) distributed throughout the core. Very slightly burrow-mottled in Sections 2 and 3.</p> <p>Minor lithology: Volcanic ash, Section 6, 55-56 cm, altered, distinct, greenish gray (5G 6/1).</p> <p>SMEAR SLIDE SUMMARY (%):</p> <table border="0"> <tr> <td></td> <td>1, 100</td> </tr> <tr> <td>TEXTURE:</td> <td>D</td> </tr> <tr> <td>Silt</td> <td>15</td> </tr> <tr> <td>Clay</td> <td>85</td> </tr> <tr> <td>COMPOSITION:</td> <td></td> </tr> <tr> <td>Foraminifers</td> <td>15</td> </tr> <tr> <td>Nannofossils</td> <td>85</td> </tr> </table>		1, 100	TEXTURE:	D	Silt	15	Clay	85	COMPOSITION:		Foraminifers	15	Nannofossils	85
	1, 100																											
TEXTURE:	D																											
Silt	15																											
Clay	85																											
COMPOSITION:																												
Foraminifers	15																											
Nannofossils	85																											
	CG	<i>Spongaster pentas</i>																										
	RP	<i>T. convexa</i>																										
	CC																											



SITE 709 HOLE B CORE 7H CORED INTERVAL 3090.2-3099.9 mbsl; 52.0-61.7 mbsf

TIME-ROCK UNIT	BIOSTRAT. ZONE/ FOSSIL CHARACTER				PALEOMAGNETICS	PHYS. PROPERTIES	CHEMISTRY	SECTION	METERS	GRAPHIC LITHOLOGY	DRILLING DISTURB.	SED. STRUCTURES	SAMPLES	LITHOLOGIC DESCRIPTION
	FORAMINIFERS	NANNOFOSSILS	RADIOLARIANS	DIATOMS										
← UPPER MIOCENE	AM ← NN 11													<p>NANNOFOSSIL OOZE and CLAY-BEARING NANNOFOSSIL OOZE</p> <p>Major lithologies: Nannofossil ooze and clay-bearing nannofossil ooze, very light gray (N8), with 9 faint, thin interbedded light gray horizons (N7), 4 thin interbedded light greenish gray (5G7/1) horizons, and 3 thin interbedded couplets of light gray (N7) below light greenish gray (5G 7/1).</p> <p>SMEAR SLIDE SUMMARY (%):</p> <p style="padding-left: 40px;">1, 100 D</p> <p>TEXTURE:</p> <p>Sand 4 Silt 1 Clay 95</p> <p>COMPOSITION:</p> <p>Volcanic glass Tr Foraminifers 5 Nannofossils 95 Sponge spicules Tr</p>
		CN 10c - CN 11 (NN 13 - NN 15)						0.5 1.0						
		CN 10a+b (NN 12)						2						
		<i>T. convexa</i>						3						
								4						
								5						
								6						
← LOWER PLIOCENE								7						



SITE 709 HOLE B CORE 9H CORED INTERVAL 3109.5-3119.2 mbsf: 71.3-81.0 mbsf

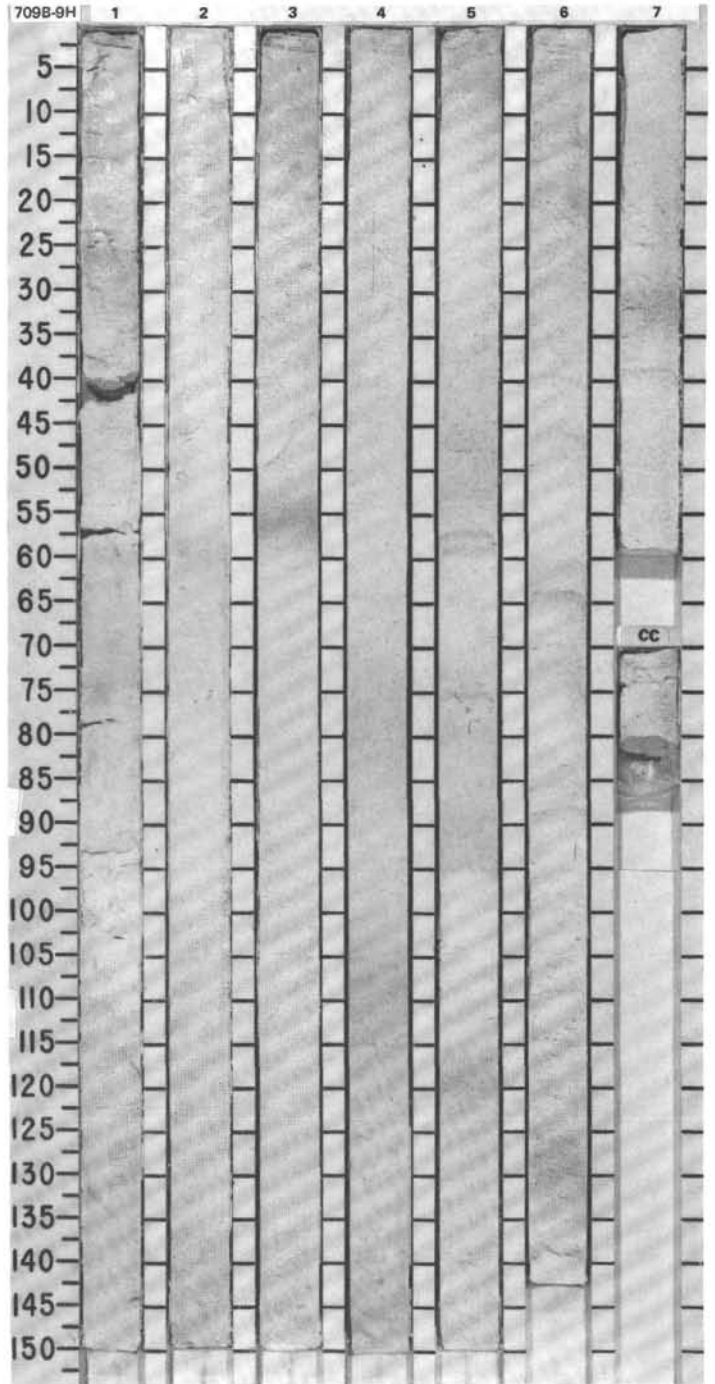
TIME-ROCK UNIT	BIOSTRAT. ZONE/ FOSSIL CHARACTER				PALEOMAGNETICS	PHYS. PROPERTIES	CHEMISTRY	SECTION	METERS	GRAPHIC LITHOLOGY	DRILLING DISTURB.	SED. STRUCTURES	SAMPLES	LITHOLOGIC DESCRIPTION																					
	FORAMINIFERS	NANNOFOSSILS	RADIOLARIANS	DIATOMS																															
UPPER MIOCENE														<p>NANNOFOSSIL OOZE</p> <p>Major lithology: Nannofossil ooze, very light gray (N8) to light gray (N7), with 5 thin interbedded horizons of light greenish gray (5G 7/1) and 5 thin couplets of light gray (N7) light greenish gray (5G 7/1) concentrated in Sections 5, 6, and 7.</p> <p>SMEAR SLIDE SUMMARY (%):</p> <table border="0"> <tr> <td></td> <td>2, 75</td> <td>5, 75</td> </tr> <tr> <td>D</td> <td>D</td> <td>D</td> </tr> </table> <p>TEXTURE:</p> <table border="0"> <tr> <td>Sand</td> <td>2</td> <td>2</td> </tr> <tr> <td>Clay</td> <td>98</td> <td>98</td> </tr> </table> <p>COMPOSITION:</p> <table border="0"> <tr> <td>Volcanic glass</td> <td>Tr</td> <td>—</td> </tr> <tr> <td>Foraminifers</td> <td>2</td> <td>2</td> </tr> <tr> <td>Nannofossils</td> <td>98</td> <td>98</td> </tr> </table>		2, 75	5, 75	D	D	D	Sand	2	2	Clay	98	98	Volcanic glass	Tr	—	Foraminifers	2	2	Nannofossils	98	98
	2, 75	5, 75																																	
D	D	D																																	
Sand	2	2																																	
Clay	98	98																																	
Volcanic glass	Tr	—																																	
Foraminifers	2	2																																	
Nannofossils	98	98																																	
AM	CN 9b (NN 11)						1	0.5																											
RP							2	1.0																											
							3																												
							4																												
							5																												
							6																												
							7																												

T. convexa

*

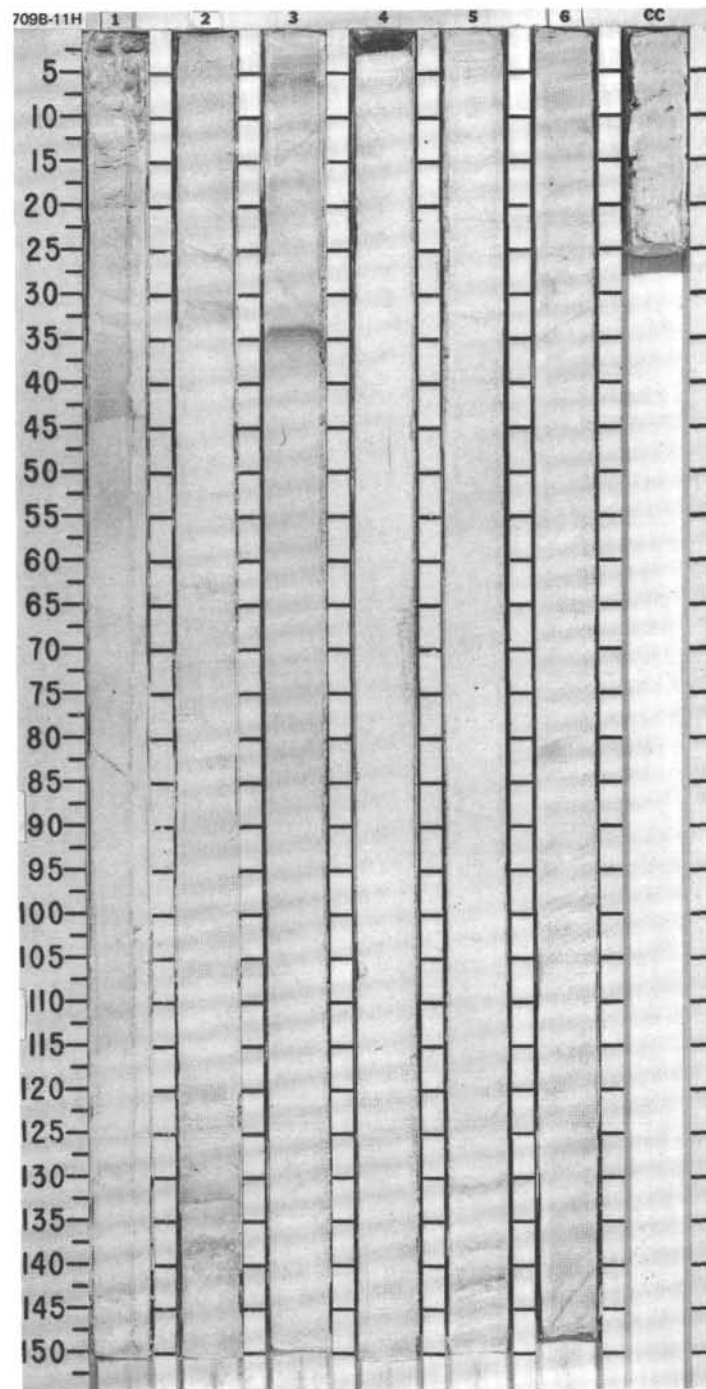
*

HP

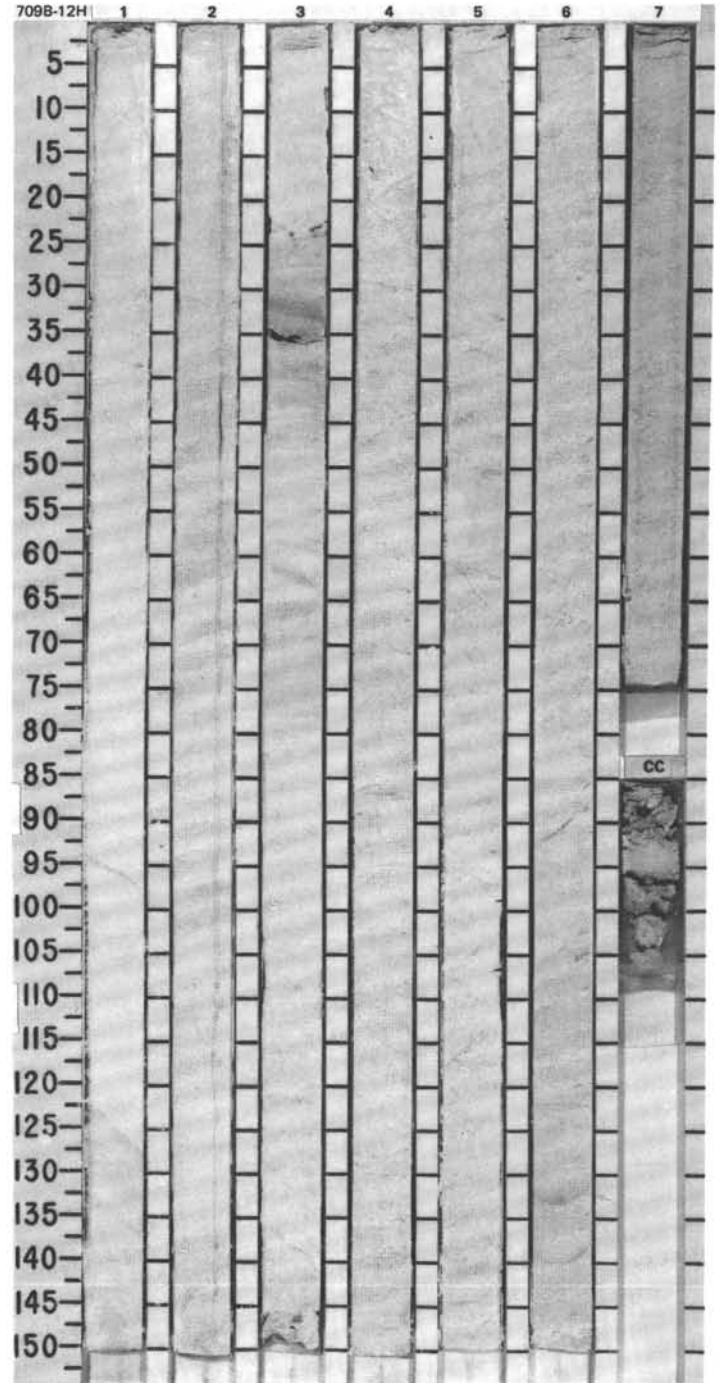


SITE 709 HOLE B CORE 11H CORED INTERVAL 3128.8-3138.5 mbsf; 90.6-100.3 mbsf

TIME-ROCK UNIT	BIOSTRAT. ZONE/ FOSSIL CHARACTER			PALEOMAGNETICS	PHYS. PROPERTIES	CHEMISTRY	SECTION	METERS	GRAPHIC LITHOLOGY	DRILLING DISTURB.	SED. STRUCTURES	SAMPLES	LITHOLOGIC DESCRIPTION																											
	FORAMINIFERS	NANNOFOSSILS	RADIOLARIANS DIATOMS																																					
UPPER MIOCENE	AM	CN 9B (NN 11)					1	0.5 1.0					<p>NANNOFOSSIL OOZE</p> <p>Major lithology: Nannofossil ooze, very light gray (N8) with horizons of light gray (N7), faintly burrow-mottled in Section 2, wavy, distorted, inclined, and curved light gray (N7) layers in Section 5, 140 cm, to CC; slump.</p> <p>SMEAR SLIDE SUMMARY (%):</p> <table border="1"> <tr> <td></td> <td>2, 75</td> <td>5, 75</td> </tr> <tr> <td></td> <td>D</td> <td>D</td> </tr> </table> <p>TEXTURE:</p> <table border="1"> <tr> <td>Sand</td> <td>5</td> <td>6</td> </tr> <tr> <td>Silt</td> <td>2</td> <td>3</td> </tr> <tr> <td>Clay</td> <td>93</td> <td>91</td> </tr> </table> <p>COMPOSITION:</p> <table border="1"> <tr> <td>Volcanic glass</td> <td>Tr</td> <td>Tr</td> </tr> <tr> <td>Foraminifers</td> <td>7</td> <td>8</td> </tr> <tr> <td>Nannofossils</td> <td>93</td> <td>91</td> </tr> <tr> <td>Sponge spicules</td> <td>Tr</td> <td>1</td> </tr> </table>		2, 75	5, 75		D	D	Sand	5	6	Silt	2	3	Clay	93	91	Volcanic glass	Tr	Tr	Foraminifers	7	8	Nannofossils	93	91	Sponge spicules	Tr	1
		2, 75	5, 75																																					
		D	D																																					
	Sand	5	6																																					
	Silt	2	3																																					
	Clay	93	91																																					
Volcanic glass	Tr	Tr																																						
Foraminifers	7	8																																						
Nannofossils	93	91																																						
Sponge spicules	Tr	1																																						
		CN 9a (NN 11)				2																																		
			Barren			3																																		
						4																																		
						5																																		
						6																																		
						CC																																		

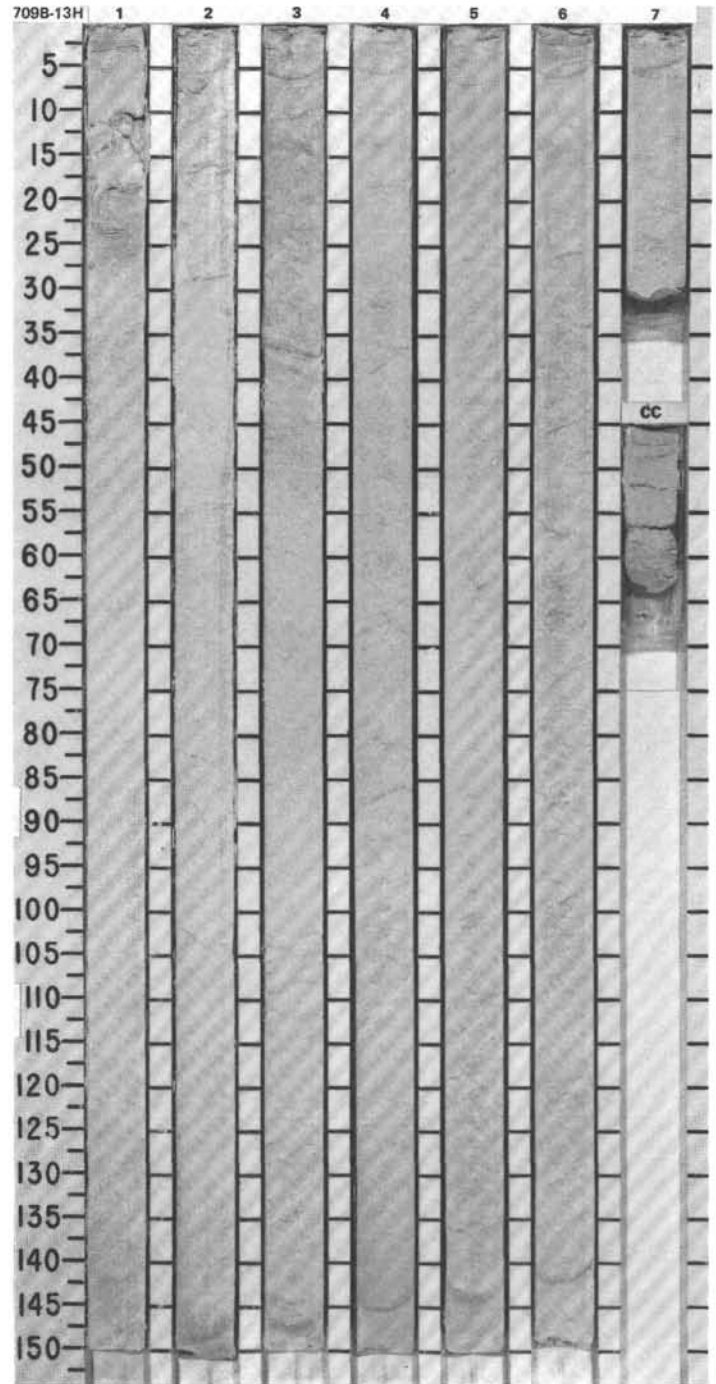


TIME-ROCK UNIT	BIOSTRAT. ZONE/ FOSSIL CHARACTER			PALEOMAGNETICS	PHYS. PROPERTIES	CHEMISTRY	SECTION	METERS	GRAPHIC LITHOLOGY	DRILLING DISTURB.	SED. STRUCTURES	SAMPLES	LITHOLOGIC DESCRIPTION																								
	FORAMINIFERS	NANNOFOSSILS	RADIOLARIANS																																		
UPPER MIOCENE	AM	CN 8 (NN 10)	CN 9a (NN 11)					0.5					<p>NANNOFOSSIL OOZE and CLAY-BEARING NANNOFOSSIL OOZE</p> <p>Major lithologies: Nannofossil ooze and clay-bearing nannofossil ooze, very light gray (N8, 5Y 8/1), with thin light gray horizons (N7) in Sections 1, 2, and 3; homogeneous and featureless in Sections 4-7; steeply inclined and wavy light gray (N7) horizons. Section 1, 125 cm, to Section 2, 70 cm; possible slump.</p> <p>SMEAR SLIDE SUMMARY (%):</p> <table border="1"> <tr> <td></td> <td>2, 75</td> <td>5, 75</td> </tr> <tr> <td>D</td> <td>D</td> <td>D</td> </tr> </table> <p>TEXTURE:</p> <table border="1"> <tr> <td>Sand</td> <td>4</td> <td>8</td> </tr> <tr> <td>Silt</td> <td>10</td> <td>12</td> </tr> <tr> <td>Clay</td> <td>86</td> <td>80</td> </tr> </table> <p>COMPOSITION:</p> <table border="1"> <tr> <td>Foraminifers</td> <td>4</td> <td>8</td> </tr> <tr> <td>Nannofossils</td> <td>96</td> <td>92</td> </tr> <tr> <td>Sponge spicules</td> <td>—</td> <td>Tr</td> </tr> </table>		2, 75	5, 75	D	D	D	Sand	4	8	Silt	10	12	Clay	86	80	Foraminifers	4	8	Nannofossils	96	92	Sponge spicules	—	Tr
		2, 75	5, 75																																		
	D	D	D																																		
	Sand	4	8																																		
	Silt	10	12																																		
	Clay	86	80																																		
	Foraminifers	4	8																																		
Nannofossils	96	92																																			
Sponge spicules	—	Tr																																			
							1.0																														
							2				*																										
							3																														
							4																														
							5				*																										
							6																														
							7																														
							CC																														

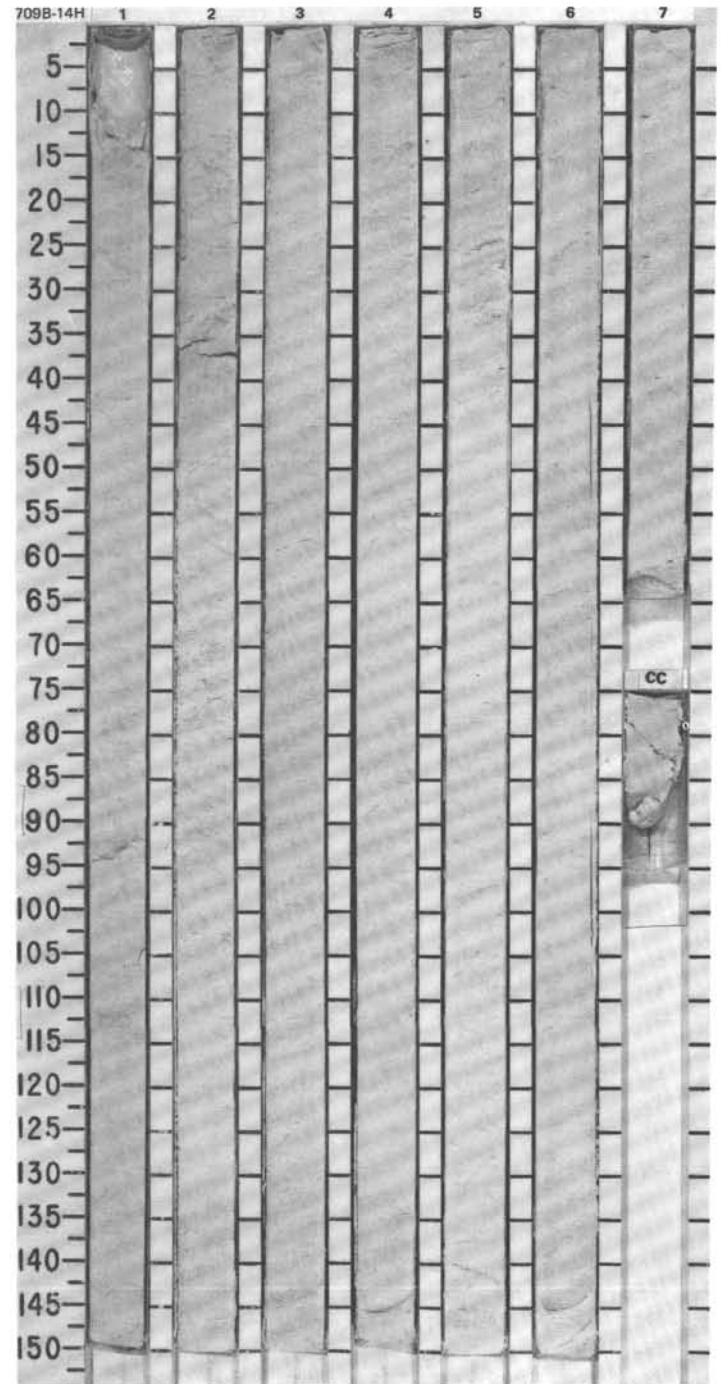


SITE 709 HOLE B CORE 13H CORED INTERVAL 3148.1-3157.7 mbsl; 109.9-119.5 mbsf

TIME-ROCK UNIT	BIOSTRAT. ZONE/ FOSSIL CHARACTER			PALEOMAGNETICS	PHYS. PROPERTIES	CHEMISTRY	SECTION	METERS	GRAPHIC LITHOLOGY	DRILLING DISTURB.	SED. STRUCTURES	SAMPLES	LITHOLOGIC DESCRIPTION																								
	FORAMINIFERS	NANNOFOSSILS	RADIOLARIANS																																		
UPPER MIOCENE																																					
AM	CN 5 ? (NN 6 ?)	CN 7 + CN 8	(NN 8 + NN 9)				1	0.5					<p>NANNOFOSSIL OOZE and CLAY-BEARING NANNOFOSSIL OOZE</p> <p>Major lithologies: Nannofossil ooze and clay-bearing nannofossil ooze, homogeneous and featureless, very light gray (N8) and light gray (N7) to white (10YR 8/1).</p> <p>SMEAR SLIDE SUMMARY (%):</p> <table border="0"> <tr> <td></td> <td>2, 75</td> <td>5, 75</td> </tr> <tr> <td></td> <td>D</td> <td>D</td> </tr> </table> <p>TEXTURE:</p> <table border="0"> <tr> <td>Sand</td> <td>8</td> <td>8</td> </tr> <tr> <td>Silt</td> <td>20</td> <td>20</td> </tr> <tr> <td>Clay</td> <td>72</td> <td>72</td> </tr> </table> <p>COMPOSITION:</p> <table border="0"> <tr> <td>Foraminifers</td> <td>8</td> <td>8</td> </tr> <tr> <td>Nannofossils</td> <td>92</td> <td>92</td> </tr> <tr> <td>Sponge spicules</td> <td>Tr</td> <td>Tr</td> </tr> </table>		2, 75	5, 75		D	D	Sand	8	8	Silt	20	20	Clay	72	72	Foraminifers	8	8	Nannofossils	92	92	Sponge spicules	Tr	Tr
	2, 75	5, 75																																			
	D	D																																			
Sand	8	8																																			
Silt	20	20																																			
Clay	72	72																																			
Foraminifers	8	8																																			
Nannofossils	92	92																																			
Sponge spicules	Tr	Tr																																			
							2	1.0			*																										
							3																														
							4																														
							5				*																										
							6																														
							7																														
							CC																														



TIME-ROCK UNIT	BIOSTRAT. ZONE/ FOSSIL CHARACTER			PALEOMAGNETICS	PHYS. PROPERTIES	CHEMISTRY	SECTION	METERS	GRAPHIC LITHOLOGY	DRILLING DISTURB. SED. STRUCTURES	SAMPLES	LITHOLOGIC DESCRIPTION																																	
	FORAMINIFERS	NANNOFOSSILS	RADIOLARIANS DIATOMS																																										
MIDDLE MIOCENE									VOID			<p>CLAY-BEARING NANNOFOSSIL OOZE</p> <p>Major lithology: Clay-bearing nannofossil ooze, homogeneous and featureless, very light gray (5Y 8/1) to white (10YR 8/1).</p> <p>SMEAR SLIDE SUMMARY (%):</p> <table border="0"> <tr> <td></td> <td>2, 75</td> <td>5, 75</td> </tr> <tr> <td></td> <td>D</td> <td>D</td> </tr> </table> <p>TEXTURE:</p> <table border="0"> <tr> <td>Sand</td> <td>1</td> <td>4</td> </tr> <tr> <td>Silt</td> <td>10</td> <td>11</td> </tr> <tr> <td>Clay</td> <td>89</td> <td>85</td> </tr> </table> <p>COMPOSITION:</p> <table border="0"> <tr> <td>Volcanic glass</td> <td>—</td> <td>Tr</td> </tr> <tr> <td>Dolomite</td> <td>—</td> <td>Tr</td> </tr> <tr> <td>Accessory minerals</td> <td>Tr</td> <td>—</td> </tr> <tr> <td>Foraminifers</td> <td>3</td> <td>8</td> </tr> <tr> <td>Nannofossils</td> <td>97</td> <td>92</td> </tr> <tr> <td>Sponge spicules</td> <td>Tr</td> <td>Tr</td> </tr> </table>		2, 75	5, 75		D	D	Sand	1	4	Silt	10	11	Clay	89	85	Volcanic glass	—	Tr	Dolomite	—	Tr	Accessory minerals	Tr	—	Foraminifers	3	8	Nannofossils	97	92	Sponge spicules	Tr	Tr
	2, 75	5, 75																																											
	D	D																																											
Sand	1	4																																											
Silt	10	11																																											
Clay	89	85																																											
Volcanic glass	—	Tr																																											
Dolomite	—	Tr																																											
Accessory minerals	Tr	—																																											
Foraminifers	3	8																																											
Nannofossils	97	92																																											
Sponge spicules	Tr	Tr																																											
							1	0.5																																					
							1	1.0																																					
							2																																						
							3																																						
							4																																						
							5																																						
							6																																						
							7																																						
							CC																																						

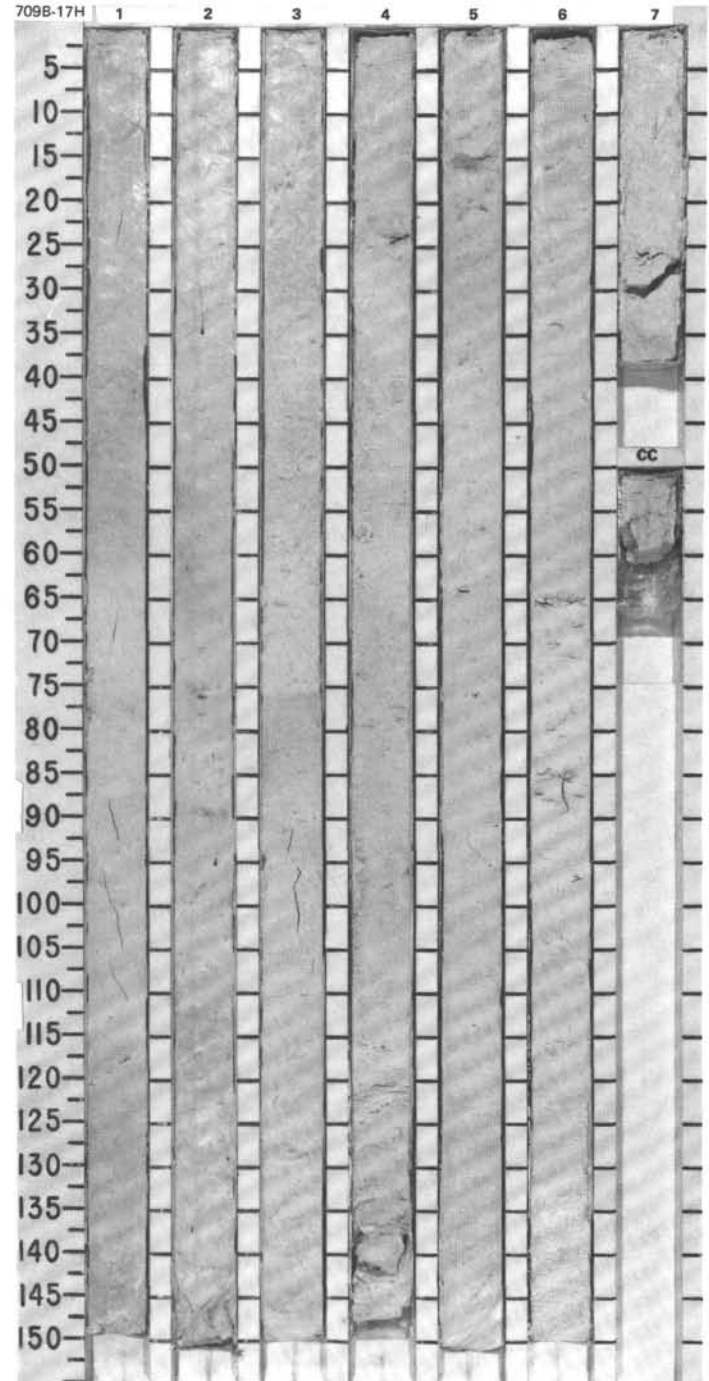


TIME-ROCK UNIT	BIOSTRAT. ZONE/ FOSSIL CHARACTER			PALEOMAGNETICS	PHYS. PROPERTIES	CHEMISTRY	SECTION	METERS	GRAPHIC LITHOLOGY	DRILLING DISTURB. SED. STRUCTURES	SAMPLES	LITHOLOGIC DESCRIPTION
	FORAMINIFERS	NANNOFOSSILS	RADIOLARIANS									
LOWER-MIDDLE MIOCENE	AM	CN 2 - CN 4 (NN 3 - NN 5)	Barren				1	0.5 1.0				<p>NANNOFOSSIL OOZE and CLAY-BEARING NANNOFOSSIL OOZE</p> <p>Major lithologies: Nannofossil ooze and clay-bearing nannofossil ooze, white (10YR 8/2) to very pale brown (10YR 8/3).</p> <p>Minor lithologies: Nannofossil chalk and clay-bearing nannofossil chalk, white (10YR 8/2) to very pale brown (10YR 8/3), occurs in thin lenses sporadically distributed throughout core.</p> <p>SMEAR SLIDE SUMMARY (%):</p> <p style="margin-left: 40px;">2, 75 D</p> <p>TEXTURE:</p> <p style="margin-left: 40px;">Sand 1 Silt 9 Clay 90</p> <p>COMPOSITION:</p> <p style="margin-left: 40px;">Foraminifers 2 Nannofossils 98</p>
							2			*		
							3					
							CC					



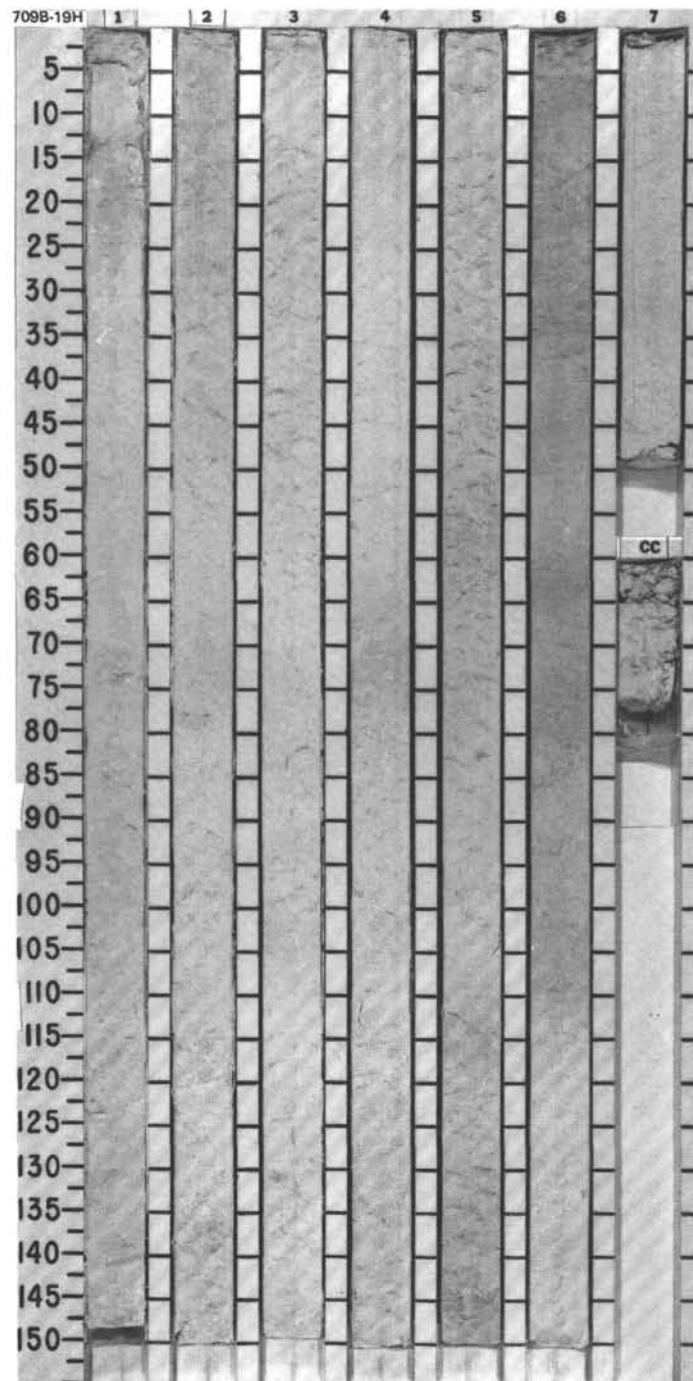
SITE 709 HOLE B CORE 17H CORED INTERVAL 3186.8-3196.5 mbsf; 148.6-158.3 mbsf

TIME-ROCK UNIT	BIOSTRAT. ZONE/ FOSSIL CHARACTER				PALEOMAGNETICS	PHYS. PROPERTIES	CHEMISTRY	SECTION METERS	GRAPHIC LITHOLOGY	DRILLING DISTURB.	SED. STRUCTURES	SAMPLES	LITHOLOGIC DESCRIPTION																														
	FORAMINIFERS	NANNOFOSSILS	RADIOLARIANS	DIATOMS																																							
LOWER-MIDDLE MIOCENE	AM	CN 2 - CN 4 (NN 3 - NN 5)	Barren					0.5					<p>NANNOFOSSIL OOZE and CLAY-BEARING NANNOFOSSIL OOZE</p> <p>Major lithologies: Nannofossil ooze and clay-bearing nannofossil ooze, white (10YR 8/2) to very pale brown (10YR 8/3), slightly burrow-mottled in Section 2.</p> <p>Minor lithologies: Nannofossil chalk and clay-bearing nannofossil chalk, white (10YR 8/2) to very pale brown (10YR 8/3), occurring in lenses irregularly distributed throughout core.</p> <p>SMEAR SLIDE SUMMARY (%):</p> <table border="1"> <tr> <td></td> <td>2, 75</td> <td>5, 75</td> </tr> <tr> <td>D</td> <td>D</td> <td>D</td> </tr> </table> <p>TEXTURE:</p> <table border="1"> <tr> <td>Sand</td> <td>2</td> <td>3</td> </tr> <tr> <td>Silt</td> <td>8</td> <td>9</td> </tr> <tr> <td>Clay</td> <td>90</td> <td>88</td> </tr> </table> <p>COMPOSITION:</p> <table border="1"> <tr> <td>Volcanic glass</td> <td>Tr</td> <td>—</td> </tr> <tr> <td>Dolomite</td> <td>Tr</td> <td>—</td> </tr> <tr> <td>Accessory minerals</td> <td>—</td> <td>Tr</td> </tr> <tr> <td>Foraminifers</td> <td>4</td> <td>6</td> </tr> <tr> <td>Nannofossils</td> <td>96</td> <td>94</td> </tr> </table>		2, 75	5, 75	D	D	D	Sand	2	3	Silt	8	9	Clay	90	88	Volcanic glass	Tr	—	Dolomite	Tr	—	Accessory minerals	—	Tr	Foraminifers	4	6	Nannofossils	96	94
									2, 75	5, 75																																	
								D	D	D																																	
								Sand	2	3																																	
								Silt	8	9																																	
								Clay	90	88																																	
								Volcanic glass	Tr	—																																	
Dolomite	Tr	—																																									
Accessory minerals	—	Tr																																									
Foraminifers	4	6																																									
Nannofossils	96	94																																									
1																																											
2									*																																		
3																																											
4																																											
5									*																																		
6																																											
7																																											



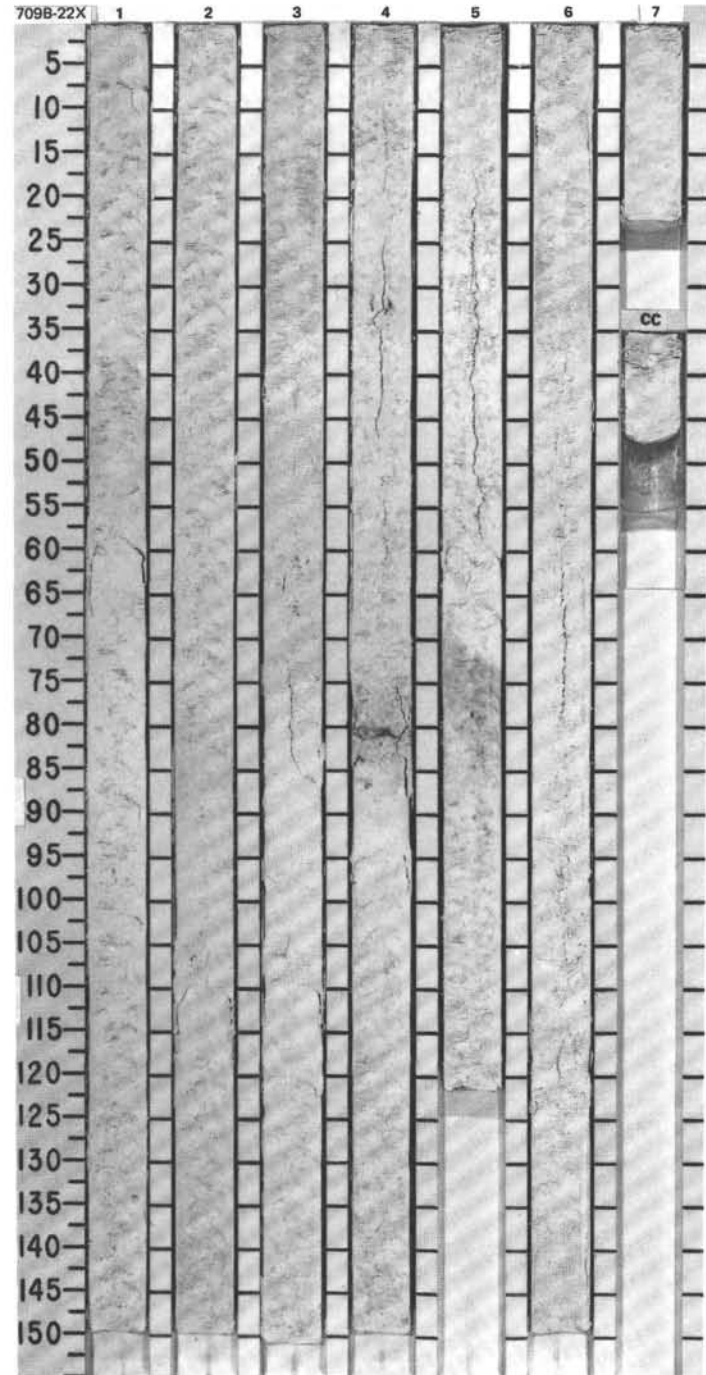
SITE 709 HOLE B CORE 19H CORED INTERVAL 3206.2-3215.8 mbsl; 168.0-177.6 mbsf

TIME-ROCK UNIT	BIOSTRAT. ZONE/ FOSSIL CHARACTER				PALEOMAGNETICS	PHYS. PROPERTIES	CHEMISTRY	SECTION	METERS	GRAPHIC LITHOLOGY	DRILLING DISTURB.	SED. STRUCTURES	SAMPLES	LITHOLOGIC DESCRIPTION	
	FORAMINIFERS	NANNOFOSSILS	RADICULARIANS	DIATOMS											
LOWER MIOCENE	AM													<p>NANNOFOSSIL OOZE and CLAY-BEARING NANNOFOSSIL OOZE</p> <p>Major lithologies: Nannofossil ooze and clay-bearing nannofossil ooze, white (10YR 8/2) to very pale brown (10YR 8/3), homogeneous except for slight burrow-mottling in Sections 5 and 6.</p> <p>Minor lithologies: Nannofossil chalk and clay-bearing nannofossil chalk, white (10YR 8/2) to very pale brown (10YR 8/3), occurring predominantly as thin lenses sporadically distributed through core; one continuous interval, Section 6, 10-30 cm.</p> <p>SMEAR SLIDE SUMMARY (%):</p> <p style="padding-left: 40px;">2.75 D</p> <p>TEXTURE:</p> <p>Sand 5 Silt 10 Clay 85</p> <p>COMPOSITION:</p> <p>Foraminifers 8 Nannofossils 92 Calcareous spicules(?) Tr</p>	
		CN 1 (NN 1 - NN 2)						0.5							
								1							
								1.0							
		Barren						2				*			
								3							
								4							
								5							
								6							
								7							
								CC							

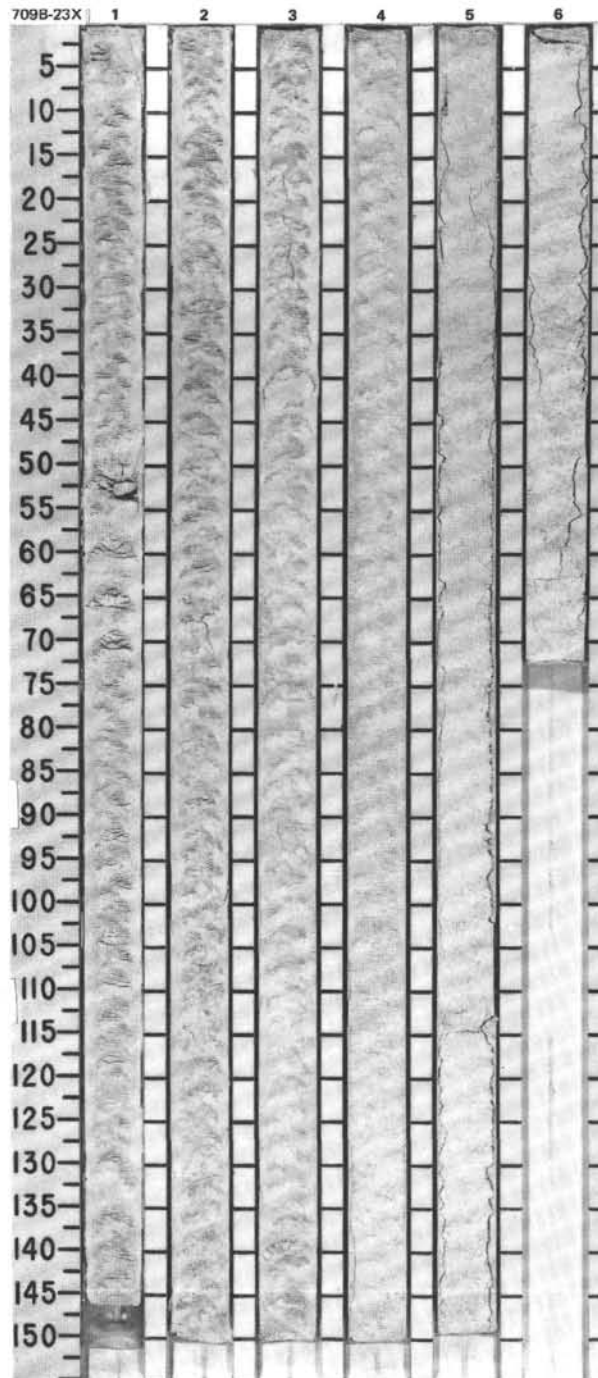


SITE 709 HOLE B CORE 22X CORED INTERVAL 3235.0-3244.7 mbsf; 196.8-206.5 mbsf

TIME-ROCK UNIT	BIOSTRAT. ZONE/ FOSSIL CHARACTER				PALEOMAGNETICS	PHYS. PROPERTIES	CHEMISTRY	SECTION METERS	GRAPHIC LITHOLOGY	DRILLING DISTURB.	SED. STRUCTURES	SAMPLES	LITHOLOGIC DESCRIPTION																											
	FORAMINIFERS	NANNOFOSSILS	RADIOLARIANS	DIATOMS																																				
LOWER MIOCENE		AM	CN 1 (NN 1)										<p>NANNOFOSSIL OOZE and CLAY-BEARING NANNOFOSSIL OOZE, alternating with NANNOFOSSIL CHALK and CLAY-BEARING NANNOFOSSIL CHALK</p> <p>Major lithologies:</p> <p>a. Nannofossil ooze and clay-bearing nannofossil ooze, homogeneous, white (10YR 8/2), distinctly less consolidated than in previous cores.</p> <p>b. Nannofossil chalk and clay-bearing nannofossil chalk, homogeneous, white (10YR 8/2), occurring in irregularly spaced nodules and highly fractured layers.</p> <p>Minor lithology: Volcanic ash, Section 4, 80-81 cm, dark grayish brown (10YR 4/2), grading above and below to light gray (N7).</p> <p>* SMEAR SLIDE SUMMARY (%):</p> <table border="1"> <tr> <td></td> <td>2, 75</td> <td>5, 75</td> </tr> <tr> <td>D</td> <td>D</td> <td>D</td> </tr> </table> <p>TEXTURE:</p> <table border="1"> <tr> <td>Sand</td> <td>5</td> <td>1</td> </tr> <tr> <td>Silt</td> <td>10</td> <td>7</td> </tr> <tr> <td>Clay</td> <td>85</td> <td>92</td> </tr> </table> <p>COMPOSITION:</p> <table border="1"> <tr> <td>Foraminifers</td> <td>10</td> <td>5</td> </tr> <tr> <td>Nannofossils</td> <td>90</td> <td>95</td> </tr> <tr> <td>Radiolarians</td> <td>Tr</td> <td>Tr</td> </tr> <tr> <td>Sponge spicules</td> <td>-</td> <td>Tr</td> </tr> </table>		2, 75	5, 75	D	D	D	Sand	5	1	Silt	10	7	Clay	85	92	Foraminifers	10	5	Nannofossils	90	95	Radiolarians	Tr	Tr	Sponge spicules	-	Tr
	2, 75	5, 75																																						
D	D	D																																						
Sand	5	1																																						
Silt	10	7																																						
Clay	85	92																																						
Foraminifers	10	5																																						
Nannofossils	90	95																																						
Radiolarians	Tr	Tr																																						
Sponge spicules	-	Tr																																						
		AM					1																																	
		AM					2																																	
		AM	<i>Lychnocanoma elongata</i>				3																																	
		AM					4																																	
UPPER OLIGOCENE	P22	AM					5																																	
		AM	<i>Dorcadospyris ateuchus</i>				6																																	
		FP		Barten			7																																	
							CC																																	

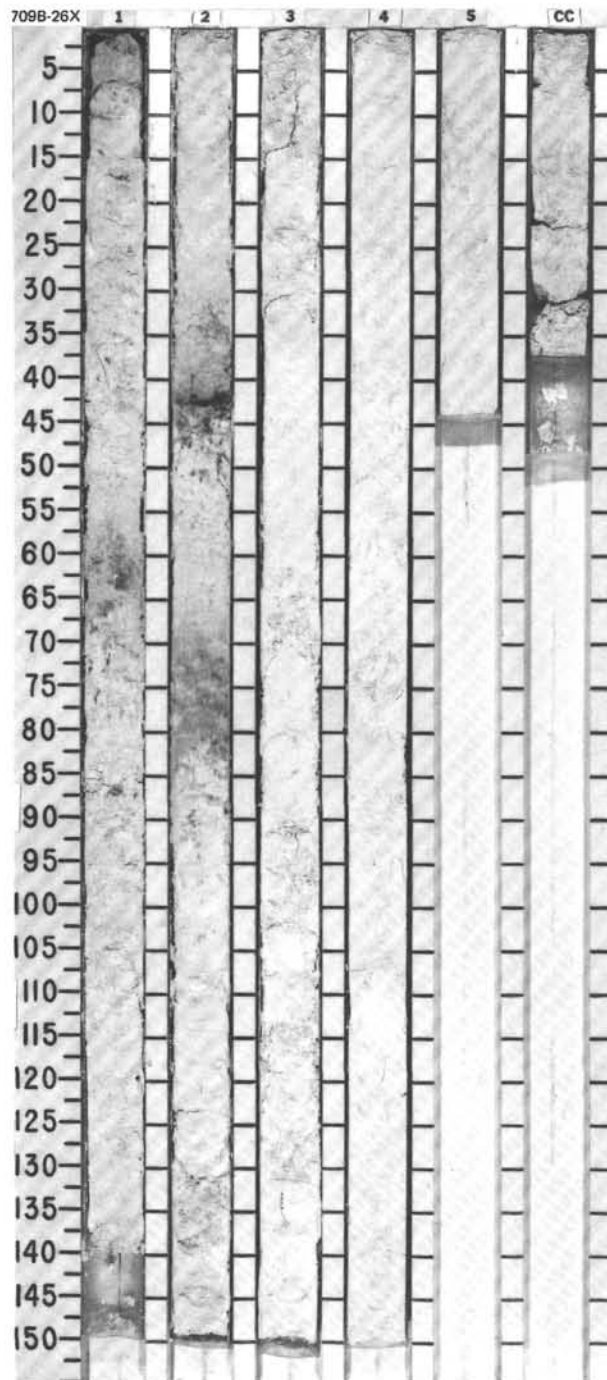


TIME-ROCK UNIT	BIOSTRAT. ZONE/ FOSSIL CHARACTER				PALEOMAGNETICS	PHYS. PROPERTIES	CHEMISTRY	SECTION	METERS	GRAPHIC LITHOLOGY	DRILLING DISTURB.	SED. STRUCTURES	SAMPLES	LITHOLOGIC DESCRIPTION
	FORAMINIFERS	NANNOFOSSILS	RADIOLARIANS	DIATOMS										
UPPER OLILOCENE	AM	CP 19b (NP 25)							0.5					<p>NANNOFOSSIL OOZE, alternating with NANNOFOSSIL CHALK</p> <p>Major lithologies:</p> <p>a. Nannofossil ooze, homogeneous, white (10YR 9/2), firm.</p> <p>b. Nannofossil chalk, homogeneous, white (10YR 9/2), occurring as irregularly spaced nodules and larger layers throughout entire core.</p> <p>SMEAR SLIDE SUMMARY (%):</p> <p>1, 100 D</p> <p>TEXTURE:</p> <p>Silt 5 Clay 95</p> <p>COMPOSITION:</p> <p>Volcanic glass Tr Foraminifers 5 Nannofossils 95 Radiolarians Tr Sponge spicules Tr</p>
	RP	<i>Dorcadospiris atauchus</i>						1.0						
		Barten						2						
								3						
								4						
								5						
								6						



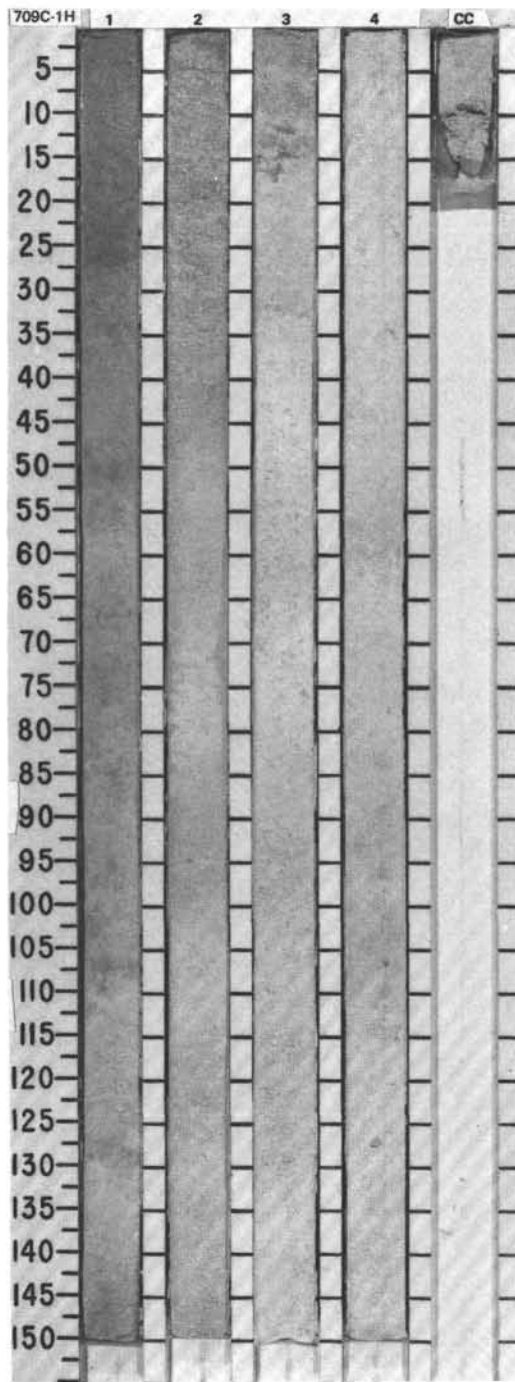
SITE 709 HOLE B CORE 26X CORED INTERVAL 3273.3-3283.3 mbsl; 235.5-245.1 mbsf

TIME-ROCK UNIT	BIOSTRAT. ZONE/ FOSSIL CHARACTER				PALEOMAGNETICS	PHYS. PROPERTIES	CHEMISTRY	SECTION	METERS	GRAPHIC LITHOLOGY	DRILLING DISTURB.	SED. STRUCTURES	SAMPLES	LITHOLOGIC DESCRIPTION
	FORAMINIFERS	NANNOFOSSILS	RADIOLARIANS	DIATOMS										
LOWER OLILOCENE	AM	CP 17 - CP 18 (NP 23)						1	0.5 1.0					FORAMINIFER-BEARING NANNOFOSSIL CHALK and CLAY-BEARING FORAMINIFER-BEARING NANNOFOSSIL CHALK
	FP	<i>Theocyrtis tuberosa</i>						2						Major lithologies: Foraminifer-bearing nannofossil chalk and clay-bearing foraminifer-bearing nannofossil chalk, homogeneous, white (10YR 9/2), continuous.
		Barren						3						Minor lithology: Volcanic ash, Section 2, 41-42 cm, distinct, very dark brownish gray (10YR 3/2), disseminated above and below in 5 cm bioturbated intervals of light gray (N7); Section 1, 0-12 cm, probable disseminated ash, altered and burrow-mottled, light gray (N7); Section 1, 56-70 cm, and Section 2, 68-84 cm, disseminated, altered, burrow-mottled, light gray (N7).
								4						SMEAR SLIDE SUMMARY (%):
								5						4, 100
								CC						D
														TEXTURE:
														Silt 10
														Clay 90
														COMPOSITION:
														Volcanic glass Tr
														Foraminifers 10
														Nannofossils 89
														Radiolarians 1
														Sponge spicules Tr

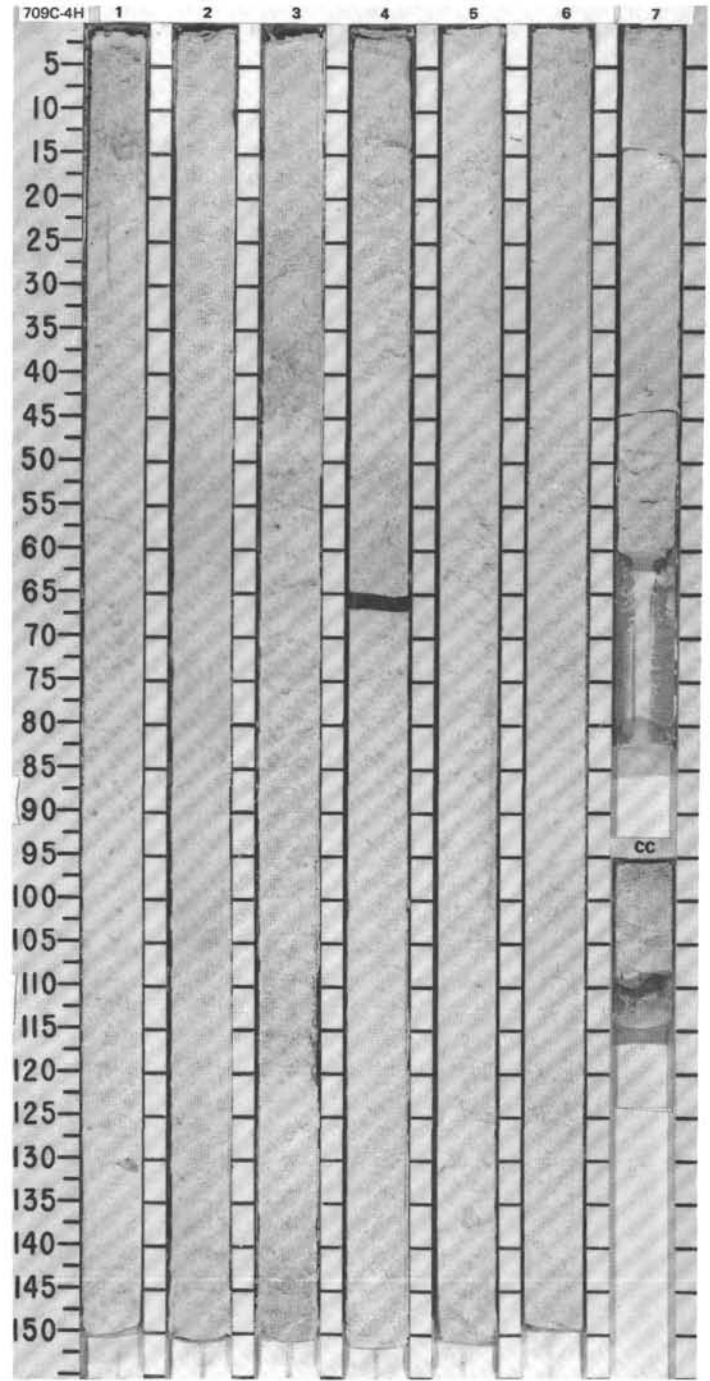


SITE 709 HOLE C CORE 1H CORED INTERVAL 3038.2-3044.0 mbsf; 0.0-5.8 mbsf

TIME-ROCK UNIT		BIOSTRAT. ZONE/ FOSSIL CHARACTER		PALEOMAGNETIC	PHYS. PROPERTIES	CHEMISTRY	SECTION METERS	GRAPHIC LITHOLOGY	DRILLING DISTURB.	SED. STRUCTURES	SAMPLES	LITHOLOGIC DESCRIPTION
FORAMINIFERS	NANNOFOSSILS	RADIOLARIANS	DIATOMS									
PLEISTOCENE												
AM	CN 14a	CN 14b (NN 20)	CN 15 (NN 21)				1					<p>FORAMINIFER-NANNOFOSSIL OOZE and CLAY-BEARING FORAMINIFER-NANNOFOSSIL OOZE</p> <p>Major lithologies: Foraminifer-nannofossil ooze and clay-bearing foraminifer-nannofossil ooze, burrow-mottled, very pale brown (10YR 7/3) and light gray (N7) to homogeneous, white (10YR 8/1, 8/2) and very pale brown (10YR 8/3).</p>
FP		<i>P. ootoolus-N. reinholdii</i>				2						
						3						
						4						
						CC						

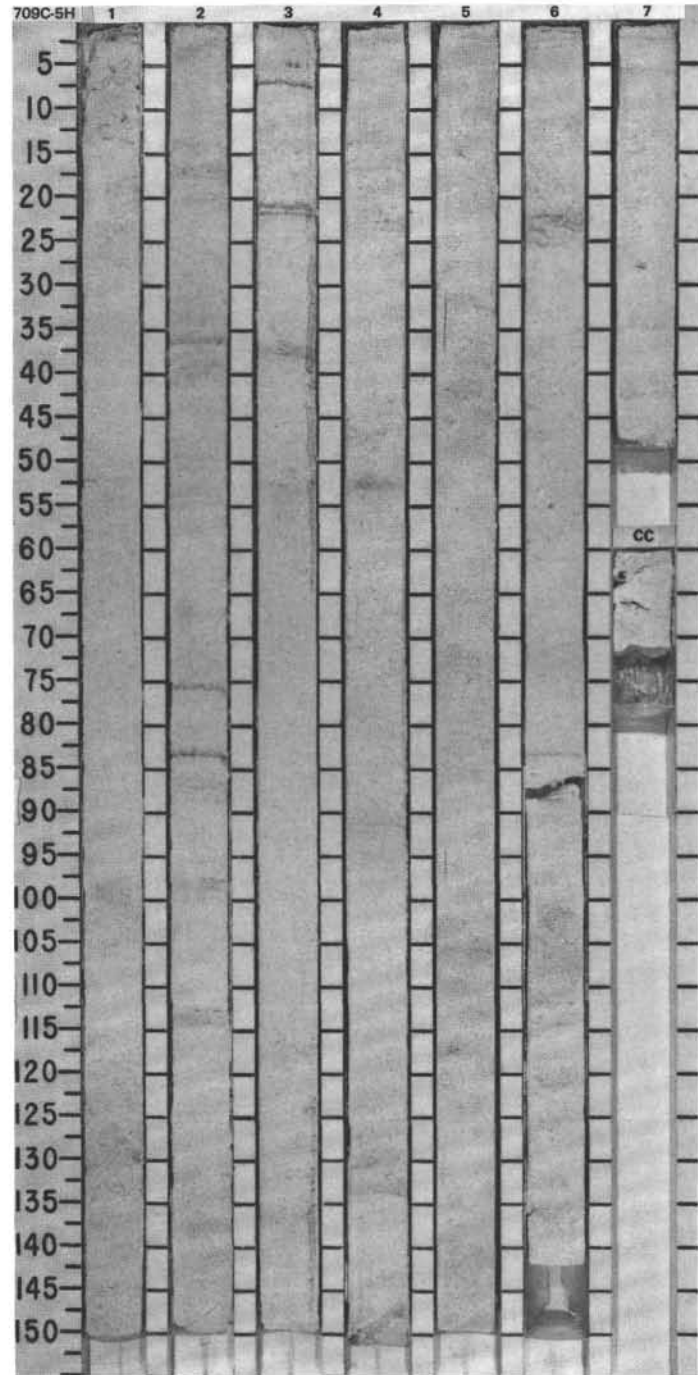


TIME-ROCK UNIT	BIOSTRAT. ZONE/ FOSSIL CHARACTER				PALEOMAGNETICS	PHYS. PROPERTIES	CHEMISTRY	SECTION	METERS	GRAPHIC LITHOLOGY	DRILLING DISTURB. SED. STRUCTURES	SAMPLES	LITHOLOGIC DESCRIPTION
	FORAMINIFERS	NANNOFOSSILS	RADIOLARIANS	DIATOMS									
UPPER PLIOCENE	AM	CN 12a (NN 16)		CN 12b+c (NN 16)				1	0.5 1.0				FORAMINIFER-BEARING NANNOFOSSIL OOZE and CLAY-BEARING FORAMINIFER-BEARING NANNOFOSSIL OOZE Major lithologies: Foraminifer-bearing nannofossil ooze and clay-bearing foraminifer-bearing nannofossil ooze, white (N9) to very light greenish gray (5G 8/1), homogeneous.
	RP		<i>N. jouseae</i>				2						
							3						
							4						
							5						
							6						
							7						
							CC						

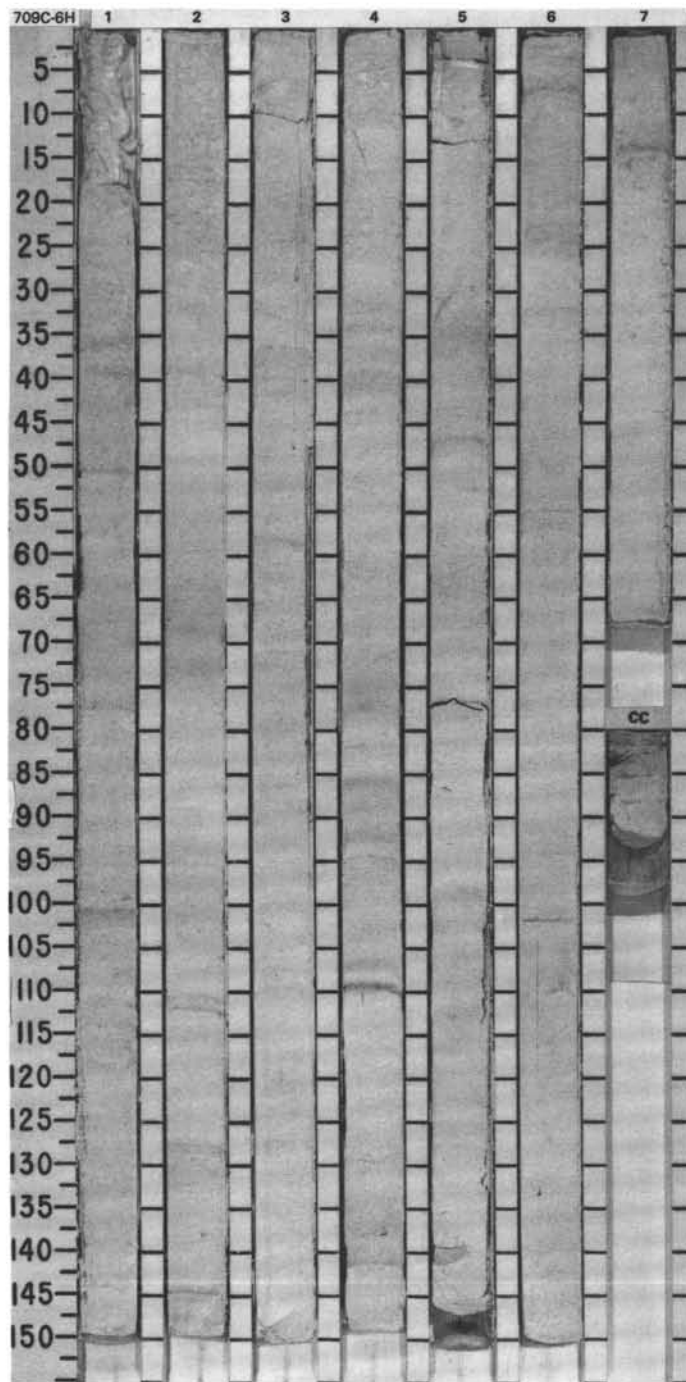


SITE 709 HOLE C CORE 5H CORED INTERVAL 3072.9-3082.5 mbsf; 34.7-44.3 mbsf

TIME-ROCK UNIT	BIOSTRAT. ZONE/ FOSSIL CHARACTER				PALEOMAGNETICS	PHYS. PROPERTIES CHEMISTRY	SECTION METERS	GRAPHIC LITHOLOGY	DRILLING DISTURB.	SED. STRUCTURES	SAMPLES	LITHOLOGIC DESCRIPTION
	FORAMINIFERS	NANNOFOSSILS	RADIOLARIANS	DIAZONS								
LOWER PLIOCENE	AM	CN 12a (NN 16)					0.5 1.0					FORAMINIFER-BEARING NANNOFOSSIL OOZE and CLAY-BEARING FORAMINIFER-BEARING NANNOFOSSIL OOZE Major lithologies: Foraminifer-bearing nannofossil ooze and clay-bearing foraminifer-bearing nannofossil ooze, white (N9) to very light greenish gray (5G 8/1), with 26 thin interbedded horizons of very light gray (N8) and light greenish gray (5G 7/1), most concentrated in Sections 2-4.
	RP	CN 10c - CN 11 (NN 13 - NN 15)					2 3 4 5 6 7					

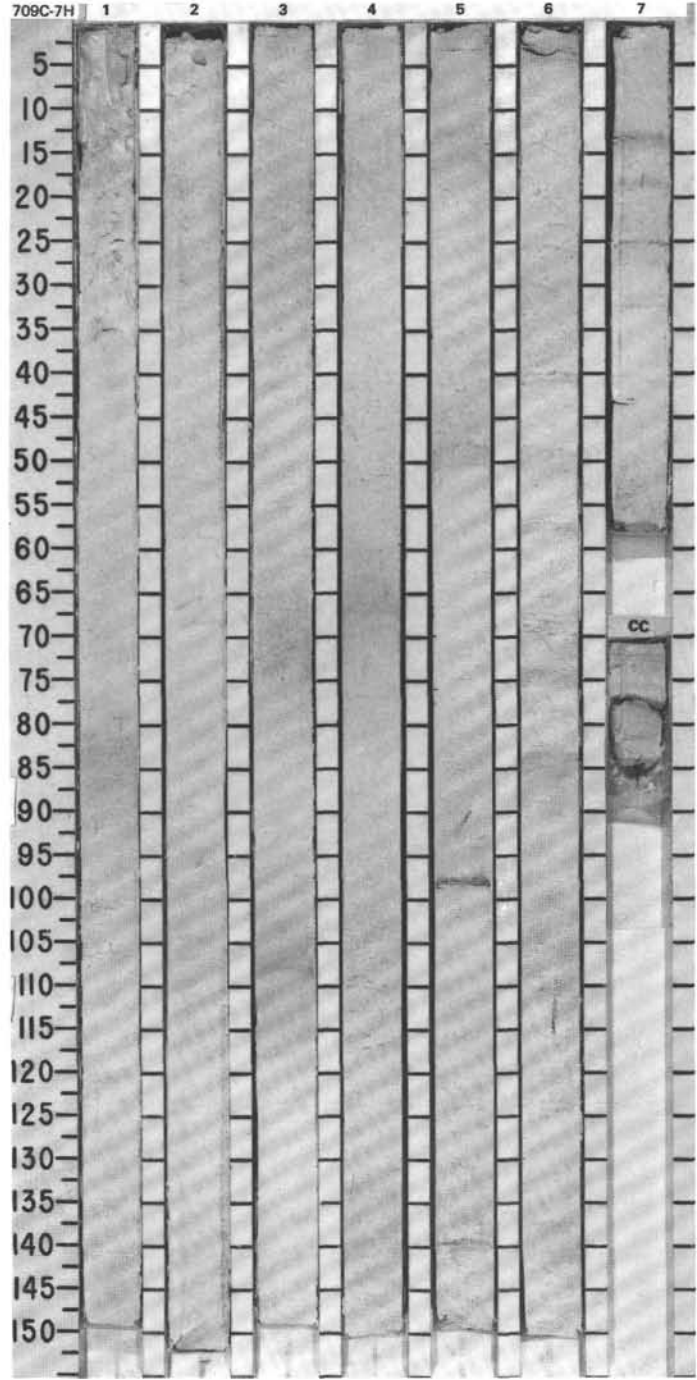


TIME-ROCK UNIT		BIOSTRAT. ZONE/ FOSSIL CHARACTER	SECTION	METERS	GRAPHIC LITHOLOGY	DRILLING DISTURB.	SED. STRUCTURES	SAMPLES	LITHOLOGIC DESCRIPTION
LOWER PLIOCENE	AM CN 10b								
		CN 10c - CN 11 (NN 13 - NN 15)							<p>FORAMINIFER-BEARING NANNOFOSSIL OOZE and CLAY-BEARING FORAMINIFER-BEARING NANNOFOSSIL OOZE</p> <p>Major lithologies: Foraminifer-bearing nannofossil ooze and clay-bearing foraminifer-bearing nannofossil ooze, white (N9) to very light greenish gray (5G 8/1), with 35 thin interbedded horizons of very light gray (N8), light gray (N7), and very light greenish gray (5G 7/1) distributed throughout the core; one thin couplet of very light gray (N8) below light greenish gray (5G7/1), Section 3, 107-110 cm.</p>
		<i>? N. jouseae</i>							

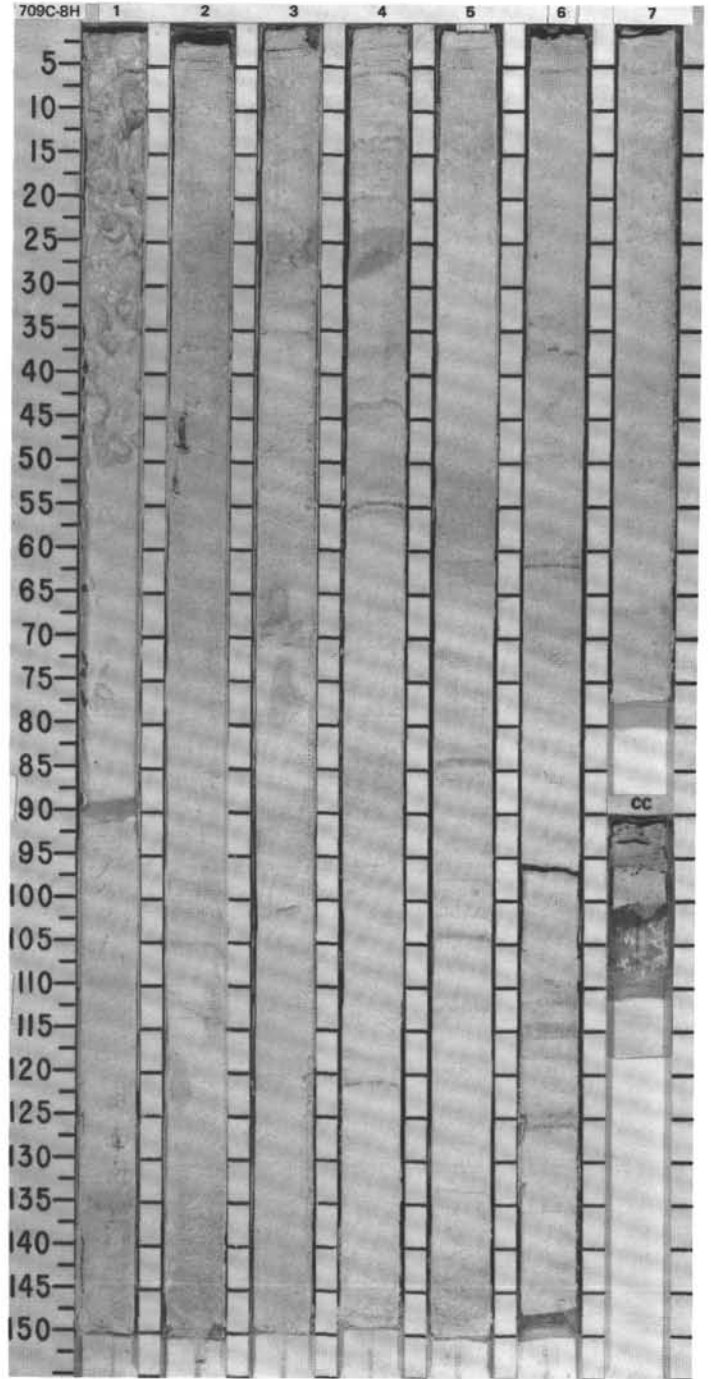


SITE 709 HOLE C CORE 7H CORED INTERVAL 3092.1-3101.8 mbsl; 53.9-63.6 mbsf

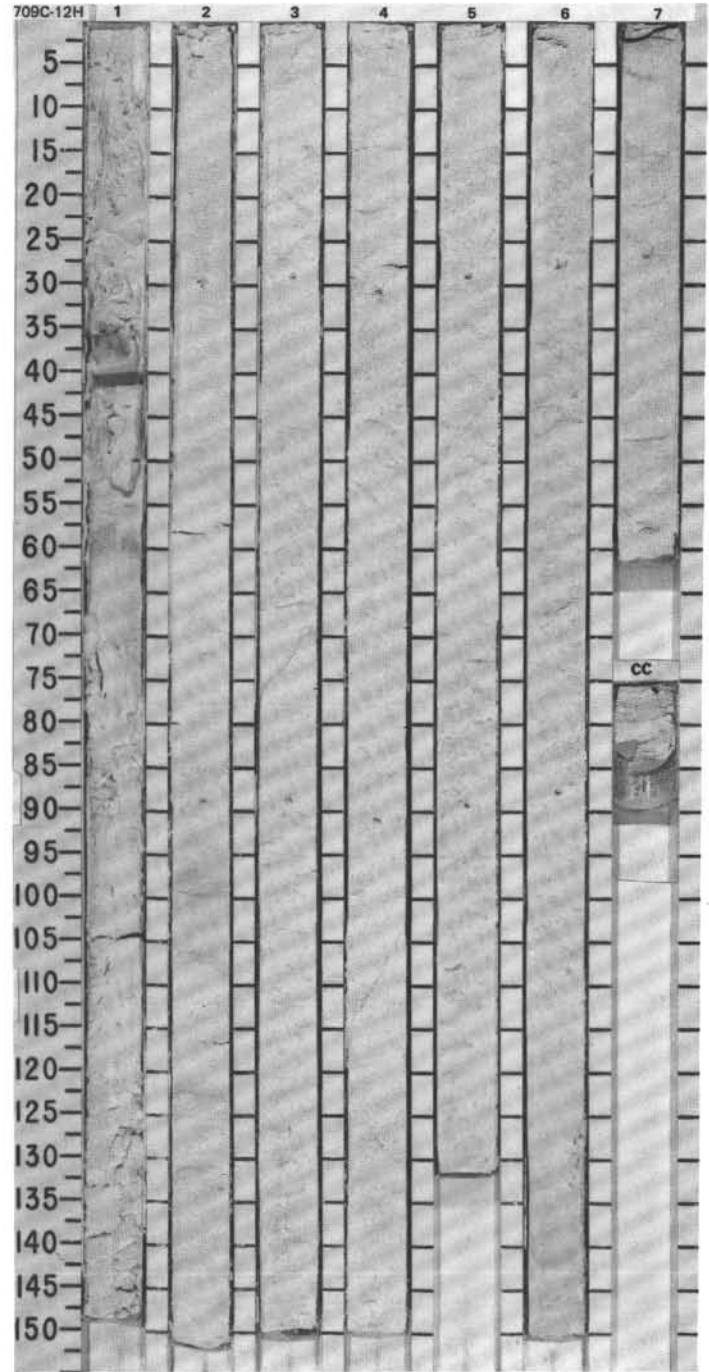
TIME-ROCK UNIT	BIOSTRAT. ZONE/ FOSSIL CHARACTER				PALEOMAGNETICS	PHYS. PROPERTIES	CHEMISTRY	SECTION METERS	GRAPHIC LITHOLOGY	DRILLING DISTURB.	SED. STRUCTURES	SAMPLES	LITHOLOGIC DESCRIPTION
	FORAMINIFERS	NANNOFOSSILS	RADIOLARIANS	DIATOMS									
UPPER MIOCENE	AM	CN 9b (NN 11)	CN 10b (NN 12)	CN 10a (NN 12)				0.5 1.0					<p>NANNOFOSSIL OOZE and CLAY-BEARING NANNOFOSSIL OOZE</p> <p>Major lithologies: Nannofossil ooze and clay-bearing nannofossil ooze, very light gray (N8) to very light greenish gray (5G 8/1), with 13 thin interbedded horizons of very light gray (N7) and very light greenish gray (5G 7/1) occurring in Section 5-CC.</p> <p>Minor lithology: Volcanic ash(?), altered, Section 5, 98-99 cm, distinct, greenish gray (5G 6/1).</p>
LOWER PLIOCENE	RP						2						
							3						
							4						
							5						
							6						
							7						



TIME-ROCK UNIT	BIOSTRAT. ZONE/ FOSSIL CHARACTER				PALEOMAGNETICS	PHYS. PROPERTIES	CHEMISTRY	SECTION	METERS	GRAPHIC LITHOLOGY	DRILLING DISTURB.	SED. STRUCTURES	SAMPLES	LITHOLOGIC DESCRIPTION
	FORAMINIFERS	NANNOFOSSILS	RADIOLARIANS	DIATOMS										
UPPER MIOCENE														<p>NANNOFOSSIL OOZE and CLAY-BEARING NANNOFOSSIL OOZE</p> <p>Major lithologies: Nannofossil ooze and clay-bearing nannofossil ooze, very light gray (N8) to very light greenish gray (5G 8/1), with 17 thin interbedded horizons of light greenish gray (5G 7/1), light gray (N7), and gray (N6), and four thin couplets of light gray (N7) below light greenish gray (5G 7/1) in Sections 2-6.</p>
AM	CN 9b (NN 11)							0.5						
RP	<i>T. convexa</i>							1.0						

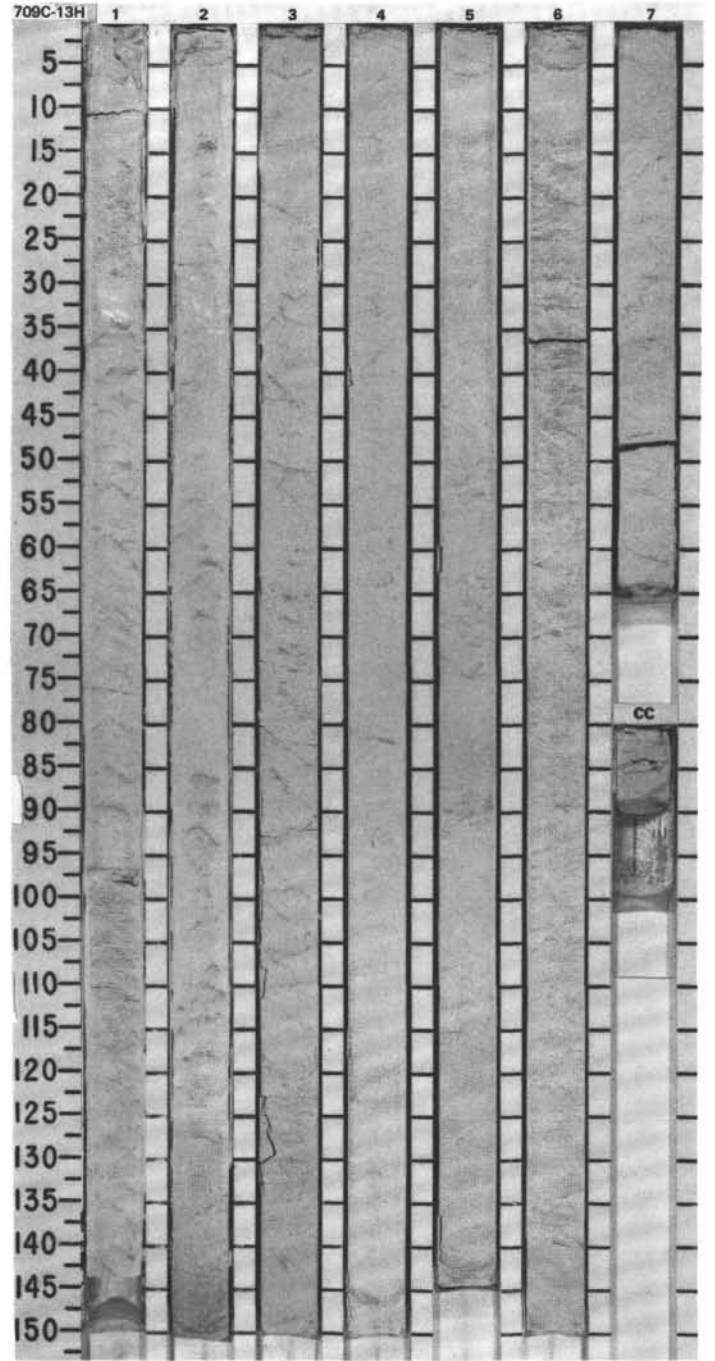


TIME-ROCK UNIT	BIOSTRAT. ZONE/ FOSSIL CHARACTER				PALEOMAGNETICS	PHYS. PROPERTIES	CHEMISTRY	SECTION	METERS	GRAPHIC LITHOLOGY	DRILLING DISTURB.	SED. STRUCTURES	SAMPLES	LITHOLOGIC DESCRIPTION
	FORAMINIFERS	NANNOFOSSILS	RADIOLARIANS	DIAATOMS										
UPPER MIOCENE	AM	AM						1	0.5 1.0				<p>NANNOFOSSIL OOZE and CLAY-BEARING NANNOFOSSIL OOZE</p> <p>Major lithologies: Nannofossil ooze and clay-bearing nannofossil ooze, very light gray (N8), with 10 thin interbedded light gray (N7) horizons, gently dipping, in Sections 3, 4, and 5.</p>	
		CN 9a (NN 11)					2							
		CN 8 (NN 10)					3							
		Barten					4							
							5							
							6							
							7							

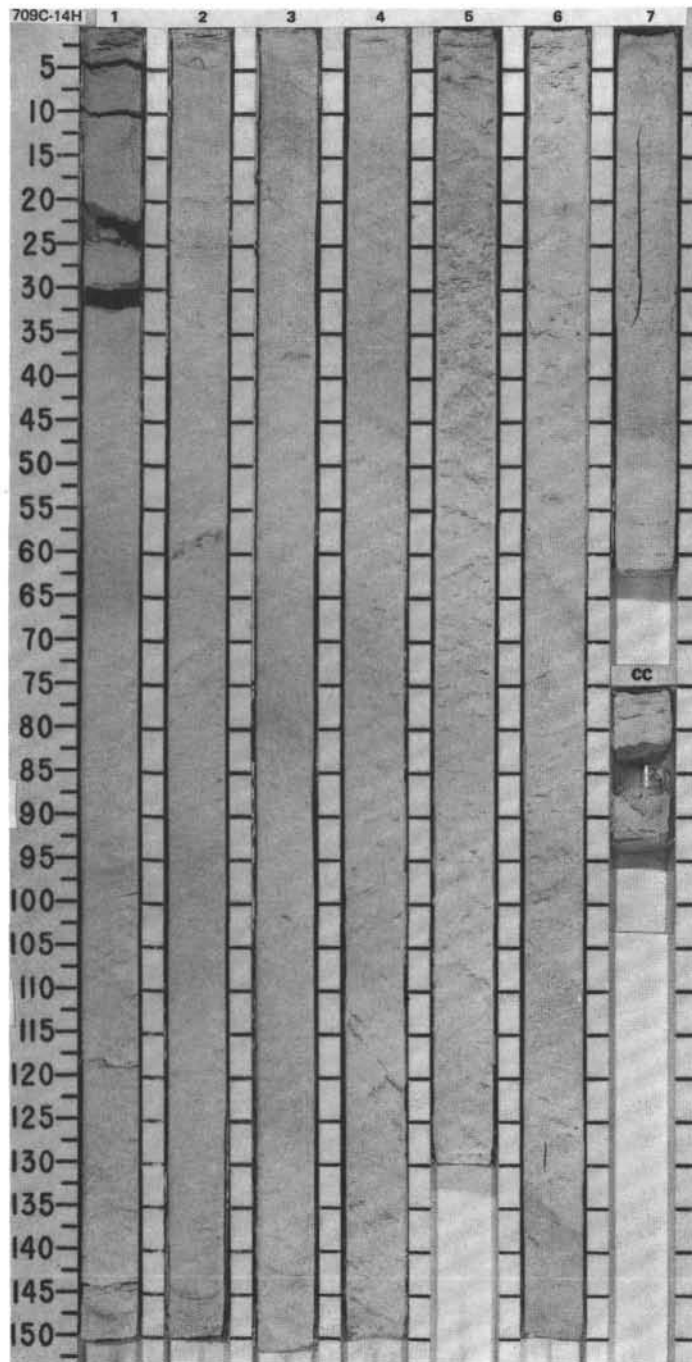


SITE 709 HOLE C CORE 13H CORED INTERVAL 3150.0-3159.6 mbsl; 111.8-121.4 mbsf

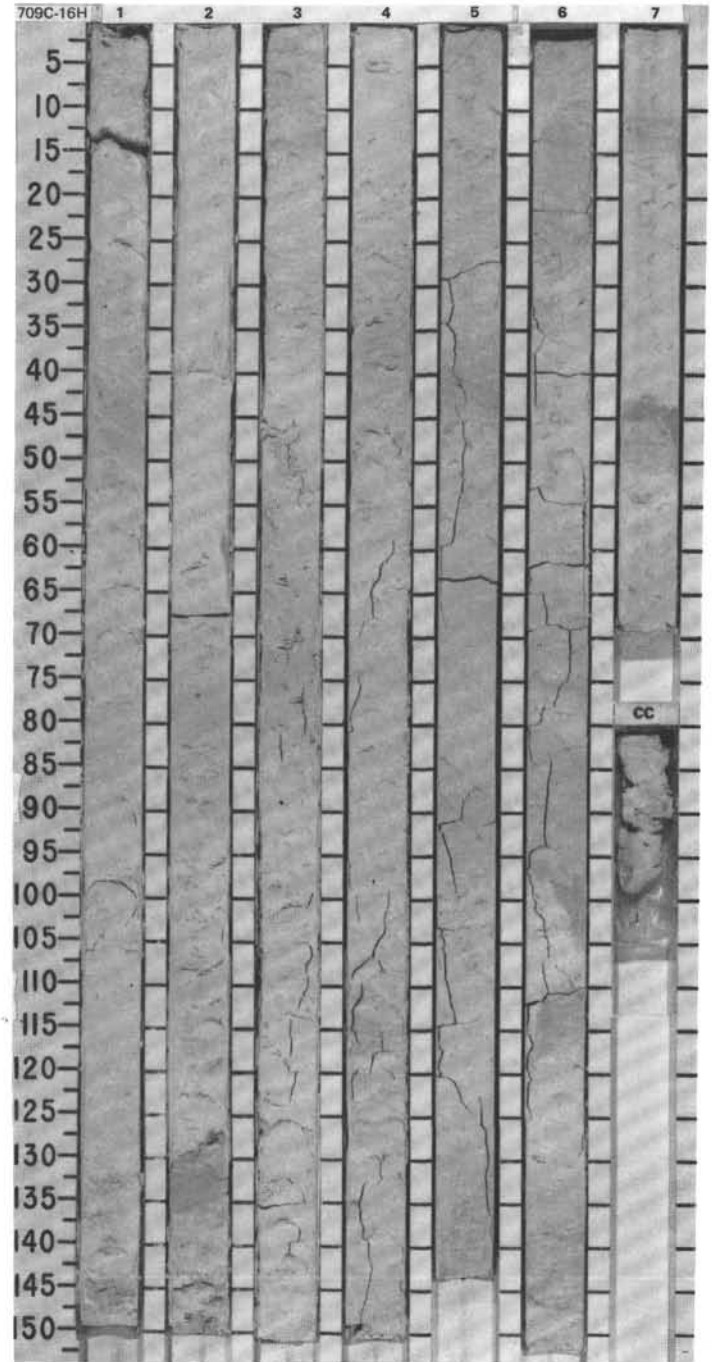
TIME-ROCK UNIT	BIOSTRAT. ZONE/ FOSSIL CHARACTER				PALEOMAGNETICS	PHYS. PROPERTIES	CHEMISTRY	SECTION	METERS	GRAPHIC LITHOLOGY	DRILLING DISTURB.	SED. STRUCTURES	SAMPLES	LITHOLOGIC DESCRIPTION
	FORAMINIFERS	NANNOFOSSILS	RADIOLARIANS	DIAZONS										
MIDDLE MIOCENE	CN 5 (NN 6 - NN 7)	CN 6 (NN 8)	CN 7 (NN 9)	CN 8 (NN 10)				1	0.5					<p>NANNOFOSSIL OOZE and CLAY-BEARING NANNOFOSSIL OOZE</p> <p>Major lithologies: Nannofossil ooze and clay-bearing nannofossil ooze, homogeneous and featureless, very light greenish gray (5G 8/1) to very light gray (N8) from Section 1 through Section 5, 10 cm, where a distinct color change occurs to white (10YR 8/1) for remainder of core (Section 5, 10 cm, through CC).</p>
UPPER MIOCENE							2	1.0						
							3							
							4							
							5							
							6							
							7							



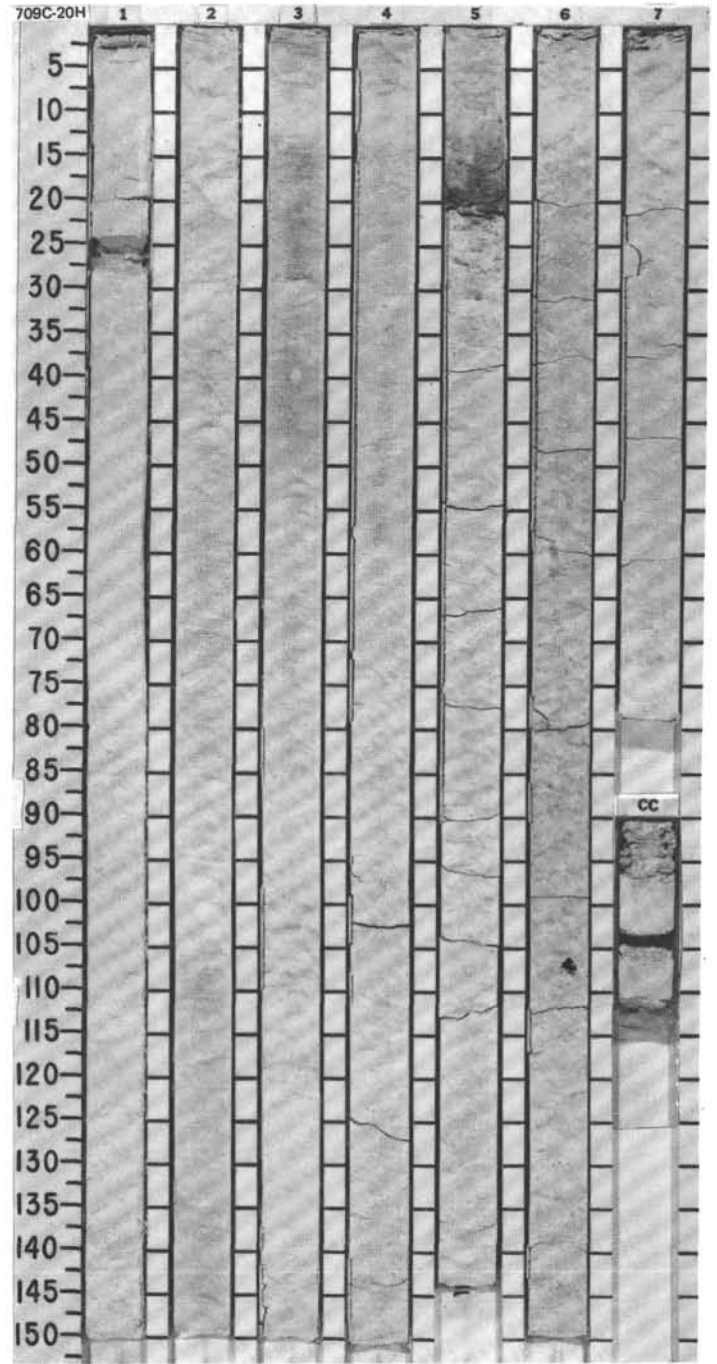
TIME-ROCK UNIT		BIOSTRAT. ZONE/ FOSSIL CHARACTER		PALEOMAGNETICS	PHYS. PROPERTIES	CHEMISTRY	SECTION METERS	GRAPHIC LITHOLOGY	DRILLING DISTURB.	SED. STRUCTURES	SAMPLES	LITHOLOGIC DESCRIPTION
FORAMINIFERS	NANNOFOSSILS	RADIOLARIANS	DIAATOMS									
MIDDLE MIOCENE		CN 5 (NN 6 - NN 7)					0.5 1.0					CLAY-BEARING NANNOFOSSIL OOZE Major lithology: Clay-bearing nannofossil ooze, extremely homogeneous, featureless, white (10YR 8/2).
AM	CN 4 (NN 5)	Barren					2					
							3					
							4					
							5					
							6			PP		
							7					
							CC					



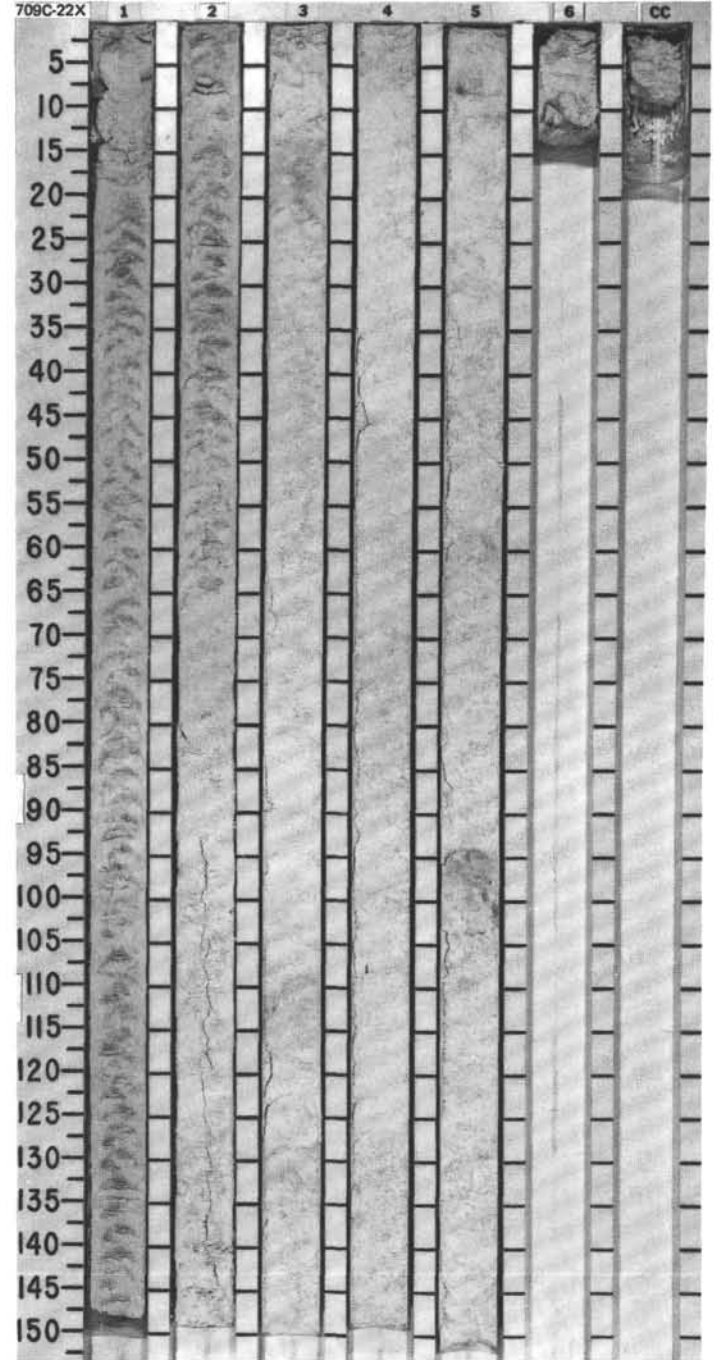
TIME-ROCK UNIT	BIOSTRAT. ZONE/ FOSSIL CHARACTER				PALEOMAGNETICS	PHYS. PROPERTIES	CHEMISTRY	SECTION	METERS	GRAPHIC LITHOLOGY	DRILLING DISTURB.	SED. STRUCTURES	SAMPLES	LITHOLOGIC DESCRIPTION
	FORAMINIFERS	NANNOFOSSILS	RAD/OLARIANE	DIATOMS										
LOWER-UPPER MIOCENE	CN 4 - CN 3 (NN 4 - NN 5)								0.5 1.0					<p>NANNOFOSSIL OOZE and CLAY-BEARING NANNOFOSSIL OOZE</p> <p>Major lithologies: Nannofossil ooze and clay-bearing nannofossil ooze, homogeneous, white (10YR 8/2) to slightly burrow-mottled, very pale brown (10YR 8/3), firm.</p> <p>Minor lithologies: Nannofossil chalk and clay-bearing nannofossil chalk, homogeneous, white (10YR 8/2) to slightly burrow-mottled, very pale brown (10YR 8/3); occur as thin lenses, sporadically distributed in Sections 1-4 and more abundantly in Sections 5 and 6 (making up around 20% of Sections 5 and 6).</p>
AM	Barren							2						
								3						
								4						
								5						
								6				PP		
								7						
								CC						



TIME-ROCK UNIT	BIOSTRAT. ZONE/ FOSSIL CHARACTER				PALEOMAGNETICS	PHYS. PROPERTIES	CHEMISTRY	SECTION	METERS	GRAPHIC LITHOLOGY	DRILLING DISTURB.	SEP. STRUCTURES	SAMPLES	LITHOLOGIC DESCRIPTION
	FORAMINIFERS	NANNOFOSSILS	RADIOLARIANS	DIATOMS										
LOWER MIOCENE	NN 2 (CN 1c + CN 2 ?)							1	0.5					<p>NANNOFOSSIL OOZE and CLAY-BEARING NANNOFOSSIL OOZE</p> <p>Major lithologies: Nannofossil ooze and clay-bearing nannofossil ooze, homogeneous, uniformly consolidated, somewhat firmer in Sections 6 and 7, white (10YR 8/2).</p> <p>Minor lithology: Volcanic ash, Section 5, 18-20 cm, sharp, distinct lower boundary, grayish brown (10YR 5/2) grading upward to light gray (10YR 7/2) and white (10YR 8/2).</p>
	Barren							2	1.0					
								3						
								4						
								5						
								6						
								7						
	AM NN 1 (CN 1a+b)							CC						

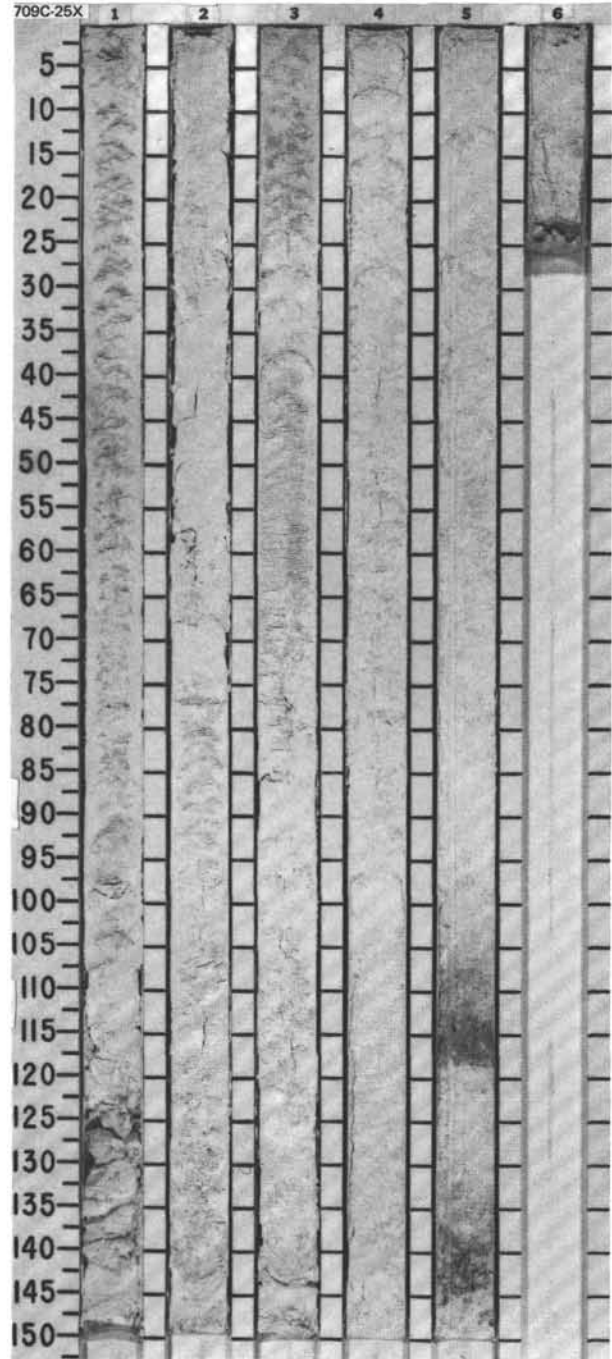


TIME-ROCK UNIT	BIOSTRAT. ZONE/ FOSSIL CHARACTER				PALEOMAGNETICS	PHYS. PROPERTIES	CHEMISTRY	SECTION	METERS	GRAPHIC LITHOLOGY	DRILLING DISTURB.	SED. STRUCTURES	SAMPLES	LITHOLOGIC DESCRIPTION
	FORAMINIFERS	NANNOFOSSILS	RADIOLARIANS	DIATOMS										
UPPER OLIIGOCENE	CP 19b (NP 25)													<p>NANNOFOSSIL OOZE and CLAY-BEARING NANNOFOSSIL OOZE, alternating with NANNOFOSSIL CHALK and CLAY-BEARING NANNOFOSSIL CHALK</p> <p>Major lithologies:</p> <p>a. Nannofossil ooze and clay-bearing nannofossil ooze, homogeneous, white (10YR 8/2).</p> <p>b. Nannofossil chalk and clay-bearing nannofossil chalk, homogeneous, white (10YR 8/2), irregularly spaced lenses, nodules, and layers, most highly concentrated in Sections 5-6.</p> <p>Minor lithology: Volcanic ash(?), Section 5, 93-102 cm, altered, light gray (N7), burrow-mottled with indistinct gradational boundaries.</p>
LOWER MIOCENE	NN 3 (CN a+b)													
P22	Barren													
CP														
AM														

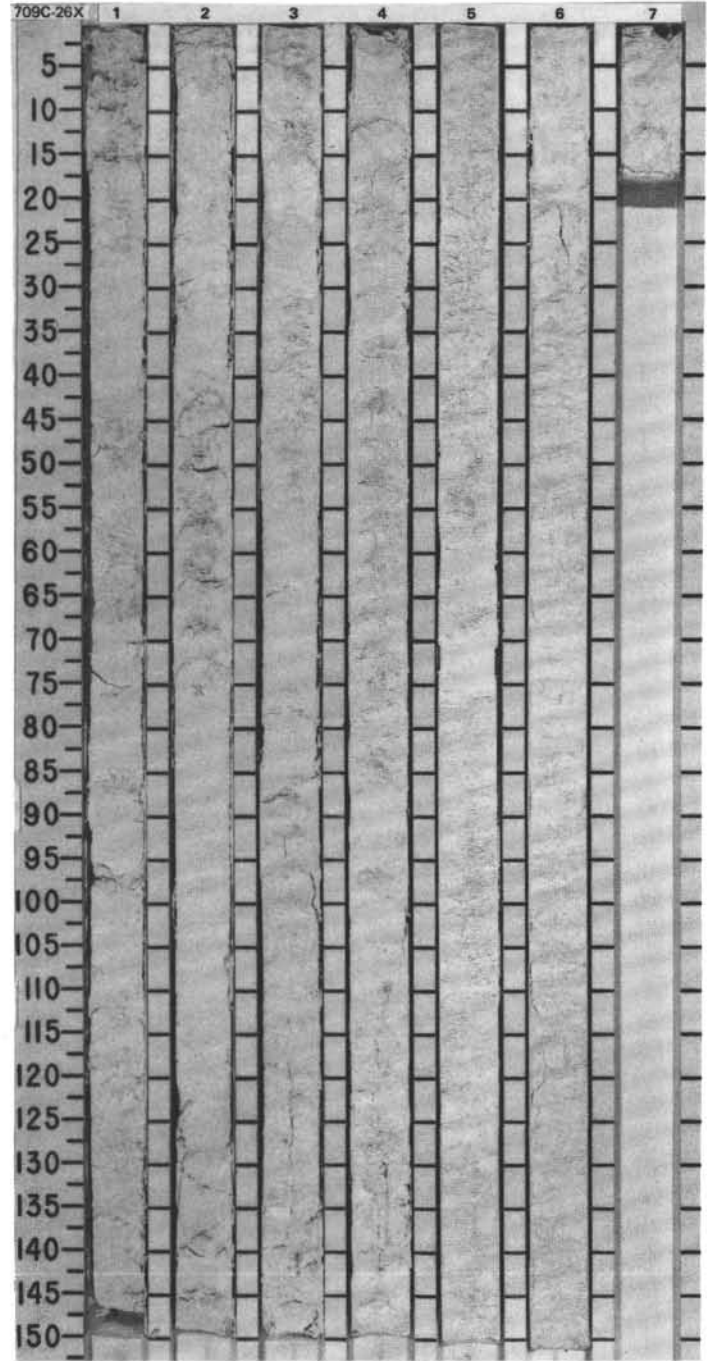


SITE 709 HOLE C CORE 25X CORED INTERVAL 3265.9-3275.6 mbsf; 227.7-237.4 mbsf

TIME-ROCK UNIT	BIOSTRAT. ZONE/ FOSSIL CHARACTER				PALEOMAGNETICS	PHYS. PROPERTIES CHEMISTRY	SECTION METERS	GRAPHIC LITHOLOGY	DRILLING DISTURB.	SED. STRUCTURES SAMPLES	LITHOLOGIC DESCRIPTION
	FORAMINIFERS	NANNOFOSSILS	RADIOLARIANS	DIAZONS							
UPPER OLIGOCENE											<p>NANNOFOSSIL OOZE and CLAY-BEARING NANNOFOSSIL OOZE, alternating with NANNOFOSSIL CHALK and CLAY-BEARING NANNOFOSSIL CHALK</p> <p>Major lithologies:</p> <ul style="list-style-type: none"> a. Nannofossil ooze and clay-bearing nannofossil ooze, homogeneous, white (10YR 8/2). b. Nannofossil chalk and clay-bearing nannofossil chalk, homogeneous, white (10YR 8/2), occurring as irregularly spaced nodules, lenses, and layers throughout core. <p>Minor lithology: Volcanic ash, Section 5, 116-124 cm, sharp distinct lower boundary, light brownish gray (10YR 6/2), grading upward to light gray (N7); Section 5, 130-145 cm, less distinct, light gray (N7), gradational boundaries. Light gray (N7) pyrite(?) staining, Section 1, 40-60 cm.</p>
AM	CP 19a (NP 24)					0.5 1.0					
				Barren							

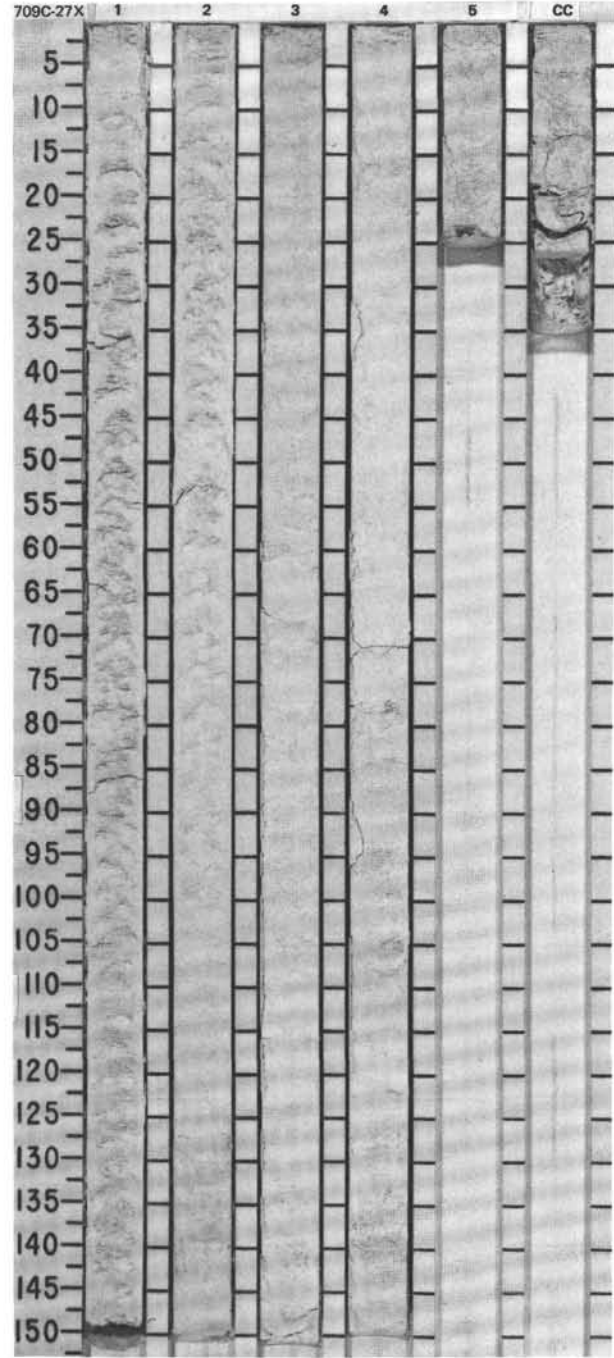


TIME-ROCK UNIT	BIOSTRAT. ZONE/ FOSSIL CHARACTER				PALEOMAGNETICS	PHYS. PROPERTIES	CHEMISTRY	SECTION	METERS	GRAPHIC LITHOLOGY	DRILLING DISTURB.	SED. STRUCTURES	SAMPLES	LITHOLOGIC DESCRIPTION
	FORAMINIFERS	NANNOFOSSILS	RADIOLARIANS	DIALOMS										
LOWER OLIGOCENE														<p>NANNOFOSSIL CHALK and CLAY-BEARING NANNOFOSSIL CHALK, alternating with NANNOFOSSIL OOZE and CLAY-BEARING NANNOFOSSIL OOZE</p> <p>Major lithologies:</p> <ol style="list-style-type: none"> Nannofossil chalk and clay-bearing nannofossil chalk, very homogeneous, white (10YR 8/2), occurring as layers, nodules, and layers. Nannofossil ooze and clay-bearing nannofossil ooze, very homogeneous, white (10YR 8/2), distributed in and around chalk lenses, nodules, and layers.
CP	upper P 20						1	0.5						
AM	CP 17 - CP 18 (NP 23)						2	1.0						
	Barren						3							
							4							
							5							
							6							
							7							



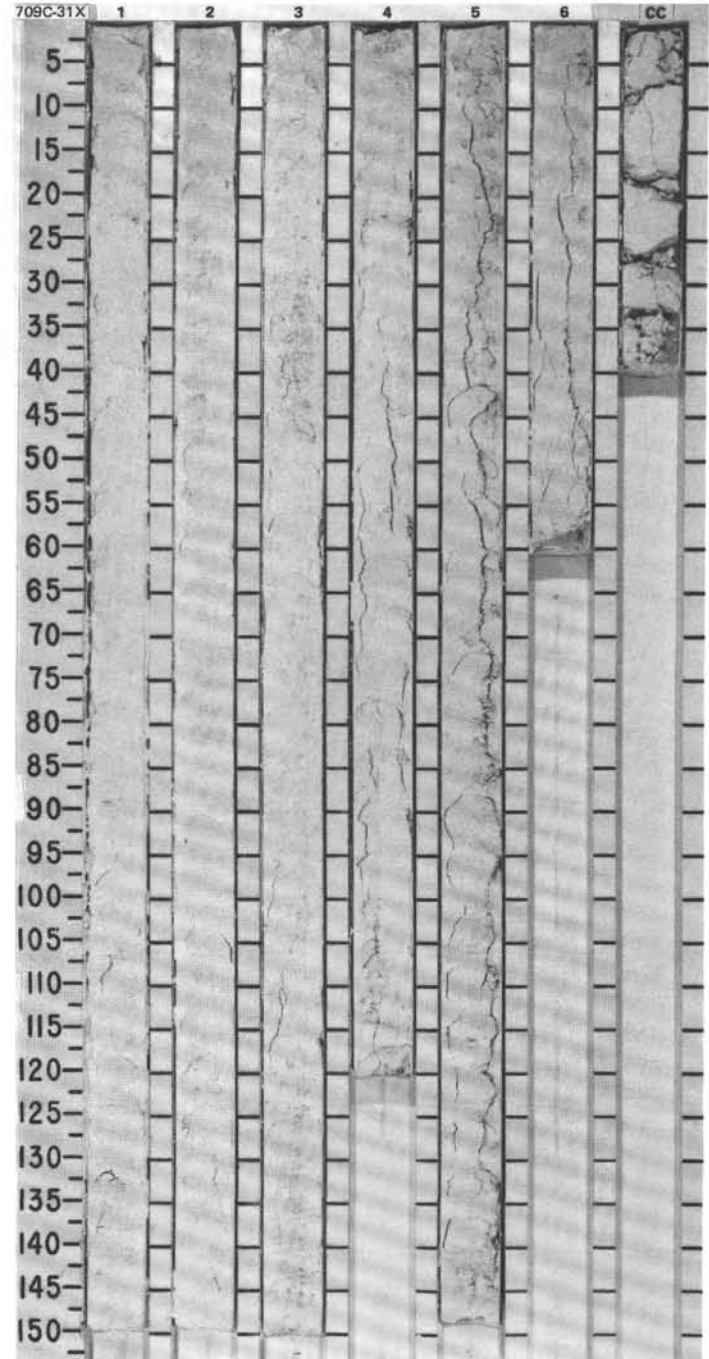
SITE 709 HOLE C CORE 27X CORED INTERVAL 3285.2-3294.9 mbsl; 247.0-256.7 mbsf

TIME-ROCK UNIT	BIOSTRAT. ZONE/ FOSSIL CHARACTER				PALEOMAGNETICS	PHYS. PROPERTIES	CHEMISTRY	SECTION	METERS	GRAPHIC LITHOLOGY	DRILLING DISTURB.	SED. STRUCTURES	SAMPLES	LITHOLOGIC DESCRIPTION
	FORAMINIFERS	NANNOFOSSILS	RADIOLARIANS	DIATOMS										
LOWER OLILOCENE														<p>NANNOFOSSIL CHALK, alternating with NANNOFOSSIL OOZE</p> <p>Major lithologies:</p> <p>a. Nannofossil chalk, homogeneous, white (10YR 8/2), occurring as lenses, nodules, and layers.</p> <p>b. Nannofossil ooze, homogeneous, white (10YR 8/2), distributed between and around chalk lenses, nodules, and layers.</p>
AM	CP 17 - CP 18 (NP 23)						1	0.5						
RM	<i>Theocyrtis tuberosa</i>						2	1.0						
	LOWER OLILOCENE						3							
	TRACE						4							
							5							
							CC							

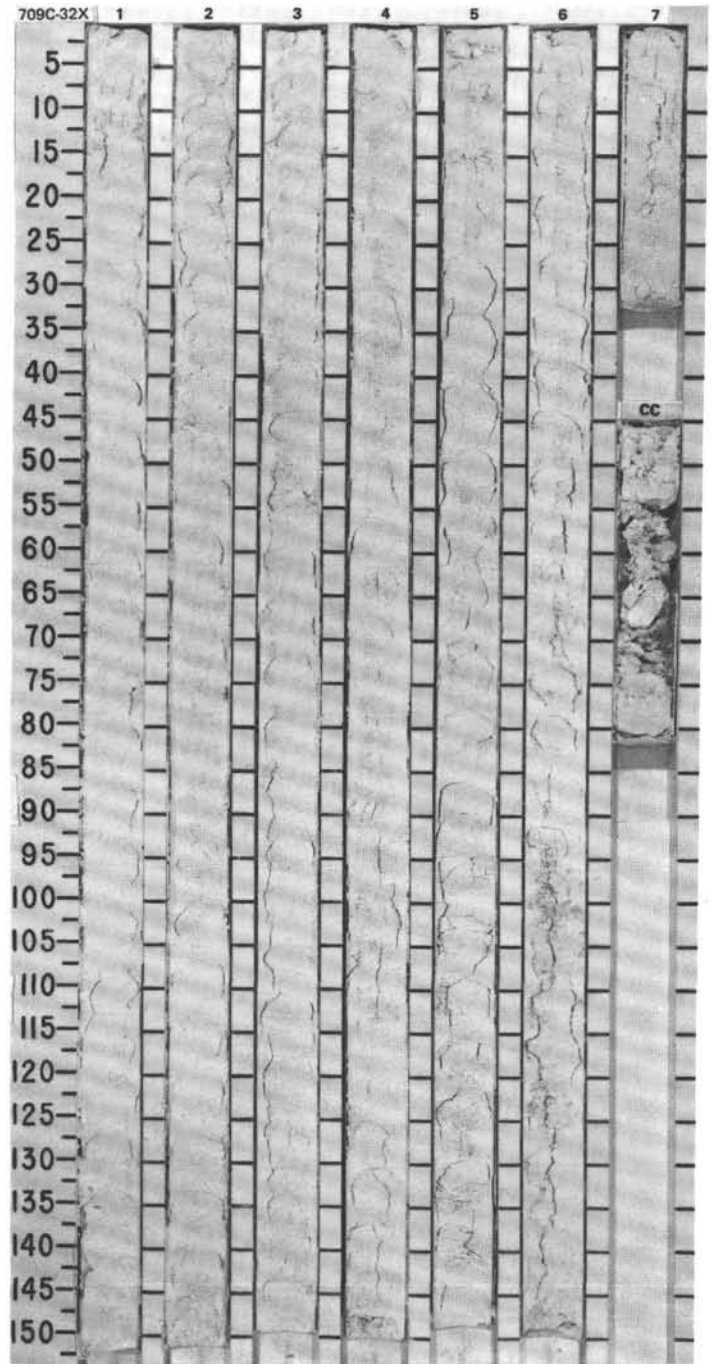


SITE 709 HOLE C CORE 31X CORED INTERVAL 3324.0-3333.6 mbsf; 285.8-295.4 mbsf

TIME-ROCK UNIT	BIOSTRAT. ZONE/ FOSSIL CHARACTER				PALEOMAGNETICS	PHYS. PROPERTIES	CHEMISTRY	SECTION	METERS	GRAPHIC LITHOLOGY	DRILLING DISTURB	SED. STRUCTURES	SAMPLES	LITHOLOGIC DESCRIPTION																								
	FORAMINIFERS	NANNOFOSSILS	RADIOLARIANS	DIFATOMS																																		
UPPER EOCENE																																						
CM	P 16?							1	0.5				*	<p>FORAMINIFER-BEARING NANNOFOSSIL OOZE and CLAY-BEARING FORAMINIFER-BEARING NANNOFOSSIL OOZE, alternating with FORAMINIFER-BEARING NANNOFOSSIL CHALK and CLAY-BEARING FORAMINIFER-BEARING NANNOFOSSIL CHALK</p> <p>Major lithologies:</p> <p>a. Foraminifer-bearing nannofossil ooze and clay-bearing foraminifer-bearing nannofossil ooze, homogeneous, white (10YR 8/2), uniformly less consolidated than ooze in previous cores (drilling paste?).</p> <p>b. Foraminifer-bearing nannofossil chalk and clay-bearing foraminifer-bearing nannofossil chalk, homogeneous, white (10YR 8/2), occurring as uniformly spaced nodules (drilling biscuits?), 2-3 cm thick and spaced 6-8 cm apart.</p> <p>Note: This core and cores 115-709C-32X to 115-709C-37X were split using a band saw; all previous cores were split with piano wire.</p> <p>SMEAR SLIDE SUMMARY (%):</p> <table> <tr><td>1</td><td>80</td></tr> <tr><td>D</td><td></td></tr> </table> <p>TEXTURE:</p> <table> <tr><td>Silt</td><td>24</td></tr> <tr><td>Clay</td><td>76</td></tr> </table> <p>COMPOSITION:</p> <table> <tr><td>Quartz</td><td>Tr</td></tr> <tr><td>Volcanic glass</td><td>1</td></tr> <tr><td>Foraminifers</td><td>10</td></tr> <tr><td>Nannofossils</td><td>76</td></tr> <tr><td>Radiolarians</td><td>5</td></tr> <tr><td>Sponge spicules</td><td>3</td></tr> <tr><td>Silicoflagellates</td><td>Tr</td></tr> <tr><td>Calcispheres</td><td>5</td></tr> </table>	1	80	D		Silt	24	Clay	76	Quartz	Tr	Volcanic glass	1	Foraminifers	10	Nannofossils	76	Radiolarians	5	Sponge spicules	3	Silicoflagellates	Tr	Calcispheres	5
1	80																																					
D																																						
Silt	24																																					
Clay	76																																					
Quartz	Tr																																					
Volcanic glass	1																																					
Foraminifers	10																																					
Nannofossils	76																																					
Radiolarians	5																																					
Sponge spicules	3																																					
Silicoflagellates	Tr																																					
Calcispheres	5																																					
AM	CP 15 (NP 18 - NP 20)						2	1.0																														
CM	<i>Thyrsocyrtis bromia</i>						3																															
	Barren						4																															
							5																															
							6																															
							CC																															

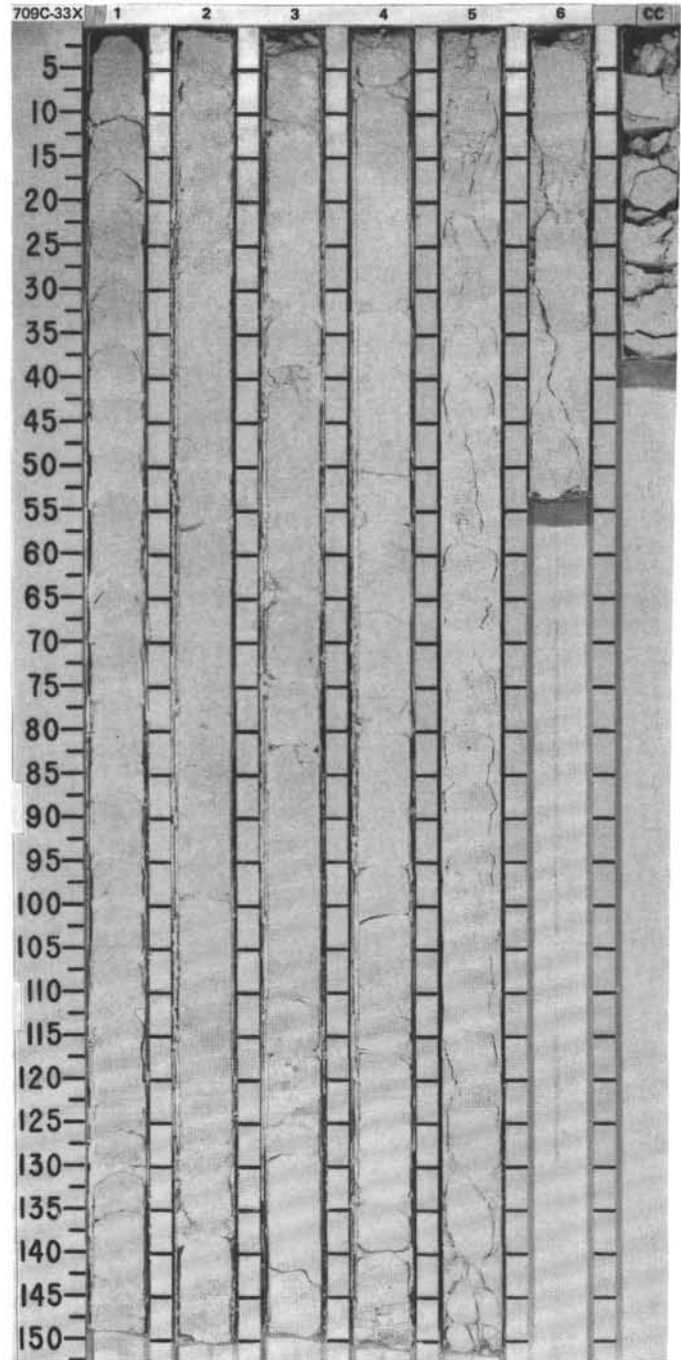


TIME-ROCK UNIT		BIOSTRAT. ZONE/ FOSSIL CHARACTER	PALEOMAGNETICS	PHYS. PROPERTIES	CHEMISTRY	SECTION	METERS	GRAPHIC LITHOLOGY	DRILLING DISTURB. SED. STRUCTURES	SAMPLES	LITHOLOGIC DESCRIPTION
FORAMINIFERS	NANNOFOSSILS										
UPPER EOCENE											FORAMINIFER-BEARING NANNOFOSSIL OOZE and CLAY-BEARING FORAMINIFER-BEARING NANNOFOSSIL OOZE, alternating with FORAMINIFER-BEARING NANNOFOSSIL CHALK and CLAY-BEARING FORAMINIFER-BEARING NANNOFOSSIL CHALK Major lithologies: a. Foraminifer-bearing nannofossil ooze and clay-bearing foraminifer-bearing nannofossil ooze, homogeneous, white (10YR 8/2), soft (drilling paste?). b. Foraminifer-bearing nannofossil chalk and clay-bearing foraminifer-bearing nannofossil chalk, homogeneous, white (10YR 8/2), occur as uniformly spaced nodules (drilling biscuits?), 2-3 cm thick and 6-8 cm apart. SMEAR SLIDE SUMMARY (%): 1, 80 D TEXTURE: Silt 22 Clay 78 COMPOSITION: Quartz Tr Volcanic glass Tr Foraminifers 15 Nannofossils 78 Radiolarians 4 Sponge spicules 2 Silicoflagellates Tr Fish remains Calcispheres 1
CP	P 16?					0.5				*	
AM	CP 15 (NP 18 - NP 20)					1.0					
CM	<i>Thyrsocypris bromia</i>										
	Barren										
						2					
						3					
						4					
						5					
						6					
						7					
						CC					



SITE 709 HOLE C CORE 33X CORED INTERVAL 3343.3-3353.0 mbsl; 305.1-314.8 mbsf

TIME-ROCK UNIT		BIOSTRAT. ZONE/ FOSSIL CHARACTER		PALEOMAGNETICS	PHYS. PROPERTIES	CHEMISTRY	SECTION METERS	GRAPHIC LITHOLOGY	DRILLING DISTURB. SED. STRUCTURES	SAMPLES	LITHOLOGIC DESCRIPTION																																	
FORAMINIFERS	NANNOFOSSILS	RADIOLARIANS	DIATOMS																																									
UPPER EOCENE		P 13-P 14					0.5 1.0				<p>FORAMINIFER-BEARING NANNOFOSSIL CHALK and CLAY-BEARING FORAMINIFER-BEARING NANNOFOSSIL CHALK, alternating with FORAMINIFER-BEARING NANNOFOSSIL OOZE and CLAY-BEARING FORAMINIFER-BEARING NANNOFOSSIL OOZE</p> <p>Major lithologies:</p> <p>a. Foraminifer-bearing nannofossil chalk and clay-bearing foraminifer-bearing nannofossil chalk, homogeneous to faintly burrow-mottled, white (10YR 8/2), occurring as regularly spaced nodules (drilling biscuits?) in Sections 1 and 5, and as continuous layers and fractured layers in Sections 2, 3, 4, and CC.</p> <p>b. Foraminifer-bearing nannofossil ooze and clay-bearing foraminifer-bearing nannofossil ooze, homogeneous to faintly burrow-mottled, white (10YR 8/2), soft, uniformly unconsolidated (drilling paste?).</p> <p>* SMEAR SLIDE SUMMARY (%):</p> <table border="1"> <tr> <td></td> <td>2, 80</td> <td>5, 80</td> </tr> <tr> <td>TEXTURE:</td> <td>D</td> <td>D</td> </tr> <tr> <td>Sand</td> <td>10</td> <td>10</td> </tr> <tr> <td>Silt</td> <td>5</td> <td>5</td> </tr> <tr> <td>Clay</td> <td>85</td> <td>85</td> </tr> <tr> <td>COMPOSITION:</td> <td></td> <td></td> </tr> <tr> <td>Foraminifers</td> <td>15</td> <td>15</td> </tr> <tr> <td>Nannofossils</td> <td>85</td> <td>83</td> </tr> <tr> <td>Radiolarians</td> <td>—</td> <td>Tr</td> </tr> <tr> <td>Sponge spicules</td> <td>Tr</td> <td>Tr</td> </tr> <tr> <td>Calcspheres</td> <td>Tr</td> <td>2</td> </tr> </table>		2, 80	5, 80	TEXTURE:	D	D	Sand	10	10	Silt	5	5	Clay	85	85	COMPOSITION:			Foraminifers	15	15	Nannofossils	85	83	Radiolarians	—	Tr	Sponge spicules	Tr	Tr	Calcspheres	Tr	2
	2, 80	5, 80																																										
TEXTURE:	D	D																																										
Sand	10	10																																										
Silt	5	5																																										
Clay	85	85																																										
COMPOSITION:																																												
Foraminifers	15	15																																										
Nannofossils	85	83																																										
Radiolarians	—	Tr																																										
Sponge spicules	Tr	Tr																																										
Calcspheres	Tr	2																																										
MIDDLE EOCENE		CP 15 (NP 18 - NP 20)					2																																					
AM							3																																					
AM	CP 14b (NP 17)	<i>Thyrocystis bromia</i>					4																																					
CM	<i>Podocystis goetheana</i>	Barten					5																																					
							6																																					
							CC																																					



TIME-ROCK UNIT	BIOSTRAT. ZONE/ FOSSIL CHARACTER				PALEOMAGNETICS	PHYS. PROPERTIES	CHEMISTRY	SECTION	METERS	GRAPHIC LITHOLOGY	DRILLING DISTURB.	SED. STRUCTURES	SAMPLES	LITHOLOGIC DESCRIPTION																																				
	FORAMINIFERS	NANNOFOSSILS	RADIOLARIANS	DIATOMS																																														
MIDDLE EOCENE														<p>CLAY-BEARING FORAMINIFER-BEARING NANNOFOSSIL CHALK, alternating with CLAY-BEARING FORAMINIFER-BEARING NANNOFOSSIL OOZE</p> <p>Major lithologies:</p> <p>a. Clay-bearing foraminifer-bearing nannofossil chalk, fairly homogeneous, white (10YR 8/2), occurring in somewhat regularly spaced nodules (drilling biscuits?) throughout core, many nodules fractured.</p> <p>b. Clay-bearing foraminifer-bearing nannofossil ooze, homogeneous, uniformly unconsolidated, white (10YR 8/2), occurring between and around chalk nodules (drilling paste?).</p> <p>* SMEAR SLIDE SUMMARY (%):</p> <table border="1"> <tr> <td></td> <td>2, 58</td> <td>4, 38</td> </tr> <tr> <td></td> <td>D</td> <td>D</td> </tr> </table> <p>TEXTURE:</p> <table border="1"> <tr> <td>Sand</td> <td>10</td> <td>15</td> </tr> <tr> <td>Silt</td> <td>10</td> <td>15</td> </tr> <tr> <td>Clay</td> <td>80</td> <td>70</td> </tr> </table> <p>COMPOSITION:</p> <table border="1"> <tr> <td>Volcanic glass</td> <td>Tr</td> <td>—</td> </tr> <tr> <td>Dolomite</td> <td>—</td> <td>5</td> </tr> <tr> <td>Accessory minerals</td> <td>Tr</td> <td>—</td> </tr> <tr> <td>Foraminifers</td> <td>15</td> <td>15</td> </tr> <tr> <td>Nannofossils</td> <td>84</td> <td>77</td> </tr> <tr> <td>Radiolarians</td> <td>1</td> <td>2</td> </tr> <tr> <td>Sponge spicules</td> <td>Tr</td> <td>1</td> </tr> </table>		2, 58	4, 38		D	D	Sand	10	15	Silt	10	15	Clay	80	70	Volcanic glass	Tr	—	Dolomite	—	5	Accessory minerals	Tr	—	Foraminifers	15	15	Nannofossils	84	77	Radiolarians	1	2	Sponge spicules	Tr	1
	2, 58	4, 38																																																
	D	D																																																
Sand	10	15																																																
Silt	10	15																																																
Clay	80	70																																																
Volcanic glass	Tr	—																																																
Dolomite	—	5																																																
Accessory minerals	Tr	—																																																
Foraminifers	15	15																																																
Nannofossils	84	77																																																
Radiolarians	1	2																																																
Sponge spicules	Tr	1																																																
AM	P 11						1	0.5																																										
AM	CP 13c (NP 15)						1	1.0																																										
CM	<i>Podocyrthis ampla</i> (EOCENE) TRACE						2																																											
							3																																											
							4																																											
							CC																																											

